REGULATION OF APICAL POLARITY COMPLEXES

By

Jay Nicholas Pieczynski

A dissertation submitted in partial fulfillment
of the requirements for the degree of
Doctor of Philosophy
(Biological Chemistry)
in the University of Michigan
2010

Doctoral Committee:

Professor Benjamin L. Margolis, Chair
Professor Eric R. Fearon
Professor Robert S. Fuller
Assistant Professor Daniel A. Bochar
Assistant Professor Hisashi Umemori

Acknowledgements

I would like to thank my mentor Dr. Ben Margolis for his guidance and support throughout the process of earning my doctorate degree. He has taught me that being a scientist means being your own toughest critic and to always remember that your work represents who you are and what you have accomplished. I would also like to thank the current and former members of the Margolis laboratory who made my time in the lab very enjoyable. Each person past and present has brought their own personality to the lab and contributed to the success of the group. It has been an honor to be associated with truly gifted scientists, yet even better people. The work contained within this thesis is also dedicated to my former mentors especially Michael Baxter and Dr. Todd Weaver. Michael Baxter was a former teacher of mine growing up in Wisconsin and recognized my potential as a scientist at a very early age. He taught me that science is not about how intelligent you are, but asking the write questions. Dr. Todd Weaver was also very instrumental in my scientific career, allowing me to begin my independent research career during the first years of college. Dr. Weaver recognized my desire to always know more, and challenged me to work outside the classroom in his laboratory for most of my undergraduate career; an experience that I am forever indebted to.

Finally, I would like to thank my friends and family. I am blessed to have some of the best friends that one could ask for and my success can only be attributed to having

people back me up all the way. My brother Tad has been my best friend my entire life and always encouraged me to be the best at whatever I do. My parents, Guy and Liz, have always been there for me especially when times got tough. They taught me that nothing in life is free and that hard work always eventually pays off. I am truly lucky to have two of the best parents who always wanted more for their children than they had.

Preface

Chapter 1 will be submitted as part of an invited review for the American Journal of Physiology Renal Physiology. Chapter 2 was published in December of 2006 in the Journal of Biological Chemistry and contains work completed by Dr. Samuel Straight and Jay Pieczynski. Chapter 3 contains data that will be submitted as a manuscript to Experimental Cell Research and is collaboration between Jay Pieczynski, Dr. Sanjeevkumar Patel, and Dr. Peter Arvan. Chapter 4 contains work that will be published in a future manuscript. Appendix A contains the full data sets of the microarray analysis completed in Chapter 3. Appendix B contains data that was published in Schlüter et al. in Molecular and Cellular Biology in September of 2009 and unpublished data related to that manuscript.

Table of Contents

List of Figures

List of Tables

List of Appendices

Chapter 1

Development and Maintenance of Renal Epithelial Cell Polarity

1.1 Introduction

Cell polarization refers to the asymmetry that arises in cells based on their ability to sequester biomolecules to different subcellular localizations, resulting in membranes of specialized function. The epithelial cell layer is a highly polarized layer of cells covering the surfaces of the body exposed to the outside environment and organ compartments such as the kidney. In the case of polarized cubiodial epithelia found in the renal tubules, segregation of proteins and phospholipids results in the formation of distinct surfaces referred to as domains. The formation of membrane domains in renal epithelial cells allows for a structure-function relationship that facilitates function of the kidney as a unit. Functions of renal epithelia derived from polarized epithelial structure include but are not limited to secretion, filtration, absorption, adhesion and sensory function. An intricate framework that combines protein-protein interactions, regulated transcription, ion flux, genetics, and the environment establishes polarity and therefore structure-function relationship of renal epithelial cells. The ability for epithelial cells to first establish and then maintain their polarized nature is essential to the physiology of any tubular organ system. Abrogation of polarization factors leads to an either partial or perhaps overall

loss of polarity that may be temporary or chronic based on genetic predisposition or acquired through disease, injury, or infection. Renal diseases, collectively referred to as nephropathies, can often be traced to a defect in a polarity mechanism at a molecular level.

Understanding how renal epithelial polarization is acquired and maintained in higher mammals is essential for the treatment of nephropathies. Due to a prevalence of polarized epithelial cells in the kidney, the kidney provides an excellent model system for the study of epithelial polarity in general. The identification of patients suffering from various nephropathies has allowed for an in depth genetic study of renal polarity. Model systems for the study of renal cell polarization in the mammalian system include cell culture and a limited number of mouse models. Fortunately, epithelial polarization is a highly conserved evolutionary phenomenon. Classic models such as the *C. elegans* zygote, *Drosophila melanogaster* (fruit fly), and *Danio rerio* (zebrafish) can be utilized to deduce the role of cell polarity *in vivo* in instances where manipulation of polarity genes/proteins is not practical. Albeit slightly different, polarity in lower organisms is often analogous to mammalian polarity, and many functional homologues of polarity proteins have been identified (10). Additionally, advancements in cell culture technique and imaging have allowed for a more accurate representation of cell polarity in a 3-dimesional context, allowing for study of polarization and development at the molecular level (reviewed in (214, 245)).

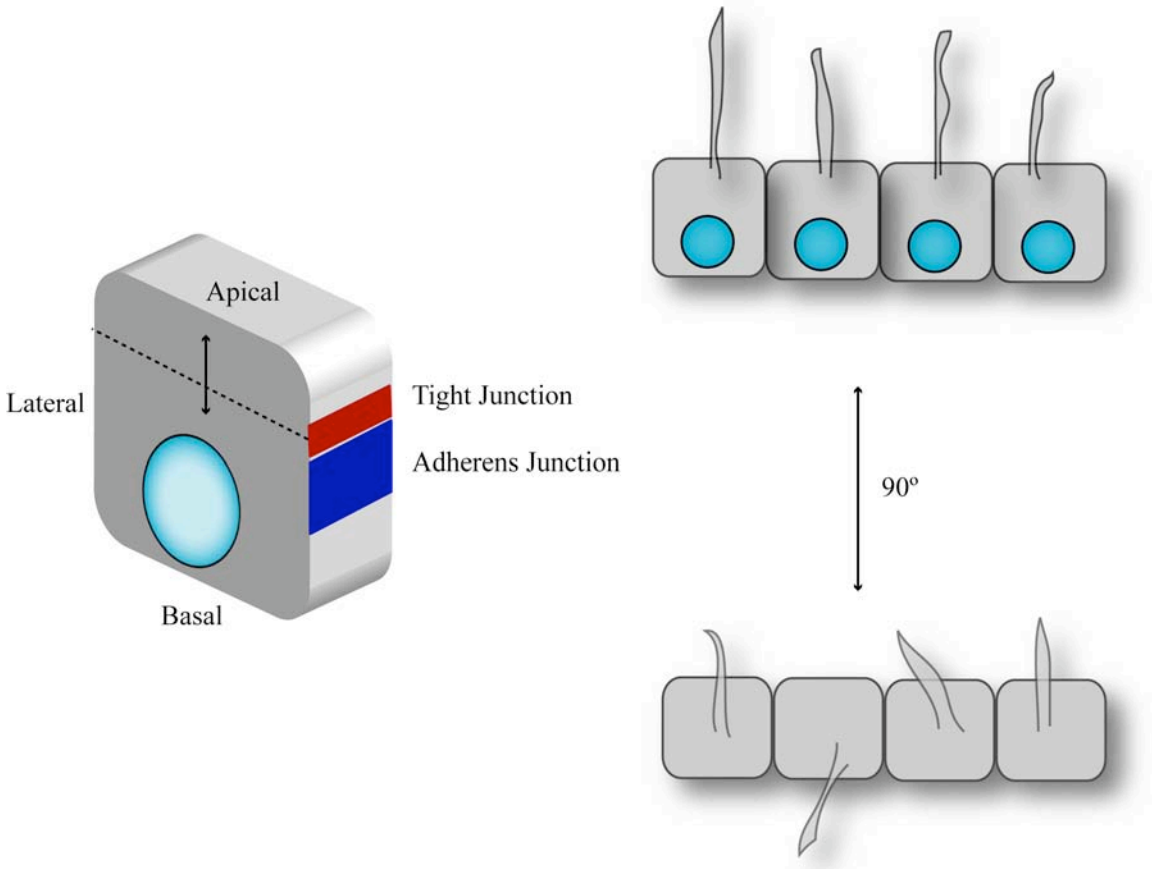

Figure 1-1: Model of basic cubodial epithelial cells. Epithelial cells arrange themselves in monolayers and are connected by junctions. Tight junctions (red) delineate apical versus basolateral sufaces while adherens junctions (blue) adhere cells to eachother. A primary cilium extends from the apical surface of many polarized epithelial cells, such as MDCKII cells. The relationship between polarity and cilia function is discussed in section 1.4.3.

1.2 Molecular Interactions Governing the Establishment of Mammalian Epithelial Cell Polarity

The structure of basic, cuboidal epithelia allows these cells to form a continuous monolayer which lines the tubular network of a particular organ, forming a barrier between the luminal space and the underlying tissue (Figure 1-1). Two major subdomains are created in polarized epithelial cells to facilitate the formation of the monolayer. The membrane subdomain facing the luminal space is termed the apical domain. The apical membrane surface is comprised of a network of microvilli, and the membrane contains a specific compliment of apical transporters and receptors as well as a distinct preference for particular phospholipids of which the membrane is constructed (45, 175). In the case of renal epithelia, there also exists a single non-motile primary cilium (reviewed in (80)). The second major subdomain of the epithelial membrane is known as the basolateral domain. The basolateral domain extends from just below the top of the cell, comprising both the lateral edges and the basement membrane. The basolateral domain faces neighboring cells and the underlying tissue making it distinctly different from the apical domain. The basolateral domain has its own set of transporters, receptors, phospholipids along with a host of cell-to-cell adhesion molecules and the extracellular matrix. The ability of epithelial cells to form distinct apical versus basolateral surfaces and therefore establish polarity is a result of protein-rich cell-to-cell contact points known as junctions. Junctions form a continuous belt around single polarized epithelial cells allowing for the formation of a continuous epithelial monolayer where the cell is an individual unit in 3-dimensional space. This phenomenon is referred to as apical-basal polarity (A-B polarity) in the context of planar-cell polarity (PCP). Both types of polarity are essential to the physiology of the epithelial monolayer. This

chapter will focus on the establishment and maintenance of A-B polarity, but it is important to keep PCP in mind, and it will be discussed by name where appropriate.

Junction formation, and therefore maintenance of epithelial polarity, is regulated by a series of protein-protein interactions. There are at least four types of junctions formed in polarized epithelial cells as a result of protein-protein interactions: tight junctions, adherens junctions, desomosomes, and gap junctions. Tight junctions are the most apical of the junctions, delineating apical versus basolateral surfaces and preventing "mixing" of the components of each respective membrane domain. This ability to establish preventative delineation of membranous surfaces is often referred to as the "fence" function of tight junctions. Yet another function of the tight junction is to be selectively permeable, preventing material from the luminal space from moving in between epithelial cells towards the underlying tissue. The selective permeability of the tight junction is referred to as the "gate" function. In essence, the tight junction allows for the epithelial monolayer to function as an entire unit, where each individual cell combines to maintain the integrity of the barrier layer. The formation of the tight junctions in a single cell gives context to the physiology of the entire epithelial monolayer. With the formation of the tight junction, the epithelial monolayer can be seen as a sealed sheet, covered with specialized surfaces for absorption and sensation. Since the majority of material passing through the luminal space is unable to directly pass between cells (passive transport), most material that the cell may need must be actively transported or endocytosed across the apical membrane into the cell. Likewise, any solute that must be expelled from the epithelial cell in to the lumen must be actively transported in the opposing direction. Additionally, the presence of the primary cilium on

the apical surface is essential for signal transduction from the luminal space to the cell interior (80).

Adherens junctions, desomosomes, and gap junctions are found on the lateral membrane of polarized epithelial cells. These junctions are protein-rich cell-to-cell contacts, but primarily function to facilitate adherence of neighboring cells. Cell-to-cell adhesion is important, as proximity and adhesion result in cell signaling and feedback. These feedback signals have been dissected and have illustrated the epithelial cell's ability to distinguish area and orientation and adjust cell morphology accordingly. Although the major focus of this review is not concerned with cell adhesion, it is important to note its role in cell polarity. The major epithelial adhesion protein, E-cadherin, has an extensive role in maintaining the epithelial monolayer through genetic and physical interactions with conserved proteins that are involved with the establishment of apico-basal polarity (92).

Large conserved polarity complexes are formed to facilitate tight junction formation. There are at least three major polarity complexes: the Par complex, the Scribble complex, and the Crumbs complex (10). Polarity protein complexes function both independently and synergistically and are complemented by a number of associated proteins not considered part of the core complex but essential to the stability, signaling, and/or localization of conserved polarity proteins. A general model for the mechanisms of polarity complexes is as follows: the Crumbs complex establishes and maintains the distinct apical domain in balance with the Scribble complex, which establishes and maintains the lateral domain. This balance is regulated through a system of exclusivity through phosphorylation by the Par complex. Polarity complexes consist of proteins

involved in a multitude of cellular functions including scaffolding, signaling, and membrane anchorage. Each member of the core polarity complexes is discussed in detail below, including important interactions, the role each protein plays in it's respective complex, and the role each protein has in overall epithelial cell polarity. For brevity, only established interactions and mechanisms of mammalian homologues will be discussed while homologues of lower organisms will only be mentioned to highlight specific interactions.

1.3 Mammalian Polarity Complexes and Their Interactions

1.3.1 The Par Complex Overview

The mammalian Par complex is comprises the proteins **P**artitioning defective-**3** (Par3/Par-3/Pard3), **Par**titioning defective-**6** (Par6/Par-6/Pard6), and **A**typical **P**rotein **K**inase **C** isoform **zeta** (aPKCζ). The Par complex provides us with the classical model of cell polarity, first studied in the *C. elegans* zygote (reviewed in (169)). Knockout studies in *C. elegans* provided the first insights into the asymmetrical distribution of proteins in developing organisms, as removal of the Par proteins leads to a failure of the zygote to correctly segregate proteins needed to begin proper development through asymmetrical cell division (62). The Par polarity complex is a transient complex, where Par3 is excluded or included to modulate the formation of both the apical surface and the tight junction (Figure 1-2 and (195, 201)).

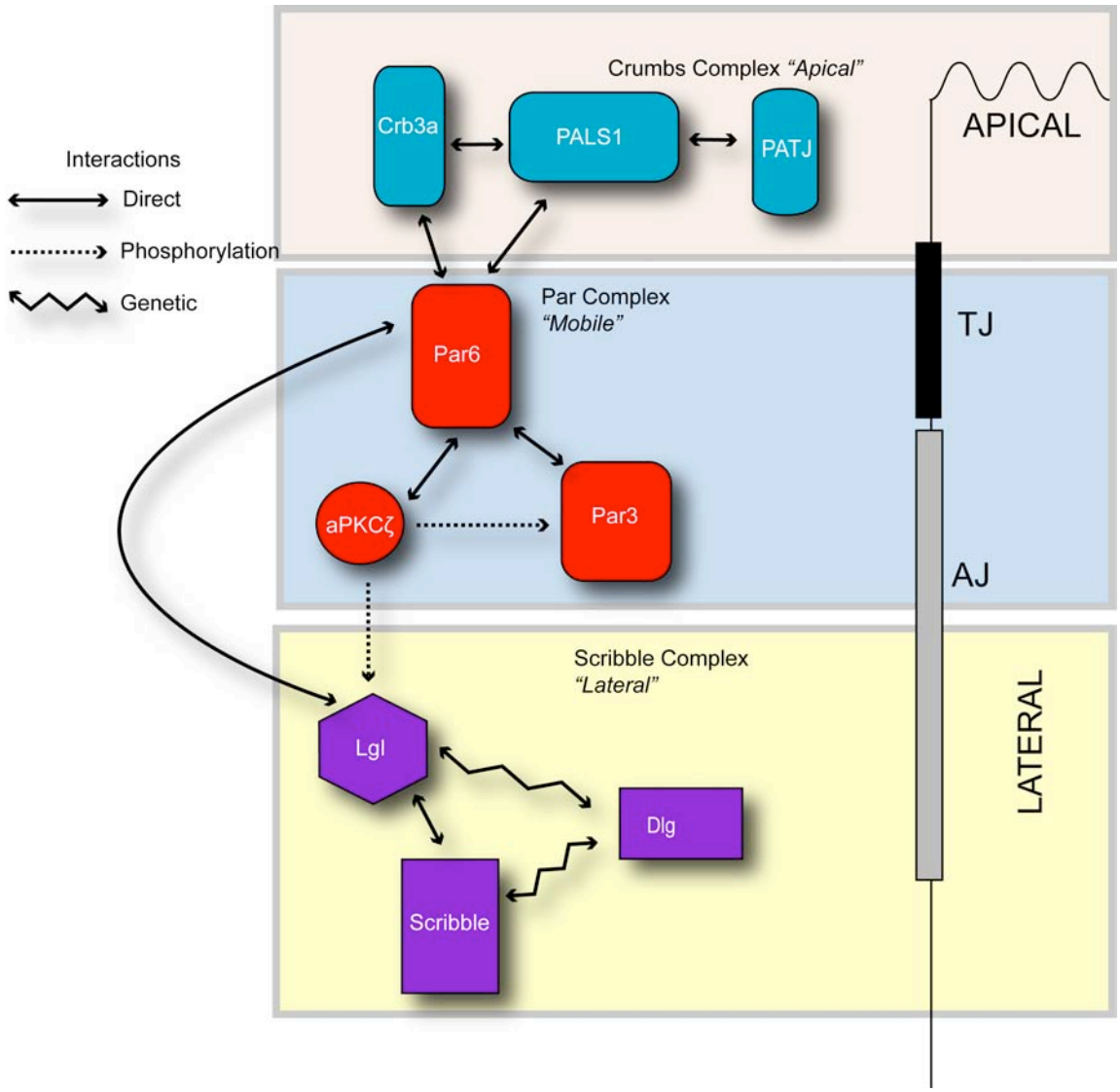

Figure 1-2: The conserved polarity complex interactome. The Crumbs, Par, and Scribble polarity complexes interact with eachother to modulate the formation of junctions and epithelila polarity. The Crumbs complex regulates the formation of the apical surface. The Scribble complex regulates formation of the lateral surface. The Par complex modulates the balance between apical and lateral surfaces via mulitple interactions.

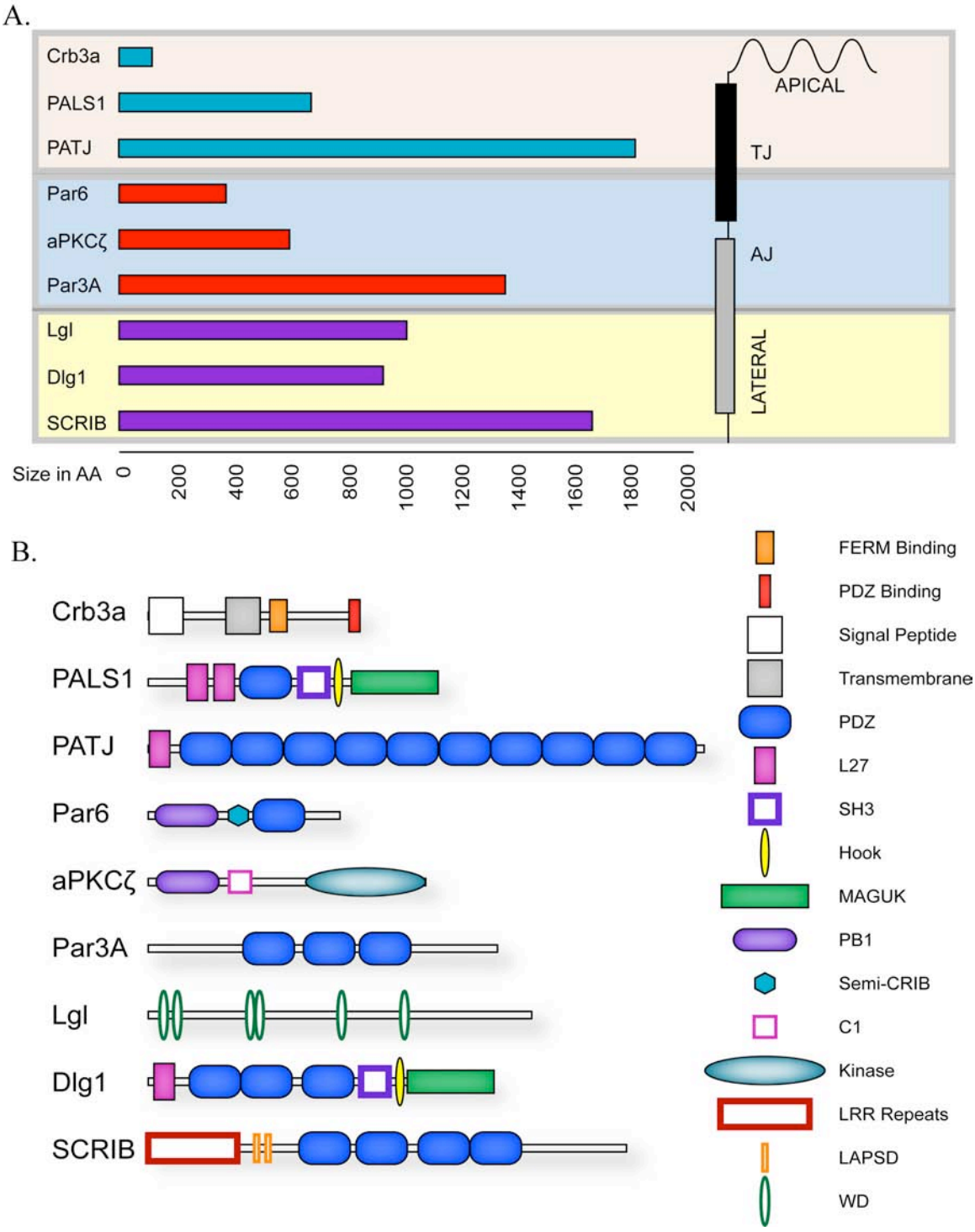

Figure 1-3: Sizes and domains of conserved polarity proteins. (A) Relative sizes of polarity proteins in amino acids (AA). (B) Domain structures of polarity proteins. Scale is approximate with the exception of Crb3a which is enlarged to show domains.

1.3.2 Par3

Par3 was first identified in a genetic screen for defects in asymmetrical cell division in the *C. elegans* zygote (62, 138). Deletion of the *Par3* gene leads to the defective partitioning of biomolecules during the first cell division, hence its namesake (138). In mammalian epithelia, Par3 is localized to both the tight junction and lateral membrane and has been shown to be necessary for tight junction formation and the localization of other members of the Par complex (73, 142, 268). Par3 is a multi-domain scaffold protein, consisting of multiple phosphorylation sites and three important protein-protein interaction domains, known as PSD95/DlgA/Zona Occludins-1 (PDZ) domains (Figure 1-3 and (120)).

In mammals, there are two Par3 proteins Par3A and Par3B (73). Although expressions of these proteins overlap in renal epithelial and localize to the lateral membrane, Par3B does not interact with aPKCζ (73). This exclusion is not fully understood as Par3B can still bind Par6 and overexpression of the N-terminus of Par3B can block tight junction formation similar to overexpression of Par3A (73). Interestingly, there are also three different Par3A protein isoforms due to alternate splicing in mammalian epithelia, and only two of which can bind aPKCζ (73). Each Par3A isoform is distinguishable due to significant differences in the molecule weights of the transcribed sequence (180kd, 150kd, and 100kd respectively); they still possess a similar domain structure. The 180kd and 150kd isoforms of Par3A bind aPKCζ on their C-terminus while the 100kd isoform lacks such a domain but is still considered an isoform of Par3A due to sequence homology (159).

Although Par3A is found in an evolutionarily conserved polarity complex with with Par6 and aPKCζ, Par3A is also found as a homodimer, which may be significant with regards to cell polarity. It has been demonstrated that Par3A can dimerize via its N-terminus and this interaction is important to the apical localization of Par3A (191). In the same study, the authors showed that the extreme N-terminus of Par3A is necessary for proper localization of the other Par complex and tight junction proteins (191). Like other PDZ-domain containing proteins, Par3A acts as a molecular scaffold at the tight junction. The first PDZ domain of Par3A interacts with Par6 (125). The interaction between Par3A with Par6 and aPKCζ is indispensable for the development of cell polarity (104, 125, 159). Interestingly, the binding between Par3A and Par6 is atypical. Normally, PDZ domain is found at the extreme C-terminus of a protein and is bound to a PDZ binding domain found somewhere on the internal structure of the binding partner. In the case of Par3A and Par6, there is an internal PDZ to PDZ binding not often described (125). Typical PDZ domain interactions involve a single PDZ domain that binds to a PDZ binding domain (PBD) located at the extreme C-terminus of the interacting protein (65, 238).

The identity of the Par polarity complex is regulated at least in part by the ability of aPKCζ to interact with and phosphorylate Par3A (97, 120). Phosphorylation of Par3 at S827 by aPKCζ is required for proper tight junction localization of Par3A (97, 201, 267). Overexpression of either a non-phosphorylatable mutant of Par3A or a dominant negative aPKCζ result a similar phenotype, an expanded lateral surface and a reduced apical surface suggesting this phosphorylation event is key to epithelial structure (201). The necessity of Par3A-aPKCζ interaction has been further demonstrated as essential by

knockdown experiments in both two and three dimensional tissue culture models. In a Par3A knockdown system, MDCKII cells formed intercellular lumens in monolayer culture and exhibited a multiple lumen phenotype in three-dimensions (104). In complementation assays, these Par3A knockdown phenotypes can only be rescued by introduction of Par3A that can specifically interact with aPKCζ (104).

In addition to phosphorylation by aPKCζ, it seems that phosphorylation of Par3A by other kinases also dictate functions of the protein in polarized epithelia. De-phosphorylation of serines in Par3A is mediated by Protein Phophastase 1 alpha (PP1α). Repression of PP1α in MDCKII cells caused delays in tight junction formation, further supporting the view of Par3A as a potent antagonist to cell polarity in PP1α regulated manner (278). Phosphorylation of S144 and S885 of Par3A by polarity kinase Par-1 (EMK1/MARK2) are necessary for the binding of protein 14-3-3 (also known as Par5) to Par3A in both canine and murine models (16). Disruption of Par3A S144 phosphorylation prevents a Par3A 14-3-3 interaction, resulting in polarity defects in three-dimensional culture (109). Importantly, 14-3-3 isoforms bind many other proteins including phosphorylated Yes-Associated-Protein (Yap), a terminal transcription factor of the Hippo signaling pathway known to be responsible for growth in a cell density dependent manner (304). Important questions remain to be answered on how the Hippo signaling pathway intersects with epithelial polarity, however recent studies in *Drosophila* suggest further roles for polarity proteins in attenuation of the Hippo pathway (14, 88, 160, 233, 304).

In MDCKII cells, Y1127 of Par3A is phosphorylated by c-Src or c-Yes through an epidermal growth factor (EGF) dependent mechanism and the phosphorylation event is

necessary for EGF induced tight junction formation (290). It is speculated that Y1127 phosphorylation of Par3A may contribute to its interaction with Ras-family GTPases that also bind the C-terminus of Par3A (290). Ras-family GTPases are famously known for regulating a multitude of cellular functions, including modulating cytoskeleton and perhaps epithelial architecture through cytoskeleton dynamics. Tiam1/2 is a Rac1 guanine nucleotide exchange factor (GEF) that binds the C-terminus of Par3A. The interaction of Tiam1/2 to Par3A spatially regulates activation of Rac1 at the cell periphery leading to a stabilization of epithelial junctions (39). Another Ras-family member, RhoA, is a potent antagonist of Rac1 activity (39). RhoA activates Rho-kinase (ROCK) downstream, leading to phosphorylation of yet another site on Par3A, T833 (204). The phosphorylation of Par3 at T833 has been recently demonstrated to prevent formation of the Par polarity complex, leading to the inactivation of Rac1, presumably by impairing the function of Tiam1/2 bound to Par3A (204). Overexpression of Par3A in subconfluent and non contact-inhibited MDCK cells leads to Rac1-induced fibroblastic phenotypes suggesting that the binding of Par3A to Tiam1/2 alone is not sufficient for the entire mechanism of junctional stability (190). In fact, evidence has shown that a functional Par polarity complex (consisting of Par3A, Par6, and aPKCζ) enhances Rac1 activity and is antagonized by Rho activity (204). Mechanisms for spatial and temporal control of Rac/Rho activity has been recently put forth that may explain how epithelial cells so carefully control their morphology. It has been suggested that aPKCζ phosphorylation of Par3 decreases the stability of the Par polarity complex which subsequently has the downstream effect of modulating Rac/Rho GTP levels, ultimately controlling the cytoskeletal framework of the epithelial cell (195). In this model, aPKCζ

phosphorylation of Par3A defines the apical-lateral border by controlling the identity of the Par polarity complex at a given time (195).

Par3A also has been shown to interact with cytoplasmic keratin via the keratin binding protein Albatross. The association of Par3A with Albatross enforces the identity of the basolateral surfaces (266). In an Albatross knockdown cell, lateral membrane components are mislocalized in the cell (266). Also, Par3A is implicated in the genesis of the primary cilium in epithelial cells by interacting with Kinesin-II (249). In this study, it is suggested that Par3A is dispensable for end-stage polarity, but absolutely required for ciliogenesis indicating that Par3A has a role in creating new apical membrane but not maintaining existing membrane. The authors of this study found that stable Par3A knockdown delayed tight junction formation, suggesting that Par3A only plays a role in early polarization, a process that is analogous to new apical membrane formation (249).

The second and third PDZ domains of Par3A have been suggested to anchor the Par complex to the cell membrane and to be associated with phosphoinositide signaling. PDZ2 of Par3A binds phospholipids found in the inner leaflet of the plasma membrane while PDZ3 of Par3A has been shown to bind the protein Phosphatase and Tensin homolog (PTEN) (67, 297). The localization of PTEN to the lateral membrane of polarized MDCKII cells is essential for proper cell polarization (67). Studies suggesting a link between cell polarity and phosphoinositide signaling will provide ground for studying the integrated signaling networks involve in epithelial polarization and cytokinesis (45, 175)(45, 168). Par3A also directly interacts with Junction Adhesion Molecule (JAMS) via PDZ domains 1 and 3 (61, 117). The binding of JAMs to Par3A is found at the lateral membrane and not in the cytosol and occurs specifically at the tight

junction, suggesting that JAMs are an anchor for the Par polarity complex at the tight junction as cells polarize. It has yet to be determined if PDZ3 of Par3 exhibits mutually exclusive binding between the JAMs and PTEN, and further study is needed to elucidate whether or not this binding is polarization dependent.

1.3.3 Par6

Par6 is a multi-domain protein localized to tight junctions of renal epithelial cells and a member of the conserved Par polarity complex. In mammals, there are three identified *Par6* genes, Par6A, Par6B, and Par6G, and all appear to be ubiquitously expressed, albeit with slightly different temporal-spatial and sub-cellular localizations (72). Par6A and Par6B are more enriched in the kidney, and will thus be the focus of this review. Regardless of the isoform, it appears that Par6 is a multifunctional protein in kidney epithelial cells, being a key adapter protein that allows the Par complex to interact with both the Crumbs and Scribble polarity complexes (110, 153, 289). Par6 contains an N-terminal Phox and Bem1 (PB1) domain, followed by a semi-Cdc42/Rac Interactive Binding (Semi-CRIB) domain, and a C-terminal PDZ domain (Figure 1-3).

Par6A directly interacts with Crumb3 (Crb3) via Par6A's PDZ domain and this binding is an absolute requirement for proper tight junction formation (110, 153). Interestingly, Par6 binding to Crb3 appears to be isoform dependent (72). Although the PDZ domain of Par6A binds Crb3, the PDZ domain of Par6B binds a different member of the Crumbs complex, Protein Associated with Lin Seven 1 (PALS1), with higher affinity (72). Par6B binding to PALS1 can interrupt the binding of PALS1 to the third member of the Crumbs polarity complex, PALS1 Associated Tight Junction Protein (PATJ).

Interruption of PALS1-PATJ binding by Par6-PALS1 binding interferes with the formation of the tight junction (289). The difference in binding preference between Par6A and Par6B may be explained by the conformation of the protein when bound with another binding partner, Cdc42, which is discussed below (72).

The Par6 isoforms interact with members of the aPKC family in a multitude of tissues. In the kidney, the most notable contribution to renal polarity is aPKCζ, which binds Par6 via an N-terminal PB1 domain (268). The function of Par6 binding to aPKCζ is to link Par6 and the previously mentioned Par3 into a complex that may be dependent on the phosphorylation status of Par3 and to control the activity of the complex. The semi-CRIB domain and the PDZ domain of Par6 binds the N-terminus of Par3 forming a stable tripartite complex that promotes junction formation (125). Par6 is thought to activate aPKCζ through direct interaction, allowing aPKCζ to phosphorylate Par3 (301).

Par6 has the ability to activate aPKCζ and begin the cascade of polarization due its ability to bind the GTP-bound forms of Cdc42 and Rac1. Par6 interacts with Cdc42 and Rac1 via the semi-CRIB domain (125, 126). The interaction between Par6 and Cdc42 and/or Rac1 leads to dynamic cytoskeletal rearrangement for overall epithelial polarization. Par6 is able to bind the GTP-bound form of Cdc42 as a result of Cdc42-GTP assembly via E-cadherin trans-homodimerization at the adherens junction between neighboring epithelial cells (126). The interaction of Par6 with Cdc42 renders a conformational change in Par6 altering the binding between Par6 to PALS1 and/or Crb3 (72, 76). When activated, GTP-bound Cdc42 binds Par6; the PDZ domain of Par6 most likely becomes hidden through conformational change resulting in masking of the PDZ domain of Par6, leaving Par6 unable to bind PALS1 or Crb3 (72).

It is through this conformational change that Par6, and the entire Par complex for that matter, is thought to antagonize the formation of polarity and/or the tight junction. There is conflicting evidence however, on whether Par6 function is related to promotion or prevention of polarization. Overexpression of Par6 in MDCK cells inhibits tight junction formation but not adherens junction formation, providing evidence that Par6 does act as an antagonist to the establishment of tight junctions (71). On the other hand, Par6 overexpression has also been linked to cell hyperproliferation without loss of apico-basal polarity suggesting tight junction formation is not regulated via Par6 and that the hyperproliferative phenotype is due to increased levels GTP-Cdc42 induced cytoskeletal changes (213). Hypothetically, the phenotypes described could possibly describe the same scenario, with the suggestion that during Par6 overexpression, mature tight junctions are short lived due to the overwhelming presence of a potent antagonist to their formation. An alternative and increasingly likely explanation for these phenotypes is that the Par complex as a whole acts in a context-dependent manner facilitating both the formation and disassembly of tight junctions depending on nature of the complex. Evidence suggesting that the Par complex contains transient components due to the presence of aPKCζ, an active kinase in the complex, supports this theory. Recent studies have shown that Par6 can interact directly with a member of conserved Scribble polarity complex, namely Lethal-giant Larvae (Lgl), and that this interaction is upstream of canonical Par complex formation (230, 299). The basolateral Scribble polarity complex is hypothesized to antagonize formation of the apical surface. Tony Pawson's group illustrated that Lgl effectively interacts with PDZ domain of Par6B (230). The binding of Lgl to Par6B is mutually exclusive to that the binding of Par3 and PALS1 to Par6 (300).

With the binding between PALS1 and Lgl to Par6 being mutually exclusive, Par6 is likely a regulator of the delicate balance between the formations of distinct apical versus basolateral domains in polarized epithelial cells. In this case, Par6 shuttles back and forth, reinforcing both basolateral and apical identities through alternate binding between conserved polarity complexes.

1.3.4 aPKCζ

Atypical protein kinase C zeta (aPKCζ) is the kidney specific isoform of the atypical protein kinase family that also includes lambda and iota isoforms (221, 248). Members of the atypical protein kinase C family lack most of the C1 and all of the C2 domains, distinguishing themselves from typical PCKs (96). However, the C-terminal kinase domains of aPCKs are active, placing them in the proteins kinase C family due to similarities of these kinase domains (5). With regards to epithelial polarity, aPKCζ is a member of the Par polarity complex localized to the lateral membrane of renal epithelial cells via directly binding to Par6 and Par3 via an N-terminal PB1 domain on aPKCζ (Figure 1-3 and (120)). aPKCζ can also localize to the nucleus. Upon binding of GTP-Cdc42 to Par6, aPKCζ is translocated from the nucleus to the cytoplasm to form a stable complex with Par6 (211). Translocation from the nucleus and subsequent binding of aPKCζ to Par6 is downstream of cell-cell adhesion where GTP-loading of Cdc42 and other Rho GTPases occurs upon cadherin based cell to cell contacts (121). Current models suggest that upon E-cadherin mediated cell adhesion; Cdc42 converts from its GDP-bound inactive form to its GTP-bound active form that then binds Par6, which in turn sequesters aPKCζ in the cytoplasm (211).

aPKCζ is the only conserved polarity protein that contains an active kinase domain. It is believed that the function of aPKCζ in polarized epithelial cells is to act as a molecular switch controlling the identity of apical and lateral domains. This is accomplished by the selective phosphorylation of known targets of aPKCζ in mammals, including the previously mentioned Par3A and Lgl (97, 120, 159, 230, 300). aPKCζ phosphorylation of Par3 and Lgl is believed to modulate the identity of the Par-complex in mammalian cells where as the phosphorylated species of either Par3A or Lgl are excluded or included in a particular complex based on conformational change. Phosphorylation of Par3A by aPKCζ results in a Par3-Par6 dissociation, beginning a cascade resulting in the stabilization of tight junctions and the development of apical-basal polarity (97, 201). In a similar way, aPKCζ phosphorylates Lgl inducing Lgl dissociation from Par6 and the inclusion of Lgl in the Scribble complex (230, 299, 300). Liberated phospho-Lgl is free to associate with other binding partners, reinforcing Par complex formation resulting in subsequent phosphorylation and dissociation of Par3 with the complex leaving Par6 free to potentially associate potentially, with either Crb3 or PALS1. The dissociation of Lgl from Par6 leads to Par complex reformation, and results in cytoskeletal rearrangements that reinforce surface identity through Ras-family GTPases (section 1.3.3). In *Drosophila,* aPKCs have been shown to also phosphorlyate dCrumbs (the *Drosophila* homologue of mammalian Crb) (259). In mammals however, this phenomenon has not been observed. The above evidence suggests that in mammals, the Par complex and the Scribble complex are functional antagonists with regards to cell polarity where aPKCζ acts as the molecular switch to facilitate polarity and junction formation.

1.3.5 The Scribble Complex Overview

The mammalian Scribble complex comprises the genetically linked conserved polarity proteins **Scrib**ble (SCRIB), **D**iscs **L**ar**g**e (Dlg), and **L**ethal **g**iant **l**arvae (Lgl). Although the evidence for physical interaction between these proteins is limited, studies in lower organisms suggest that they function in the same genetic pathway. The Scribble complex localizes to the lateral membrane in polarized epithelia; a location consistent with a role in defining the lateral versus the apical surface of these cells (Figure 1-2).

1.3.6 Scribble

Scribble (SCRIB) is a large, cytoplasmic scaffold protein associated with the lateral membrane in polarized renal epithelial cells (56, 203). Originally described in *Drosophila,* SCRIB's name is derived from the disorganized phenotype described in the developing embryo, imaginal wing discs, and follicles of the fly (20, 21). SCRIB is a member of the Leucine-rich repeat (LRR) and PDZ domain (LAP) family of proteins due to the 16 LRRs on the N-terminus and 4 PDZ domains on the C-terminus of its structure (Figure 1-3 and (19)).

The functional role of Scribble in renal epithelia is still a mystery, however interactions between Scribble and its binding partners have given insight to how this protein affects cell polarity. The N-terminal of 16 LRRs of SCRIB are necessary for binding to Lgl2 and targeting SCRIB to the lateral membrane in polarized renal epithelia (128, 206). The association of Scribble with the lateral membrane however appears to be cell-type specific. In intestinal epithelia, Scribble associates with the tight junction

structural protein ZO-1 and regulates tight junctions stability, a phenomenon not seen in renal epithelia (119). The lateral targeting of SCRIB depends on the presence of E-cadherin, and in MCF10A cells lacking E-cadherin; SCRIB is no longer associated with the membrane (206). The association of SCRIB with intracellular domain of E-cadherin at the lateral membrane of polarized renal epithelia is necessary for proper cell-cell adhesion as SCRIB knockdown effects adherens junction stability (231). In this study, shRNAs against SCRIB in MDCK cells was shown to increased motility and adhesion, a phenotype similar to that seen with the knockdown of E-cadherin (231). The association of Scribble with E-cadherin suggests that Scribble may have a role in both epithelial cell migration and the initiation of epithelial polarity. The PDZ domains of SCRIB bind βPix, a Rac/Cdc42 GEF involved in exocytosis (11). SCRIB has been shown to regulate directed migration and wound healing in association with Rac1, Cdc42, and presumably the Par complex (58, 212). Also, PDZ domains 3 and 4 of SCRIB bind the tight junction structural protein ZO-2 in contact naïve epithelial cells, but not fully polarized epithelia further suggesting a role for SCRIB in cell migration (187). Similarly, mice displaying mutated variants of SCRIB display impaired directed epithelial migration phenotypes (58).

A SCRIB-E-cadherin genetic interaction also suggest SCRIB may associate with both canonical and non-canonical Wnt signaling. SCRIB knockdown phenotypes could be rescued by expression of an alpha-catenin-E-cadherin fusion protein suggesting canonical-Wnt signaling is associated with SCRIB expression (231). PDZ domains 2, 3, and 4 of SCRIB bind to the planar cell polarity factor and non-canonical Wnt-signaling molecule Vangl2, and this interaction is responsible for proper orientation of polarized

structures in mammals (128, 194). Abrogation of Vangl2 in mouse reproductive tract epithelium in turn resulted in a mislocalization of SCRIB and defects in apical membrane formation further strengthening the association of Scibble with both methods of Wnt-signaling (284).

Human SCRIB has been demonstrated to be an effective tumor suppressor; confirming apico-basal cell polarity, preventing tumorgenic overgrowth, and contributing to the proper orientation of planar cell polarity (56, 193). A recent study suggests that SCRIB tumor suppressor function is related to the ability of SCRIB to regulate the Ras-MAPK pathway, and overexpressed SCRIB was able to effectively suppress oncogenic Ras-associated invasiveness (57). *Drosophila* models of tumor formation confirm that oncogenic-Ras and SCRIB mutants cooperate to form metastatic tumors similar to those found in human cancers (298). The tumor suppressor APC also binds SCRIB through PDZ1 and PDZ4 suggesting that SCRIB is involved with cell signaling regulating the cell cycle, cell growth, and cell morphology (269). Perhaps the most compelling evidence however, of SCRIB controlling growth in epithelial cells is the fact that the SCRIB protein is a target of oncogenic viruses. High-risk human papilloma virus oncoprotein E6-E6AP is an ubiquitin ligase complex that tags SCRIB with an ubiquitin signature causing proteosomal degradation of the SCRIB protein (203). Degradation of SCRIB via this pathway leads to a reduction in tight junctions and tumor formation.

1.3.7 Lgl

Mammals contain multiple Lethal giant larvae (Lgl) proteins, termed Lgl1-4. In mammalian renal epithelia, Lgl1 is highly expressed and however studies have shown

that Lgl proteins have highly similar/redundant functions and may be interchangeable and therefore are given the name mLgl for mammalian Lgl. mLgl is characterized by a series of WD-40 repeats in its N-terminus that are thought to facilitate binding to SCRIB (Figure 1-3 and (128)). No direct link to Dlg1 has been reported for mLgl, but they are thought to genetically interact via a similar mode of action.

Mammalian Lgl localizes to basolateral membrane in renal epithelia upon cell-to-cell contacts, and is localized to the cytoplasm in contact naïve cells (193). mLgl binds Par6/aPKCζ prior to GTP Cdc-42 binding to Par6 and this binding is found only in the absence of Par3 (230, 300). As mentioned previously, mLgl is phosphorlyated by aPKCζ and the phosphorylation of Lgl inactivates Lgl and restricts its localization to the basolateral membrane, as a non-phosphorylatable mutant of mLgl was shown to localize with apical membrane markers (200, 230). In human cancers, overexpression of aPKC at the membrane results in a cytosolic accumulation of Lgl from the membrane, suggesting that membrane bound Lgl is necessary for tissue homeostasis (86, 161). In terms of vertebrate development, it has been demonstrated that Lgl gives identity to the basolateral membrane and the interaction between Lgl and aPKC results in definition of apical versus basolateral surfaces (38). Likewise, in depolarization models, knockdown of Lgl prevented the dissociation of the Par polarity complex resulting in cellular overgrowth (299). This data suggests that there exists a coordinated series of events where the action of Lgl and aPKC function to define the apical and basolateral surfaces by mutual inhibition and scaffolding.

Lgl has also been demonstrated to interact with trafficking machinery. Lgl interacts with myosin II heavy chain and syntaxin-4 suggesting it plays a role in the

trafficking of membrane components (200). More studies are needed on this phenomenon in mammalian systems, however work in *Drosophila* has illustrated that Lgl may be involved with the regulated endocytosis and exocytosis of dCrumbs (22, 167). In particular, disrupting exocytosis of dCrumbs resulted in an expanded lateral membrane but suppression of Lgl in this system resulted in a rescue of dCrumbs presentation on the apical surface (22).

1.3.8 Dlg

Dlg (Discs large) is the mammalian homologue of the *Drosophila* gene *Discs large* of which there are 5 family members (Dlg1-5) with Dlg1 being the most throughly studied in the kidney (184). Dlg1 (also known as SAP97) localizes to the lateral membrane in polarized epithelia (168). Dlg1 contains from N-terminus to C-terminus: an L27 domain, 3 PDZ domains, and SH3 domain, a 4.1 binding domain, and a membrane associated kinase-deficient GUK (MAGUK) domain (Figure 1-3 and (168)).

The Scribble complex consisting of SCRIB, Lgl, and Dlg1 have a strong genetic interaction, however any physical interaction between Dlg1 and the other members of the complex has yet to be determined. Dlg1 contains a similar domain structure to other MAGUK domain containing proteins, including the polarity protein PALS1 (section 1.3.10); suggesting Dlg1 is also a molecular scaffold protein. The interactions of Dlg1 and its binding partners have been extensively studied, yet the functional significance of these interactions is still poorly understood. Proteins that bind the L27 domain of Dlg1 include membrane palmitolyated protein (MPP) family members MPP2, MPP3, and MPP7 (130). The interaction between Dlg1 and MPP7 demonstrates the necessity of a

tripartite complex consisting of Dlg1, MPP7, and the small polarity protein Lin-7 (section 1.3.10) for tight junction formation and stability of Dlg1 (23, 264). This interaction functionally links the Crumbs and Scribble complexes through the common binding partner Lin-7 and may help establish the tight junction (261). Interestingly, knockdown of Lin-7 in MDCKII cells results in a destabilization of Dlg1 (Straight and Pieczynski, unpublished observation). Dlg1 also interacts with Lin2, another associated MAGUK polarity protein via an L27-L27 domain dimerization interaction (151). Lin2 (also known as CASK) is a serine-threonine kinase shown to be necessary for arrangement of the basolateral membrane (44).

The PDZ domains of Dlg1 interact with key signaling proteins in mammalian epithelia making Dlg1 essential to renal physiology. Dlg1 interacts with adenomatous polyposis coli (APC) via it PDZ domains (181). APC is a tumor suppressor that binds β-catenin in polarized epithelial cells and negatively regulates Wnt signaling suggesting that Dlg1 may play a role in planar cell polarity (144, 198). The interaction of Dlg1 and APC has been clearly shown to affect cell cycle progression as overexpressed Dlg1 leads to over proliferation most likely due to an increase in Wnt signaling (116). Adey and colleagues also identified Dlg1 as a binding partner to the tumor suppressor PTEN via yeast two hybrid and show that unphosphorylated PTEN interacts with the second PDZ domain of Dlg1 (3). Although the functional significance of PTEN binding to Dlg1 is not known at this time, it is possible that Dlg1 acts to stabilize PTEN. Dlg1 would then facilitate PTEN phosphorylation effecting PTEN interactions with other PDZ domain containing proteins including Par3A (280).

A Dlg1 knockout mouse has been generated, and the phenotype included many urogenital defects associated with lack of epithelial development (111). The C-terminal SH3, Hook, and GUK domains alone of Dlg1 are also known to function in development. A gene trap mouse that leads to a C-terminal truncation of Dlg1 displays an array of developmental phenotypes including defects in nephrogenesis and cleft palate (35, 202). Identifying the protein-protein interactions needed at the C-terminus of Dlg1 will be essential to understanding these phenotypes. Data suggests that the C-terminal SH3 domain of Dlg1 may also bind Lin-2 and/or undergo internal regulation similar to other polarity proteins containing SH3 and GUK domains (210, 283).

Post-translational modifications to the Dlg1 protein have also given insight into the role of Dlg1 in epithelial polarity. Dlg1 is phosphorylated in epithelial cells, and phosphorylation appears to have a significant role in maintaining the structural integrity of the adherens junction (148). Additionally, the phosphorylation of Dlg1 may confer its subcellular localization and stability during the cell cycle and be regulated by cyclin-dependent kinases (CDK) 1 and 2 (205). The stability and half-life of Dlg1 in epithelial cells is regulated by ubiquitination (172, 173). Ubiquitination of Dlg1 can be a result of viral infection, where oncogenic viruses coding for ubiquitin ligases selectively target PDZ polarity proteins for degradation. Virally mediated ubiquitination of polarity proteins like Dlg1 or SCRIB results in a breakdown of the polarity program (75, 173, 277).

1.3.9 Crumbs complex Overview

In renal epithelia, the Crumbs complex consists of three major components, and multiple associated proteins. The core complex itself consists of the proteins **C**r**u**m**b**s**3a** (Crb3a), **P**rotein **A**ssociated with **L**in-**S**even **1** (PALS1/MPP5), and **P**ALS1 **a**ssociated **T**ight **J**unction Protein (PATJ) or **Mu**ltiple **P**DZ Domain **P**rotein-**1** (MUPP1) all of which are highly conserved from invertebrates to vertebrates (Figure 1-2 and (52, 152, 170, 186, 237)).

1.3.10 PALS1

PALS1 is a multi-domain adapter protein associated with the conserved Crumbs complex in mammalian epithelia (235, 237). In fully polarized epithelia, the PALS1 protein is localized to the tight junction (12, 129). PALS1 contains six distinct protein interacting domains: two Lin-2-7 (L27) domains (referred to as L27N and L27C respectively), a single PDZ domain, a single SH3 domain, a Hook domain, and a GUK domain (Figure 1-3 and (129)). The GUK domain of PALS1 lacks kinase activity and is speculated to be involved in only protein-protein interactions (182, 183, 271).

PALS1 an essential molecular scaffold with a multitude of binding partners that have been extensively mapped; most significantly it is found in a complex with the other essential polarity proteins Crb3a and PATJ (235, 237). PALS1 binds Crb3a via its PDZ domain and PALS1 binds PATJ via its L27N domain (156). Domain deletion analysis has illustrated that PALS1 interaction with both Crb3a and PATJ essential for tight junction formation in mammals (156, 262). Also, PALS1 provides an important link between the Crumbs complex and the Par complex via the N-terminus of PALS1 binding

the PDZ domain of Par6 (109, 226, 289). Knockdown studies of PALS1 indicate that PALS1 is necessary for timely junction formation, stability of PATJ, and the ability of aPKCζ to localize to the tight junction (262, 289).

The regulation of PALS1 in mammalian epithelia is maintained by association and binding to accessory proteins illustrating the complex nature of the tight junction. PALS1 was identified in a screen for proteins associated with the Lineage defective protein-7 (Lin-7, also known as MALS, or Veli3). Lin-7 is a small PDZ domain containing protein necessary for proper development in *C. elegans* (129). There are 3 isoforms of mammalian Lin-7, with Lin-7c being highly enriched in the kidney (114). Lin-7 stabilizes PALS1 protein in MDCKII cells by binding to the L27C domain found in PALS1 (23, 217, 261). In Lin-7 knockdown MDCKII cells, tight junction formation is delayed, but not destroyed suggesting that PALS1 is essential for the establishment of the tight junctions but not the maintenance of the tight junction (261). Lin-7 also binds the lateral membrane protein IRSp53 which is a RhoA adapter protein therefore linking PALS1 to the cytoskeleton (180). Additionally, PALS1 is destabilized by the lack of Crb3a in MDCK cells. In the epithelial to mesenchymal transition (EMT) there is a decrease PALS1 protein and only a modest decrease in transcription of the *PALS1* gene (294). Likewise, interruption of the PALS1-PATJ binding results in PALS1 moving from the tight junction to being dispersed through the cytosol (109).

The above data pose an interesting question of the dynamics concerning the continued expression and stability of junctional complexes. It has been suggested that GUK domain containing proteins such as PALS1 may exist as dimers or be involved in internal regulation via conformational change dependent on the presence of specific

binding partners. PALS1 may "fold back" on itself and be regulated by internal binding between its SH3 and GUK domains or exhibit "tail to tail" dimerization which would presumably effect the function of the protein by either exposing or blocking the availability of multiple protein-protein interaction domains. A similar phenomenon is found in the MAGUK proteins Dlg1, which has a similar SH3 domain and GUK domain structure and has been shown to be highly flexible (183, 271, 283).

Knockdown of PALS1 in MDCKII cells indicates that tight junction biogenesis may also affect the architecture of the lateral membrane. Wang et al. illustrated that PALS1 knockdown effected the trafficking of E-cadherin to the lateral surface of MDCKII cells by affecting the exocyst complex (288). This study implies that the formation of the tight junction is essential to the overall architecture of the epithelial cell, and there exists a complex feedback network coordinating exocytic events essential to maintain the integrity of the epithelial monolayer. At this point, our understanding of the interplay between tight junction formation and modulation of epithelial cell structure is limited. Functionally, likely candidates for studying this phenomenon are the spatio-temporal interactions between PALS1 to Crb3a and Par6.

1.3.11 PATJ and MUPP1

PATJ (PALS1 Associated Tight Junction protein) and MUPP1 (Multiple PDZ-domain Protein-1) are two highly related, multiple PDZ-domain containing proteins found in mammalian epithelia and localized to the tight junction (Figure 1-3). With multiple PDZ domains, PATJ and MUPP1 are both molecular scaffolds at the tight junction (152, 279). PATJ contains 10 PDZ domains while MUPP1 contains 13 PDZ

domains. PDZ domains 6 and 8 of PATJ directly bind to the tight junction structural proteins ZO-3 and Claudin-1 respectively (236). Claudin and Occludin family proteins are transmembrane proteins that form the physical "fence" and "gate" of the tight junction, while the Zona Occulidin (ZO)-family of protein are cytoplasmic adapters of the Occludin family of structural proteins (70). The binding of the ZO and Claudin families to PATJ suggests a role of PATJ in maintaining the epithelial monolayer, distinguishing apical versus lateral surfaces, and maintaining the functional identity of the tight junction itself. Similarly, MUPP1 is also linked to tight junction structural proteins, including those of the Claudin family but also to the Junctional Adhesion Molecule (JAM) family (91, 150). Both PATJ and MUPP1 contain an N-terminal L27 domain that binds the L27N domain of PALS1, and MUPP1 has also been shown to directly interact with MPP4 (also known as Dlg6) via this L27 domain (237, 281). The L27-L27 interaction between PALS1 and either PATJ is necessary for tight junction in renal epithelia (237).

Interestingly, PATJ has been illustrated to be significant in the process of maintenance and establishment of epithelial tight junctions, while the highly similar MUPP1 protein has been shown to be not necessary for tight junction formation (2). Knockdown studies have reinforced the role of PATJ in epithelial polarity. Deletion of PATJ via shRNA in MDCKII cells reveal that PATJ is necessary for the formation of tight junctions in both 2D and 3D models but knockdown of PATJ does not effect stability of other members of the conserved Crumbs polarity complex (254). However, abrogation of PATJ in epithelia did effect localization of apical and lateral components of the tight junction suggesting PATJ is a molecular scaffold and not functioning to define tight

junctions (189). Wound healing assays performed on MDCKII monolayers have shown PATJ to be localized to the leading edge of migratory epithelia and to be partly responsible for the establishment of new cell-to-cell contacts upon wound repair. Additionally, knockdown of PATJ slowed this process (255). PATJ at the leading edge of migrating cells seems to result in the localization of members of the Par polarity complex and wound healing seemed to be at least some what dependent on the cytoskeletal modulation provided by the Par polarity complex (255). Related to wound healing and directional migration of epithelial cells is the question as to whether PATJ and MUPP1 near the leading edge functions as a scaffold for proper membrane formation of if PATJ and MUPP1 are needed for positioning receptors key to signaling of extracellular migration cues, or both. PATJ has recently been shown to interact with Angiomotin (AMOT) and his interaction may provide clues into the role PATJ plays as a signaling molecule in polarized epithelia (265). AMOT binds PDZ 2 and 3 of PATJ and has a large number of interactions that may contribute to epithelial barrier maintenance. AMOT, besides binding PATJ, also associates with Rich1, a Cdc42 GAP. The PATJ-AMOT-Rich1 interaction may link the Crumbs complex with the Rho-family GTPases and the Par polarity complex through down-regulation of GTP-Cdc42 (265). Cdc42 has been shown to affect the trafficking of PALS1 and Par3 to the plasma membrane through the polarity protein Par6 (125, 293). A recent report by Leiw et al demonstrates a clear interaction between MUPP1 and the human somatostatin receptor 3 (hSSRT3), a G-protein coupled receptor (GPCR) (158). Leiw and colleagues demonstrate that the interaction between hSSRT3 and PDZ 10 of MUPP1 may allow for GPCR regulated transepithelial permeability (158). Similarly, PATJ has recently been shown to interact

with members of the dopamine signaling family, most notably Na+/K+ ATPase subunit α (40). Na+/K+ ATPase, in addition to regulating renal ion flux, has been suggested to be a member of a novel epithelial polarity complex also consisting of Yurt, Coracle, and Neurexin IV in *Drosophila* responsible for lateral membrane stability (147). Although further study is needed in mammalian systems, this finding further strengthens the hypothesis that PATJ is a scaffold involved in the establishment of apico-basal polarity.

1.3.12 Crumbs3

The eponymous Crb3 protein is a human homologue of the *Drosophila* protein DCrumbs, a regulator of epithelial polarity (273). There are three human homologues of the *Crb* gene termed *Crb1, Crb2,* and *Crb3*. *Crb1* is primarily localized to the retinal pigmented epithelium of the eye and mutations in the gene have been linked to retinitis pigmentosa and other retinal defects (52, 282). *Crb2* gene expression has been seen in brain, testis, uterus, eye, and embryonic tissue, but its full function remains to be fully elucidated and may play a role in the glomerulus (60, 134). The *Crb3* gene is highly expressed and is the predominant isoform in the kidney and therefore can be readily studied in cultured renal cells, such as MDCKII cells.

Crb3 is the smallest and least conserved member of the *Crb* gene family. Each member of the *Crb* family encodes for a single pass transmembrane protein with an extracellular N-termini and highly similar cytoplasmic C-terminus. The cytoplamic C-termini of the Crumbs proteins contains a FERM binding domain and a PDZ binding domain (170). Crb1 and Crb2 share sequence homology in their EGF-repeat rich-extracellular domains while the extracellular domain of Crb3 is markedly shorter and

lacks any identified domain structure (Figure 1-3 and (170)). Additionally, Crb3 exists in two unique isoforms due to alternate splicing of the final exon of the *Crb3* gene. Alternate splicing of Crb3 results in a 22 amino-acid difference in the C-termini of each isoform; changing the sequence of the PDZ binding domain at the extreme C-termini (63). Crb3a is termed ERLI for the terminal glutamic acid-arginine-leucine-isoleucine (E-R-L-I in single letter code) amino acids that comprise its PDZ binding motif. Crb3b is known as the CLPI isoform, named for the four terminal cysteine-leucine-proline-isoleucine (C-L-P-I in single letter code) sequence comprising its PDZ binding domain sequence.

The difference in PDZ binding domains of Crb3 has been shown to alter the function of each Crb3. Both Crb3 isoforms have been shown to localize to the tight junction, the apical membrane, and the primary cilium of polarized MDCKII cells (63, 64, 152, 170). However, Crb3b has also been shown to localize to the spindle pole of mitotic MDCKII cells and specific knockdown of Crb3b disrupts cell division and cytokinesis, with cells showing a multinuclear phenotype (63). Mutational analysis involving Crb3a illustrates the requirement of Crb3a for the formation of the tight junction and establishment of polarity (69, 153, 235). These results indicate that both Crb3 isoforms are essential for epithelial formation and function. Interestingly, the regulatory mechanism concerning the abundance of each splice variant is not yet understood. The ability to accurately monitor the production of both splice variants of the *Crb3* gene will be essential to understanding how epithelial integrity is maintained.

Crb3a is localized to both the tight junction, along the apical membrane, and to the primary cilium (64). Of both Crb3 isoforms, Crb3a is noted for its inclusion in the

Crumbs polarity complex. Crb3a is found in a complex at the tight junction with PALS1 and PATJ, and links the Crumbs complex with the Par complex via its interaction with Par6 (100, 110, 153, 237). Crb3a binds to both PALS1 and Par6 via its C-terminal PDZ binding domain (110, 153). The necessity of Crb3a binding to both PALS1 and Par6 is illustrated by specific deletion of the ERLI tail of Crb3a, mutation of the PDZ domain of Par6, or mutation of the PALS1 N-terminus; all of which inhibit tight junction formation (110, 153, 235).

The intracellular FERM binding domain of Crb3a has been shown to be functionally important for Crb3a in MDCK cells (69). However, proteins interacting with the FERM binding domain of Crb3a are far less understood in mammalian cells, but are beginning to be identified. The protein Yurt was shown to bind the FERM binding domain of *Drosophila* dCrumbs and function as a negative regulator of dCrumbs (146). Studies have also suggested the mammalian orthologs of Yurt, YMO1, EHM2, and EPB41L5 have a similar function in mammalian cells and form a novel complex with Crb3a and PALS1 (83, 146, 147). Similarly, the homolouge for Yurt in zebrafish, known as *mosaic eyes (moe),* also codes for a FERM binding protein and knockouts of this gene give rise to a phenotype similar to that of a PALS1 knockdown (known as *nagie oko* in zebrafish nomenclature) (122). Further characterization of these proteins in mammalian systems is needed to fully elucidate their specific functions in regards to apico-basal cell polarity.

1.4 Molecular Mechanisms Establishing Renal Epithelial Cell Polarity

1.4.1 Establishing Renal Polarity: MET vs. EMT

The developing kidney is a well-studied organ model, matching the development of polarity with acquired physiologic properties. Epithelial to mesenchymal transition (EMT) and the converse mesenchymal to epithelial transition (MET) describe the process in which cells undergo phenotypic changes to facilitate growth and development, including organogenesis. EMT is characterized by a morphological change where the cell undergoes massive reorganization to its transcription, translation, and cytoskeletal networks to become fibroblastic. For the reciprocal process of MET, morphological changes again must take place, this time rearranging epithelial cells into their normally highly ordered morphology with specialized surfaces for function. Change in morphology of cells during EMT/MET can be attributed at least partially due to loss and gain of expression of polarity proteins (27, 165, 197). During EMT/MET polarity proteins can be either regulated at the transcription level by activation or suppression of transcription, at the translational level by microRNAs, or at the proteins level by redistribution of their subcellular localization and/or loss of stability (85). In the case of EMT, in addition to silencing of genes there is a marked activation of genes that provide the cell with resistance to apoptosis, loss of contact inhibited growth, resistance to anoikis, and increased invasive properties (197, 274).

Functional EMT/MET is a cornerstone of mammalian development initiating the ability of cells to form complex cells and tissues at the proper location with temporal significance. During development, the initial steps in organogenesis of the renal tubule network are the condensation of unorganized mesenchymal cells to organized epithelia through the EMT/MET process (37, 59). The canonical Wnt signaling cascade initiates

this process (247). During MET of the kidney, the migrating ureteric bud secretes Wnt9b inducing the metanephric mesenchyme to aggregate and undergo planar cell division and forming the beginnings of the pretubular aggregate (34, 132). Autocrine Wnt4 signaling from this initial condensation of the pretubular aggregate combined with continued activation from Wnt9b from the ureteric bud promotes β-catenin survival and TCF/Lef1 mediated transcripitional activation beginning the process of cellular differentiation and the beginnings of renal tubule formation (222). Interestingly, canonical Wnt-signaling derived from, Wnt4, Wnt9b, or forced β-catenin expression does not effectively induce *Cdh1* (the gene for E-cadherin) transcription to allow for epithelial adhesion and progression to a polarized epithelial phenotype (222).

How do polarized renal epithelial cells arise from these differentiated pro-epithelial structures? Regulatory proteins of EMT/MET program have been identified and the activities of these regulators may explain how mesenchyme can condense into epithelial structures. The Snail family (Snail, Slug) consists of zinc-finger transcriptional repressors that can lead to EMT by binding E-boxes in the promoter regions of essential genes controlling the epithelial phenotype (26, 162, 208, 275). In addition to the Snail-family of transcription factors, the basic helix-loop-helix (bHLH) family of transcriptional repressors also initiates the EMT program (225, 258). Although a multitude of EMT initiation factors have been described, it seems as though specific EMT transcriptional repressors each have common and unique targets of repression (196).

EMT transcription factors in both the Snail and bHLH families repress the promoter activity of *Cdh1* that codes for the major adherens junction molecule E-

cadherin (33, 196). Reduction of the Snail family of transcription repressors positively regulates the expression of cadherins and tight junction proteins and facilitates epithelial polarization by releasing E-box motif mediated gene silencing (33, 207, 276, 294). With repression of EMT transcription repressors in the developing kidney, cadherin based cell-to-cell adhesions could presumably form allowing for continued maturation of the pretubular aggregate into fully polarized epithelia (15, 26, 47). At this stage in renal development however, Wnt-signaling must be attenuated as illustrated by the fact that canonical Wnt-signaling can lead to inhibition of the epithelial phenotype (222). There is an established relationship between Wnt-signaling and control of EMT factors, however the exact mechanisms and temporal significance of these interactions during development are not well understood (162).

1.4.2 Regulation and Maintenance of Renal Epithelial Polarity: A Trail of Crumbs

As MET is essential to proper renal development, the converse EMT can be seen as, according to Boutet et al, a "reversed embryogeneis" with regards to renal fibrosis and carcinomas (27). The regulation of proper renal epithelial phenotype is undoubtedly tied to the regulation of *Crb3* transcript (26, 27, 294). Not surprisingly, the *Crb3* gene is also a target of the transcriptional repressors Snail1 and ZEB1 in renal epithelia implicating EMT transcription factors to the regulation of tight junction protein complexes (4, 294). At this time it is not known which bHLH factors repress *Crb3* transcription but it will be important to further characterize the bHLH transcription factors to determine what role, if any; they have on repressing this gene. Although EMT transcriptional repressors can only affect specific target regions within the promoter regions of certain genes, the

downstream effects of genetic repression often manifest in an extended EMT program. Deregulation of polarity genes by EMT factors forces feedback whereby transcriptional repression and stability of polarity proteins can be reduced furthering the cycle of EMT. Examples of such genes are those coding for PALS1 and PATJ, where Snail overexpression results in direct repression of the *Crb3* promoter followed by a smaller, yet noticable decrease in transcription of the genes coding for these two conserved binding partners of Crb3a (294).

The fact that the *Crb3* gene is highly regulated suggests Crb3 may be at the centerpiece of the polarized epithelial program. There lies a body of evidence to suggest that Crb3a has the intrinsic ability to delineate epithelial morphology by establishment of the tight junction. Crb3a physically binds Par6 linking two highly conserved essential polarity complexes. Crb3a, being a transmembrane protein, also must be functionally exocytosed and endocytosed to modulate any activity. Forced expression of high levels of the *Crb3* gene in normally unpolarized epithelia can lead to the establishment of tight junctions, including the sequestering of tight junction structural proteins including those of the zona occludin (ZO-family), claudin, and occludin families (69). Also, overexpression of Crb3a in normally polarized epithelia leads to an expansion of the apical surface, an extended tight junction, and a reduced basolateral membrane similar to neoplastic tumor growth (153, 235). And finally, knockdown or reduction of the *Crb3a* transcript results in cells completely devoid of tight junctions (69, 133, 235).

Crb3a is unique that it is the only transmembrane protein in any of the three conserved polarity complexes; it must travel through an exocytic pathway to arrive at its proper apical location. It is been hypothesized that transmembrane proteins destined for

the apical surface are recruited to that surface via N or O-linked glycosylation and lectins or via their association with lipid rafts. Crb3a does not associate with lipid rafts (Hurd and Pieczynski, unpublished results); however Crb3a contains at least one N-linked glycosylation site on its extracellular domain at position 36. This N-linked glycosylation site appears to be dispensable for the apical targeting of Crb3 however (170). Galectin-3 has been identified as a possible apical sorting protein in polarized epithelial cells (49, 50). Since N-linked glycosylation of Crb3a is not necessary for apical targeting it seems unlikely Galectin-3 is responsible for Crb3a localization along the apical membrane at least in recognition of asparagine 36. The exocyst complex has also been shown to regulate ciliogenesis, however in exocyst mutants the tight junctions remained intact again suggesting that the exocyst may not be responsible for the trafficking of Crb3a, at least to the apical surface and the tight junction (305). Since Crb3a has three different subcellular localizations it is quite likely that there is more than one mechanism that directs transmembrane proteins to the apical surface.

Studies by in 3-dimenstional systems have given insight into the role of Crb3a in apical membrane formation however (141, 176). Using lumen formation models, it has been demonstrated that the formation and delineation of both the apical and basolateral surfaces are a result of coordinated endo- and exocytitic events. In these models, proteins destined for the apical membrane first appear on the plasma membrane in a one cell, unpolarized stage. Upon the initiation of cell division, apical membrane proteins are endocytosed and trafficked to the eventual site of the apical membrane. It is at this point where apical membrane proteins accumulate and begin to 1.) Form the apical surface by exclusion of basolateral proteins, 2.) Establish a lumen, and 3.) Begin the formation of

the tight junction. Although this model is in its infancy, it illustrates the exocytic events that may lead to the maintenance of the apical membrane during steady state.

Schluter et al. illustrated that Crb3 trafficking to the apical surface is essential for lumen formation during the first cell division and this movement is not only dependent on Rab11a activity but also sets the basis for aPKCζ localization (246). Concurrently, the role of Rab11 in dCrumbs trafficking was confirmed in *Drosophilia* as Rab11 insult caused a defect in apical surface integrity (234). Both the previously mentioned studies were concerned with the exocystosis of dCrumbs, but perhaps the most striking evidence for the role of dCrumbs in epithelial homeostasis is a dissection of endocytic events. In *Drosophila* deletion of *avalanche,* the fly equivalent of Syntaxin-7, gives an overgrowth phenotype quite similar to Crb3a overexpression and neoplastic tumor growth (167). Similarly, in flies knockdown or mutation of the gene *erupted* (*ept,* mammalian TSG101) again leads to cell overgrowth and apical expansion (92, 192). TSG101 is a member of the ESCRT-I complex (endosomal-sorting-complex- required for-transport-I) and an identified neoplastic tumor suppressor linked to cell polarity (18). In mammals, the role of TSG101 as a tumor suppressor is still debatable and seems to be tissue specific, but it is known that TSG101 is involved in multitude of functions including the entry into the endocytic MVB pathway to internalize transmembrane proteins for degradation either through fusion with the lysosome or inclusion of proteins in exosomes (250). Taking into consideration the evidence in *Drosophila* it can by hypothesized that endocytosis of Crb3a is essential for controlling epithelial growth and development in mammals. There is a limited evidence of the role of the MVB pathway in Crb3a regulation in the

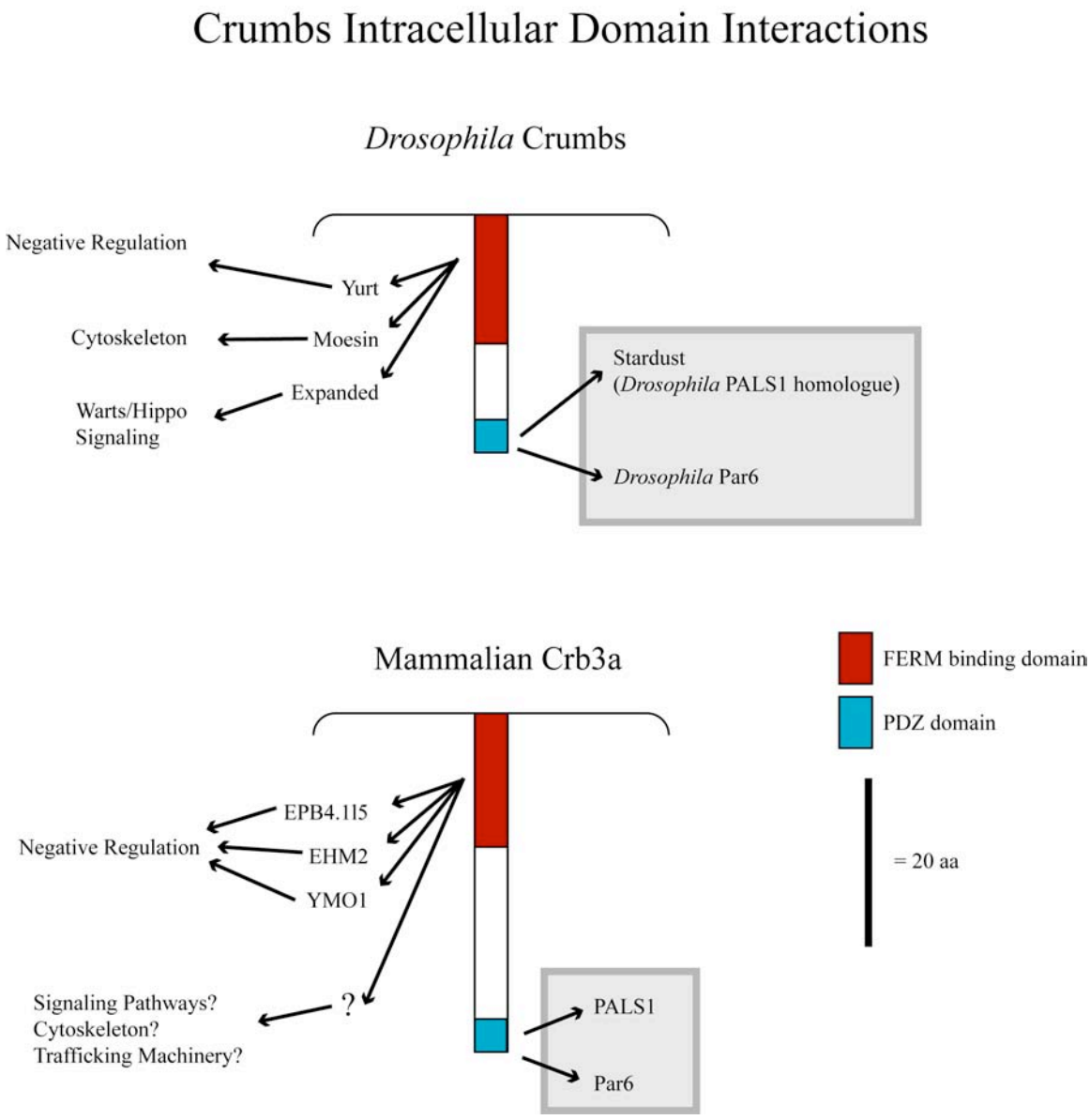

Figure 1-4: Identified regulators of Crumbs in *Drosophila* and mammalian systems. The cytoplasmic domains of dCrumbs and mammalian Crb3a are highly conserved, however, binding partners of the FERM binding domain have only been readily identified and studied in *Drosophila* and have been shown to regulate epithelial growth and morphology. Idenitifcation of FERM binding domain partners for mammalian Crb3a will be of importance in the future.

mammalian renal system, however the urinary exosome proteome includes numerous polarity proteins, including Crb3a (82).

A body of recent evidence also in *Drosophila* suggests that dCrumbs could possibly act as an upstream member of one arm of the conserved Hippo signaling cascade (Figure 1-4 and (88, 160, 233)). In flies and mammals, the Hippo pathway controls the exit from the cell cycle and controls apoptosis by nuclear shuttling of the transcription factor Yorkie/Yap (87). Fly knockouts of Hippo members result in an enlargement of the apical surface, although this is independent of Yorkie/Yap activity and has been suggested to be a result of impaired endocytosis (77, 90). These findings are significant in that they provide a functional link to the amount of dCrumbs localized to the apical surface and the ability of the cell to control tissue growth and proliferation. Additionally, recent data suggest that dCrumbs overexpression leads to tissue overgrowth by binding the protein Expanded, with Expanded being a negative regulator of Yorkie/Yap activity (88, 233). It will be interesting to confirm these results in mammalian systems to further understand how Crb3a controls cellular growth.

1.4.3 Renal Apico-Basal Epithelial Polarity in Context: A Link to Nephropathies, Planar Cell Polarity, and Renal Cilia

There is an established link between some of the most well studied nephropathies and the basic molecular mechanisms governing renal epithelial cell polarity. In the establishment of apico-basal polarity in the developing renal tubule network we must keep in mind the context in which individual cells exist. Individual renal epithelial cells

are single functional units in a continuous three-dimensional epithelial sheet that must maintain its integrity while undergoing cell division and apoptosis. The ability for epithelial cells to form a cohesive polarized functional sheet is facilitated by the relationship between apical-basal cell polarity and planar cell polarity (PCP). PCP involves spatio-temporal control over symmetry perpendicular to the apical-basal axis based on mitotic organization and is a result of the formation and function of the primary renal cilium (131, 185). In the development of kidney tubules PCP is controlled through both canonical and non-canonical Wnt-signaling pathways (131, 185). The formation of the primary cilium is an essential step of developmental epithelial polarization, orientating the cell in space during development and providing signal transduction (80). Defects in vertebrate cilia and ciliogenesis, referred to as ciliopathies, result in abnormal PCP (68). Ciliopathies may be a result of failure for the primary cilium to form or defects in cilia trafficking, known as intraflaggelar transport (IFT, reviewed in (224)). In these scenarios, there is a failure of proteins to traffic either in or out of the cilia, resulting in decreased signaling. The primary monocilium of renal epithelia arises from the basal body, a structure associated with the mother centriole orientated in space above the nucleus. Failure of the basal body and centrioles to be correctly oriented results in defects in ciliogenesis and cell division. Lack of a primary cilium in polarized epithelia leads to loss of sensory function, as the primary cilium in renal epithelia is host a number of receptors and channels that are essential to cellular function.

There is an established link between PCP and apico-basal polarity as PCP affects many polarity proteins. The conserved polarity protein SCRIB is considered a PCP protein, where mutation in the protein causes aberrant PCP (193). Congenital renal

defects have given insight to the relationship between renal physiology, apical-basal polarity and PCP. The congenital, autosomal dominant disease Von Hippel-Lindau is a result of the loss of function of the tumor suppressor von Hippel-Lindau (VHL) potentially resulting in renal cell carcinoma (RCC) and loss of PCP. VHL controls EMT via HIF1-α where VHL loss of function results in an upregulation of Snail resulting in the Snail mediated repression of the genes which encode Occludin and Claudin-1, both components of the tight junction (32, 93, 113). The VHL protein additionally has been identified as a binding partner of the Par polarity complex and shown to be necessary for the growth of the primary renal cilium and ubiquitination of aPKC isoforms (118, 216, 244).

Polycystic Kidney Disease (PKD) is another well-studied example of aberrant PCP in renal epithelia. The PKD proteins polycystin 1 (PC1) and polycystin 2 (PC2) localize to the lateral membranes and the primary cilium of polarized renal epithelium (107, 263). Traditionally, PC1 and PC2 are seen as intricate members of primary cilium formation and cilium signaling through the IFT system (reviewed in (224)). The loss of functional Polycystins leads to aberrant cell cycle progression and hyperproliferation, hallmarks of not only cyst formation but of the EMT phenotype. However, Polycystins also may be involved with the establishment of apico-basal polarity in renal epithelia. PC1 in part seems to regulate the formation of E-cadherin positive adherens junctions in MDCK cells (107, 263). Additionally, overexpression of the exocyst protein Sec10 has been shown to lead the a cystic phenotype and this phenotype has been linked to expression of Par3, since Par3 can localized to the primary cilium and both knockdown of Sec10 and Par3 give a strikingly similar phenotype (249, 305).

Nephronophthisis (NPHP) is a ciliopathy involving the well-defined nephrocystin gene family. NPHP the gene products localize to the primary cilium and/or basal body (95). Co-immunoprecipitation experiments show a physical interaction between PALS1 and nephrocystins 1 and 4 and these interactions suggest that PALS1 and the nephrocystins contribute to overall cell morphology. Nephrocystin-1 and Nephrocystin-4 knockdown cells exhibit a similar phenotype to PALS1 knockdowns (51). An established link between PALS1 and Nephrocystin-1 and Nephrocystin-4 and their effect on cell morphology links the molecular mechanisms of apical-basal cell polarity with the aberrant cilia physiology associated with NPHP. Interestingly, the known NPHP patient mutation p.L180P results in a mutation of the Nephrocystin-1 when this mutation is recapitulated *in vitro* the interaction of Nephrocystin-1 and PALS1 is severely decreased (51). As mentioned above, the protein Lin-7 contributes to the stability of PALS1 and when Lin-7 is knocked out in mice, the mice also exhibit a cystic kidney phenotype (217). Continued study of how nephropathies are related to the core polarity complex proteins will only strengthen these models and provide further areas for study.

1.5 Concluding Remarks

The molecular mechanisms underlying the development of basic renal epithelial polarity are numerous. Although many protein-protein interactions have been mapped, we are only now beginning to understand the complexity of these interactions. Considering that most of our understanding of the basic molecular mechanisms of epithelial polarity have only been discovered and studied in the last twenty years, it will be interesting to see what the next twenty will bring. Now that functional interactions

have been mapped, as a research community we will have to evolve to understanding how polarity is controlled both spatially and temporally. Although answers to these questions will undoubtedly be complex, they are important questions to ask, as they will only further our understanding of development and disease.

Chapter 2

Mammalian Lin-7 Stabilizes Polarity Complex Proteins

2.1 Introduction

Polarization of mammalian epithelia is characterized by the asymmetrical partitioning of proteins to specific membrane domains. The cellular boundary of the apical and basolateral membranes in polarized epithelia is demarcated by the tight junction that forms a fence between the two membrane compartments. Junctions within and between cells are defined by the localization of, and interactions between, specific protein complexes. The interaction of these proteins is mediated by evolutionarily conserved protein-protein interaction domains. Many studies have shown an important role for PDS-95/Discs large/ZO-1 (PDZ) domain-containing proteins in tight junctions and the polarized localization of proteins (65, 238). One of the earliest studies to show this relationship was the work of Kim and co-workers that demonstrated an important role for the Lin-2, Lin-7, and Lin-10 proteins in the basolateral targeting of the *Caenorhabditis elegans* epidermal growth factor receptor (127, 256). Mutation in any one of these genes led to a vulva-less phenotype, presumably due to mistargeting of the epidermal growth factor receptor (127, 256). Lin-2, Lin-7, and Lin-10 all contain PDZ

domains and form a conserved heterotrimeric protein complex (25, 31, 127). Mammalian Lin-7 (also known as vertebrate Lin-7 (VELI) or MALS) is a small protein (~197 amino acids), and in the worm its PDZ domain directly binds the epidermal growth factor receptor (25, 31, 114, 124, 256). Lin-2 is a member of the membrane-associated guanylate kinase (MAGUK) family of proteins, whereas Lin-10 is a multidomain scaffold protein (25, 31, 54) (105, 127) (151). Lin-7 binds to Lin-2 via an L27 domain; however, it is important to note that Lin-10 is not associated with Lin-2 and Lin-7 in mammalian epithelial cells (55, 260).

Recent work in mammalian cells as well as *Drosophila* has identified additional binding partners for the Lin-7 L27 domain. The L27 domain of Lin-7 has been demonstrated to bind a family of MAGUK proteins highly related to Lin-2, collectively referred to as PALS or Proteins Associated with Lin-Seven (129). The archetype for these proteins is known as PALS1 in mammalian cells and Stardust in *Drosophila*. PALS1/Stardust contains several protein interaction motifs, including two adjacent L27 domains, and binds to Lin-7 via the L27 domain nearer its carboxyl terminus (L27C) (236). The amino-terminal L27 domain (L27N) of PALS1/Stardust binds to the polarity protein PATJ (229). Additionally, the PDZ domain of PALS1/Stardust binds to the carboxyl terminus of Crumbs, an apical transmembrane protein (12, 100, 170). Studies in mammalian and invertebrate systems have shown an important role for the Crumbs-PALS1-PATJ complex in polarity determination in epithelial cells (253). In turn, these proteins bind to the highly evolutionarily conserved Par3-Par6-atypical protein kinase C polarity effector complex via an interaction between PALS1 and Crumbs with Par6 (110, 153). In mammalian cells, the loss of PATJ or PALS1 via RNA interference knock down

leads to loss of polarization of epithelial cells under certain experimental conditions (254, 262). In addition, the loss of these proteins results in defects in tight junction formation. Although PALS1 binds to Lin-7, the exact role of Lin-7 in tight junction formation and polarity determination by these proteins remains unclear. As mentioned, Lin-7 also binds to other MAGUK proteins related to Lin-2 and PALS1, including PALS2, DLG2, and DLG3 (129). The role of these other Lin-7 binding partners in protein targeting and epithelial polarization is still unclear, although some clues have been provided by studies of invertebrate systems (13, 143).

It is not clear at this time why Lin-7 binds to several mammalian MAGUK proteins. Recent reports of Lin-7 knock-out mice indicate Lin-7 might not be crucial for epithelial morphogenesis (219). Accordingly, further work on the exact roles of Lin-7 is indicated. In this study, we examined the role of Lin-7 in Madin-Darby canine kidney (MDCK) cells. After stable transfection of the mammalian epithelial cell line MDCKII with Lin-7 small hairpin RNA (shRNA), we found that the resulting loss of Lin-7 correlated with the loss of expression of several Lin-7-binding proteins, including PALS1. The loss of these polarity proteins resulted in defects in tight junction formation in the Lin-7 knockdown cell lines. From these data, we hypothesize that Lin-7 is essential for the stable expression of several MAGUK family members that are in turn required for proper formation of tight junctions in mammalian epithelial cells.

2.2 Materials and Methods

2.2.1 DNA Constructs

To create the shRNA constructs, two 19-base pair sites within canine Lin-7C were chosen, and pairs of complementary oligonucleotides were synthesized by Invitrogen

custom primers. These oligonucleotides contained the following target sequences: 5`-GGCTCGGTGAAGCTGGTGG-3`, corresponding to the amino acids NH_3-GSVKLV-COOH, and 5`-GGCCACAGTGGCAGCCTTC-3', corresponding to the amino acids NH_3-ATVAAF-COOH. These sequences were checked for significant homology to other genes in the canine genome database, and none was found. The sense and antisense sequences were separated by a 9-base pair loop region, and each oligonucleotide was terminated with restriction endonuclease half-sites. After annealing the complementary oligonucleotides, the dimers were ligated into the pre-cut pSilencer 2.0-U6/neomycin plasmid (Ambion, Austin, TX) as directed by the manufacturer, followed by amplification of the resulting plasmids. All plasmid sequences were verified by automated sequencing at the University of Michigan DNA Sequencing Core.

The various rescue plasmids used in this study express Myc-tagged constructs from a cytomegalovirus promoter in the plasmid pRK5-myc and contain the human or murine gene indicated in the text and figures. These constructs, mycLin-7FL, mycLin-7N (amino acids 1–97), mycLin-7PDZ (amino acids 89–197), mycPALS1, mycLin-2, mycPALS2, and mycDlg2, have been previously published (25, 170, 236, 260). In the case of the murine Lin-7 constructs, these contained such significant differences in their RNA sequence as to be unaffected by the canine Lin-7-targeted shRNA constructs.

2.2.2 Cell Culture and Transfection

MDCKII cells were cultured in Dulbecco's modified Eagle's medium plus 10% fetal bovine serum supplemented with penicillin, streptomycin, and L-glutamine. All cell culture media and supplements were purchased from Invitrogen. To create the cell lines

stably expressing shRNA constructs, MDCKII cells were transfected with 5μg of plasmid DNA using FuGENE 6 reagent (Roche Applied Science). Cells were transfected with either construct individually or with a mixture of the two constructs to create cell lines. After selection with 500 μg of active G418/ml (Invitrogen) for 14 days, surviving clones were isolated for the generation of cell lines. These lines were screened for loss of Lin-7 expression by both immunostaining and Western blot analysis using affinity purified anti-Lin-7 sera.

Rescue clones were created by co-transfection of the C19 and C20 shRNA Lin-7 lines with 5 μg of the Myc-tagged rescue plasmid and 0.5 μg of zeocin resistance plasmid, followed by selection with 200 μg of zeocin/ml (Invitrogen) for 14 days and the isolation of cell lines. Clones were screened for the expression of the Myc-tagged protein and the maintained loss of endogenous Lin-7 expression using both immunostaining and Western blot analysis. For immunostaining or calcium switch assays, MDCKII cell lines were seeded at confluence onto 12- or 24-mm Transwell clear polyester filters (Corning Inc.; Corning, NY) in low calcium medium (with 5% dialyzed fetal bovine serum, 5 μM Ca^{2+}). After allowing the cells to adhere to the substrate overnight, the non-adherent cells were removed by gently washing with PBS and the medium was replaced with normal growth medium. The cells were then grown at least 72 h so that a tightly packed columnar epithelial monolayer was formed.

2.2.3 Calcium Switch Assay and Transepithelial Electrical Resistance Measurement

MDCKII cell lines were grown to confluence on 24-mm Transwell filters and were then washed extensively with PBS and grown in low calcium medium overnight to

dissociate cell-cell contacts. The low calcium medium was replaced the next day with normal growth medium (containing1.8 μM Ca^{2+}), and the cells were prepared for immunostaining at various times afterward (typically 0, 3, 6, or 29 h).

To measure the transepithelial electrical resistance (TER) a similar experiment was performed using 12-mm Transwell filters. The TER was determined with a Millicell-ERS volt-ohm meter (Millipore, Billerica, MA) immediately after the addition of normal growth medium (time=0) and at 30–60-min intervals for up to 48 h. Prior to each measurement, the Millicell was "zeroed" according to the manufacturer's directions and the background resistance was determined using cell-free filters. Each cell line was measured in triplicate, background was subtracted, and the means and the S.D. from the means (n=3) for each time point were plotted using Microsoft Excel.

2.2.4 Antibodies

Lin-7 (UM199)-, Lin-2 (UM195 and UM196)-, PALS1 (UM349)-, PATJ (UM356)-, and CRB3 (UM369)-specific antisera were generated in rabbits and affinity purified as previously described (25, 170, 236, 260). Mouse anti-Myc antibody was purified from hybridoma clone 9E10 ascites fluid obtained from the University of Michigan Hybridoma Core. Antibodies directed against ZO-1, occludin, claudin-1, and claudin-4 were purchased from Zymed Laboratories Inc. (San Francisco, CA). Antibodies to E-cadherin and actin were purchased from Sigma. Antibodies to Par3 and protein kinase C ζ were obtained from Upstate (Lake Placid, NY). Fluorochrome-conjugated antibodies used for immunofluorescence were purchased from Molecular

Probes (Eugene, OR). Horseradish peroxidase-conjugated antibodies used in immunoblotting were obtained from Amersham Biosciences.

2.2.5 Immunoprecipitation and Immunoblotting

MDCKII cell lysates were prepared from confluent 15-cm dishes with 1 ml of ice-cold lysis buffer (50 mM Tris-HCl, pH 7.4, 150 mM NaCl, 10% glycerol, 1% Triton X-100, 1.5 mM $MgCl_2$, 1 mM EGTA, 1mM phenylmethylsulfonyl fluoride, 10 μg/ml leupeptin, 20 μg/ml aprotinin, and phosphatase inhibitor mixture) (Sigma) and cleared by centrifugation at 14,000 x g for 20 min at 4 °C. A portion of the lysate was reserved, mixed with LDS loading buffer (Invitrogen), and used as input. For immunoprecipitation, 1–5 μl of antibody was mixed with 200 μl of lysate and 50 μl of 50% slurry of protein A-Sepharose beads (Zymed Laboratories Inc.; San Francisco, CA) and incubated overnight at 4 °C. The beads were washed three times with ice-cold HNTG and resuspended in LDS loading buffer. Samples were separated on 4–12% NuPAGE NOVEX gels (Invitrogen) in MOPS-SDS running buffer and transferred to nitrocellulose membranes in Bicine-MeOH. The transfer efficiency was assessed by staining with 0.5% Ponceau S red in 10% acetic acid, and then the membranes were blocked by incubation in 5% bovine serum albumin (Calbiochem; San Diego, CA) in Tris-buffered saline (TBS). The membranes were incubated with primary antibody in 5% bovine serum albumin/TBS for 2 hr. at room temperature and then washed with 0.1% Triton X-100/TBS. Membranes were incubated with horseradish peroxidase-conjugated secondary antibody in 5% skimmed milk/TBS for 1 hr. at room temperature and then

washed with 0.1% TritonX-100/TBS. Protein bands were visualized using ECL reagent (PerkinElmer Life Sciences).

2.2.6 CRB3 Peptide Beads

CRB3 peptide-coupled agarose beads were created using the SulfoLink Coupling gel kit (Pierce Biotechnology, Rockford, IL) and were linked via a terminal cysteine residue added to a peptide corresponding to the carboxyl-terminal 18 amino acids of CRB3 (wild type, NH_3-CARVPPTPNLKLPPEERLI-COOH) or the same sequence missing the terminal ERLI. The CRB3 peptides were synthesized at the University of Michigan Protein Structure Facility. For the CRB3 peptide bead pulldown assays, 20 μl of 50% slurry of CRB3 peptide beads were added to 200 μl of cell lysate and incubated overnight at 4 °C. The beads were washed three times with ice-cold HNTG (50 mM HEPES, pH 7.5, 150 mM NaCl, 0.1% Triton X-100, and 10% glycerol) and resuspended in LDS loading buffer. Samples were separated on 4–12% NuPAGE NOVEX gels, transferred to nitrocellulose, and processed for Western blotting as described above for immunoprecipitations.

2.2.7 Pulse-Chase Labeling

The rate of degradation of PALS1protein was determined using a pulse-chase protocol. MDCKII cell lines grown to confluence on 15-cm dishes were incubated for 2 hr. in methionine-free Dulbecco's modified Eagle's medium (Invitrogen) supplemented with 10% dialyzed fetal bovine serum. Cells were then pulse labeled for 1 h at 37°C by the addition of 250 mCi/ml 35S-Easytag Express label (PerkinElmer). Unincorporated

label was washed away, and cells were incubated at 37°C for 0–12 h in complete growth medium. Cell lysates were collected and utilized as described above for immunoprecipitation. The precipitated proteins were separated by SDS-PAGE, and the gel was fixed in 30% methanol/10% acetic acid, soaked for 30 min in Amplify (AmershamBiosciences), and dried. Densitometry was performed using a Molecular Dynamics laser scanner, model STORM860, and ImageQuant software (GE Healthcare). Each sample was prepared in triplicate (n =3) so that the standard deviation from the means could be determined.

2.2.8 Immunostaining and Confocal Microscopy

Cells grown on Transwell filters were cut from the support with a scalpel, washed with PBS, and fixed with 4% paraformaldehyde/PBS for 30 min, permeabilized with either 0.1% Triton X-100/PBS or 1% SDS/PBS for 15 min, and then blocked with 2% goat serum/PBS for 1 hr. The filters were then incubated with primary antibodies in goat serum/PBS for overnight at 30 °C in a humidified chamber. After washing extensively with goat serum/PBS, fluorochrome-conjugated secondary antibodies in goat serum/PBS were added overnight at 4 °C. Finally, filters were washed with PBS and mounted onto glass slides using ProLong antifade reagent (Molecular Probes, Eugene, OR). All images were obtained using an Olympus FluoView 500 confocal laser-scanning confocal microscope at the Morphology and Image Analysis Core of the Michigan Diabetes Research and Training Center. Samples were scanned with appropriate lasers and filter sets, and images were collected at 0.5-μm intervals on an Olympus IX-71 inverted

microscope using an x100 oil objective. FluoView v4.3 software was used to collect images, and subsequent preparation was performed using Adobe Creative Suite software.

2.2.9 Quantitative Real-time PCR

Messenger RNA from cell lines was isolated following the manufacturer's protocol found in the RNeasy kit (Qiagen). cDNA was reversed transcribed from isolated mRNA by Superscript III First-Strand Synthesis Supermix (Invitrogen) according to the published protocol. Real-time PCR was performed using Platinum SYBR Green qPCR Supermix UDG with Rox (Invitrogen) in an Applied Biosystem 7300 real-time PCR system with the following parameters: 50 °C (2 min), 95 °C (10 min), 40 cycles of 95 °C (15 s), 54 °C (30 s), 72 °C (1 min), followed by a dissociation cycle to verify one product by melting curve analysis. Primers to desired amplicons were designed using PerlPrimer software (174) and are as follows: *Canis familiaris* Lin-7C (5`-GCCTTACAAAGAGTCCTTCA-3` (forward)), (5`-TGATGTCCACAGTCTCATAG-3` (reverse)); *C. familiaris* PALS1 (5`-TAGAACCCTTTACAGATGAGAG-3`(forward)), (5`-ACTATCCGACTAATGATGACA G-3` (reverse)); *C. familiaris* glyceraldehyde-3-phosphate dehydrogenase (5`-ATTCTATCCACGGCAAATCC-3` (forward)), (5`-GGACTCCACAACATACTCAG-3`(reverse)). Primer pairs were validated by subjecting the quantitative PCR reactions to agarose gel electrophoresis to confirm the presence of single products at the expected size. In addition, each amplicon was sequenced to verify its identity. Experimental samples were performed in duplicate. Results were compiled from two independent experiments.

2.3 Results

2.3.1 Lin-7 shRNA affects the formation of tight junctions

Previous work from our group had shown that MDCKII cells, a canine kidney-derived epithelial cell line, express only one of the three Lin-7 genes, Lin-7C (260). Lin-7B is not expressed in the kidney tubule; and Lin-7A is larger than Lin-7C and this size is not seen on Western blotting of MDCKII cell lysates with anti-Lin-7 antibodies (220, 260). We generated shRNA expression plasmids to specifically target the canine Lin-7C sequence (Figure 2-1A) based on the genomic information available in the public database. These shRNA constructs had several mismatches with mouse Lin-7C allowing for eventual rescue of the phenotype using murine Lin-7 constructs (Figure 2-1A). We chose two different shRNA constructs (shRNA 1 and shRNA 2, respectively) and transfected them into MDCKII cells separately and in combination in order to knockdown the endogenous expression of Lin-7. We isolated several stable cell lines, including both controls, that exhibited little or no knockdown (clones 1, 12 and 21), and Lin-7 knockdown clones that had greatly reduced expression of Lin-7 (Figure 2-1B, clones 6, 10, 17, 19, and 20). Immunostaining with affinity-purified anti-Lin-7 antibodies confirmed markedly reduced Lin-7 at cell-cell junctions (Figure 2-2). In contrast, E-cadherin was correctly localized to lateral cell-cell junctions (Figure 2-2), suggesting that Lin-7 shRNA had little or no effect on the integrity of adherens junctions. We next tested the MDCKII cell lines for the formation of tight junctions using a calcium switch assay, in which cells were placed in low calcium medium overnight to dissociate the cells by breaking adherens junctions, followed by the readdition of calcium to allow the MDCKII cells to form junctions. Tight junction function was measured by the establishment of TER.

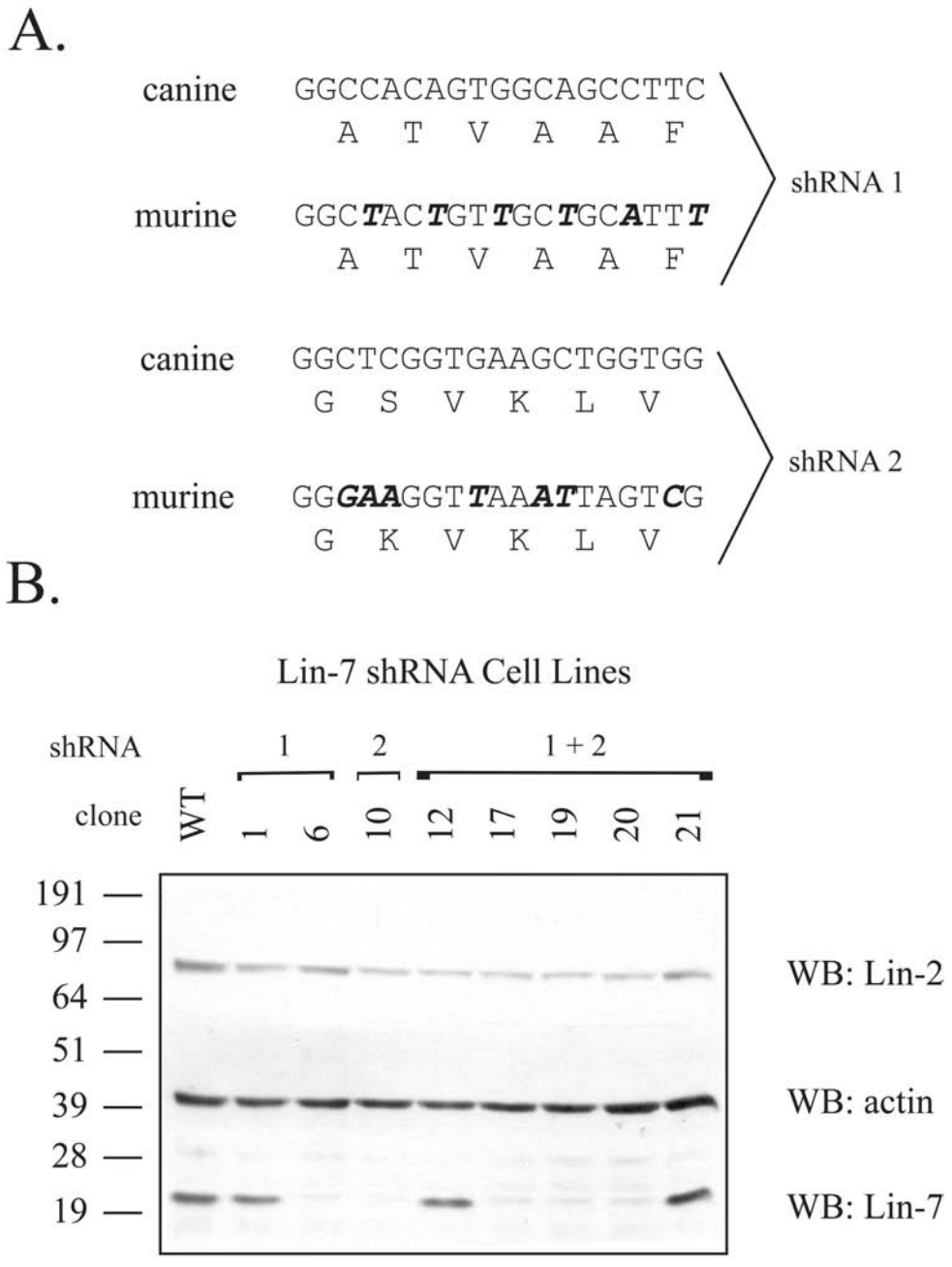

Figure 2-1: Lin-7 shRNA clones. (A) Sequences of canine Lin-7 short hairpin RNAs (shRNAs) compared to the murine Lin-7 sequence used for rescue experiments. Differences are indicated in bold. (B) Western blots of Lin-7 shRNA MDCKII cells. The shRNAs used are indicated above. Clones 19, 20 were used for future experiments and clone 21 was used as a control. Lin-7 shRNAs had no effect on Lin-2, a Lin-7 binding partner.

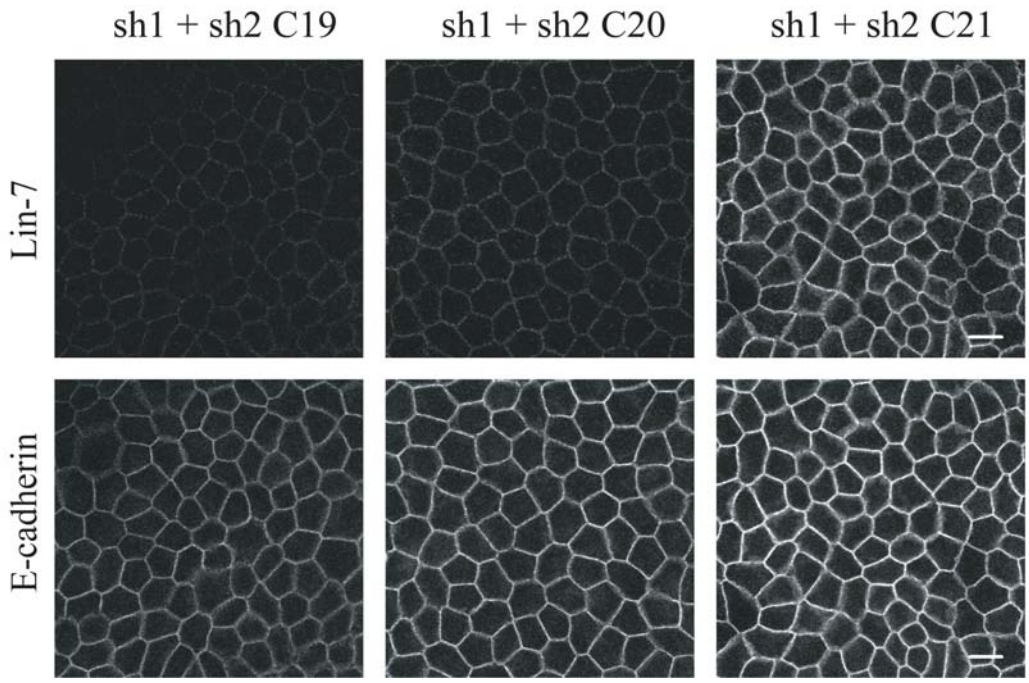

Figure 2-2: Immunofluorescence (IF) staining of Lin-7 shRNA clones 19, 20, and 21. Knockdown of Lin-7 reduced cellular levels of Lin-7 but had no effect on the adherens junction protein E-cadherin.

A.

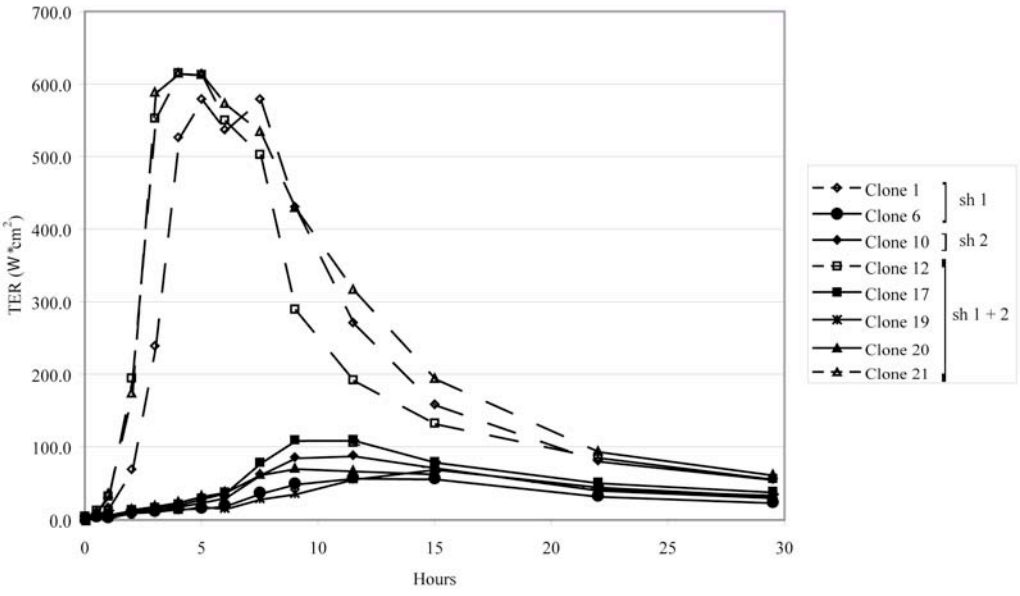

B.

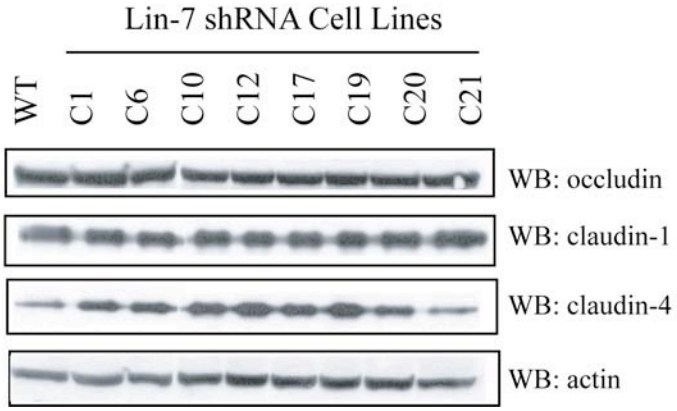

Figure 2-3: Knockdown of Lin-7 effects tight junction formation but not expression of tight junction structural proteins. (A) Trans-epithelial resistance (TER) of Lin-7 shRNA clones. Control clones (dashed lines with open shapes) show normal TER profiles while Lin-7 knockdown clones (solid lines with closed shapes) have reduced TER profiles indicating defects in tight junction formation. (B) Western blots of tight junction structural proteins in Lin-7 shRNA clones. Lin-7 shRNA does not effect expression of tight junction structure components.

Cell lines in which Lin-7 had been knocked down had markedly abnormal TER profiles (Figure 2-3A, solid lines) compared with wild-type and control cells (Figure 2-3A, dashed lines). However, western blotting indicated no change in expression of several tight junction component proteins including claudin-1, claudin-4 and occludin in cells with or without Lin-7 (Figure 2-3B). Furthermore, immunostaining of the MDCKII cells that had been grown on filters for 7 days showed that the tight junction marker proteins claudin-1 and ZO-1 were similarly localized in both control and Lin-7 knockdown cell lines (results not shown). However, using the calcium switch assay, abnormal, incomplete localization of ZO-1 was observed in the Lin-7 knockdown cells (Figure 2-4) in contrast to control cells. In conjunction with the TER data, this suggests that Lin-7 plays a role in the formation of tight junctions and the loss of Lin-7 expression results in a delay in tight junction formation during polarization.

2.3.2 Lin-7 shRNA affects expression of MAGUK family members

We have previously demonstrated that Far-Western blotting with a radiolabeled Lin-7 probe could reveal multiple MAGUK proteins that bind to Lin-7 (129). These include Lin-2/CASK, PALS1/MPP5, PALS2/Vam-1, Dlg2/MMP2, and Dlg3/MPP3. In the Lin-7 knockdown cells the expression of these MAGUKs, except for Lin-2, was significantly reduced (Figure 2-5A). Of the MAGUK family members with reduced expression, we chose to focus our study on PALS1 because of its known roles in polarity and tight junction formation, which had been previously demonstrated, by our laboratory and others (12, 100, 235, 237, 239, 262). The PDZ domain of PALS1 binds to the carboxyl-terminal amino acids of Crumbs proteins and these two proteins are in a

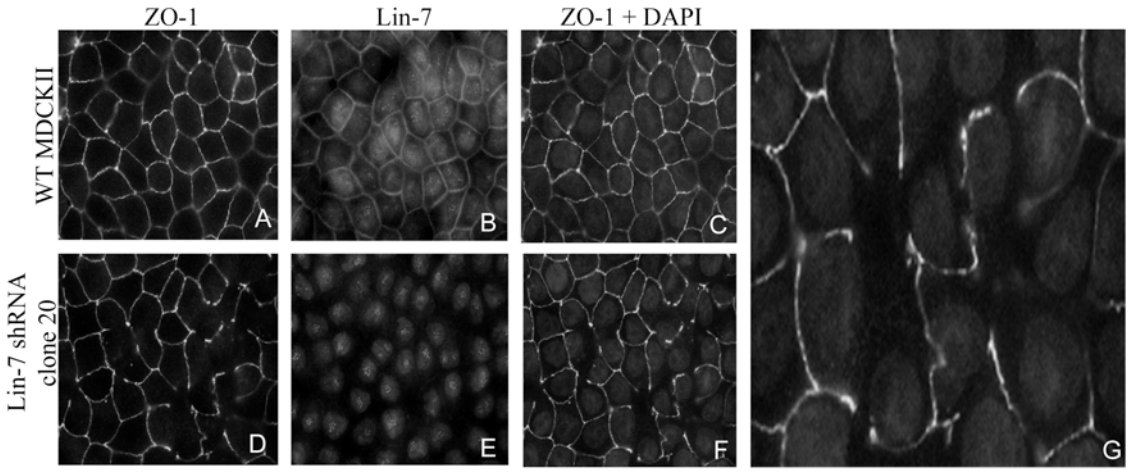

Figure 2-4: Lin-7 shRNA causes defects in tight junction formation during cell polarization. In cell polarization assays (calcium switch) Lin-7 shRNA cells fail to form complete tight junctions compared to wild type cells as indicated by ZO-1 staining. (A-C) Wild type MDCKII cells 24 hr. post calcium switch. (D-F) Lin-7 shRNA clone 20 24 hr. post calcium switch. (G) Zoom in of panel F illustrating that complete tight junctions failed to form in Lin-7 shRNA cells.

complex with PATJ (12, 100, 152, 236). Using a Sepharose bead coated with a peptide corresponding to the carboxyl-terminus of Crumbs3 (CRB3) we are able to precipitate PALS1 and PATJ from MDCKII cell lysates. In accord with Figure 2-5B, Crumbs beads precipitated PALS1 from control cells, but not from cells where Lin-7 was knocked down. PATJ expression was also reduced in the Lin-7 knockdown cells, although CRB3 expression was similar in control and wild type cells (Figure 2-6A). This agrees with our previously published result that PATJ protein levels are reduced when PALS1 expression is knocked down (262). However, the knockdown of Lin-7 did not affect expression of Par3 or aPKCζ (Figure 2-6B).

2.3.3 The L27 domain of Lin-7C is essential for correct tight junction formation

To determine whether these effects were specific to the loss of Lin-7, we rescued the Lin-7 shRNA MDCKII cells using mouse Lin-7C constructs. Murine Lin-7C is resistant to the effect of the shRNA constructs we used to knockdown canine Lin-7 due to nucleotide sequence differences between species (Figure 2-1A). We transfected Lin-7 knockdown cell lines with Myc-tagged mouse Lin-7C constructs: full length Lin-7C (mycLin-7FL), the amino-terminus containing the L27 domain (amino acids1-97; mycLin-7N) and the carboxyl-terminus containing the PDZ domain (amino acids 89-197; mycLin-7PDZ). Several MDCKII cell clones expressing Zeocin only were also selected as controls. Full length murine Lin-7 and the amino-terminal/L27 domain construct rescued the expression of the MAGUK proteins, including PALS1, as determined by Far-western blotting with radiolabeled GST-Lin-7 (Figure 2-7). In contrast, the carboxyl-terminus/PDZ domain construct and Zeocin alone did not rescue MAGUK expression

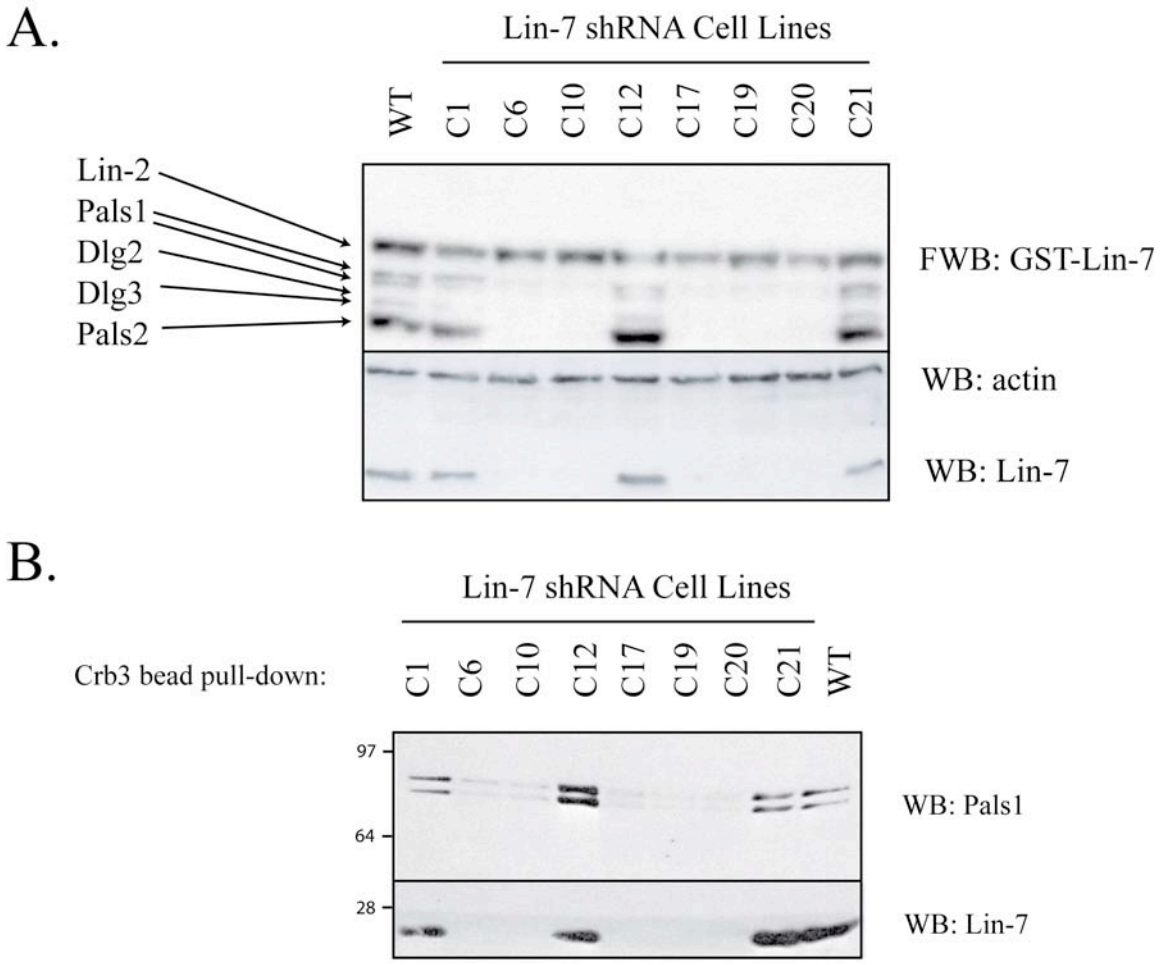

Figure 2-5: Lin-7 shRNA reduces expression of MAGUK family members. (A) Far Western blot of MAGUK family members that bind Lin-7. Knockdown of Lin-7 effects expression of PALS1, Dlg2, Dlg3, and PALS2 but not Lin-2. (B) Crb3 bead pull-down of PALS1 demonstrates that knockdown of Lin-7 correlates to reduced binding and expression of the conserved polarity protein PALS1.

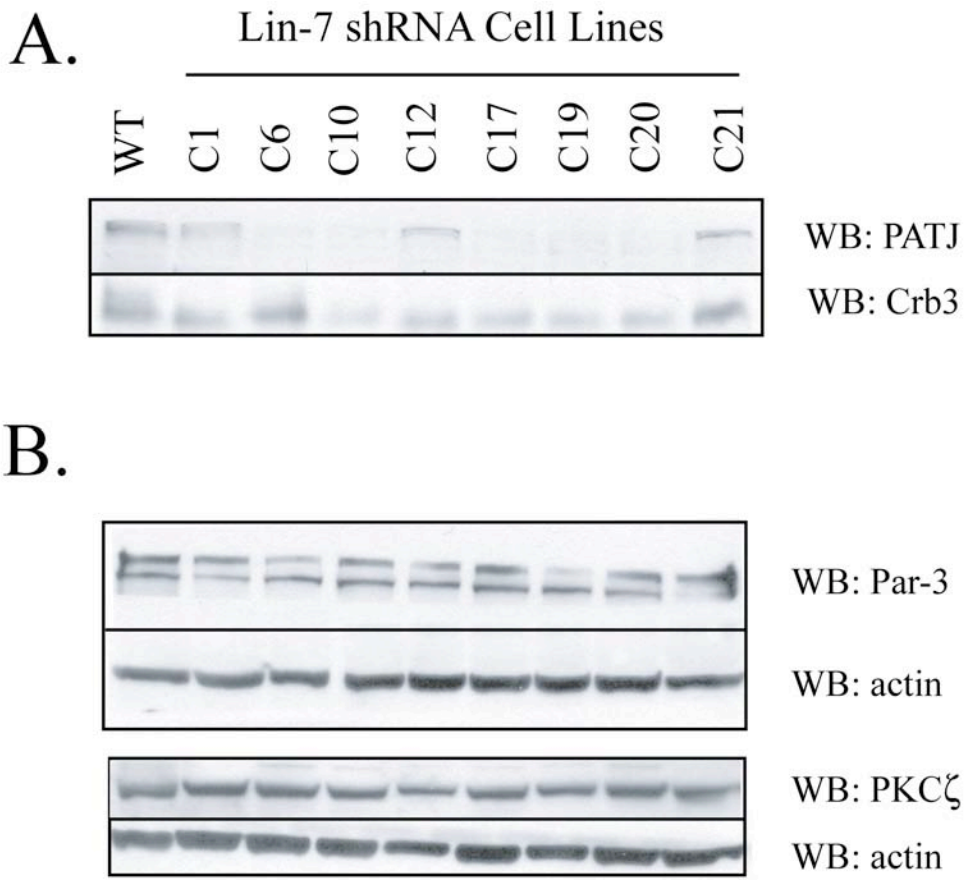

Figure 2-6: Lin-7 shRNA effects expression of PATJ, but not Crb3 or Par polarity complex proteins. (A) Lin-7 shRNA correlates to reduced expression in PATJ. (B) Lin-7 shRNA does not effect expression of Par3 or aPKCζ, two members of the Par polarity complex.

(Figure 2-7). PATJ protein expression was also rescued by the Myc-Lin-7FL and Myc-Lin-7N constructs (Figure 2-7). Both the Myc-Lin-7FL and Myc-Lin-7N constructs also rescued the TER after calcium switch (Figure 2-8, dashed lines and open shapes). Additionally, immunostaining for ZO-1 after calcium switch illustrated that Myc-Lin-7FL and Myc-Lin-7N constructs rescued normal tight junction formation (Figure 2-9). Thus, these experiments indicate that the L27 domain, but not the PDZ domain, of Lin-7 is required to rescue the Lin-7 knockdown phenotype.

2.3.4 Reexpression of PALS1 can reverse the tight junction defect seen in Lin-7 knockdown cells

Next, we wanted to determine if loss of the MAGUK proteins could explain the tight junction defects. In particular, we suspected that loss of PALS1 was responsible for the tight junction defects in that PALS1 is required for tight junction formation (262). To this end, the Lin-7 knockdown cell lines were transfected with a vector expressing mycPALS1 and stable cell lines were selected. Two Lin-7 shRNA cell lines overexpressing mycPALS1 were chosen for further study. In these cell lines, mycPALS1 rescued the expression of endogenous PATJ (Figure 2-10A). Endogenous Lin-7 protein was still low to undetectable in these PALS1 rescue clones (Figure 2-10B). mycPALS1 targeted correctly to the tight junction in the absence of endogenous Lin-7 (Figure 2-10B) and was also able to partially rescue the TER after calcium switch (Figure 2-11, dashed lines). In contrast, expression of Myc-tagged PALS2, Dlg2 or overexpressing Lin-2 could not rescue either the TER or tight junction immunostaining defects seen in Lin-7

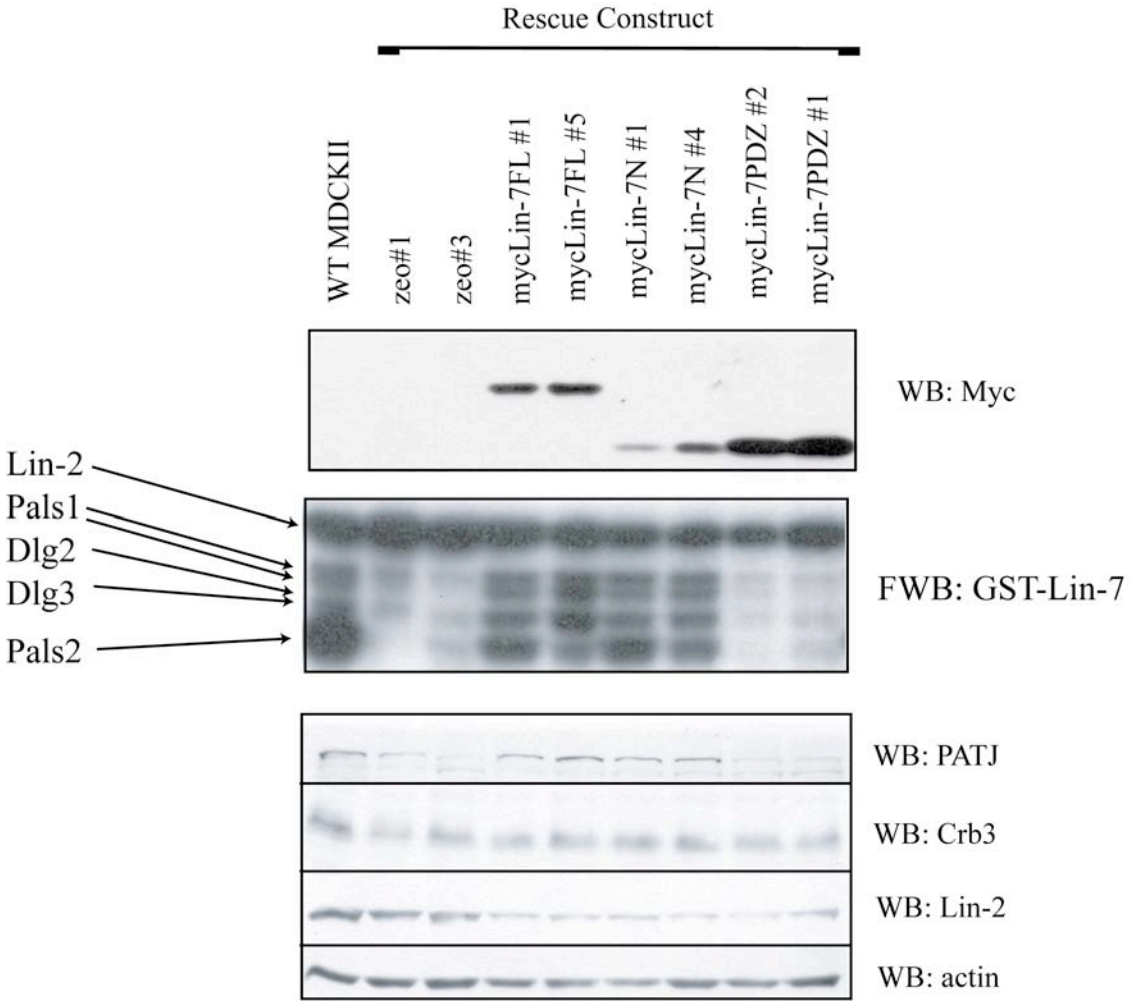

Figure 2-7: Rescue of protein expression with murine mycLin-7 FL and mycLin-7N in Lin-7 shRNA cell lines. Introduction of either full length (FL) or the N-terminal half (the L27 domain) of murine Lin-7 can rescue protein expression of MAGUK family members and PATJ.

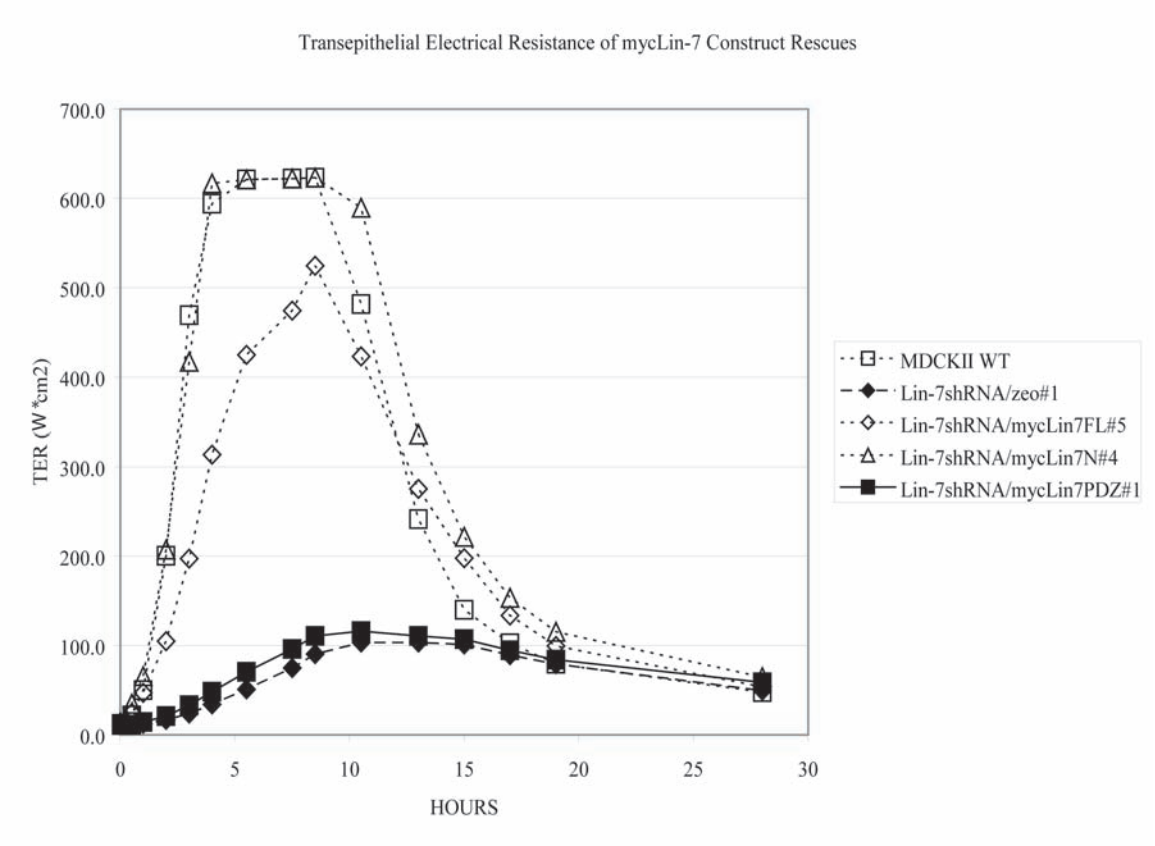

Figure 2-8: TER of murine mycLin-7 rescue constructs. Both mycLin-7FL and mycLin-7N (dashed lines with open shapes) can rescue tight junction formation but mycLin-7PDZ or control cells (solid lines with closed shapes) cannot rescue tight junction defects.

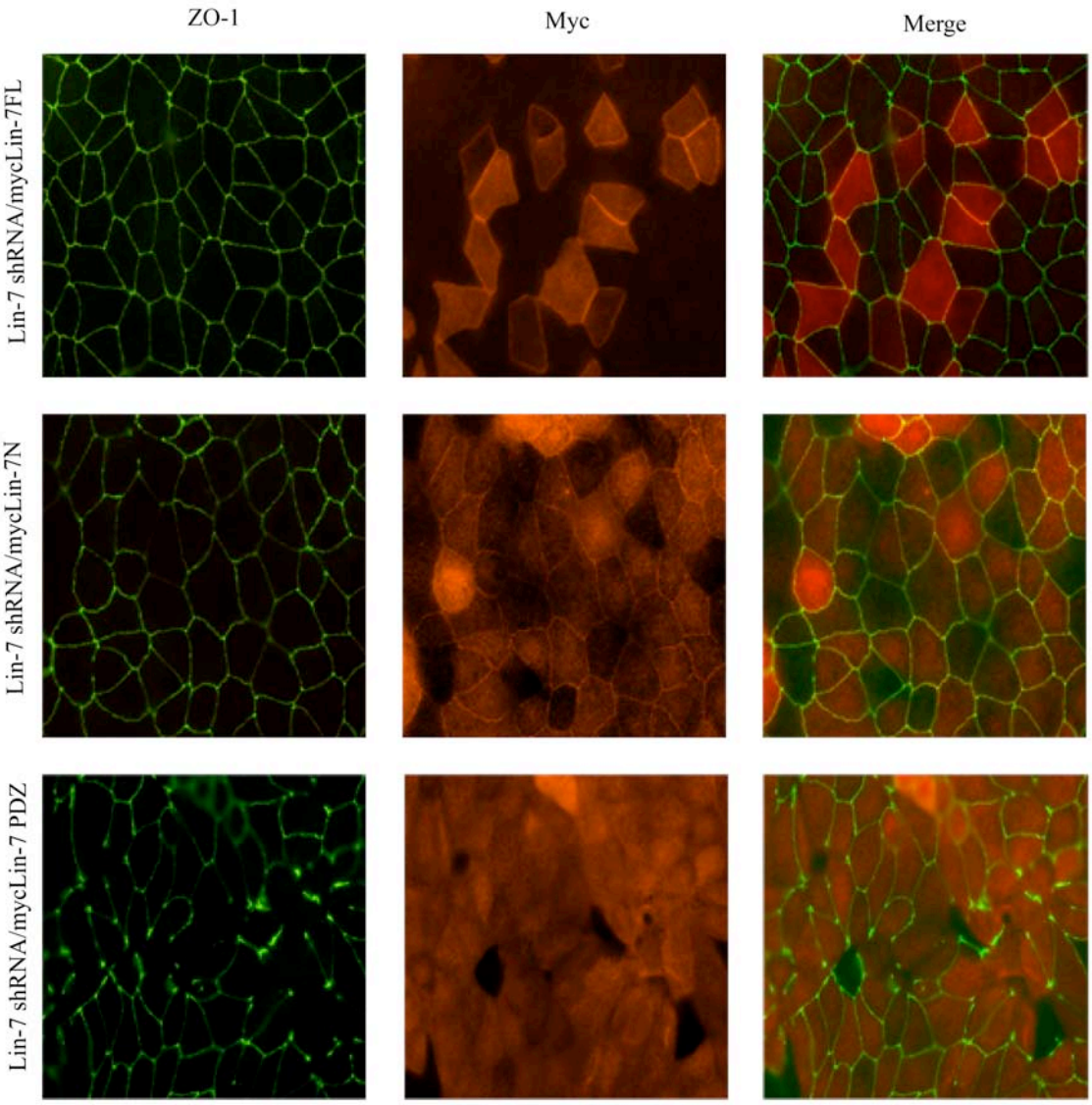

Figure 2-9: IF of murine Lin-7 rescues. Full-length (FL) and N-terminal (N) mycLin-7 can rescue the defect in tight junction formation 24 hr. post calcium switch. A mycLin-7 PDZ construct corresponding to the C-terminus of murine Lin-7 cannot rescue tight junction defects post calcium switch.

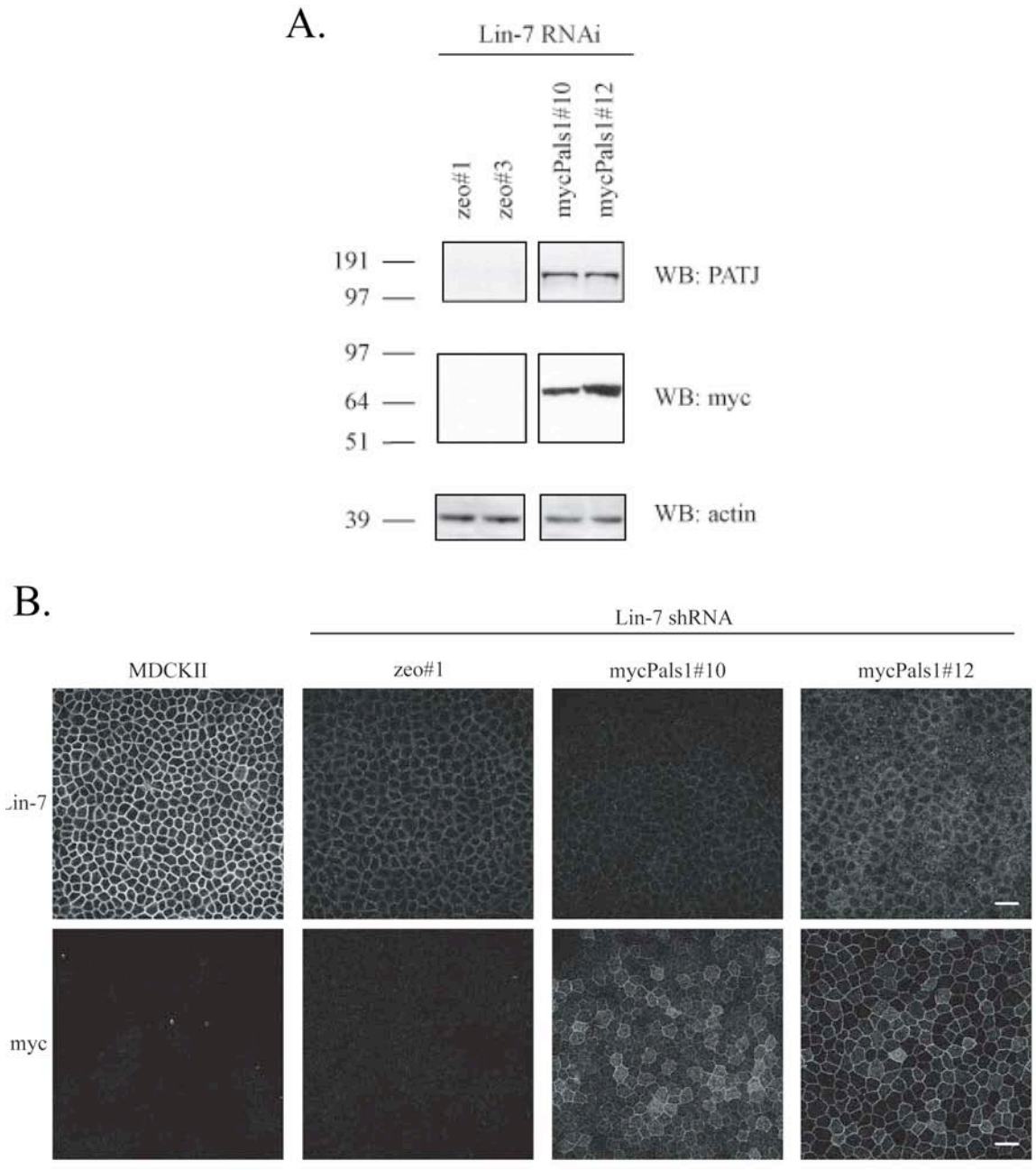

Figure 2-10: Rescue of Lin-7 shRNA cells with mycPALS1. (A) Expression of mycPALS1 in Lin-7 shRNA cells can rescue protein expression of PATJ. (B) IF of mycPALS1 rescue. PALS1 correctly localizes to the lateral surface in rescue cells.

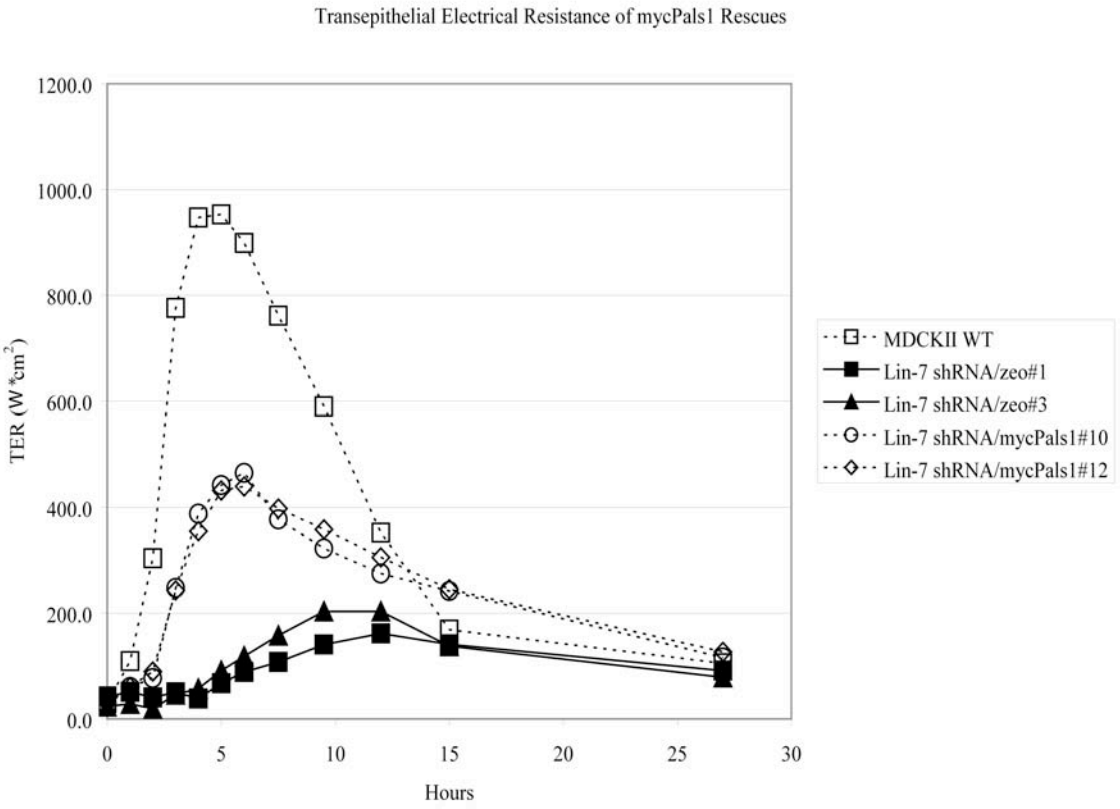

Figure 2-11: Expression of mycPALS1 can partially rescue TER profiles of Lin-7 shRNA cells. Overexpression of mycPALS1 in Lin-7 shRNA cells (dashed lines with open shapes) partially rescues tight junction formation compared to control resuce cell lines (solid lines with closed shapes)

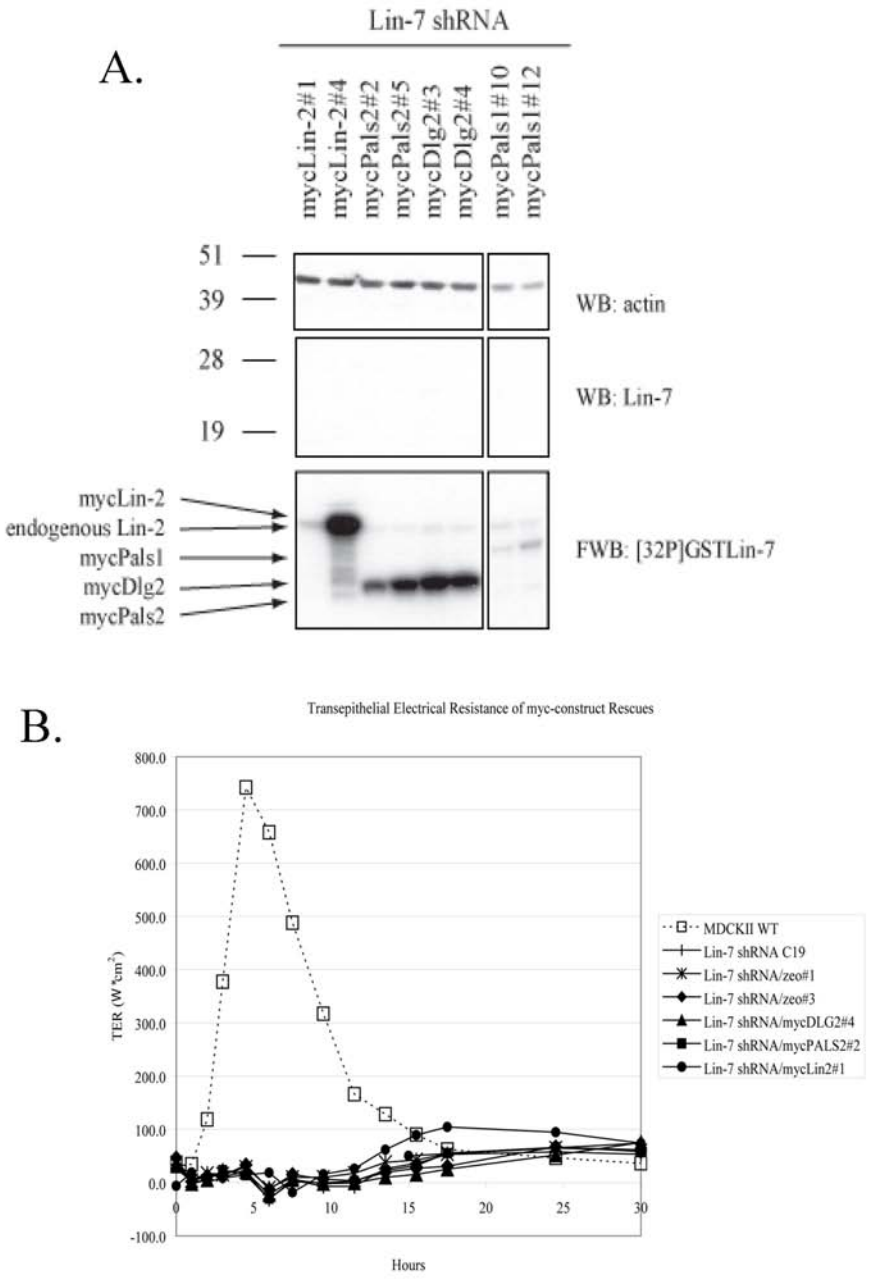

Figure 2-12: Other Lin-7 L27 domain binding partners cannot rescue Lin-7 shRNA tight junction defects. (A) Far Western blot using GST-Lin-7 on Lin-7 shRNA cells overexpressing other Lin-7 binding partners. (B) TER profiles of Lin-7 binding partner rescue cells lines (solid lines with closed shapes).

shRNA cells (Figure 2-12A-B). These results indicate that the defects we observed in Lin-7 knockdown cells were primarily due to the loss of PALS1.

2.3.5 Lin-7 expression affects stability of PALS1 in polarized MDCKII cells

Finally we sought to determine the manner by which PALS1 expression was reduced in Lin-7 shRNA cells: The loss of Lin-7 might be affecting the PALS1 mRNA or the expression and stability of the PALS1 protein. We performed quantitative reverse transcripiton-PCR to measure PALS1 transcripts in both Lin-7 shRNA and a previously published PALS1 shRNA cell line (262). We found no difference in the mRNA levels between control and Lin-7 knockdown cells (Figure 2-13A) suggesting PALS1 mRNA levels are not altered in Lin-7 shRNA cells. Control PALS1 knockdown cells illustrate our primer pairs were specific for the PALS1 transcript. Subsequently, we undertook pulse-chase radiolabeling to examine the degradation rate of the PALS1 protein. Our antibodies do not immunoprecipitate PALS1, so instead we examined wild type cells and Lin-7 shRNA cells transfected with mycPALS1. Thus we were able to immunoprecipitate tagged PALS1 and follow its half-life in the presence and absence of Lin-7. The pulse-chase assay found that the half life of PALS1 was much shorter in the Lin-7 knockdown cells in comparison to controls, with only 1.7-3.9% of radiolabeled mycPALS1 protein remaining in Lin-7 knockdown cell lines after 12 hours, compared to 18.7% in control cells (Figure 2-13B and C). These data indicate that Lin-7 stabilizes the PALS1 protein in MDCKII cells.

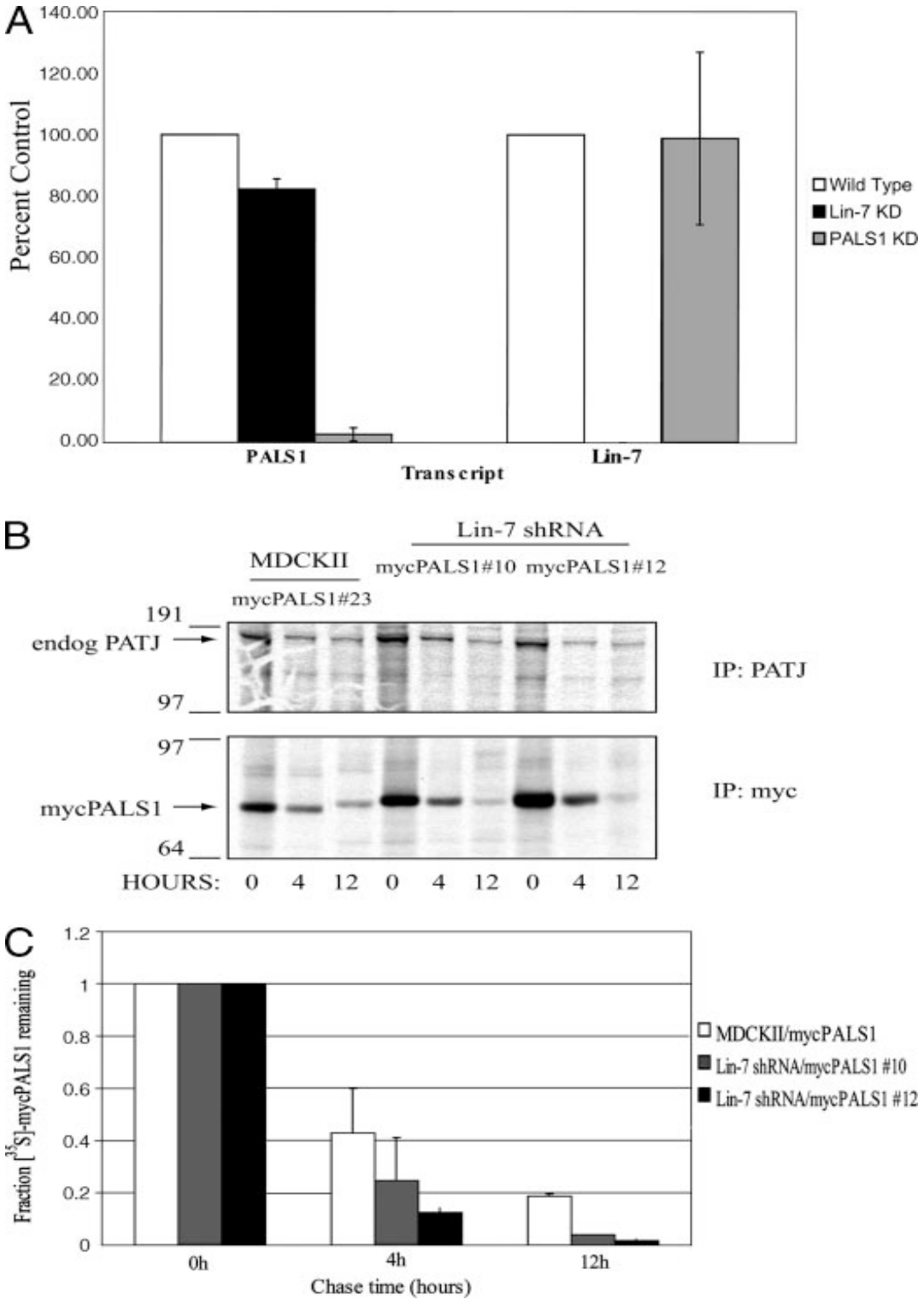

Figure 2-13: PALS1 protein degradation is increase in Lin-7 knockdown cells. (A) Quantitative real-time PCR of Lin-7 and PALS1 transcripts. (B) Pulse chase labeling of PATJ and mycPALS1 in Lin-7 shRNA cells. (B) Quantification of PALS1 degradation in Lin-7 shRNA cells.

2.4 Discussion

Lin-7, a small PDZ domain-containing protein has been shown to play a role in the polarized localization of proteins in both invertebrates and mammals. Here we show that Lin-7 regulates the expression of many other MAGUK family proteins, most notably PALS1, in polarized mammalian kidney cells. To study the role of Lin-7 in mammalian epithelia, we generated stable Lin-7 shRNA MDCKII and control cell lines. Lin-7 knockdown cell lines showed a specific reduction in endogenous Lin-7C and, under static conditions, cell-cell junction integrity appeared normal. However, when subjected to calcium switch, where we could monitor phenotypes under polarizing conditions, transepithelial electrical resistance and immunostaining data clearly demonstrated that Lin-7 shRNA cells were unable to efficiently form tight junctions, suggesting that Lin-7 affects the formation of tight junctions in polarizing epithelial cells by delaying their formation.

Lin-7 knockdown reduced the expression of MAGUK family proteins that are known binding partners of the L27 domain of Lin-7. The cause for the reduction in expression of the MAGUK PALS1 was due to a reduced half-life as seen by pulse chase experiments with no difference seen in mRNA levels. The reduced expression of PALS1 and other MAGUKs was rescued by expression of the L27 domain of Lin-7 but not by expression of the Lin-7 PDZ domain. It is likely that the binding of the Lin-7 L27 domain to the PALS1 L27 domain stabilizes the fold of the PALS1 protein making it more stable. As L27 domains interact via large hydrophobic surfaces, it is not hard to

understand how L27 domain interactions would stabilize folding of proteins containing this domain (66, 156) (229).

Knockdown of PALS1 leads to a loss of PATJ expression and loss of PATJ was also seen in cells missing Lin-7 (262). This was due to the lack of PALS1 as re-expression of PALS1, even in the absence of Lin-7, restored PATJ expression. PALS1 also binds to PATJ via an L27 domain interaction involving a single L27 domain in the amino-terminus of PATJ. Again it is possible that an unliganded L27 domain in PATJ leads to protein misfolding, instability and reduced expression in cells missing PALS1. It is interesting to note however that PALS1 expression in PATJ knockdown cells is only moderately affected (254). This suggests the relationship between L27 domain binding and protein stability is complex. Similarly the expression of the MAGUK protein, Lin-2/CASK, appeared unaffected by the Lin-7 knockdown although it binds Lin-7 like PALS1. It is interesting to note however that Lin-2/CASK expression was reduced in the brains of Lin-7 knockout mice (219). The differential effects of L27 binding on MAGUK stability may point to simple structural differences amongst the proteins or might suggest that the L27 domains of these MAGUKs have alternate binding partners.

The effects we saw with Lin-7 were due to loss of the L27 domain and not the PDZ domain. The role of the PDZ domain of Lin-7 was best described in worms where it targets the epidermal growth factor receptor to the lateral surface (256). Several binding partners for the PDZ domain of mammalian Lin-7 have been described. One binding partner is β-catenin although we saw no defects in cadherin staining in cells missing Lin-7 (227). Defects in other Lin-7 binding partners such as potassium channels or other transporters would not be detected in our studies (218, 228). It has been found that

mammalian epidermal growth factor receptor family members can bind to the first 13 amino acids of Lin-7C in a region N terminal to the PDZ domain, however deleting this region in mouse Lin-7C had no effect on the ability of this Lin-7 to rescue knockdown MDCK cells ((251) and S. Straight and B. Margolis, unpublished observations).

We demonstrated that the tight junction defect of Lin-7 shRNA was due to the reduction in endogenous PALS1. Even without Lin-7, exogenously expressed PALS1 still trafficked properly to the tight junction and partially rescued tight junction formation. Its inability to completely rescue TER measurements (Figure 2-11) could have been due to the presence of the Myc tag or the expression level of the mycPALS1 protein. Another possibility could be the loss of other Lin-7 binding MAGUK proteins such as DLG2, DLG3 or PALS2 whose function in epithelia is unclear. Again further studies in the Lin-7 knockout mice may be instructive. These mice with all Lin-7 genes removed die shortly after birth due to respiratory failure (219). These studies indicate no gross defects in tissue morphogenesis suggesting epithelial polarity is not overtly perturbed. Defects in tight junctions may not appear until later in knockout animals where they manifest as deficiencies in the skin barrier (70). Although it is likely that PALS1 is reduced in these Lin-7 knockout animals, they may have sufficient PALS1 to mediate epithelial polarity. In summary, our results show an expanding role for Lin-7 in epithelial function by stabilizing a large number of MAGUK proteins. Further studies of defects in knockout mice will reveal if the defects we observed in tissue culture cells extends to the whole animal.

Chapter 3

Slug Represses *Crumbs3* in Epithelial Cells

3.1 Introduction

The epithelial monolayer is formed by a combination of timed transcription events and protein-protein interactions to facilitate the formation of two biochemically distinct membrane domains. These are the apical domain that faces the lumen, and the basolateral domain that faces neighboring cells and the basement membrane. Protein complexes, containing a subset of conserved proteins from invertebrates to higher mammals, control segregation of epithelial cells into distinct apical versus basolateral domains by the formation of tight junctions. The Crumbs polarity complex consisting of Crumbs3a, Protein associated with Lin-7 1, and PALS1 associated tight junction protein (Crb3-PALS1-PATJ) controls tight junction formation (235). Knockdown of either PALS1 or PATJ in epithelia causes a delay in tight junction formation (254) (262). Cells deficient in Crb3 fail to form tight junctions and do not polarize properly (133, 294). Both Crb3 and PALS1 interact with Par6, a member of the Par complex (110, 153). In addition to Par6, the Par complex contains the proteins Par3 and atypical Protein Kinase C isoform zeta (aPKCζ). The Par complex also interacts with Lethal Giant Larvae (Lgl),

a member of the SCRIB-Lgl-Discs large (Dlg) protein complex (300). The Crumbs complex confirms the formation of the apical domain, while the Scribble complex modulates the formation of the lateral membrane. The function of the Par complex is to maintain the balance between membranous surfaces (10, 38).

Maintenance of epithelial membrane surfaces is essential to maintain epithelial morphology. The epithelial to mesenchymal transition (EMT) is the genetic rearrangement of epithelial cells resulting in loss of polarity with increased invasion, lack of contact inhibition, and resistance to apoptosis (197). The reciprocal process, mesenchymal to epithelial transition (MET) has also been extensively characterized. Maintaining EMT/MET balance is essential in development and wound healing while the loss of the EMT/MET balance manifests in fibrotic disease and cancers of epithelial origin (165, 274, 275). In cancer or fibrotic disease EMT has been shown to cause a drastic and prolonged repression of proteins essential for maintaining polarity (108, 188). During EMT/MET there is also a rearrangement of the cytoskeleton and an acquisition of invasive properties such as expression of the intermediate filament vimentin, an increase in smooth-muscle actin, and migration of the microtubule organizing center (302). Activation of signaling pathways results in upregulation of transcriptional repressors responsible for the genetic rearrangements associated with EMT (303).

One family of transcription factors implicated in EMT is the zinc-finger transcription factors Snail (*Snai1*) and Slug (*Snai2*). Snail and Slug bind E-box motifs in the promoters of genes necessary for maintaining epithelial integrity including *Cdh1,* the gene for E-cadherin, and the major epithelial cell adhesion protein (24, 33, 89). It appears that Snail and Slug, although related, may have divergent targets suggesting a

level of specificity (196). Slug was identified as an EMT factor in the neural crest of the migrating mesoderm of chick embryos and has subsequently been described in numerous cancers (6, 208). Validated targets of Slug include tight junction structural proteins of the claudin and occuldin families (177, 243, 291). Slug has also been shown to block transcription in a transient capacity, allowing for EMT at the leading edge of cutaneous wounding to faciltate wound closure (242).

Epithelial tissues must polarize to function properly. For example, thyroid follicular epithelial cells (thyrocytes) require a defined apical membrane and tight junction to secrete thyroglobulin into the follicular lumen for iodination and storage. Some cultured thyroid follicular epithelial cells lack tight junctions, and these cells can be used to identify factors in tight junction biogenesis. FRTL5 cells exhibit little apico-basal polarity and fail to form proper tight junctions, yet do not exhibit markedly increased invasiveness (9, 306). FRT cells have normal apico-basal polarity and form proper tight junctions (74) (209). Although FRT cells remain fully polarized, they have lost the ability to synthesize thyroglobulin and concentrate iodine therefore they cannot be utilized to study polarized trafficking (7). Non-polarized FRTL5 cells lack tight junctions and apical membranes but synthesize high levels of thyroglobulin making them valuable for the study of polarized trafficking (306). Due to production of large amounts of secreted protein and to study cellular phenomenon such as polarization and polarized trafficking, it would be beneficial to understand why FRTL5 cells do not possess tight junctions and polarity. Since FRTL5 cells lack discernable tight junctions yet are minimally invasive, FRTL5 cells may also effectively mimic transient EMT found in both development and wound healing. Through genomic studies of transient EMT states we

can potentially elucidate genetic rearrangements that underscore the factors governing tight junction biogenesis.

For this study we chose to ask the question as to what genes of unpolarized FRTL5 thyroid cells experience reduced expression in order to keep FRTL5 cells devoid of tight junctions as compared to polarized FRT cells. We preformed a screen for components of the conserved polarity complex proteins known to establish tight junctions and revealed drastically different protein profiles between FRT and FRTL5 cells. A microarray analysis illustrated significant differences in gene expression of tight junction proteins between these two cell lines. Additionally, the unpolarized phenotype of FRTL5 cells seems to be a result of the endogenous expression of the oncogene and EMT transcriptional repressor Slug (*Snai2)*. To confirm the role of Slug in repressing cell polarity, we overexpressed Slug in a normally polarized Madin-Darby canine kidney cells (MDCKII cells) and found Slug directly inhibits polarity by binding the promoter of *Crb3*.

3.2 Materials and Methods

3.2.1 Cell lines

Wild-type FRT, FRTL5, and PCCL3 cells were a gift obtained from P. Arvan (University of Michigan). FRT cells were maintained in F-12 Coon's Modified Ham's Medium (Sigma-Aldrich, St. Louis, MO) supplemented with 2.68 g/L sodium bicarbonate (Sigma-Aldrich), 10% Fetal Bovine Serum (FBS), Gibco-Invitrogen)), and 1% Penicillin/L-Glutamine/Streptomycin (Gibco-Invitrogen). FRTL5 and PCCL3 cells were maintained in F-12 Coon's Modified Ham's Medium (Sigma-Aldrich)

supplemented with 2.68 g/L sodium bicarbonate and 5% Fetal Calf Serum (FCS), Gibco-Invitrogen)), 1% Penicillin/Glutamine/Streptomycin (Gibco-Invitrogen) and a hormone cocktail including: thyroid stimulating hormone (TSH), 1 μg/mL insulin, 5 μg/mL apo-transferrin, and 1 nM hydrocortisone. All hormones were purchased from Sigma-Aldrich and dissolved in MOSH buffer (1% BSA, 1x Hank's Buffered Saline (Gibco-Invitrogen)) in the appropriate amounts, filter sterilized in 1000x concentrations, and stored at -20 C prior to single use. MDCKI and MDCKII cells were maintained in DMEM (Gibco-Invitrogen) with 10% FBS and 1% Penicillin/L-Glutamine/Streptomycin (Gibco-Invitrogen). For retroviral transduction, 293T cells were transfected with 1 μg pGag-Pol, 1 μg pVSV, and 1 μg of the either expression plasmid or vector control plasmid using FuGene6 (Roche Applied Sciences, Madison, WI). 24 hr. post transfection, viral supernatants were collected, sterile filtered, diluted 2-fold with complete media containing 8 ng/mL polybrene, and placed directly on MDCKII cells. 2 days post infection; MDCKII cells were trypsinized and plated in selection media. For MDCKII cells expressing Slug-V5 selection medium containing 200 μg/mL hygromycin was used. MDCKI cells constitutively expressing Snail-Flag used as controls were a gift from E. Fearon (University of Michigan).

3.2.2 DNA Constructs

Plasmid cDNA containing the *H.s*. Slug and was a kind gift from the E. Fearon (University of Michigan) as published in Hajra, et al., 2002 (89). *H.s.* Slug was PCR amplified using the Roche High Fidelity PCR Kit via manufacturers protocol and a V5-tag was added to the C-terminus of the products via this PCR step. The primer sequences

are as follows: Forward (5`-TTATTGGATCCCCACCATGCCGCGCTCCTTCCTG-GTC-3`) and Reverse (5`-TTAATTGGATCCTCAAGTTGAATCCAATCCCAACAA-TGGGTTTGGGATTGGCTTTCCTCCTCCGTGTGCTACACAGCAGCCAGATTC-3`). PCR products were ligated into pQCXIH (Clonetech). The University of Michigan Automated DNA Sequencing Core confirmed sequences.

3.2.3 Antibodies and Immunostaining

Antibodies against Crb3a (UM-369), PALS1 (UM-349), and PATJ (UM-356) were affinity purified and used as described previously (170, 236). An anti-V5 antibody was purchased from Bethyl Labs. The anti-actin and anti-E-cadherin antibodies were purchased from Sigma. Anti-mouse and anti-rabbit secondary were used at 1:20,000 in 5% fat-free milk and purchased from Molecular Probes. For immunostaing, cells were seeded on Transwell filters (Corning, Corning, NY) and allowed to polarize over 4 days. Filters were excised, washed twice with PBS, fixed for 20 min. with 4% paraformaldehyde and permiablized with 0.1% SDS/PBS for 5 min. Filters were then washed twice with PBS and blocked in PBS supplemented with 2% goat serum (PBSG) for 2 – 24 hrs. Primary and fluorophore-conjugated secondary antibodies (Molecular Probes) were diluted in PBSG to appropriate concentrations. All images were obtained using an Olympus FluoView 500 confocal laser-scanning confocal microscope at the Morphology and Image Analysis Core of the Michigan Diabetes Research and Training Center. Samples were scanned with appropriate lasers and filter sets, and images were collected on an Olympus IX-71 inverted microscope using an 100x oil objective.

FluoView v4.3 software was used to collect images, and subsequent preparation was performed using Adobe Creative Suite software.

3.2.4 Microarray and Statistics

All microarray analysis and statistics were performed at the University of Michigan Microarray Core using GeneChip Rat Gene 1.0 ST Array (Affymetrix, Cat.# 901172). Total cytoplasmic RNA was extracted from FRT and FRTL5 cells using the RNeasy kit from Qiagen according to the manufacturer's protocol for isolation of total cytoplasmic mRNA. Gene arrays were completed in duplicate. Quality control steps were done to ensure accuracy. In brief, perfect match (PM), robust mulit-array average (RMA), and principal component analysis (PCA), were completed to ensure quality of the datasets (115). Data was analyzed by filtering the probe set for those with a variance less than 0.05 and then fit to a linear model of microarray analysis (257). Probesets were then selected using an adjusted p-value of 0.05%, adjusted for a false discovery rate, and a 4-fold difference (232). Analysis was done using the affy and limma packages of Bioconductor. Outputs were presented using Microsoft Excel. Relative differences in gene expression were determined by the t-statistic, where positive values represent genes highly expressed in FRT cells relative to FRTL5 cells and negative values represent genes highly expressed in FRTL5 cells relative to FRT cells.

3.2.5 qRT-PCR

Quantitative real-time PCR experiments were performed as described (261). Primer pairs used are as follows: *R.n. Snai2* - (Forward: 5'- CTTCAAGGACACATT-

AGAACAC 3' Reverse: 5' GGTATTTCTTTACATCAGAGTGGG 3'), *R.n. GAPDH*- (Forward: 5'-GCCATATTCATTGTCATACCAG-3' Reverse: 5'-ATTCTTCCACCTTT-GATGCT-3'), *R.n. Cdh*1- (Forward: 5'-AGAAGCCATTGACAAGTACCT-3' Reverse: 5'-ACAGATCCCTCAAAGACCTC-3'). *R.n Crb3*- (Forward: 5`-GAGACAACAGCCTCTGATGA-3`) Reverse: 5`- GGTCACAGTAGGAGACACAG-3`). For end point PCR, qPCR primers were used to amplify target genes from cDNA isolated for qRT-PCR experiments using Taq polymerase (Invitrogen). To verify the identity of PCR products, bands were excised from agarose gels and cloned into the pGem-Teasy vector system (Roche) and submitted for automated sequencing.

3.2.6 ChIP Assays

ChIP was performed in duplicate exactly as described (223) except for minor modifications in the sonication procedure. In brief, control MDCK cells and MDCK cells overexpressing V5 tagged-slug were fixed for 10 min at 25°C with 1% formaldehyde in culture medium. Crosslinking was stopped by the addition of glycine to 0.125 M. Cells were washed twice with ice cold PBS, scraped, and harvested by centrifugation. The cell pellet was washed in PBS, resuspended in cell lysis buffer (5 mM PIPES [pH 8.0], 85 mM KCl, 0.5% NP40, and protease inhibitors), incubated at 4°C for 5 min, and centrifuged for 5 min at 3000 g. The nuclei were resuspended in nuclei lysis buffer (50 mM Tris-HCl [pH 8.1], 10 mM EDTA, 1% SDS, protease inhibitors) and were sonicated on ice with five 20 s pulses using a microtip probe sonicator (Branson Sonifier 250) with output control set to 2.5. Sonicated lysates were clarified by centrifugation at 4°°C for 15 min. Fifteen micrograms of chromatin was diluted in IP

dilution buffer (0.01% SDS, 1.1% Triton X-100, 1.2 mM EDTA, 16.7 mM Tris-HCl [pH 8.1], and 167 mM NaCl) and preclarified with 40 μl protein A-agarose (Invitrogen). Each immunoprecipitation was performed with 5 μg antibodies. After overnight incubation at 4°C, 40 μl protein A-agarose beads were added and the incubation was continued for 1 hr. The beads were sequentially washed once in IP dilution buffer, once in TSE-500 wash buffer (0.1% SDS, 1% Trition X-100, 2mM EDTA, 20 mM Tris-HCl [pH 8.1], 500 mM NaCl), once in LiCl buffer (100 mM Tris-HCl [pH 8.1], 500 mM LiCl, 1% NP-40, 1% Na deoxycholate), and finally two times in Tris-EDTA. Bound complexes were eluted by vortexing beads twice for 15 min at 25°C in 250 ul of elution buffer (100 mM Na bicarbonate and 1% SDS). NaCl (5 M) was added to a final concentration of 0.2 M to the pooled eluates, and crosslinks were reversed by incubating samples at 65^{o}C overnight. The samples were digested with proteinase K for 1 hr at 56^{o}C, and phenol-chloroform extracted. DNA was precipitated and reconstituted in sterile water. Real-time PCR quantitation of precipitated genomic DNA relative to inputs was performed in triplicate using IQ SYBR GREEN with ROX mastermix (Bio-rad) in a Real Time PCR machine from Applied Biosystems as described (223).

Primer sequences for amplification are as follows (294):
Canis familiaris Crumbs3 promoter 5'-CGG TAA TGT CTC CAC ACT AA-3' (forward) 5'-CCC AAT TCT ATA ATA CGG AAG AG-3' (reverse) *Canis familiaris Crumbs3* "- 10 Kb" 5'-GTA TAT CGC ACA CGA TTT CCC-3' (forward) 5'-CAC ACG CAT ACA TAG ATA CGA-3' (reverse) *Canis familiaris GAPDH* promoter 5'-CAT TAC CCA TTT AGC CAA TTC C-3' (forward) 5'-TGA AAC AAC TGA GCA TAG GG-3' (reverse).

3.3 Results

3.3.1 FRTL5 thyroid epithelial cells are lacking polarized epithelial markers

Previous studies on FRTL5 thyroid epithelial cell have illustrated that although FRTL5 cells express the genes required for production of thyroid hormones such as thyroglobulin, they lack the ability to exocytose thyroglobulin in a directed manner through the apical membrane (7, 8). Presumably, the lack of polarization of FRTL5 cells is the cause of the lack of targeted secretion of thyroglobulin. We therefore initially chose to survey FRTL5 cells for their expression of key polarity proteins that have been shown to lead to the formation of suitable tight junctions and therefore a correct columnar epithelial phenotype. For controls, another non-polarized thyroid epithelial cell line, PCCL3, was included as well as fully polarized MDCKI cells and non-polarized MDCKI cells overexpressing the EMT factor Snail. Initial Western blot experiments indicate that FRTL5 cells are lacking in the essential polarity markers including Crb3 and E-cadherin (Figure 3-1A). Additionally, the tight junction proteins PALS1, PATJ, and Par3 appear to be altered in both protein level and expression of isoforms in FRTL5 cells when compared to fully polarized FRT cells (Figure 3-1A). The protein expression profile of FRTL5 cells when compared to FRT cells was curiously similar to the protein expression profile of an epithelial cell that had undergone epithelial to mesenchymal transition (EMT) by overexpression of the transcription factor Snail (294). We therefore chose to test FRTL5 cells for the presence of EMT markers to see if FRTL5 had similar

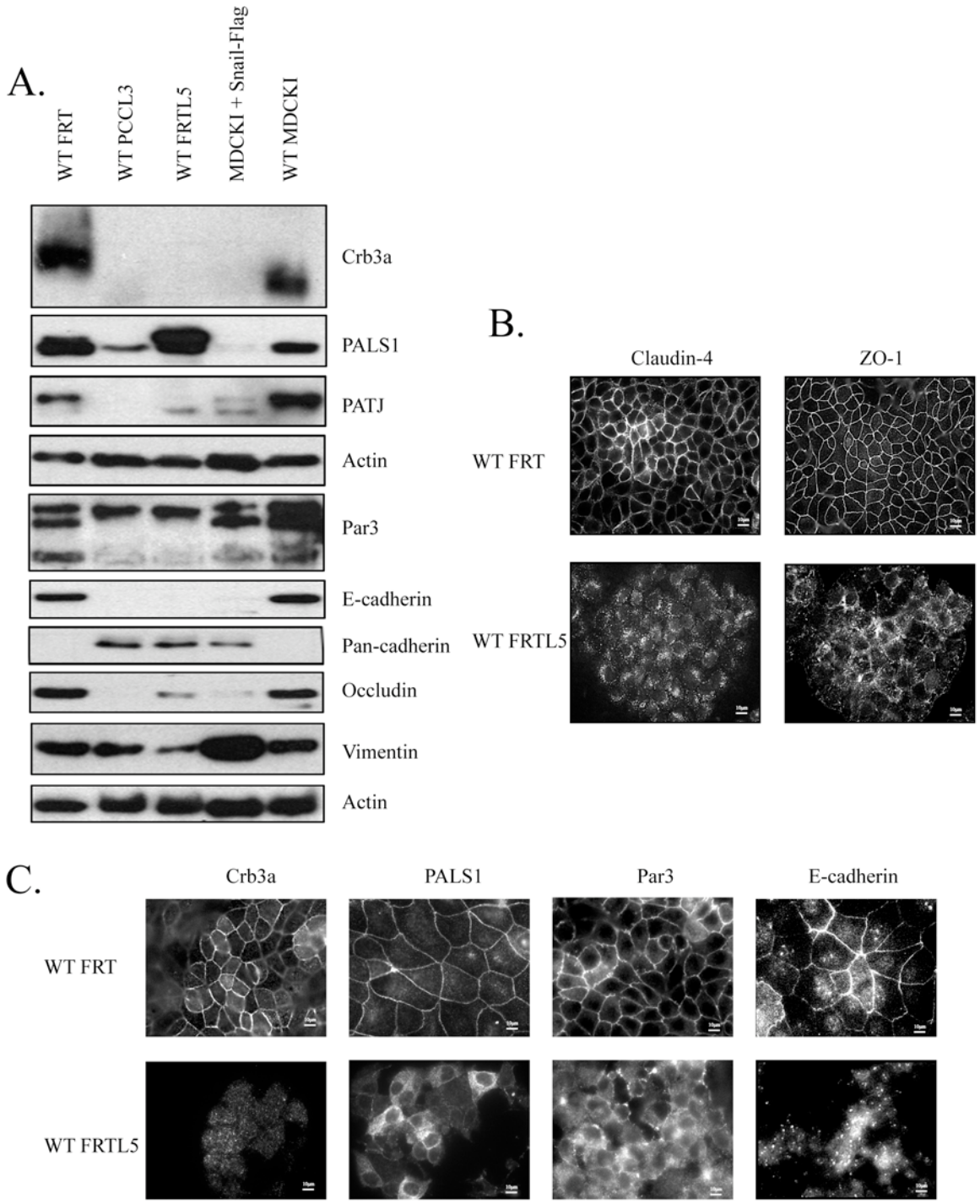

Figure 3-1: Altered expression of conserved polarity proteins and tight juction structural protines in wild type FRTL5 thyrocytes. (A). Western blots of polarity and tight junction proteins. (B) FRTL5 cells are lacking tight junctions compared to FRT cells. (C) Immunofluorescent staining of polarity proteins in FRT and FRTL5 cells.

characteristics as cells that have undergone EMT. In FRTL5 cells we see an introduction of an alternate cadherin species; presumably N-cadherin. This "cadherin switch" is often indicative that a cell has undergone some stages of EMT (Figure 3-1A).

Immunofluorescence staining of both FRT and FRTL5 cells argeed with our Western blotting data. Control FRT cells show the presence of a normal tight junction structure and correct subcellular localization of the tight junction markers Claudin-4 and ZO-1 while Claudin-4 and ZO-1 staining in FRTL5 cells shows that these cells lack a proper tight junction (Figure 3-1B). Also PALS1, normally associated with the tight junction in the cortical region of cells is now in the cytosol in FRTL5 cells. In addition to tight junction markers, FRTL5 cells lack cortical staining of endogenous E-cadherin, the major epithelial adhesion molecule while FRT cells express E-cadherin along their lateral membrane (Figure 3-1C).

3.3.2 Altered transcription of junction components in FRTL5 cells

We next chose to study global gene expression differences between FRT cells and FRTL5 cells to more fully understand which genes are involved in the loss of polarity in FRTL5 cells. We preformed a microarray analysis comparing mRNA expression levels between wild type FRT and wild type FRTL5 cells to determine differences in gene expression that could possibly explain why FRTL5 cells lack tight junctions. The full output of our microarray is included in Appendix A. Searching our data set for polarity proteins, we discovered that not only were FRTL5 cells were not expressing the key polarity genes *Cdh1* and *Crb3*, but they were also reduced in expression of genes encoding for tight junction structural proteins including claudin1, claudin4, and claudin8

Symbol	***Description***	***t-statistic***	***Fold Change***
Sdc2	syndecan 2	-64.02	-9.09
Cdh1	cadherin 1	62.82	8.57
Cldn8	claudin 8	57.71	8.64
Icam1	intercellular adhesion molecule 1	-42.2	-5.83
Cldn4	claudin 4	41.83	7.49
Cldn1	claudin 1	38.68	5.36
Crb3	crumbs homolog 3 (Drosophila)	37.45	5.23
Dsc2	desmocollin 2	-37.38	-5.46
Gjb5	gap junction membrane channel protein beta 5	31.44	4.88
LOC304000	cell adhesion molecule JCAM	30.3	4.5
Cldn7	claudin 7	27.23	6.03
Cdh2	cadherin 2	-25.08	-3.7
Jam3	junctional adhesion molecule 3	-24.65	-3.38
Cldn6_predicted	claudin 6 (predicted)	23.48	3.97
Cldn3	claudin 3	23.4	4.01
Dsp	desmoplakin	22.22	5.05
Gjb3	gap junction membrane channel protein beta 3	22.02	4.07
Fgfr1	Fibroblast growth factor receptor 1	-21.61	-4.28
Sdc1	syndecan 1	21.35	5.13
Prkch	protein kinase C, eta	20.87	2.82
Plcb4	phospholipase C, beta 4	-20.46	-4.06
Itga6	integrin, alpha 6	-19.68	-2.67
Gja4	gap junction membrane channel protein alpha 4	17.79	3.01
Prkch	protein kinase C, eta	17.47	2.43
Prkcz	protein kinase C, zeta	-17.31	-2.59
Cdh23	cadherin 23 (otocadherin)	16.96	2.57

Table 3-1: Polarity proteins differentially regulated in FRT cells relative to FRTL5 cells. The table represents 25 genes known to influence cell polarity with the largest differences in expression. Genes upregulated in FRT cells are in white and have positive values. Genes upregulated in FRTL5 cells are shaded in gray and have negative values. The absolute value of the t-statistic represents the relative level of difference where a greater absolute value represents greater difference in gene expression between FRT and FRTL5 cells.

Symbol	***Description***	***t-statistic***	***Fold Change***
Tg	thyroglobulin	-58.84	-8.88
Thrsp	thyroid hormone responsive protein	-42.24	-7.99
Titf1	thyroid transcription factor 1	-32.73	-4.91
Tpo	thyroid peroxidase	-31.72	-6.83
Foxe1	forkhead box E1 (thyroid transcription factor 2)	-21.51	-4.18
Tshr	thyroid stimulating hormone receptor	-20.01	-4.88

Table 3-2: Thyroid horome specific genes upregulated only in FRTL5 cells.

(Table 3-1. Notably, the *Cdh2* gene, which codes for N-cadherin was upregulated in FRTL5 cells further confirming the presence of the "cadherin switch" in FRTL5 cells (Table 3-1). For controls of we looked at a subset of genes that are only expressed in FRTL5 cells and are involved in the synthesis of thyroid hormones (Table 3-2). The genes for thyroglobulin (*Tg),* thyroid hormone responsive protein (*Thrsp*) thyroid transcription factor 1 (*Titf1*), thyroid peroxidase (*Tpo*), forkhead box E1 (thyroid transcription factor 2; *FoxE1*), and thyroid stimulating hormone receptor (*Thsr*) were all specifically upregulated in FRTL5 cells indicative of TSH sensitivity and the ability to produce and process thyroglobulin.

3.3.3 *Snai2* is upregulated in FRTL5 cells

Lack of expression of genes coding for polarity and tight junction proteins indicated that FRTL5 cells might be exhibiting some of the characteristics of EMT including lack of proper junctions, lack of contact inhibition, and genetic rearrangement (149). To investigate if FRTL5 cells had undergone EMT, we searched our microarray for known inducers of EMT that may cause loss of apico-basal polarity. The first indication that FRTL5 cells had undergone EMT was the alteration of expression in genes of the transforming growth factor Beta/bone morphogenic protein (TGF-β/BMP) pathways (See Appendix A). TGF-β has previously been demonstrated to upregulate endogenous expression of EMT transcription factors such as Snail (reviewed in (287, 303)). According to microarray data, FRTL5 cells were expressing increased levels of the TGF-β pathway (pro-EMT) genes including Connective Tissue Growth Factor (*CTGF*), *Id4*, and *Smad3* (287). Conversely, FRT cells were expressing genes involved

with BMP signaling (anti-EMT) such as *Gata3*, *Id2*, and *Gata4* (287). Upon analysis of the microarray data, we found annotated genes encoding the EMT transcription factors Snail (*Snai1*), Twist (*Twist1*), Transcription Factor 8 (ZEB1, *Tcf8*), and FoxC2 (*FoxC2*). All genes coding for these EMT transcription factors were not significantly different according to our microarray statistical breakdown (Table 3-3). However, one notable omission from microarray chip was the gene *Snai2,* which codes for the EMT transcription factor Slug. Slug has been previously shown to downregulate the *Cdh1* gene and lead to an EMT phenotype (24). Since our array did not contain the *Snai2* gene, we screend for the presence of *Snai2* transcript via PCR. Using primers designed specifically for rat *Snai2*, we were able to amplify a 127 base pair fragment of Slug FRTL5 cDNA reverse transcribed from total FRTL5 cytoplasmic mRNAs but not from cDNA derived by the same method from FRT cells. qRT-PCR experiments verified that there is a 60% increase in endogenous *Snai2* in FRTL5 cells compared to FRT cells.

3.3.4 Slug expression leads to polarity defects in MDCKII cells

To further elucidate the role of Slug in the repression of genes responsible for proper epithelial morphology, we chose to exogenously express Slug in Madin-Darby canine kidney cells (MDCKII cells). A V5-epitope tagged version of human Slug was stably transduced into MDCKII cells. Overexpression of Slug in MDCKII cells lead to a change in epithelial morphology including loss of ZO-1 staining at the tight junctions in Slug-V5 cells when compared to control cells (Figure 3-3A). Also, staining for E-cadherin shows a loss of E-cadherin at the cortical membrane in Slug-V5 cells (Figure 3-3A). Immunofluorescence staining using nuclear DAPI staining showed that Slug-V5

		Expression Values			
Symbol	***Description***	***FRT-A***	***FRT-B***	***FRTL5-A***	***FRTL5-B***
Snai1	snail homolog 1 (Drosophila)	6.74780035	6.848649	6.614032	6.72288
Twist1	twist gene homolog 1 (Drosophila)	4.47924204	4.457792	4.300423	4.34056
Tcf8 (ZEB1)	transcription factor 8	6.59271	6.613233	8.521425	8.541948
Foxc2	forkhead box C2	5.225509	4.869783	4.734558	4.740721

Table 3-3: Annotated genes for EMT trancription factors in FRT cells relative to FRTL5 cells.

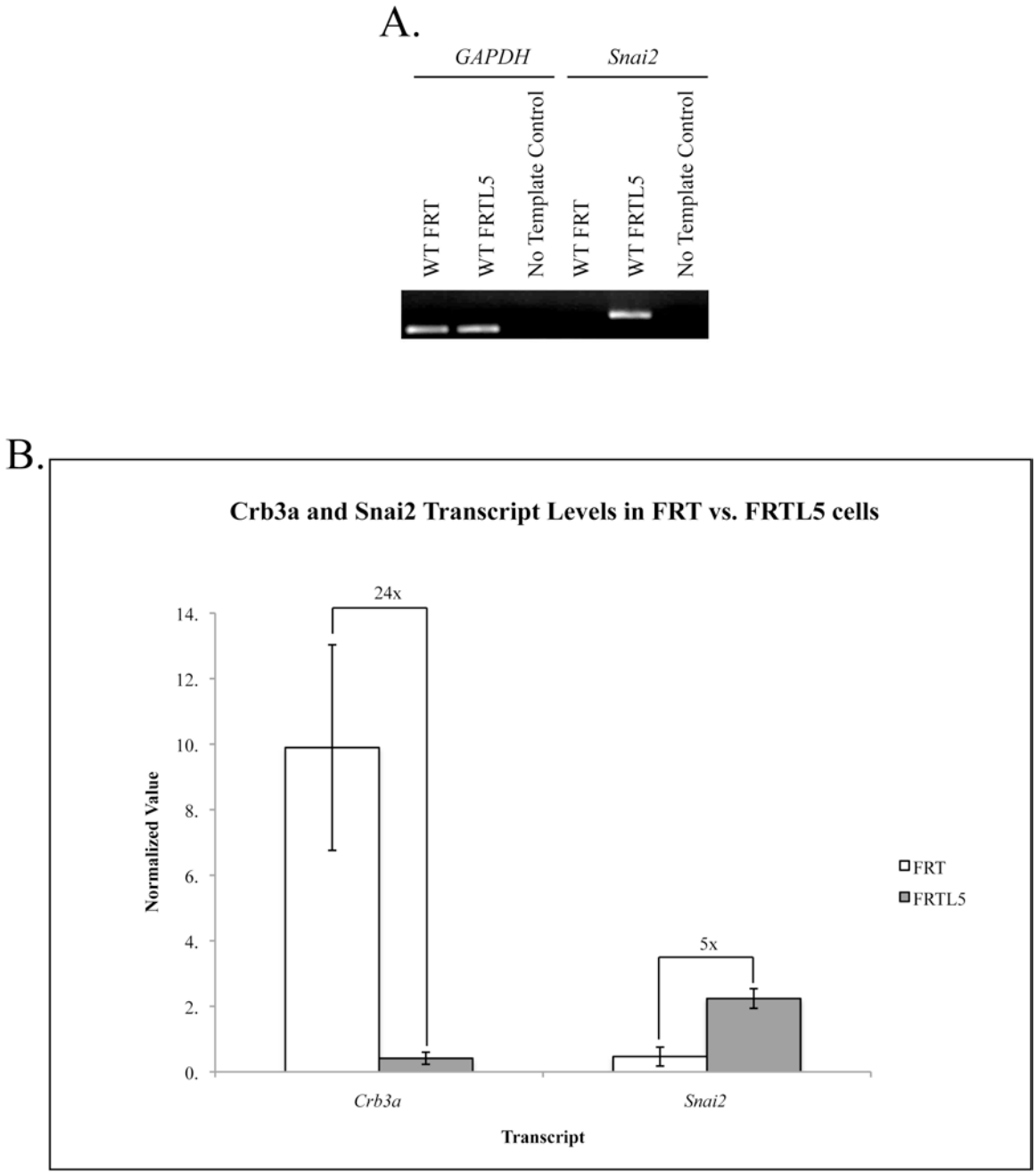

Figure 3-2: PCR of *Snai2* (Slug) transcripts from wild type FRTL5 cells. (A) End point PCR from cDNA derived from total cytoplasmic mRNA of FRT and FRTL5 cells. (B) qPCR of transcripts for *Crb3* and *Snai2* in wild type FRT and FRTL5 cells.

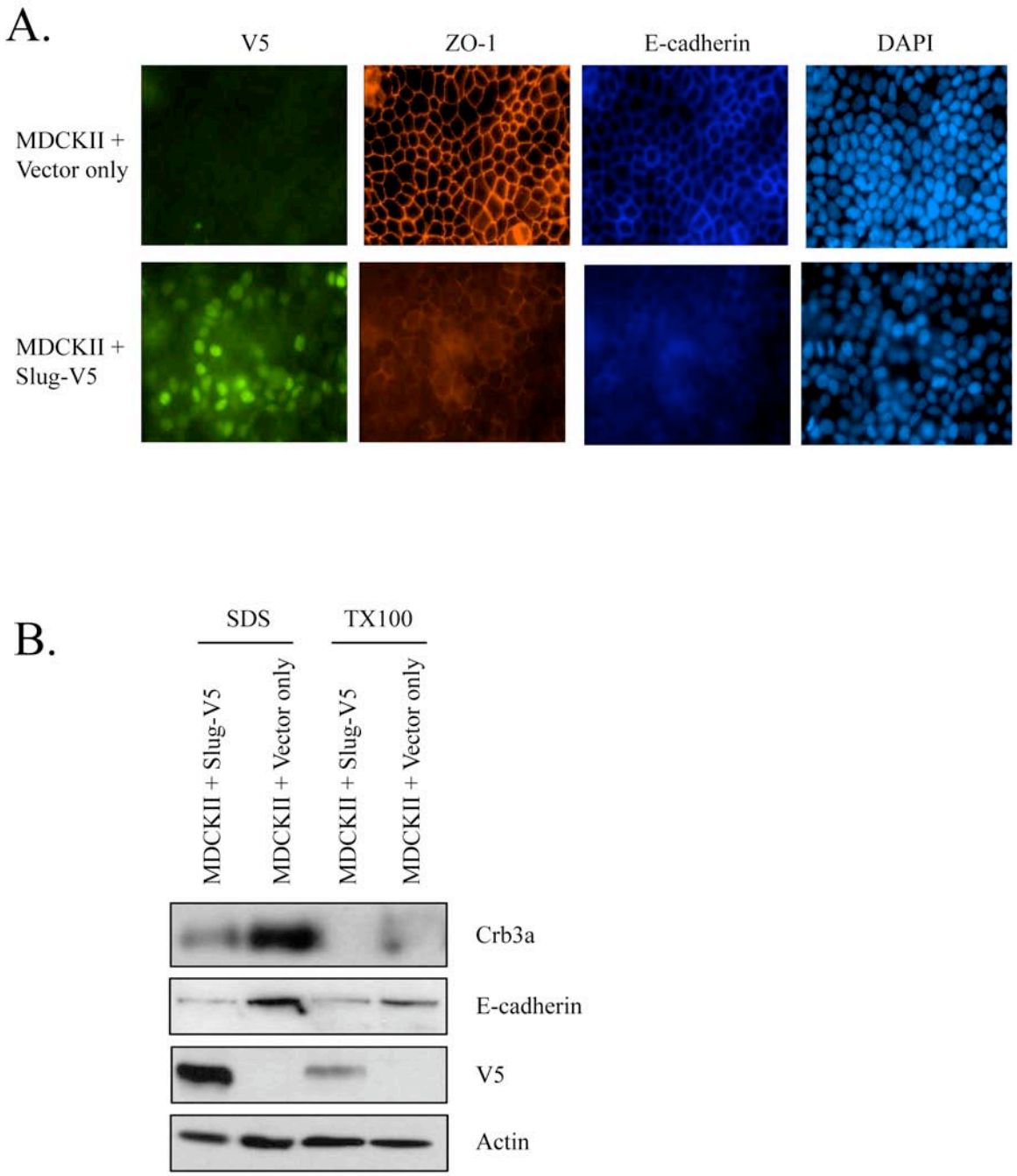

Figure 3-3: Slug overexpression leads to EMT in MDCKII cells. (A) Slug-V5 expression leads to morphology changes and reduction of tight junction ZO-1 and adherens junction E-cadherin. (B) Differential lysis of MDCKII cells expression Slug-V5. Cells were lysed in an SDS soluble fraction (lanes 1 and 2) and a Triton-X soluble fraction (lanes 3 and 4) to determine if Slug-V5 expression results in loss of protein or change in subcellular localization. Slug-V5 expression leads to loss of Crb3a and E-cadherin protein.

cells did not grow in a into a nice cobblestone monolayer typical of vector only control cells (Figure 3-3A). These morphological changes are indicative of cells that have gone through EMT.

Expression of Slug resulted in morphological changes of MDCKII cells; therefore we tested the affect of Slug on expression on the levels of Crb3 and E-cadherin proteins. Using Western blot analysis we discovered that exogenous Slug expression leads to a reduction in protein of both E-cadherin and Crb3 (Figure 3-3B). To rule out that expression of Slug-V5 was affecting the localization of both E-cadherin and Crb3, we used a crude differential lysis to differentiate between a triton-soluble cytosolic fraction and an SDS-soluble membrane associated fraction to determine if Slug-V5 expression was only causing a change in subcellular localization and not a reduction in Crb3a protein. Using this method, we verified that Slug-V5 expression lead a decrease in E-cadherin and Crb3 protein levels and not a change in subcellular localization.

3.3.5 Slug-V5 directly represses *Crb3* in MDCKII cells

Since Slug is a known transcription repressor associated with EMT, and EMT involves reduced levels of cellular Crb3a, we wanted to know if Slug could directly repress transcription of Crb3 by binding the *Crb3* promoter in MDCKII cells. To test our hypothesis, we used chromatin-immunoprecipitation (ChIP) assay to verify the presence of Slug on the *Crb3* promoter region. We used V5 antibodies to pulldown crosslinked DNA and using previously published primer sequences to canine *Crb3* and we were able

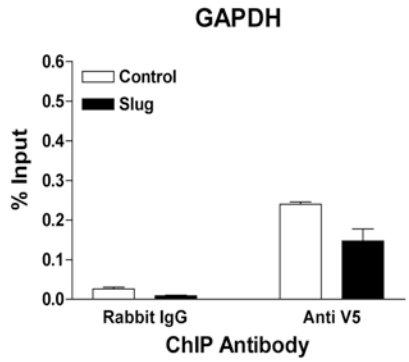

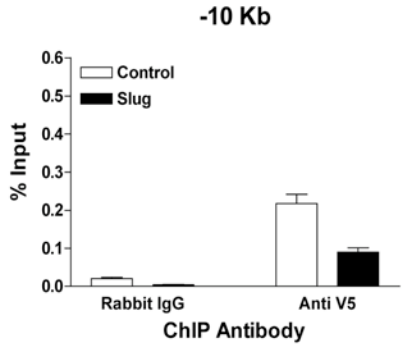

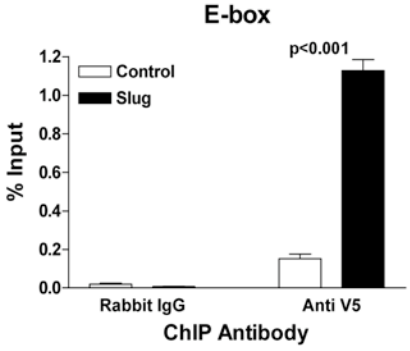

Figure 3-4: ChIP of *Crb3a* promoter with Slug-V5. Slug-V5 binds an E-box in the *Crb3* promoter previously identified as a Snail binding site. GAPDH and a 10 kb upstream sequence on the *Crb3* promoter were used as controls.

to effectively pulldown and amplify the promoter of the *Crb3* gene (294). These results indicate to us that Slug directly affects polarity at least in part by directly repressing production of Crb3.

3.4 Discussion

Here we investigated the components that affect an epithelial cells ability to form junctions and properly polarize. We found the expression of conserved polarity proteins is different in polarized FRT cells relative to non-polarized FRTL5 cells. Through genomic analysis, we determined a subset of proteins necessary for junction formation, including the polarity determinant *Crb3*. Furthermore, we show that induction of EMT by exogenous expression of the EMT transcription factor Slug specifically targets *Crb3* in epithelial cells. Reduction in Crb3 protein leads to disruption of morphology and a reduction of polarity proteins (133, 294). During the epithelial to mesenchymal transition (EMT) epithelial cells lose their epithelial morphology and take on a mesenchymal appearance complete with an increase in cell size, loss of contact inhibition, and increased invasiveness (1, 275) (302). EMT has been shown to be an important process in development and wound healing, but also detrimental as illustrated in both cancers of epithelial origin and cystic disease (165). Understanding the factors that contribute to EMT has become important to understanding these phenotypes *in vivo*. Loss of epithelial morphology is concurrent with the dissolution of epithelial tight junctions that delineate apical versus basolateral domains (113, 177). Proteins that control the structure, position, and formation of the tight junction therefore have become attractive targets to study the phenomenon of EMT.

For this study, we chose to compare polarized FRT cells and non-polarized FRTL5 cells. Both cell lines are derived from the thyroid of Fischer rats. We found that FRTL5 cells, which lack proper tight junctions, have altered protein expression profiles of the conserved polarity proteins Crb3, PATJ, and Par3. Our lab and others have previously demonstrated that each of these proteins are essential in the formation and maintenance of tight junction in other polarized epithelial cells such as MDCKs (reviewed in (10)). Tight junctions are also comprised of transmembrane scaffolds that are necessary for tight junctions structure. Protein analysis confirmed that structural claudin-4 is also missing from FRTL5 cells indicating that FRTL5 cells also have defects in tight junction structure. Additionally, when blotting for the major cell-to-cell adhesion molecule E-cadherin, we noticed that FRTL5 cells were deficient in E-cadherin, while at the same time we found an increase in Pan-cadherin signal. We believe that our Pan-cadherin antibody preferentially blots N-cadherin due to lack of signal in our control cells clearly expressing high levels of endogenous E-cadherin. This presumed increase in N-cadherin lead us to blot for the EMT marker vimentin, and we found an increase in vimentin signal in FRTL5 cells. These results suggested to us that FRTL5 cells exhibit characteristics indicative of EMT.

Determining the roles of polarity proteins in tight junction formation has involved the use of RNA interference to reduce protein levels. FRT and FRTL5 represent immortalized mammalian cells of the same tissue that represent vast differences in genetic profiles. We exploited these differences in FRT and FRTL5 cells to illustrate the genetic rearrangements involved with the EMT and specifically EMT loss of epithelial junctions. Using cultured FRT and FRTL5 cells; we used a rat microarray identify a large

number of candidate genes that could possibly explain why FRTL5 cells lack epithelial polarity relative to the polarized FRT cells. The data generated by our microarray analysis demonstrates that FRTL5 cells lack expression of genes for the tight junction structural proteins claudins-1, -3, -4, -6, -7 and -8. Claudin-1 specifically binds PATJ at the tight junction, and this interaction may contribute to the localizaton of the Crumbs polarity complex (236). Screening our microarray for conserved Crumbs complex polarity proteins, we find the gene for Crb3 and not the genes for PALS1 or PATJ as down regulated in FRTL5 cells. PALS1 and PATJ transcript levels are partially reduced in the presence of a Snail in MDCKII cells, however there is no direct evidence that PALS1 and PATJ are under direct repression by Snail in EMT (294). PATJ has been demonstrated to be under specific control by ZEB1, however neither ZEB1 nor PATJ are indicated as having significant changes in expression in our microarray (4). This is consistent with previous data that clearly demonstrates PALS1 and PATJ are under post-translational control in MDCKII cells by stabilization through binding to each other and other associated proteins (261, 262). Crb3, in contrast, has been demonstrated to be under direct genetic suppression during Snail and ZEB1-induced EMT in MDCK cells (4, 294). Likewise, previous studies have shown that Crb3 protein levels are highly regulated in polarized epithelial cells and both over abundance or lack of Crb3a lead to defects in epithelial morphology and function (235). Emerging evidence has suggested that Crb3a is essential for the establishment of the apical surface and the maintenance of that surface. Exogenous Crb3a can lead to *de novo* junctions in MCF10A cells (69). Crb3a confirms the establishment of the initial apical lumen in lumen formation assays

(246). Finally, overexpression of Crb3 alone is enough to partially rescue Snail-induced EMT (294).

Crb3 is a known target of Snail and ZEB1 mediated transcriptional repression (4, 294) yet upon comparison of FRT and FRTL5 cells we found no significant differences in expression levels of EMT factors Snail, Twist, ZEB1, or FoxC2. The transcription factor Slug was absent from our array perhaps due to lack of annotation at the time of our experiment. We performed a PCR based screen for Slug in FRT and FRTL5 cells and found significant levels of the transcript in FRTL5 cells. Snail and Slug are two highly similar zinc-finger transcription factors however, it is not known how closely related Snail and Slug in terms of specificity of targets (196). It has been suggested that Snail and Slug have both unique and overlapping targets dependent on cell type and context. Snail appears to be a more global transcriptional repressor in terms of affinity for targets and duration of activity on targets (24). Slug, on the other hand, has been hypothesized to have less affinity for target promoters lending to a more transient EMT phenotype (24, 242). We expressed a V5-epitope tagged version of human Slug in MDCKII cells to investigate the activity of Slug on epithelial polarity. We immediately noticed Slug leads to defects in epithelial polarity and junction formation indicative of EMT. Slug is a known repressor of *Cdh1* in cultured cells but it is not known if Slug has any affect on the gene for Crb3 (89). Using ChIP assays, we were able to detect a direct interaction with Snail-V5 and canine *Crb3* promoter indicating that Slug directly represses *Crb3* in MDCKII cells. This is the first report that Slug is responsible for directly repressing *Crb3*.

Our initial inspection of our microarray data illustrated a number of potential pathways deregulated during EMT conditions. TGF-β signaling is increased during EMT, and in FRTL5 cells there was a specific increase in TGF-β pathways genes. Concurrently, in FRTL5 cells we found significant decrease in the BMP signaling pathway, which is known to antagonize TGF-β signaling. We had previously utilized TGF-β treatment to stimulate endogenous expression of Snail in MDCKII cells (294). Induction of Snail *in vitro* results in a change in protein levels of tight junction proteins similar to the protein profiles found in FRTL5 cells. There is a body of evidence to suggest that TGF-β induction in thyrocytes leads to the onset of EMT In primary porcine thyrocytes TGF-β treatment lead to dedifferentiation only when combined with epidermal growth factor (EGF) treatment (84). In our microarray, EGF receptor gene expression was only significantly higher in polarized FRT cells and not FRTL5 cells. A genomic analysis of human papillary thyroid carcinomas demonstrated an upregulation of TGF-β signaling genes at the invasive front of these tumors (285). Also in anaplastic thyroid carcinoma an increase in TGF-β signaling caused by misregulation of specific microRNAs leads to invasive phenotypes (28). Interestingly, in different tumor types such as, lung adenocarcinoma TGF-β treatment lead to full EMT phenotypes, including the upregulation of endogenous Snail and Slug, but this effect could be attenuated by overexpression of TTF1 resulting in only partial EMT compared to the full complement of phenotypes associated with Snail and Slug overexpression (241). Similarly, we noted that FRTL5 cells exhibit what appears to be only a partial EMT and importantly also express high levels of TTF1. Expression of TTF1 in lung cancers has been linked to good prognoses due to limited invasive properties of tumors (270). Taken together with

our observations, the data suggest that expression of Slug in FRTL5 cells might cause a loss of polarity, but not increased invasion due to high levels of TTF1. Further experimentation is needed to verify this hypothesis and this will prove fertile ground for further study of transient EMT phenotypes.

Here we illustrate that the known EMT transcription factor Slug, can repress the gene for the epithelial polarity determinant Crb3a. We successfully used microarray analysis to identify a subset of genes required for tight junction biogenesis. Of these genes, the known EMT targets *Cdh1* and *Crb3* as well as tight junction structural proteins from the claudin and occuldin families are clearly necessary for tight junction formation and epithelial polarity. Hopefully, our data set will provide invaluable information for those studying both thyroid epithelial polarity, signaling, and trafficking.

Chapter 4

Regulation of Epithelial Polarity by Endocytosis of Crb3a

4.1 Introduction

Polarized epithelial cells consist of two biochemically distinct membrane subdomains, an apical domain facing the lumen and a basolateral domain facing neighboring cells and the underlying tissue. As a method of establishing distinct membrane domains, epithelial cells utilize differential trafficking of transmembrane proteins (106, 199, 247). Crumbs3a (Crb3a) is a resident apical domain transmembrane protein essential for epithelial polarity and part of the conserved tripartite Crumbs polarity complex consisting of Crb3a-PALS1-PATJ (152, 170, 235, 237). Crb3a interacts with the conserved Par polarity complex (Par6-Par3-aPKCζ) to modulate the formation of the distinct apical versus basolateral domains in polarized epithelial cells (110, 153). Crb3a is a highly regulated protein as both excess of Crb3a or lack of Crb3a lead to epithelial morphology defects (235). Likewise, transcriptional repression of the *Crb3* gene leads to rapid loss of epithelial morphology (133). These previous results indicate that Crb3a is essential in both the establishment and maintenance of polarized

monolayers. However, these studies do not take into consideration the role of Crb3a trafficking in the regulation of polarity.

For signal attenuation and degradation, apical surface proteins can be endocytosed into apical early endosomes (AEE) positive for Rab4 and Rab5 (30, 250). Once endocytosed, apical components are either recycled into the ARE or shuttled into an endosomal degradation pathway. Mechanisms uncovering the reciprocal exocytosis and endocytosis (apical recycling) of Crb3a in polarized epithelial cells have largely been inferred by using genetic modeling in various *Drosophila* tissues using dCrumbs (the *Drosophila* homologue of Crb3a) as a marker of apical maturation. Deposition of dCrumbs on the apical surface is necessary for epithelial polarization (272, 296). In *Drosophila* disruption of Rab11 by either introduction of a dominant negative version of the protein or knockout by introduction of a null allele leads to abnormal distribution of dCrumbs in multiple tissues (234). Decreasing output in the Rab11 gene product in flies also leads to a failure in apical dCrumbs deposition and initial apical lumen formation (41, 139). Localization of dCrumbs to the surface appears to be maintained by the balance of apical versus basolateral domains (92). Balance of apical versue basolateral surfaces is control by endocytosis and exocytosis and disruption of the endocytic syntaxin-7 or Rab5 in *Drosophila* also leads to epithelial morphology defects associated with the accumulation of dCrumbs (167).

Disrupting *Drosophila* endocytic degradation through the multi-vesicular body pathway (MVB) also leads to apical overgrowth similar to dCrumbs overexpression phenotypes (78, 79). Once endocytosed proteins reach AEE, they can be shuttled to the MVB for degradation. MVB formation and traffic is governed by Endosomal Sorting

Complex Required for Transport (ESCRT) protein complexes 0-III. From AEE, ESCRT complex proteins shuttle vesicles sequentially along membranes where vesicles are invaginated and budded into the interior of the MVB. Through this process the MVB can be seen as a vesicle containing vesicles. The resident vesicles of the MVB, now called exosomes, contain transmembrane proteins and receptors destined for degradation. For this degradation, MVBs can either fuse with the lysosome or alternatively can fuse with the plasma membrane to release exosomes into the luminal space.

Here we chose to investigate the apical recycling of a mammalian homologue of *Drosophilla* Crumbs, Crb3a, and the relationship between apical recycling and regulation of epithelial polarity in polarized MDCKII cells. Using live cell imaging and tissue culture models of the apical recycling of Crb3a, we found that once apical surfaces are established, apical recycling of Crb3a is reduced. Reduction of apical recycling suggests that Crb3a is trafficked via an alternate mechanism, and abrogation of multi-vesicular body biogenesis results in an increase in cellular levels of Crb3a. We also utilized an inducible Crb3a gene system to assess the approximate half-life of the Crb3a protein in both fully polarized and non-polarized conditions to determine if presence of an apical surface leads to Crb3a protein stabilization. Similarly, we also observed that Crb3a appears to be a very dynamic protein at both the apical surface and tight junction. Our observations lead us to conclude that Crb3a trafficking through non-recycling mediated pathways results in epithelial remodeling and contributes to epithelial polarity being a dynamic process.

4.2 Materials and Methods

4.2.1 Cell Lines and Plasmids

MDCKII cells were maintained in DMEM supplemented with 10% fetal-bovine serum and 1% penicillin-streptomycin-glutamate (all from Gibco, Invitrogen) and appropriate selection agent where noted. *H.s.* Crb3a was PCR amplified from a human kidney cDNA library (Clonetech) and ligated into pRevTRE (Clonetech). For monomeric eGFP-Crb3a (mEGFP-Crb3a) cDNA expression construct, an EcoRV site was engineered into the coding sequence of *H.s*. Crb3a via site-directed mutagenesis using Pfu Turbo (Stratagene). Monomeric eGFP (meGFP) was inserted in frame at the EcoRV site. EcoRV sites were then mutated to the original native sequence via site-directed mutagenesis (see (246)). For inducible mEGFP-Crb3a (iGFP-Crb3a) cells, cDNA for mEGFP-Crb3a was ligated into pRetroX-Tight-Puro (Clonetech) and transduced into MDCKII cells stably expressing pTet-On Advanced (Clonetech). The Dendra2-Crb3a (Den2-Crb3a) construct was created by excision of mEGFP from mEGFP-Crb3a via EcoRV restriction digest followed by ligation of Dendra2 in frame and subsequent site directed mutagenesis. Functionality of mEGFP-Crb3a and Den2-Crb3a were tested by Western blot and confocal microscopy.

For TSG101 knockdown cell lines, short hairpin sequences were obtained from (112) and are as follows: SH-1: top oligo: 5`-GATCCGCCTACTAGTT CAATGACTTTCAAGAGAAGTCATTGAACTAGTAGGCTTTTTTACGCGTG-3` bottom oligo: 5`-AATTCACGCGTAAAAAAGCCTACTAGTTCAATGACTTCTCTT GAAAGTCATTGAACTAGTAGGCG-3`. Short hairpins were annealed and ligated into pSiren-RetroQ-DsRed (Clonetech) and transduced into MDCKII cells. Clones were

picked after selection using epifluorescent microscopy selection for DsRed. The University of Michigan Automated DNA Sequencing Core verified all sequences.

4.2.2 Antibodies and Immunofluorescence Staining

Primary antibodies against Crb3a (UM510) were obtained from serum derived from inoculation of rabbits with a peptide (CARVPPTPNLKLPPEERLI) corresponding to the C-terminal sequence of human Crb3a (Cocalico Biologicals Reamstown, PA). Antibodies for PALS1 were used as described in (262). Dendra2 antibody was obtained from Evrogen. Antibodies against GFP, and fluorophore conjugated secondary antibodes as well as Wheat-germ aggultinin-594 (WGA-594) were obtained from Molecular Probes. Antibodies against Rab11, TSG101, and EEA1 were obtained from BD Biosciences. E-cadherin antibody was obtained from Zymed. Antibodies against Par6B were from Santa Cruz Biotech. Antibodies against aPKCζ and Par3 were from Upstate. HRP-conjugated secondary antibodies were obtained from Amersham-GE. For immunostaining, cells were grown on glass coverslips or transwell filters.

4.2.3 3-Dimensional Tissue Culture Cyst Assays

MDCKII cells stably expressing plasmids of interest were dissociated using enzyme free cell dissociation buffer (Gibco Invitrogen), spun down, washed twice with PBS, and counted. Cells were then resuspended in complete growth media containing 4% Geltrex (Gibco Invitrogen) and ~ 25,000 cells were seeded into one well of an 8-well chamber slide (Nunc), with each chamber containing a bed of 100% Geltrex. Cysts were allowed to grow in complete growth media with 4% geltrex for days indicated in the

figure legends. Cysts were then fixed for 1 hour with 4% paraformaldhyde and permiablized with 0.1% SDS/PBS for 30 minutes followed by blocking for 1 hour in 4% goat serum/PBS (PBSG). After blocking, primary antibodies were diluted in (PBSG) and cysts were incubated with primary antibody solution for 24-48 hours at 4 degrees. After three 30 minute washes with PBSG, secondary antibodies were diluted in PBSG and incubated with cysts for 24 hours at 4 degrees in the dark. After three 30 minute washes, cysts were placed in PBS and for visualization.

4.2.4 Imaging/Live-cell Imaging/FRAP

All images were obtained on an Olympus FV500 Confocal Microscope at the University of Michigan Diabetes Research and Training Center Morphology and Imaging Core. For FRAP analysis, MDCKII cells constitutively expressing mEGFP-Crb3a were seeded on coverslips and allowed to polarize over four days. Coverslips were then placed in a live cell-imaging chamber in Libowitz media as above. Regions of interest were photobleached using 3 iterations of the UV laser at 100% intensity and then monitored for 250 seconds. Recovery rates were determined by comparing bleached regions to control regions of approximately the same intensity. Recovery plots and statistical analysis were produced using Graphpad Prism software. Media was added as needed over the course of the assay. Images were adjusted using Adobe Photoshop software version 8.0.

4.2.5 Cell treatments and Modified Pulse chase experiments

For modified pulse chase assays iGFP-Crb3a cells were grown on in 60 mm tissue culture dishes for 4 days until confluency. Inducible cells were treated with 50 ng/mL doxycycline (Clonetech) for 1 hour at 37 degrees for the pulse. After 1-hour doxycycline incubation, cells were washed three times with complete growth media to remove any remaining doxycycline. For the chase, inducible cells were allowed to incubate in complete growth media. Four hours post washout, all samples were washed again three times with complete growth media to remove any residual doxycycline. At prescribed times, inducible cells were harvested and lysed with denaturing lysis buffer for Western blot analysis. Control induction was obtained by treating samples with vehicle for the entire length of the experiment.

For modified pulse chase assays combined with induction of EMT, iGFP-Crb3a cells were grown on transwell filters (Corning) to confluence. Recombinant TGF-β (R&D Biosystems) was added to the lower chamber to a final concentration of 5 ng/mL. Cells were treated for 2 days, washed with PBS, and boosted with an additional treatment of TGF-β for another 2 days. After 4 days of treatment with TGF-β cells were began on the modified pulse chase assay as above in the presence of TGF-β.

4.2.6 Quantitative Western Blot Analysis

For quantification of Western blots, 50 ng of total protein lysate were run on a 10% Bis-Tris/MOPS SDS-PAGE gel and transferred to PVDF. Transfer efficiency was determined by Ponceau S staining. After transfer, membranes were blocked in 5% non-fat dry milk/TBS overnight. Primary antibodies for Crb3a and Actin were diluted for

blotting in 5% milk/0.05 Tween-20/TBS and membranes were probed for two hours at room temperature with rotation. After extensive washing with 0.05% Tween-20/TBS, far-red conjugated secondary antibodies against rabbit (emission 800 nm) and mouse (emission 680nm) (Lycor) were diluted 1:10,000 in 5% milk/0.05 Tween-20/TBS and incubated for 1 hour with rotation at room temperature protected from light. Following extensive washing with wash buffer, blots were imaged using the Licor Odyssey System. After imaging, data was analyzed using Licor ImageQuant software. Regions of interest (ROI) were determined by selecting the area of the predominant band corresponding to the respective antibody signal. The ROI was copied to maintain the area for subsequent analysis. Arbitrary units for each band corresponding to either Crb3a or actin were obtained using the established ROI. Data output is given as a ratio of the signal of Crb3a to actin, back corrected to remove background signal from non-induced samples. Data points were plotted on XY-scatter plots using Microsoft Excel software to determine trend lines. Half-lives were determined by calculating exponential decay from modified pulse chase assay ratios.

4.2.7 Biotinylation Assay

iGFP-Crb3a C36 cells were plated on 10 cm tissue culture plates and grown to confluency over 4 days. Cells were treated with 50 ng/mL doxycycline for 1 hr. then chased in regular media for 4 hr. to accumulate surface iGFP-Crb3a. Cell surface biotinylation was done with the Piecre-Thermo Cell Surface Biotinylation Kit. Briefly, after induction, iGFP-Crb3 C36 cells were washed twice with ice-cold PBS and then incubated with 0.25 mg/mL Sulfo-NHS-SS-Biotin in cold PBS for 30 min. After

incubation, cells were quenched as directed, washed 3x with ice-cold PBS, and incubated with complete growth media at 37 degrees at prescribed time points to facilitate uptake. After uptake, cells were washed once with PBS and then 4 x 15 minutes with MesNA buffer (50 mM MesNA, 150 mM NaCL, 1 mM EDTA, 0.02% Bovine Serum Albumin, 20 mM Tris-Cl, pH 8.6) to reduce any non-internalized biotin linkages. Cells were then lysed in and protected biotinylated protein was isolated using NeutrAvidin pulldown as directed by manufacturers protocol.

4.3 Results

4.3.1 Efficient repopulation of Crb3a in polarized MDCKII cells

Crb3a is localized to the apical surface of polarized epithelial cells and essential for cell polarity (170, 235, 272, 296). We were interested in monitoring the production and trafficking of Crb3a vesicles in an effort to understand how Crb3a helps maintain cell polarity. To visualize Crb3a vesicles in MDCKII cells, we used the irreversibly photoswitchable protein Dendra2 (Den2) fused in frame into the Crb3a (Den2-Crb3a) extracellular domain. We tested Den2-Crb3a fusion constructs for functionality by confocal microscopy and Western blot and determined that Den2-Crb3a functioned and localized normally in MDCKII cells (Figure 4-1A). To monitor movement of Den2-Crb3a containing vesicles we used the photoswitchable properties of Den2 to monitor the accumulation of newly synthesized Den2-Crb3a. Using live cell imaging, we obtained pre-activation micrographs and then photoswitched Den2-Crb3a by activation with UV light for 1

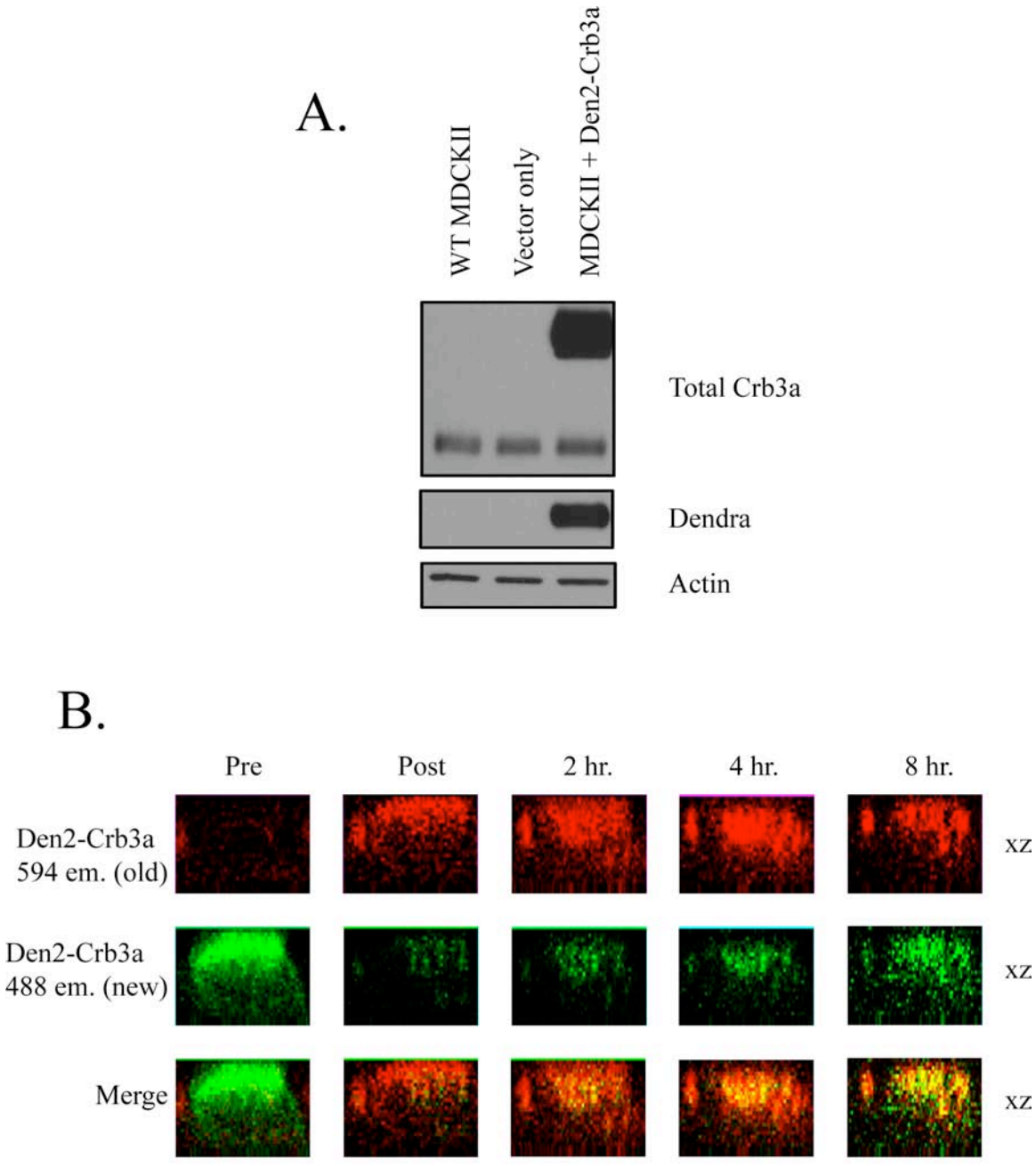

Figure 4-1: Expression and tracking of Den2-Crb3a in MDCKII cells. (A). Den2-Crb3a was stabily expressed in MDCKII cells. (B). XZ image series of a single cell expressing Den2-Crb3a. After 1 minute of activation with UV light, newly synthesized Den-Crb3a (green) was followed for 8 hr. using live cell imageing.

minute. Micrographs were taken to monitor the appearance of green color by excitation at 488nm Den2-Crb3a by taking confocal Z-stacks every 60 minutes. Theoretically, any red signal (excitation 594nm) present at time-0 represents converted Den2-Crb3a, or the pool of Den2-Crb3a present in the cell at time of activation. Conversely, any green signal obtained post activation hypothetically represents Den2-Crb3a newly synthesized. We observed significant green Den2-Crb3a signal within 60 minutes post conversion (Figure 4-1B). We saw a continuous increase in green signal from Den2-Crb3a, and by 4 hours post conversion we observed green signal from newly synthesized Den2-Crb3a had localized either at or near the apical surface and was similar intensity to the residual red signal. Although there are technical limitations to monitoring movement of Den2-Crb3a (see discussion section 4.4), we were able to conclude that the synthesis and movement of Crb3a in MDCKII cells is a rapid event and that MDCKII cells are repopulated with Crb3a within 60 minutes.

4.3.2 Inducible GFP-Crb3a system

To be able to monitor the production of a limited pool of cellular Crb3a in MDCKII cells, we constructed MDCKII cells stably expressing a tetracycline inducible (Tet-On) version of mEGFP-Crb3a (iGFP-Crb3a). We stably expressed iGFP-Crb3a in MDCKII cells picked clones and based on their ability to produce iGFP-Crb3a when treated with doxycycline compared to the same clone induced with vehicle alone. Of the clones picked, clone-36 (iGFP-Crb3a C36) appeared to have the best induction when compared to vehicle induced and was used for the majority of experiments. To optimize experimental procedures, iGFP-Crb3a C36 was used to titrate both the concentration of

doxycycline and the length of time for doxycycline treatment (Figure 4-2A). Experimentally, the optimal concentration of doxycycline was determined to be 50 ng/mL with a treatment time of 1 hour. Using these conditions, we performed time course studies on both transcript and protein levels of iGFP-Crb3a C36.

Using quantitative real-time PCR (qRT-PCR) the mRNA specific for of iGFP-Crb3a rose quickly at 0 hours post induction and declined to nearly background levels at 6 hours post induction (Figure 4-2C). The protein levels of iGFP-Crb3a C36 peaked at 4 to 6 hours post induction and by 24 hours post induction these levels appeared to return to baseline. Additionally, iGFP-Crb3a C36 were visualized using confocal microscopy to determine any effect of induction on the morphology of MDCKII cells. Morphology of iGFP-Crb3a C36 cells was determined to normal after induction conditions Figure 4-2B). We refer to this method as a modified pulse chase assay where iGFP-Crb3a C36 is produced in limited quantity to track Crb3a production.

Western blots show iGFP-Crb3a as a series of 3 distinct bands. The two bands of the highest molecular weight are the major products of iGFP-Crb3a induction and appeared as a doublet. Deglycosylation assays were performed on these cells to determine post-translational modifications (PTMs). The mEGFP-Crb3a doublet is a result of multiple N and O-linked glycosylations (Figure 4-3). We could not determine the specific identity of these glycosylated forms, however the highest molecular weight species of iGFP-Crb3a is the most highly N and O-glycosylated, leading us to believe that this band represents the most mature form of the protein, localized on the apical surface and not in a subcellular compartment.

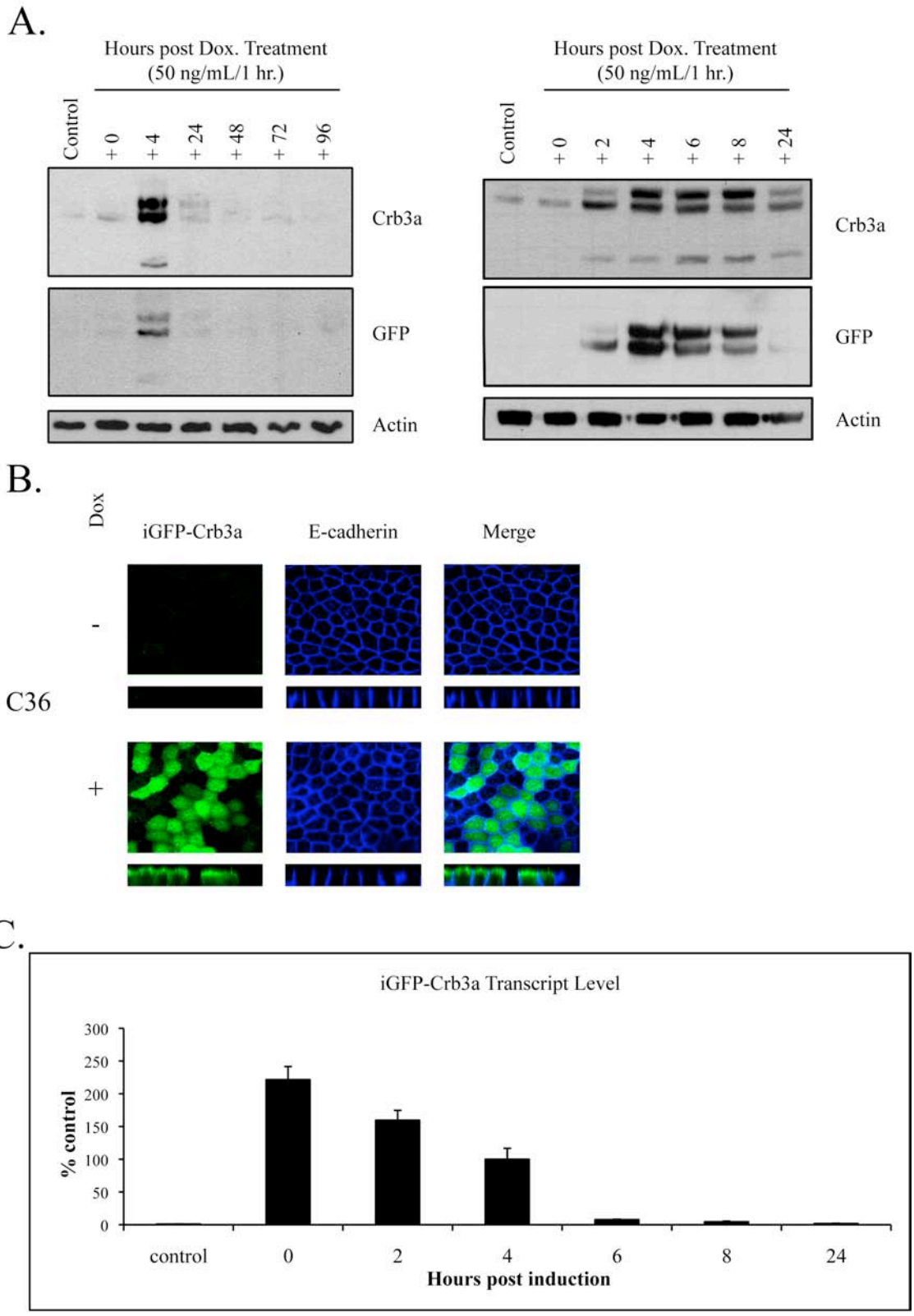

Figure 4-2: The iGFP-Crb3a sytem. (A) Western blot time course. (B) IF +/- 50ng/mL doxycycline (C) qRT-PCR of specific *H.s.* mEGFP-Crb3a.

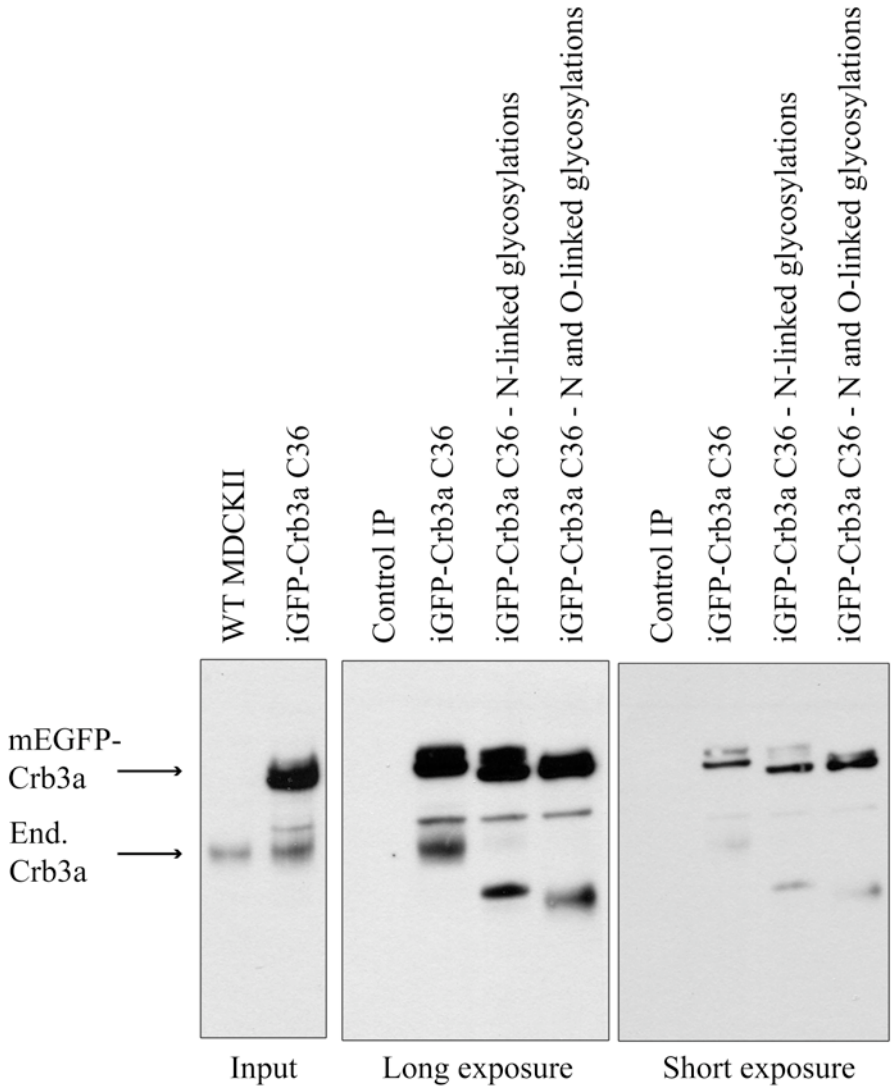

Figure 4-3: N and O-linked glycosylation of Crb3a. Both endogenous Crb3a and mEGFP-Crb3a are both highly modified proteins.

4.3.3 GFP-Crb3a is not recycled in G_0 phase MDCKII cells

Crb3a traverses a Rab11a-postive ARE during exocytosis to the apical surface in MDCKII cells (246). Our previous assays however, do not address the role of endocytosis in Crb3a recycling. In lumen formation studies, Rab11a-DN cells had exocytic defects but not defects in endocytosis but clearly mEGFP-Crb3a protein likely undergoes recycling during lumen formation. We preformed experiments to determine under what conditions apical recycling occurs. Since our previous lumen formation experiments (see Appendix B) involved the transition between a non-polarized cell to two polarized daughter cells, we examined if the presence of an apical surface and/or mitosis influence the recycling of iGFP-Crb3a. Single MDCKII cells will adhere to glass coverslips and since they lack any cell-to-cell contacts they will not form junctions and express Crb3a on the entire plasma membrane. To understand what conditions iGFP-Crb3a is recycled, we preformed modified pulse chase/antibody uptake on sub-confluent iGFP-Crb3a C36 cells in the presence or absence of serum. GFP antibody uptake illustrated that in serum free conditions where cell are not actively dividing there is limited internalization of surface iGFP-Crb3a, and GFP antibody never reached a Rab11 positive endosome (Figure 4-4 top). The only instance where we see appreciable internalization of the GFP antibody is when subconfluent cells are allowed to divide and migrate when incubated in complete growth medium containing the full compliment of serum (Figure 4-4 bottom). We also tested whether surface expressed iGFP-Crb3a endocytosis and recycling into Rab11 positive compartments was a result of neighboring cells forming junctions by performing the same experiment in medium depleted in

calcium since by depleting calcium cells will divide but not form junctions (Figure 4-4 second from bottom). Similarly, we found that in low calcium media surface GFP antibody staining could be seen in a Rab11 positive compartment suggesting that during sub-confluency where cells are actively dividing before establishing apical surfaces, does Crb3a get efficiently recycled into Rab11 positive endosomes.

In fully polarized monolayers, MDCKII cells are undergoing minimal mitosis (G_0 phase) similar to single cells in serum free media, however these cells have a fully established apical surface. To determine if the presence of an apical membrane affects the apical recycling of surface Crb3a once cells have polarized, fully confluent transwell-filters of iGFP-Crb3a C36 cells were subject to modified pulse chase assay and then incubated in media containing antibody against the extracellular GFP-tag as above.

After allowing for uptake by incubation at 37 degrees for 2 hr., filters were stained for internalized and protected GFP-antibody. At no time did we see any appreciable internalization, protection, or recycling of GFP-antibody as evidenced by co-stain with pan-Rab11 antibody (Figure 4-5A). To further examine if surface iGFP-Crb3a is internalized and recycled we subjected fully polarized monolayers to surface biotinylation assay. Fully polarized iGFP-Crb3a C36 cells were subject to modified pulse chase, surface labeled with biotin, and incubated for prescribed times at 37 degrees to allow for endocytosis. Internalized iGFP-Crb3a was analyzed by neutravidin pulldown and Western blot. To our surprise, there was very little protection of biotinylated iGFP-Crb3a over the course of the experiment (Figure 4-5B). Additionally, the small amount of biotin-iGFP-Crb3a complexes that did get internalized, cell surface biotinylation and

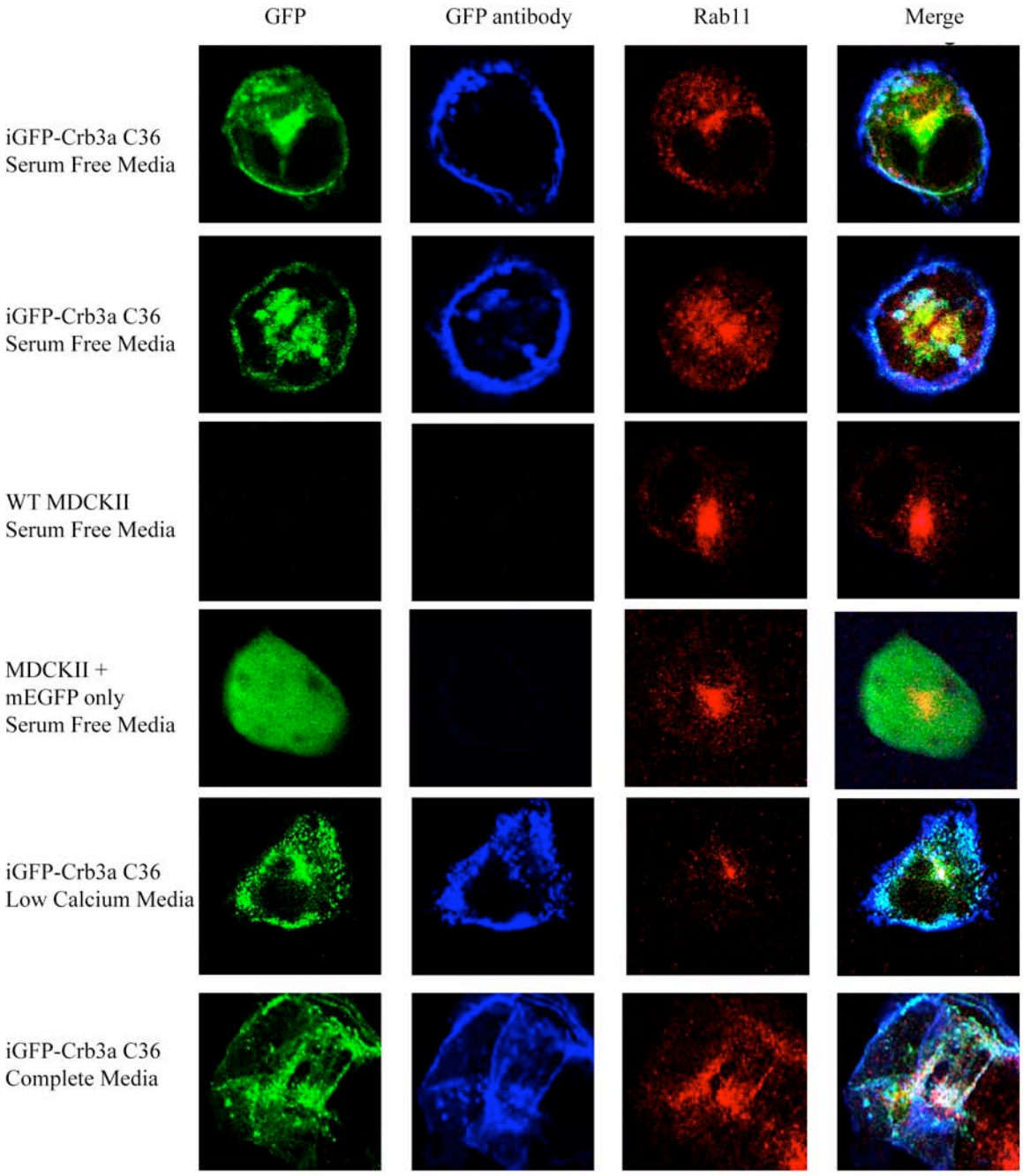

Figure 4-4: GFP-antibody uptake in single cells. Single cells were plated in on coverslips and incubated with media containing GFP-antibody. After 2 hr. incubation cells were fixed and stained for internalized GFP-antibody. Only in conditions where cells were allowed to divide (in low calcium or complete media) do we find uptake of GFP-antibody into a Rab11-positive endosome.

pulldown appeared to only isolate the upper band of the mEGFP-Crb3a doublet confirming our previous observation that the upper band represents the mature surface form of the protein. Combined with our previous results, our data suggests that surface Crb3a undergoes altered endocytosis and bypasses the apical recycling pathway once epithelial cells have established apical surfaces.

4.3.4 GFP-Crb3a can be isolated from tissue culture media

Transmembrane surface proteins must be endocytosed and then degraded for signal attenuation (136). In the case of Crb3a, protein levels must be carefully controlled to prevent overgrowth (235). Since surface labeled Crb3a was not significantly internalized and protected via antibody uptake or biotinylation, we asked the question as to how the cell is preventing an accumulation of surface Crb3a. To first approach this question, we incubated mEGFP-Crb3a expressing cells in with either bafilomycin to block lysosome function or MG132 to suppress proteosome function. Treatments with both drugs were able to stabilize Crb3a in cells (Figure 4-6). It has been reported that however, that introduction of pharmacological inhibitors to interrupt proteosome can block total protein degradation because an intact proteosome pathway is needed for lysosome-mediated degradation (140, 164). Apical transmembrane proteins may also be degraded through the multivesicular body (MVB) pathway. In this pathway, exosomes are expelled into the luminal space of an organ or into the media of cultured cells (48). Using iGFP-Crb3a C36 cells, we treated cells in serum free media with doxycycline and allowed exosomes to accumulate in the media (Figure 4-7). Using either ultracentrifugation or standard immunoprecipitation, we were able to detect iGFP-Crb3a

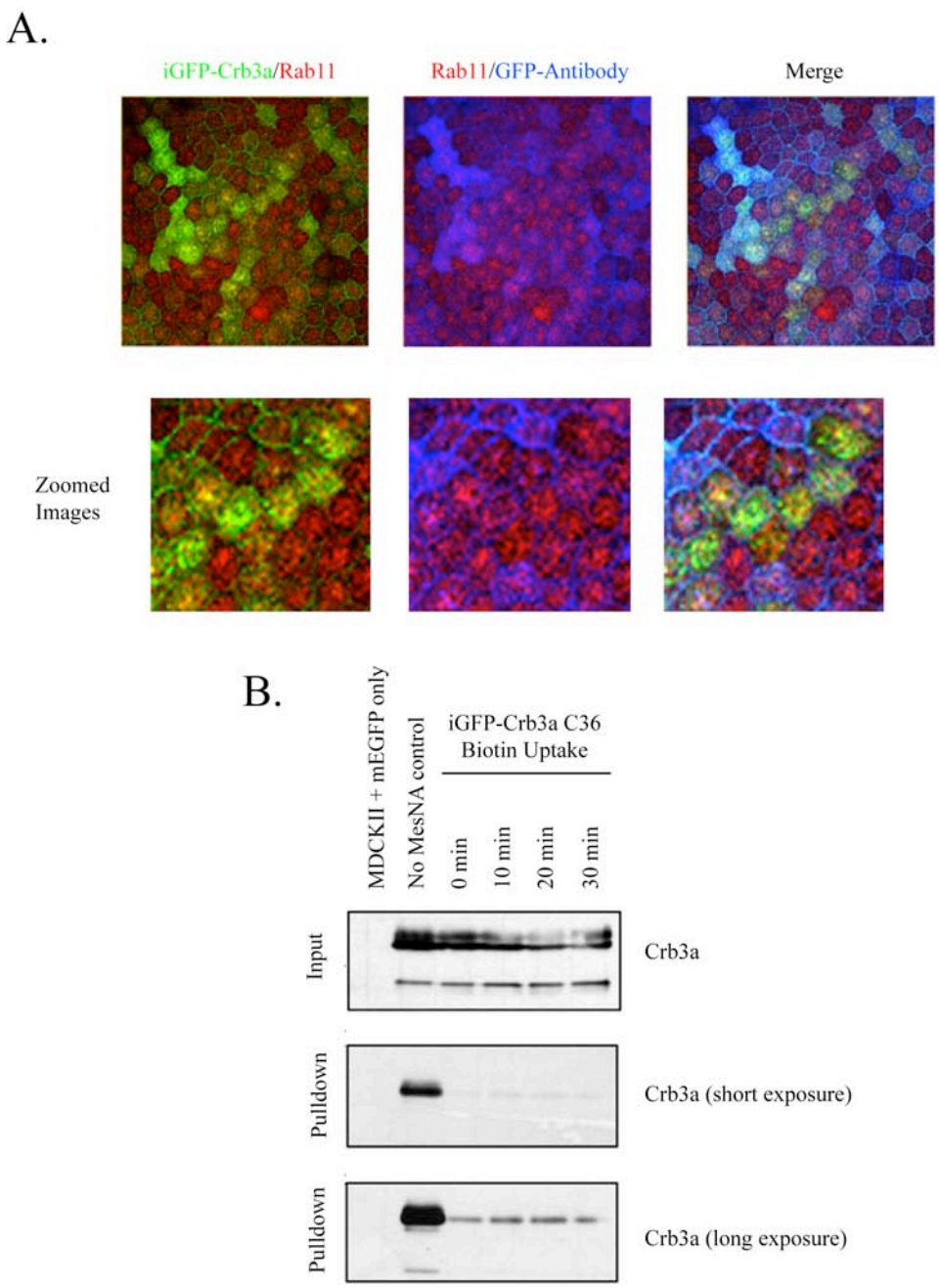

Figure 4-5: Endocytosis of iGFP-Crb3a in fully polarized monolayers. (A) GFP-antibody uptake experiments on fully formed monolayers illustrated no overlap between Rab11 and GFP-antibody indicating iGFP-Crb3a bypasses the apical recycling system. (B) Biotinylation of iGFP-Crb3a. Surface iGFP-Crb3a is not internalized and protected.

and in tissue culture supernatant. These results suggest that Crb3a may be removed from polarized MDCKII cells via dispersion into the media or luminal fluid.

4.3.5 TSG101 knockdown increases Crb3a protein levels

We next chose to investigate if the MVB pathway has a role in the regulation of Crb3a with regards to managing epithelial morphology. Tumor susceptibility gene 101 (TSG101, also Vps23) is a member of the ESCRT-I complex and implicated in MVB biogenesis (135). Short hairpin RNAs against TSG101 were transduced into MDCKII cells to determine the affect of the MVB pathway on the trafficking of endogenous Crb3a. TSG101 shRNA cells had no obvious defects in epithelial polarization of wild type MDCKII cells as they continued to form tight junctions and apical membranes in confluent monolayers. We did find differences in protein expression however. In TSG101 knockdown MDCKII cells we noted an increase in protein levels of the polarity proteins Crb3a and Par6B, while a decrease in the protein levels of the polarity kinase aPKCζ (Figure 4-8A). To rule out the possibility that TSG101 knockdown leads to an increase in endogenous Crb3a protein by increased transcription of the *Crb3* gene, we preformed qRT-PCR experiments to monitor Crb3a mRNA. Using validated primer sets specific for canine Crb3a mRNA we determined the increase in Crb3a protein was not a result of increased transcription but most likely due to accumulation of Crb3a protein (Figure 4-8B).

Notably, knockdown of TSG101 did not affect the ability of MDCKII cells to form cysts with a solitary hollow lumen. However, in TSG101 shRNA cells we saw and accumulation of cytosolic and sub-apical endogenous Crb3a when compared to control

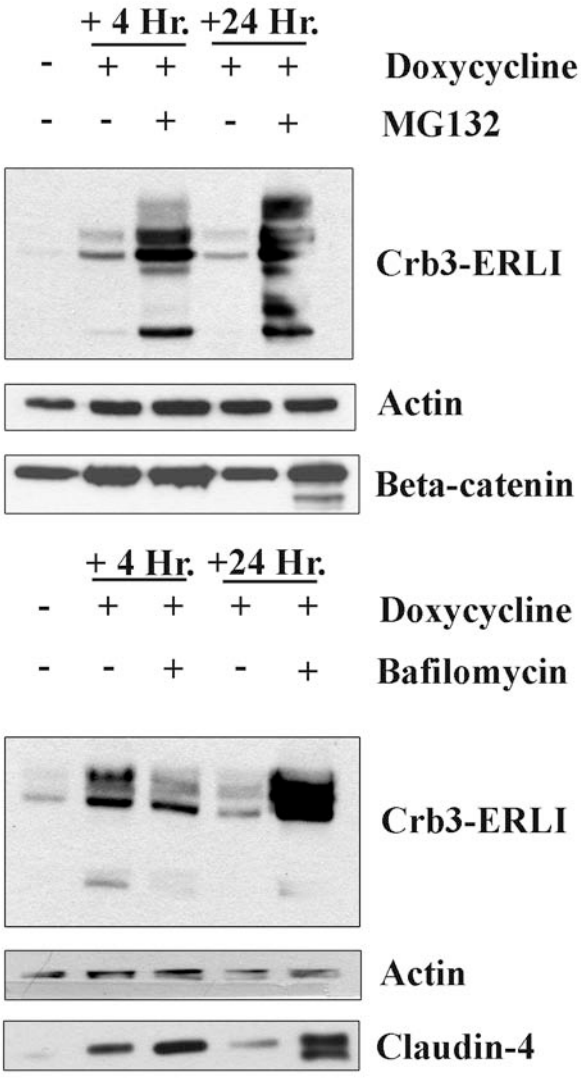

Figure 4-6: Pharmacological inhibition of Crb3a degradation. Top: Crb3a degradation is blocked by the the proteosomal inhibitor MG132. Bottom: Crb3a degradation is inhibited by the lysosomal inhibitor Bafilomycin.

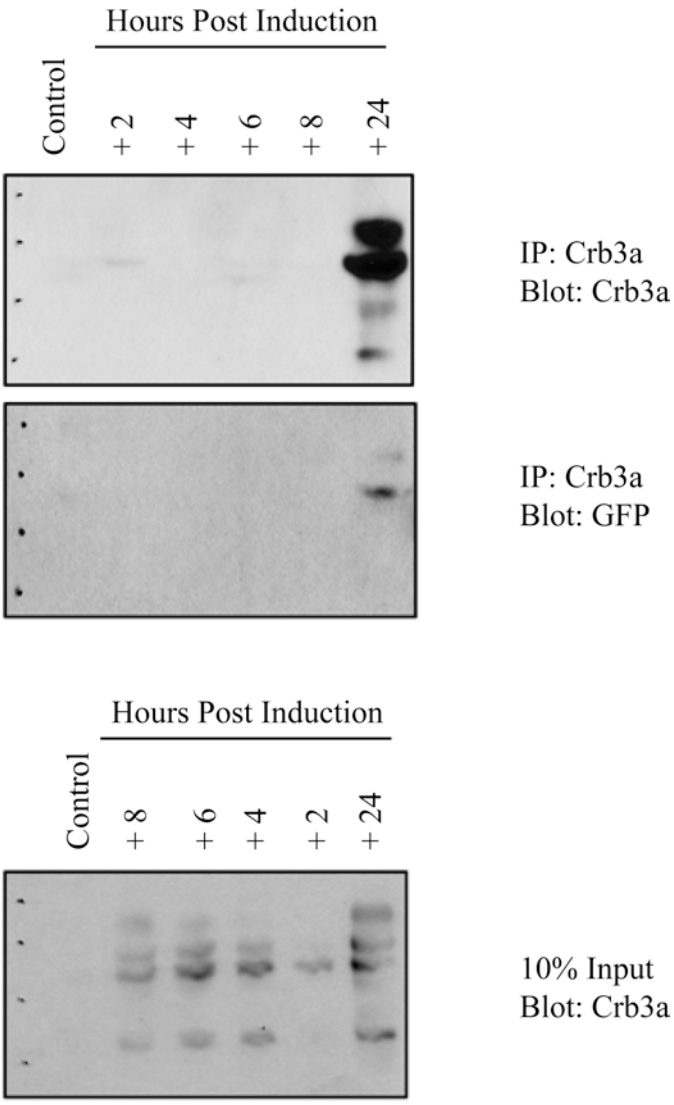

Figure 4-7: iGFP-Crb3a isolated for tissue culture media. After induction with doxycycline, iGFP-Crb3a can be immunoprecipitated from pre-cleared tissue culture media.

cells (Figure 4-9A). There were no appreciable differences in amount or localization of Par6B or aPKCζ however (Figure 4-9A). These findings were recapitulated in two different TSG101 shRNA clones using two different short hairpins. TSG101 knockdown also affects number and structure of EEA1 positive AEEs in cells (136). In our system, we also observed and increase in number and size of AEEs suggesting that endosome trafficking was disrupted in TSG101 knockdown cells. Also using three-dimesional models we wanted to observe if knockdown of TSG101 affected lumen formation through endocytosis. In the lumen formation assay, TSG101 shRNA cells did not have defects in lumen formation. However, lumens between two TSG101 shRNA cells appeared to be larger and there is a larger population of cytosolic Crb3a than in control cells (Figure 4-10). We also chose to investigate the affects of TSG101 knockdown on MDCKII cells in 12-day old cysts. It has recently been reported that disruption of TSG101 in certain tissues can lead to neoplastic tumor growth due to cellular overgrowth (79) (192). We grew cysts in geltrex for 12 days and stained them for endogenous Crb3a and monitored the cysts for overgrowth phenotypes. To our surprise, TSG101 shRNA cells continued to form complete and normal lumens (Figure 4-9A). When we took our short hairpins against TSG101 and infected them into cells expressing low levels of mEGFP-Crb3a cells we observed notable differences in cell morphology. In mEGFP-Crb3a/Control shRNA monolayers, we relatively flat cells with no discernable morphological changes. When mEGFP-Crb3a/TSG101 shRNA cells were grown as monolayers, we observed phenotypes consistent with Crb3a overexpressing including doming and expanded apical surfaces. We also observed the same morphological changes in preliminary experiments involving iGFP-Crb3a C36 cells combined with

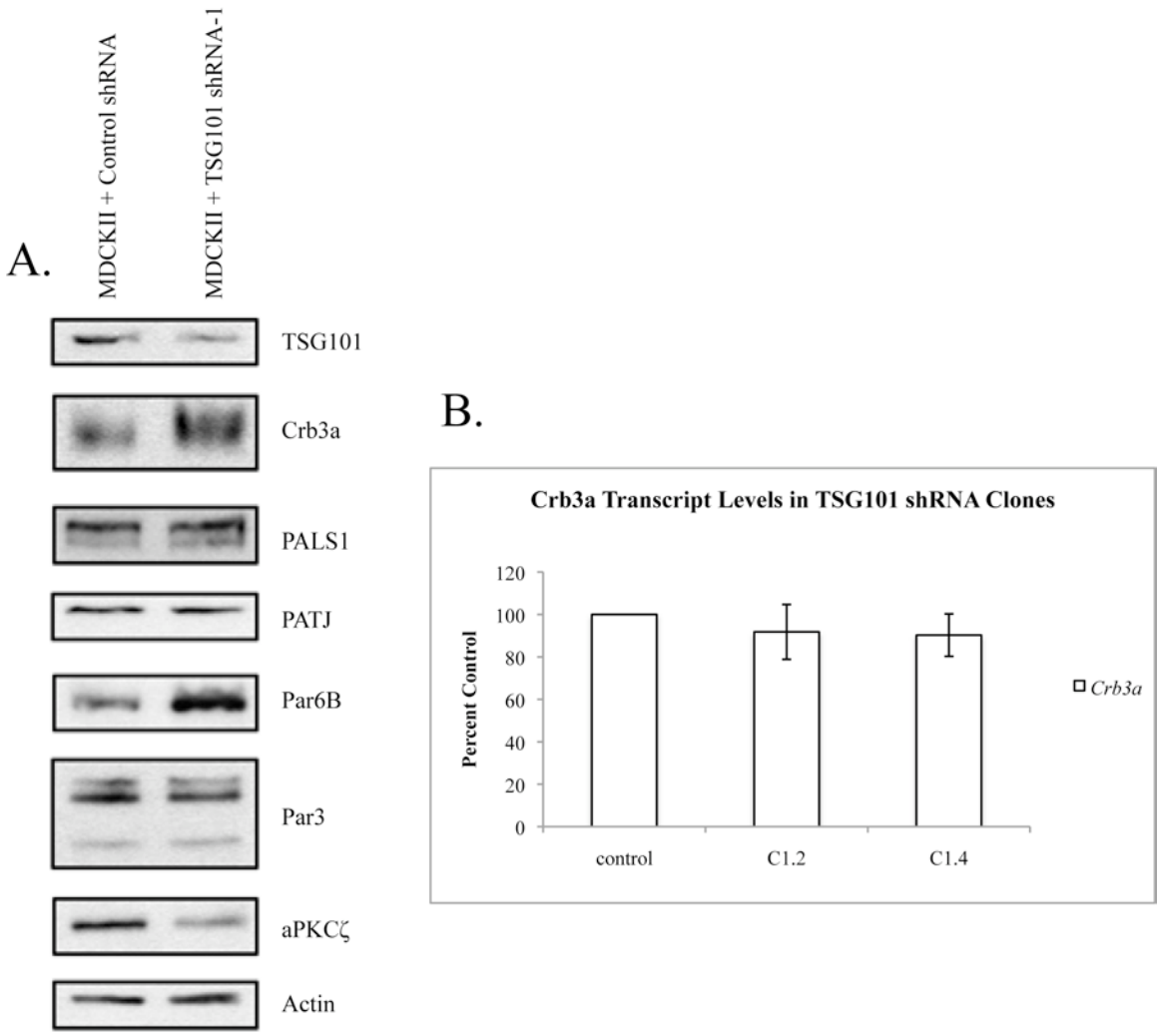

Figure 4-8: Knockdown of TSG101 is MDCKII cells. (A) Western blot of Crumbs and Par polarity complex proteins in TSG101 shRNA cells. (B) qRT-PCR of the Crb3a transcript in TSG101 shRNA cells indicating that the Crb3a protein increase is due to protein retention and not increased transcription.

TSG101 shRNAs (Figure 4-11). In cysts expressing iGFP-Crb3a with control shRNAs we found that when we expressed high levels of iGFP-Crb3a by induction with doxycycline, these cysts still maintained single large lumens. However, when we combined iGFP-Crb3a C36 cells with TSG101 shRNAs, we found cysts with invaded lumens. It also appeared that the iGFP-Crb3a C36/TSG101 shRNA cells had lost the ability to maintain their mitotic plane as perpendicular to the apical membrane. Additionally, when monitored by Western blot, overexpession of iGFP-Crb3a was enough to overcome TSG101 repression by the introduced shRNAs. Again, these results are preliminary and we are currently verifying these observations.

4.3.6 GFP-Crb3a Half-life is independent of epithelial morphology

Crb3a is a tightly regulated protein and we had previously determined that the trafficking and apical recycling of Crb3a is dependent on the presence of an established apical surface, we hypothesized that disruption of the apical surface should affect the ability of the cell to regulate Crb3a. To address this issue we wanted to determine the biological half-life of Crb3a in both polarized and non-polarized MDCKII cells to determine the relationship between trafficking of Crb3a to an established apical surface and the regulation of Crb3a protein. Due to technical limitations regarding the Crb3a protein (see discussion section 4.4), we chose to utilize our iGFP-Crb3a system to monitor the half-life of Crb3a protein. To study the half-life of Crb3a in polarized and non-polarized conditions we transduced iGFP-Crb3a C36 cells with the transcription factor Snail-Flag (Figure 4-12). Snail is a potent repressor of the endogenous *Crb3* gene

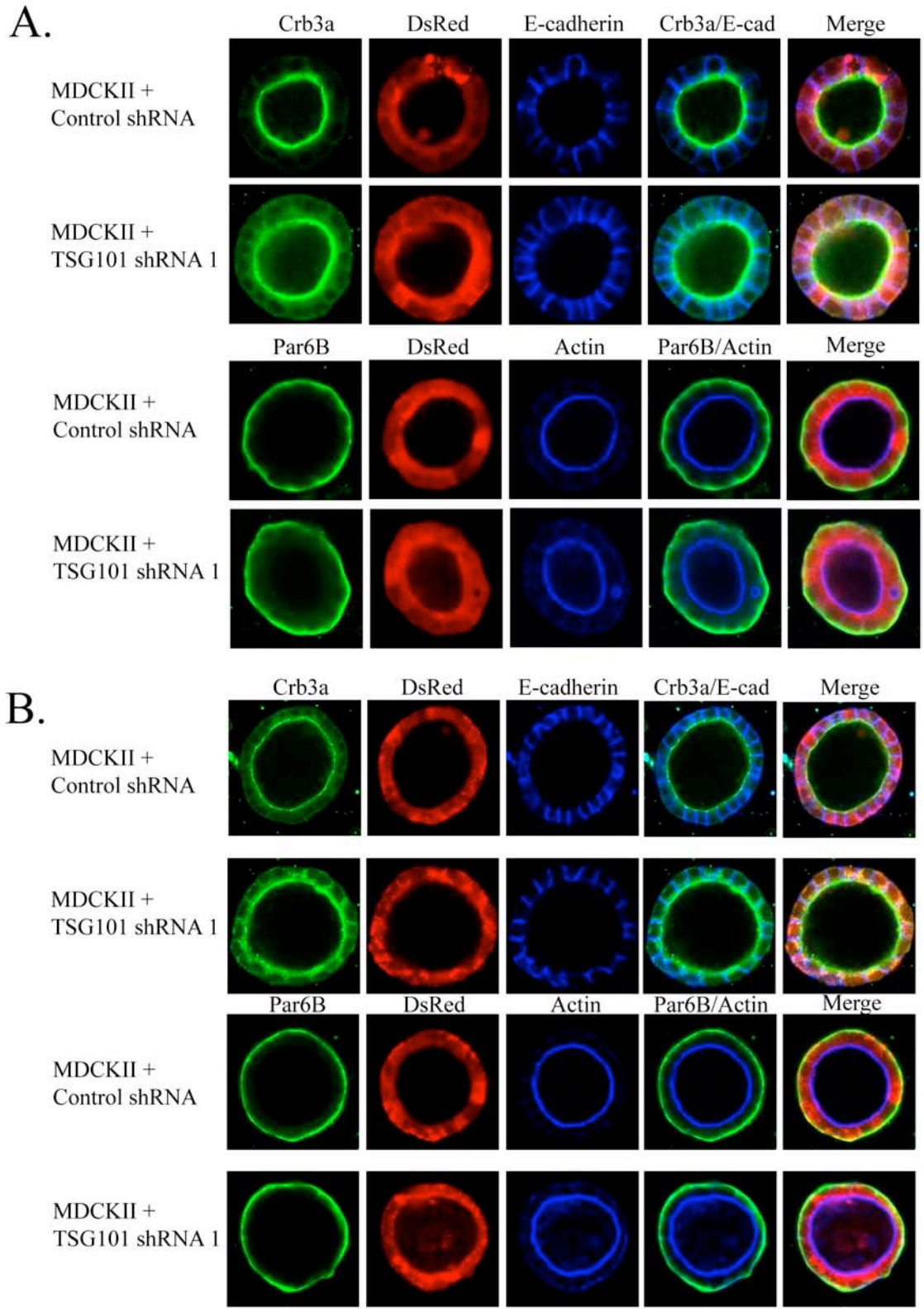

Figure 4-9: 6 and 12 day-old TSG101 shRNA 1 cysts. Note the increase in endogenous Crb3a.

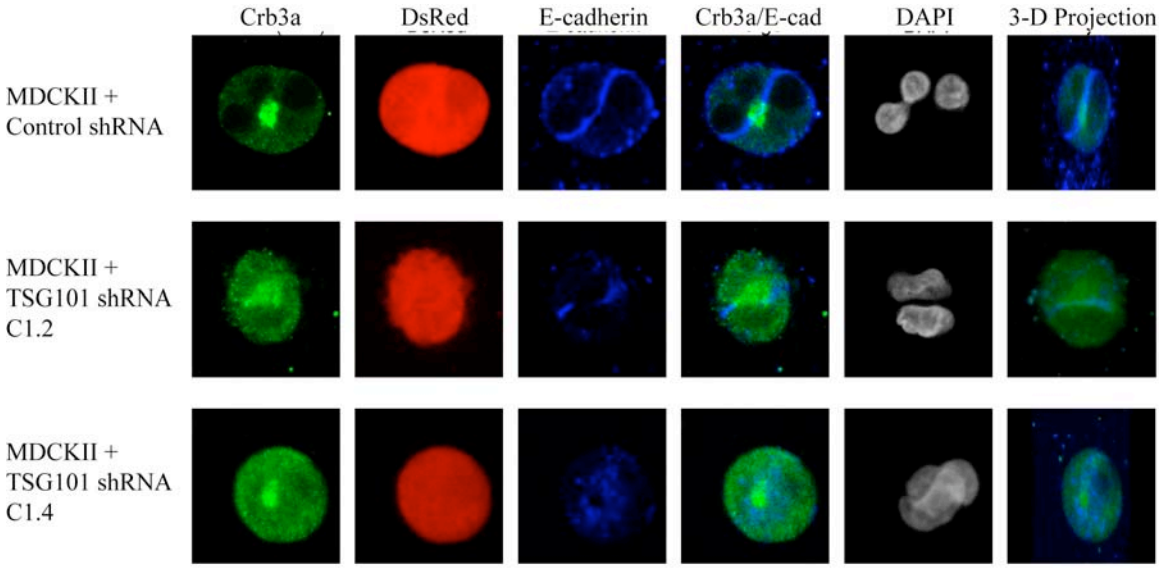

Figure 4-10: 2-cell stage of TSG101 shRNA cells. TSG101 shRNA cells were used in a lumen formation assay to for lumen formation of mitotic defects.

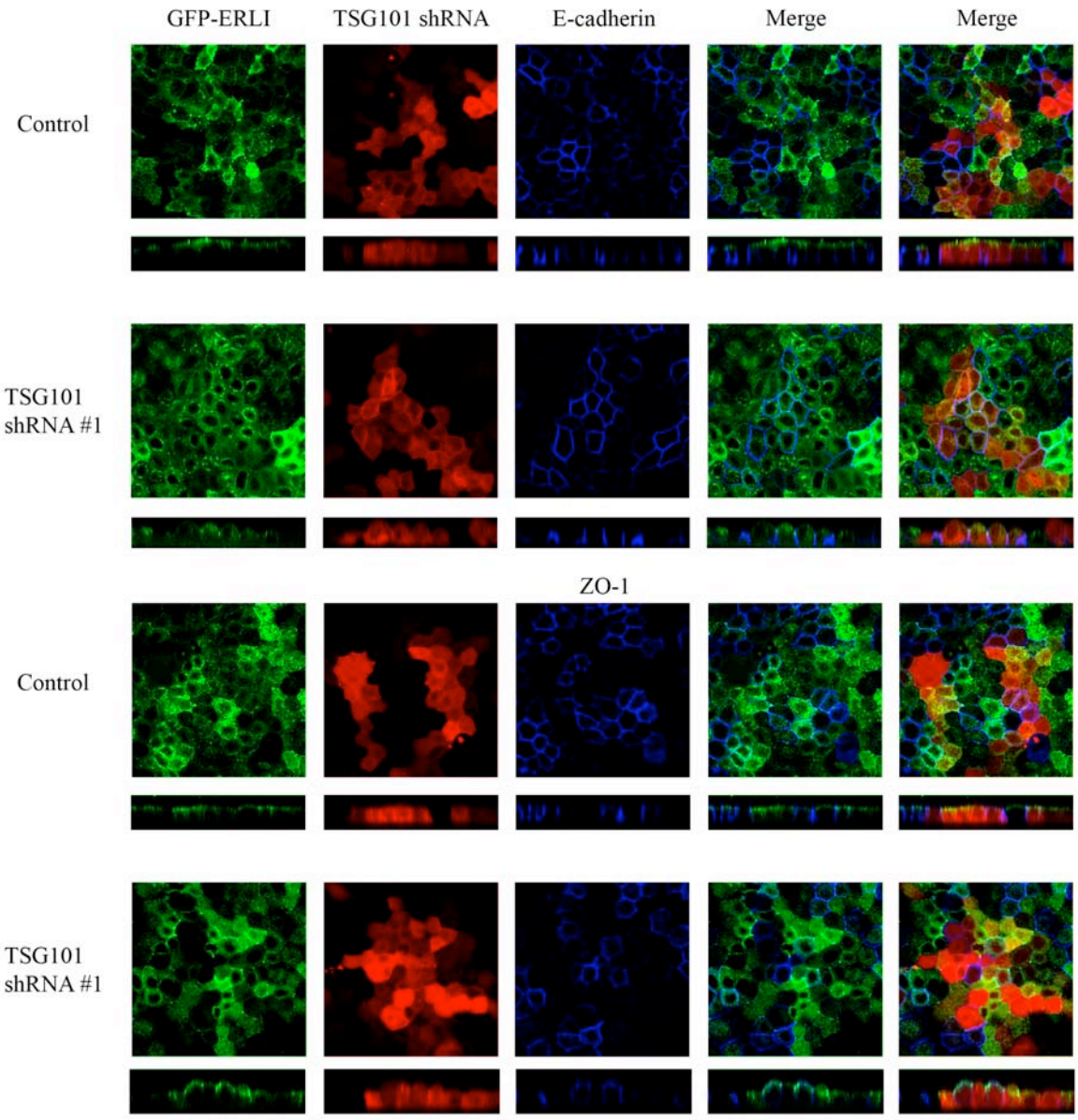

Figure 4-11: TSG101 shRNA in mEGFP-Crb3a cells. TSG101 shRNA-1 was expressed in MDCKII cells moderately overexpressing mEGFP-Crb3a. The combination of TSG101 knockdown with Crb3a overexpression leads to epithelial morphology defects.

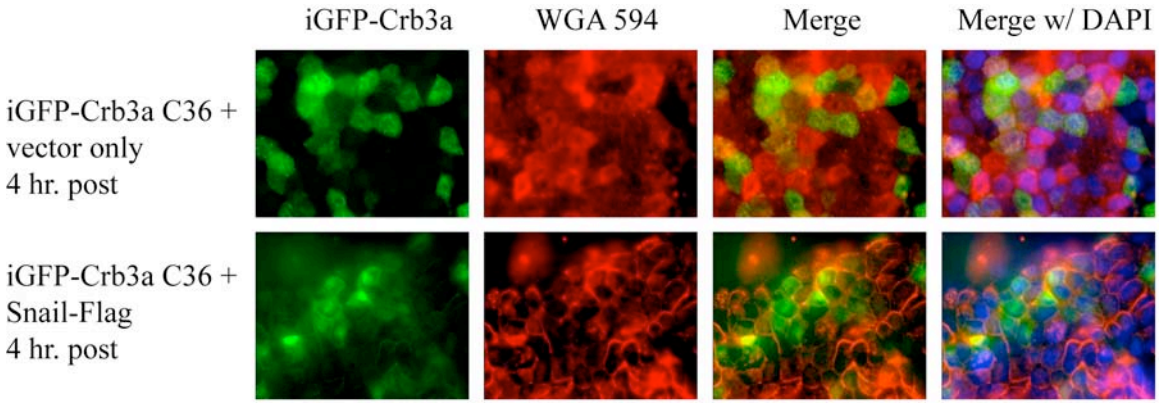

Figure 4-12: iGFP-Crb3a cells expressing Snail-Flag. iGFP-Crb3a cells were transduced with Snail-flag to disrupt polarity. iGFP-Crb3a cells continued to express iGFP-Crb3a on the surface.

and expression of Snail will cause a loss of epithelial phenotypes including formation of distinct apical surfaces through epithelial to mesenchymal transition (294). Additionally, Snail expression would not affect our exogenous iGFP-Crb3a promoter allowing us to monitor the cells ability to degrade protein in a non-polarized cell (Figure 4-13A). When we used a modified pulse chase assay with iGFP-Crb3a C36/control vector and iGFP-Crb3a C36/Snail-Flag cells we surprisingly discovered no difference in iGFP-Crb3a protein levels between experimental and control cells, and the half-life of iGFP-Crb3a protein in both conditions was 3 - 5 hours (Figure 4-13B). To rule out that our findings were a result of Snail-flag overexpression, we chose to conduct the same experiment again, this time treating the cells with TGF-β (Figure 4-14A). TGF-β is a known inducer of EMT in cells, ultimately leading to an upregulation in endogenous Snail (303). After four days of vehicle or TGF-β treatment, iGFP-Crb3a C36 cells were again subjected to modified pulse chase assay. These results demonstrated that iGFP-Crb3a had a biological half-life of 4-6 hours (Figure 4-14B).

Although there was no change in the biological half-life of Crb3a during the series of modified pulse chase experiments, there were differences in the iGFP-Crb3a protein profiles as shown by Western blot. The iGFP-Crb3a C36 cells show a robust series of bands that are positive for Crb3a on Western blot corresponding to the predicted molecular weight of Crb3a with a mEGFP tag. The highest molecular weights of mEGFP-Crb3a run as a doublet, and this doublet has been identified to be heavily modified by both N and O linked glycosylations presumably amplified due to the presence of a large extracellular mGFP-epitope. Upon analysis of the iGFP-Crb3a doublet via quantitative Western blot, we determined that although the intensities for the

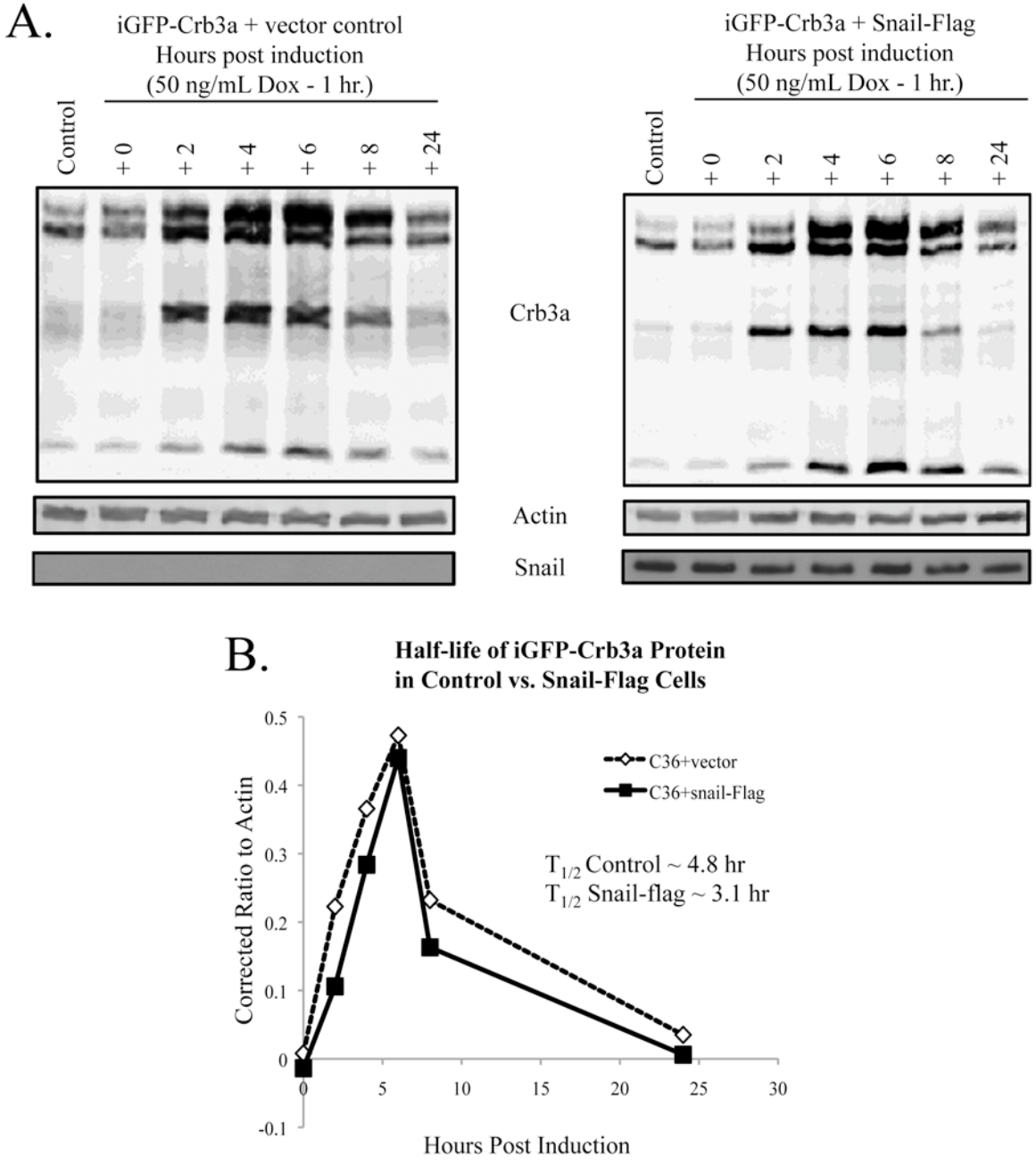

Figure 4-13: The half-life if iGFP-Crb3a. (A) The half-life of iGFP-Crb3a was determined by modified pulse chase assay followed by quantitative Western blot. (B) Half-life was determined by estimating the exponential decay of to ratio of iGFP-Crb3a to actin.

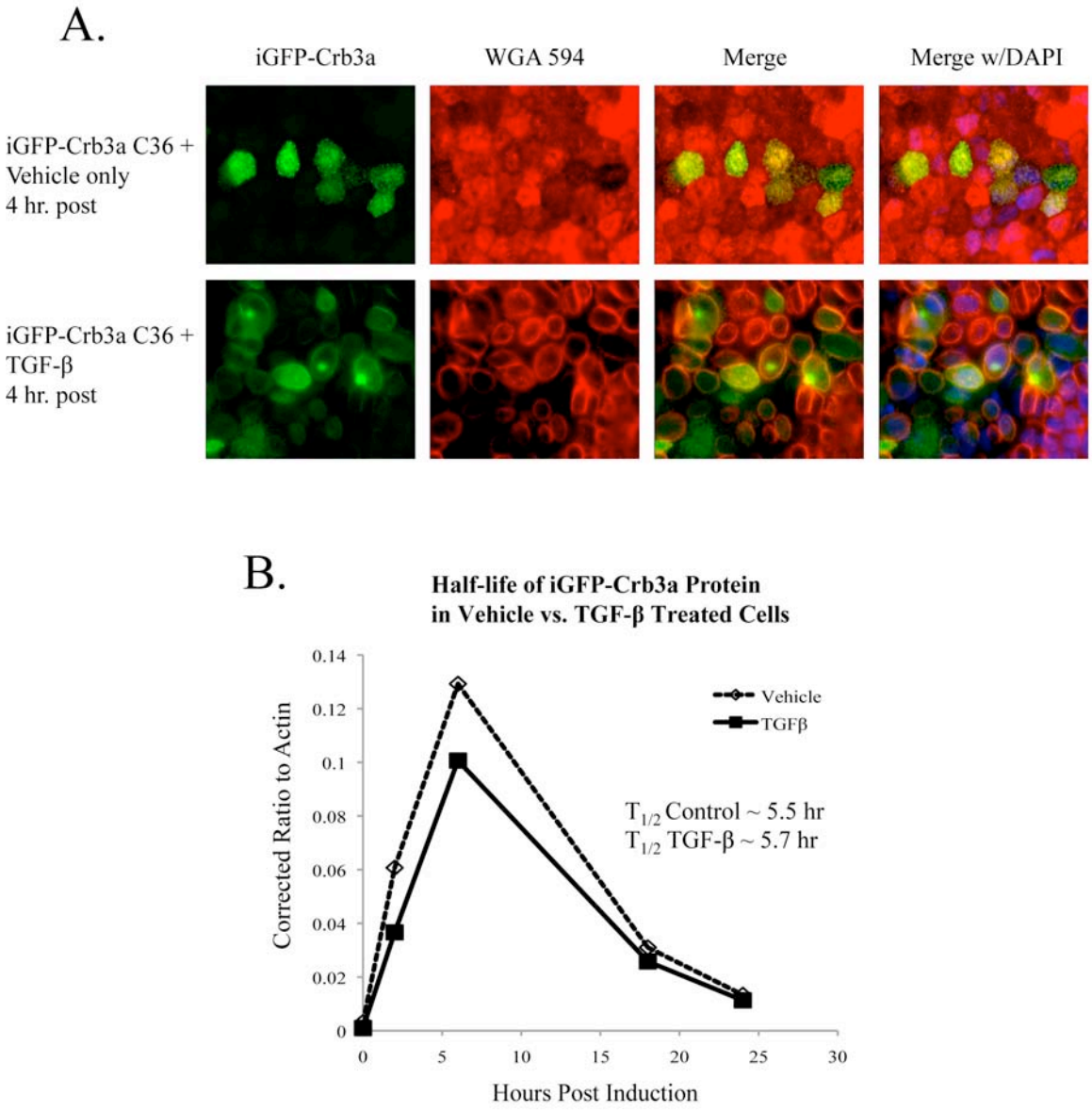

Figure 4-14: Half-life of iGFP-Crb3a with TGF-β. (A) Morphology of iGFP-Crb3a C36 cells +/- TGF-β treatment. (B) Half-life of iGFP-Crb3a using modified pulse chase assay and quantitative Western blot analysis.

A.

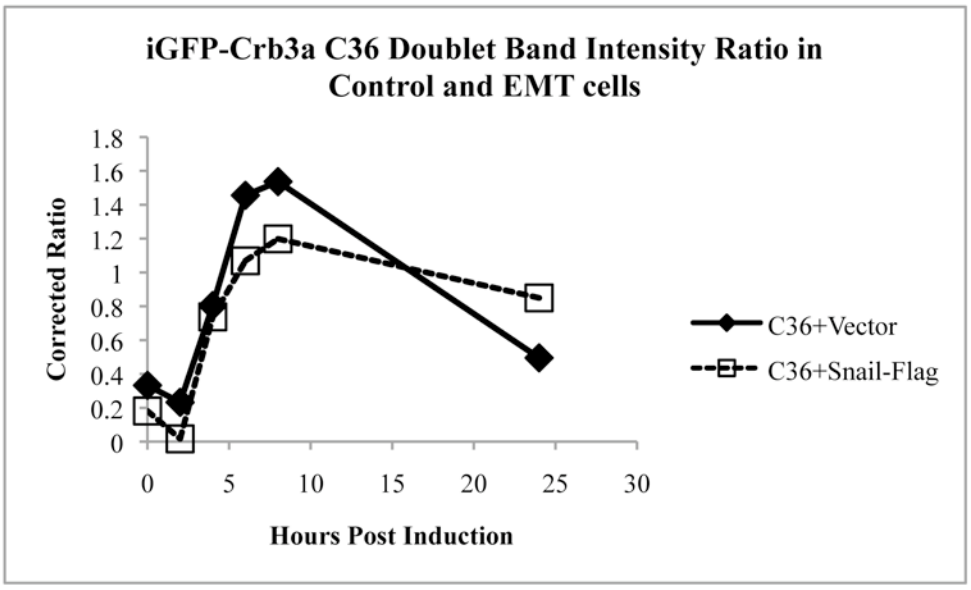

B.

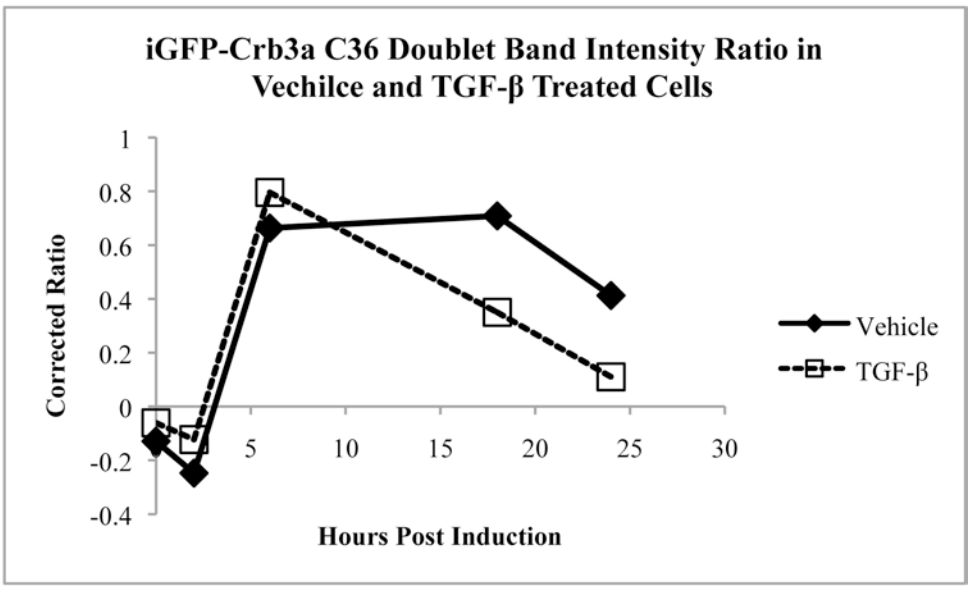

Figure 4-15: Apical identity and the maturation of iGFP-Crb3a. (A) in iGFP-Crb3a C36 cells surface Crb3a is in a ratio with immature Crb3a of 3:2. In iGFP-Crb3a C36/Snail-flag cells, the ratio is 1:1. (B) In TGF-β treated cells the ratios are similar suggesting the presence of an apical surface affects maturation and trafficking of Crb3a.

combined doublet did not change when compared to control cells, there was a difference in the intensities of the individual single bands making up the iGFP-Crb3a doublet and ratios of the doublet bands to each other were different in EMT cells versus control cells(Figure 4-15). In control cells the ratio of upper band to lower band was 3:2, suggesting an increase the more heavily glycosylated form of Crb3a. In EMT cells, the ratio of bands in the doublet was 1:1, suggesting and equal distribution between modified forms of Crb3a. Taken together, our results suggest that during steady state and EMT state, the biological half-life of mEGFP-Crb3a is approximately 3-6 hours and this does not change regardless of cellular context. There seems to be, however, a difference in the maturation and processing of Crb3a during EMT, and the maturation is dependent on the absence or presence of an apical surface.

4.3.7 Crb3a lateral mobility as measured by FRAP is constant regardless of cellular localization

Although the half-life of Crb3a did not change in each condition tested, we did note that turnover of Crb3a is high in MDCKII cells. All our previous data point to Crb3a being dynamic in polarized epithelia. To assess the dynamics and mobility of Crb3a, mEGFP-Crb3a was expressed in MDCKII cells and used for fluorescence recovery after photobleaching (FRAP). Using FRAP we completed comparative mobility analysis of Crb3a localized the apical surface and the tight junction. FRAP against either the apical surface or the junction of polarized mEGFP-Crb3a cells determined that there was no difference in the mobility of Crb3a (Figure 4-16). Apical recovery half-life was

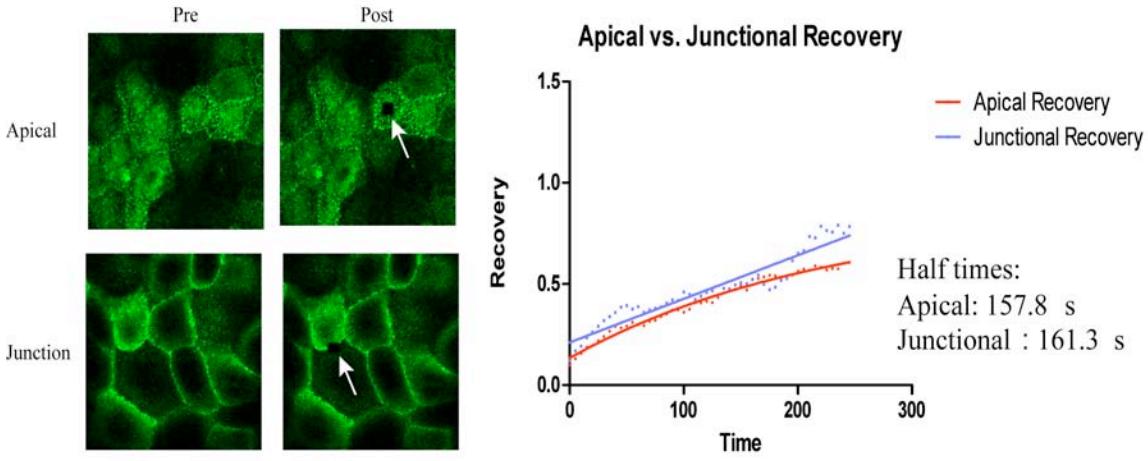

Figure 4-16: FRAP analyis of mEGFP-Crb3a cells. Both apical and junctional pools of mEGFP-Crb3a have similar lateral mobilities.

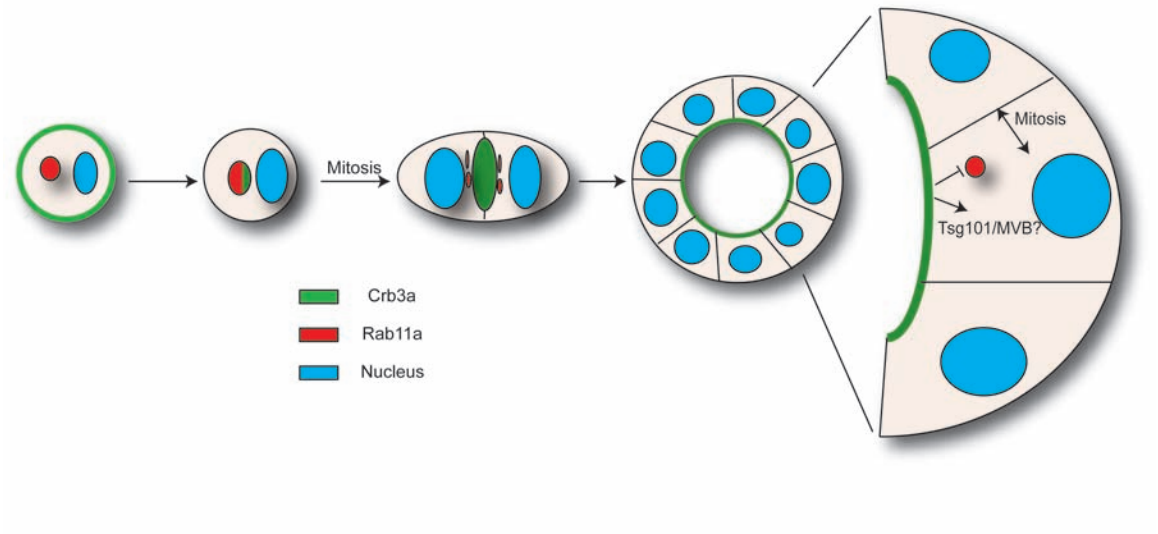

Figure 4-17: Model of Crb3a exocytosis and endocytosis.

estimated at 157.8 s while junction recovery half-life was estimated at 161.3 s. These times indicate that Crb3a has the similar mobility regardless of subcellular localization.

4.4 Discussion

Here we present evidence that apical recycling of mammalian Crb3a in polarized MDCKII cells contributes to the dynamic regulation of epithelial polarity. Newly synthesized Crb3a repopulates the cell within 1-hour and Crb3a appears to have a half-life of 4-6 hours. However, the fate of metabolized Crb3a is not yet clear. Inhibition of the MVB pathway via TSG101 knockdown prolonged the Crb3a half-life but endocytosis of the Crb3a was very difficult to detect. It is possible that a significant fraction of Crb3a is secreted into the media via exosomes and this Crumbs3a is difficult to detect with our endocytosis assays. A long-standing question in the field of epithelial polarity is how polarity is initially established and what processes are utilized to maintain polarity? Numerous studies have provided examples of the protein-protein interaction networks necessary for epithelial polarity, but how these networks are spatially and temporally regulated is not well described (12, 100, 110, 152, 153, 170, 235, 237) (254, 262). Previously, our lab and others has shown that expression of the Crb3a protein is regulated and this regulation affects the ability of epithelial cells to maintain proper polarity (69, 133, 235, 246, 294). The role of Crb3a trafficking in epithelial regulation has not been thoroughly addressed. Trafficking and junction formation assays traditionally utilize calcium depletion/repletion (switch) to monitor apical membrane formation. Calcium switch experiments probably represent endocytosis and exocytosis under artificial

conditions leaving them at a disadvantage. We believe these experiments performed above concerning the trafficking of Crb3a under steady-state conditions more closely resemble how epithelial sheets behave *in vivo*.

Crb3a is necessary for apical membrane formation and Crb3a arrives at the apical membrane in an expedited process involving the coordinated constant production of Crb3a protein and exocytosis to the apical surface via established trafficking pathways (246). Experiments with Den2-Crb3a demonstrated that newly synthesized Crb3a appears in the cell within 1-hour post photoswitch via live-cell monitoring of polarized epithelial cells. Controlled, short burst of UV light were sufficient to photoswitch a small region of Den2-Crb3a cells from excitation at 488nm (green) to excitation at 594nm (red), allowing us to qualitatively monitor turnover of the protein without detectable UV induced damage (42, 43). The newly synthesized Den3-Crb3a appeared first near the cell center and expanded to the tight junctions over time. The accumulation of new Den2-Crb3a was seen in what appears to be a sub-apical region of the cell consistent with the location of AREs. Interestingly, it has been proposed that the site of Crumbs translation is localized sub-apically and the localization of *Crumbs* transcripts is dependent on the *Crumbs* 3` untranslated region (UTR) (157). Our data does not fit with this model, as all *Crb3* genes used in this study are derived from cDNAs lacking the any 3` UTR yet Crb3a localized with markers for Golgi and endoplasmic reticulum and all cells expressing exogenous Crb3a appeared to function normally. Based on our analysis we hypothesize that during steady state (fully polarized) conditions Crb3a is trafficked directly and efficiently to the apical surface and functions to reinforce apical identity. Considering Crb3a localizes to the primary cilium, apical surface, and tight junction there exists the

possibility that Crb3a is trafficked to one location and then moves to other subcellular locations by diffusion or Crb3a is specifically targeted to distinct subellular localizations dependent on polarization. Our data cannot discount these other possibilities and other experimentation is needed to investigate this question.

Using Den2-Crb3a we were unable to determine definitively if Crb3a is endocytosed in cells. Although newly synthesized (green) sub-apical Den2-Crb3a appears to be colocalized with existing (red) Den2-Crb3a, we have no definitive method of delineating the exact apical boundary using this live-cell imaging technique. This was due to technical limitation based on microscopic resolution and our inability to monitor a novel marker for the apical surface in the far-red channel (>594 nm excitation wavelength). Using Den2-Crb3a cells, we were limited to the use of only 488 and 594 excitation channels because UV-light activates the Dendra protein. Also due to the small region of interest required for visualization of the movement of Crb3a, we were limited to only live-cell analysis. Attempts to convert entire plates or cover slips of cells using UV light only resulted in partial conversions or cell death by UV induced damage. To assess these limitations in the future we will have to employ immuno-electron microscopy.

In lumen formation models (3-dimesional tissue culture) at the single cell stage, MDCKII cells express Crb3a on the entire plasma membrane. As these cells go through mitosis and cytokinesis, Crb3a is endocytosed and then exocytosed to the cleavage furrow to initiate lumen formation (246). The apical recycling system involves coordinated endocytosis into Rab5 positive early endosomes and then passage of vesicles to the Rab11 positive recycling endosomes for reinsertion into the apical membrane (30, 36, 46, 99, 167). Accordingly, in *Rab5* null flies, there is an accumulation of apical

dCrumbs and neoplastic phenotypes indicative of endocytic defects (167). In Rab11a-DN cells, endocytosis was able to proceed; however exocytosis of Crb3a is inhibited (Chapter 4 and (246)). Using recycling into Rab11a-postive ARE is the basis for the apical recycling assay, we sought to understand how apical endocytosis and recycling regulates Crb3a. Based on our lumen formation studies (see Apendix B) we expected Crb3a to be endocytosed and eventually traverse Rab11a-postive ARE on its way back to the surface. The only conditions where uptake of GFP antibody could be detected co-localized with Rab11 were in contact naïve, yet actively dividing cells. These cells do not possess apical surfaces due to lack of cell-cell contacts but will form apical surface upon cell-cell engagement. Surprisingly, using serum-free conditions to mimic cells in G_0, we could not detect any appreciable GFP antibody internalization from single cells into Rab11 positive compartments. Fully polarized epithelial cells in monolayer are undergoing limited mitosis due to contact inhibition and most cells are in G_0 phase. Similarly, we observed very little internalization of GFP antibody in full monolayers, suggesting that there is very little apical recycling of surface Crb3a once apical membranes are fully formed. This is consistent with previous data from our lab that showed endocytosis of Crb3a into a Rab11a positive-compartment only when we eliminated junctions and membrane segregation via calcium switch yet allowed mitosis to occur. Results were made stronger considering that antibodies often dimerize on the surface of cells inducing endocytosis, yet we did not find appreciable internalization or apical recycling in our assays. Biotinylation assays also concluded that endocytosis and protection of surface labeled Crb3a either low or extremely efficient in fully polarized monolayers. The results of these experiments suggest that endocytosis and recycling of

Crb3a is differentially regulated, dependent on the presence or absence of a defined apical surface. Our observation was verified in 4-day old mature cysts where Crb3a is expressed on the apical surface. In mature cysts, apical membrane integrity is maintained once established. Even during mitosis of cells in mature cysts we are unable to detect endocytosis or recycling of Crb3a (246). Our data suggests that once apical integrity is established via a Crb3a-dependent mechanism, trafficking of Crb3a is altered to maintain the apical surface. The only instances where we find Crb3a co-localized with Rab11 after endocytosis is when the cell is actively establishing an apical surface.

If Crb3a is not recycled in fully polarized epithelium then that begs the question of how Crb3a is removed from polarized epithelial cells? Multiple groups have demonstrated that over abundance of Crb3a protein cause apical overgrowth and neoplastic tissue formation (78, 79, 167, 192). It is assumed that transmembrane proteins like Crb3a are endocytosed and degraded via established proteosomal pathways. For the degradation of transmembrane proteins the multivesicular body (MVB) pathway is used to attenuate receptor signals (136). In the MVB pathway, endocytosed proteins are passed from early endosomes and invaginated into multivesicular bodies that fuse with either the lysosome or the apical surface and release their contents into the lumen of an organ, or in our case tissue culture media. Our analysis of tissue culture supernatant determined that iEGFP-Crb3a could be isolated from these samples. This is consistent with the presence Crb3a in urinary exosomes (82).

When we knocked down a TSG101, a MVB protein, Crb3a protein increased and Crb3a increase was not caused by increased transcription. Since, traffic into the MVB pathway is down stream of the AEEs, we believe the accumulation of a Crb3a signal in

the cytosol to represent the inability of the cell to efficiently shuttle Crb3a to the MVB pathway. In *Drosophila,* a complete null of the homologue for TSG101 has been created (78, 79, 192). These flies exhibit massive overgrowths similar to neoplastic tumors in the eye and show a vast increase in cytoplasmic dCrumbs protein (79, 192). In *TSG101* mutants, cell autonomous overgrowth was attributed to changes in dCrumbs endocytosis and transcription (78). Non-autonomous overgrowth in *TSG101* mosaic mutant flies was due to increased Notch signaling (192). In flies genetically null for endocytotic *Rab5* or *Avl*, which are upstream of TSG101, development of Notch-independent neoplastic tumor growth is observed suggesting dCrumbs as a regulator of tumor growth (167). TSG101 shRNA MDCKII cells do not show cell autonomous or cell non-autonomous overgrowth phenotypes at 1, 6, or 12 days in either 2 or 3-dimensions. The role of TSG101 as a tumor suppressor continues to remain unclear as *TSG101* knockout is also embryonic lethal in mammals indicating the *TSG101* gene is necessary for development (240). Transplanted NIH3T3 cells deficient in TSG101 can form neoplastic tumors in nude mice (155). However in further studies, TSG101 has been identified as a tumor suppressor in some but not all tissues (29, 215, 286). Accordingly, in mammalian cells it has been reported that TSG101 depletion increases a cells susceptibility to apoptosis (286). Thus, in cultured cells, TSG101 shRNA may be self-selecting where only cells with moderate knockdown survive. This could potentially lead to a moderate increase in Crb3a protein that we observe. Additionally, we observed that knockdown of TSG101 in a cell moderately overexpressing mEGFP-Crb3a resulted in Crb3a overexpression phenotypes such as apical doming. Herz and Bergmann hypothesized that the role of TSG101 as a tumor suppressor in mammals remains unclear due to the necessity of a “second hit”

resulting in resistance to apoptosis (94). We therefore hypotheisize that overexpressed Crb3a could potentially act as a second genetic abrogation that results in cellular overgrowth. In this model system, TSG101 knockdown combined with Crb3a overexpression should to lead overgrowth phenotypes. In fact, induced iGFP-Crb3a cysts alone do not overgrow, but combining iGFP-Crb3a induction and TSG101 knockdown does cause overgrowth phenotypes. When analyzing these cells by Western blot, we discovered that overexpression of Crb3a was able to induce high levels of TSG101, and rescue TSG101 expression. Although speculative at this point, we conclude that overexpression of Crb3a in polarized MDCKII cells causes a feedback loop that results in upregulation of transcription of genes required to maintain cellular homeostasis. It has recently been suggested that Crumbs behaves as a tumor suppressor and is a far upstream component of the Warts/Hippo signaling pathway controlling cell size and growth (160, 233). These studies are in there infancy, but we believe this represents a fertile basis for the study of Crb3a in endocytosis mediated signaling as a epithelial regulation mechanism.

Importantly, it has been demonstrated that the majority of proteins entering into the ESCRT/MVB pathway proteins are ubiquitinated (135). Crb3a contains 3 candidate lysines in its cytoplasmic domain, and entering the intracellular sequence of Crb3a through an ubiquitination prediction algorithm produced lysine 112 as having a high probability of ubiquitination. Point mutations were made on Crb3a K112, however we could not detect any ubiquitination in a number of assays. This suggests that Crb3a is either ubiquitinated on a different lysine, the ubiquitination of Crb3a is transient, Crb3a is not ubiquitinated, or Crb3a is removed from the cell under a mechanism other than MVB

formation. There is emerging evidence that ubiquitination is not an absolute necessity for MVB inclusion and association with ubiquitinated cargo or other cytoplasmic motifs may confer entry into the MVB pathway (48). An alternative mechanism for the presence of Crb3a in the media can be attributed to a phenomenon call apical shedding. It has also been reported that other apical membrane proteins such as prominin-1 are removed from the membrane surface by direct budding into the lumen from apical surfaces (178, 179). In either exosome biogenesis or apical shedding, the presence of proteins in media supernatant suggests the protein is removed from the cell via one these two pathways and further studies by our group are underway to determine what the exact mechanism Crb3a uses to leave the polarized cell.

With Den2-Crb3a cells, after 1 minute of excitation with UV light, we were able to detect an increase in signal from newly synthesized (green) Den2-Crb3a within 1 hour. After 4 hours post photoswitch, newly synthesized Crb3a appeared to overtake the population of converted (old, red) Den2-Crb3a. These initial observations led us to speculate that Crb3a is constantly being produced in cells. To help maintain Crb3a levels, it would also require Crb3a to undergo rapid turnover and degradation. Continuing our analysis of the removal of Crb3a protein from the cell as a mode of epithelial regulation, we became interested in Crb3a protein half-life. We wanted to know if the presence or absence of a defined apical surface affects the ability of Crb3a protein to be retained in cells. Our iGFP-Crb3a system provided us with a method to circumvent technical problems associated with the endogenous Crb3a protein. Crb3a is a small transmembrane protein of only 121 amino acids, and contains only one methionine that is the start methionine and part of the cleaved signal peptide. The sequence of Crb3a

does not contain any cysteine residues therefore S35 labeling of Crb3a could only be undertaken by engineering a construct complete with sulfur containing residues in order to successfully metabolically label cells. We believe this method to be unreliable due to the transient nature of the protein and the possibility that introduction of sulfur containing amino-acids could possibly affect our results by the potential of creating disulfide linkages where none previously exist. We have also discovered that Crb3a is a highly post-translational modified protein in MDCKII cells containing both N and O linked glycosylations. We have only been able to authenticate one post-translational modification, an N-linked glycosylation event on asparagine-36 (170). Unfortunately, previous work in the lab determined that this N-linked glycosylation was not necessary for proper function of Crb3a in MDCKII cells (170).

We utilized modified pulse chase to calculate the Crb3a half-life in both fully polarized MDCKII cells and cells that have gone through the epithelial to mesenchymal transition (EMT) by exogenous expression of the oncogene Snail (33, 294). Surprisingly, our results suggest that the half-life of Crb3a is approximately 3-6 hours and the half-life is not affected by a non-polarized EMT state. These data were generated by looking at production of Crb3a without influence of the endogenous promoter that can be under EMT transcription factor control (133, 294). Even though the half-life of Crb3a did not change during EMT conditions, there was a significant difference in the maturation of the iGFP-Crb3a protein suggesting that part of the EMT program is a restructuring of trafficking machinery in cells. In iGFP-Crb3a/Snail-flag cells, iGFP-Crb3a is still found on the surface albeit at lower concentrations, and this may signify that polarization is required for the optimum delivery of Crb3a to the surface. Furthermore, our data also

suggest that EMT is a transcriptional process, changing cell morphology by genetic rearrangement and not through upregulation of conventional protein degradation machinery, at least in terms of Crb3a degradation. A half-life of 3-6 hours of Crb3a becomes significant when one considers that E-cadherin has a half-life of > 40 hours (166). During EMT, the levels of Crb3a will fall quite fast and this can contribute to the loss of cell polarization. Additionally, FRAP analysis on fully polarized MDCKII cells showed that both apical and junctional pools of mEGFP-Crb3a have very similar motilities relative to each other in fully polarized monolayers. Conventionally in the field of epithelial polarity it as been argued that the apical surface is very dynamic while the junctions are static in nature. It has been demonstrated that the tight junction structural protein ZO-1 is also mobile during steady-state (252). This data has often been unfairly dismissed due to ZO-1 being a purely cytosolic protein, however, further studies have also demonstrated other mobile tight junction components (137). Our data demonstrates that a transmembrane protein, Crb3a, is also dynamic at both the apical membrane and tight junction. This data strongly implies that epithelial tight junctions are dynamic structures undergoing constant remodeling. Furthermore, since Crb3a is such as strong inducer of polarity and has a relatively short life span, it can also be implied that polarity itself is a dynamic process and this process is essential for the maintenance of epithelial integrity.

Chapter 5

Conclusions, Perspectives, and Future Directions

The ability for cells to establish cell polarity represents a major evolutionary milestone where organisms could begin to form specialized germ layers that will eventually give rise to complex tissues. The epithelial cell layer represents a highly specialized cell layer that demonstrates a structure-function relationship of polarized cells. Over the last 20 years, our understanding of the molecular mechanisms governing the establishment, maintenance, and regulation of epithelial integrity has grown exponentially. The identification of the Crumbs, Par, and Scribble polarity complexes and the realization that these proteins represent conserved developmental mechanisms in a variety of organisms has set the basis for the study of polarization. The initial descriptions of the protein-protein interactions that are required for epithelial polarity represent only the first clues about the complexity of this system.

The work represented in this thesis explores the regulatory mechanisms governing the conserved Crumbs polarity complex. The Crumbs complex consists of the proteins Crumbs3A (Crb3a), protein associated with Lin-7 1 (PALS1), and PALS1 associated tight junction protein (PATJ) and each member of the complex has been demonstrated to be involved with the formation of the tight junction (235, 254, 262). Both PALS1 and PATJ

are cytosolic scaffold proteins consisting of multiple protein-protein interaction domains. PALS1 and PATJ are both regulated by their abilities to interact with each other and other accessory proteins found at the tight junction. Lin-7 is one of these accessory proteins, and although not part of the conserved Crumbs complex, Lin-7 is necessary to stabilize PALS1 in MDCKII cells (Chapter 2 and (261)). It has been previously demonstrated that PALS1 in turn stabilizes PATJ in MDCKII cells, leading us to conclude that during tight junction formation, Lin-7 is upstream of PALS1 and PATJ, stabilizing the formation of the Crumbs polarity complex. We believe this stabilization occurs due to the nature of Lin-7-PALS1-PATJ binding, which is mediated by L27-domain dimerization that would require proteins to be in proper conformation to interact with one another (156).

What our studies in Chapter 2 do not address is the spatial and temporal association of the Lin-7-PALS1-PATJ interaction and how these two important variables will ultimately affect the ability for cells to form tight junctions and specialized membrane domains. Our lab has briefly investigated the affect of depleting PALS1 on events leading to the trafficking of proteins. In 2007, Wang et al demonstrated that knockdown of PALS1 had an effect on the exocyst and trafficking of basolateral E-cadherin suggesting a role between tight junction formation and the ability to sequester proteins to their proper subcellular domains (288). Lin-7 stabilizes PALS1, and PALS1 stabilizes PATJ it is conceivable that depletion of either Lin-7 or PATJ would also affect trafficking of proteins. In our Lin-7 shRNA study (Chapter 2) we did not find any adherens junction defects associated with abrogated E-cadherin traffic suggesting that Lin-7 functions at the lateral membrane. At this time, we do not know where PALS1 and PATJ interact; however it has been proposed that this interaction is dependent on the

conformation of both proteins. A proposed technique that we could utilize to determine when and where these interactions occur is a fluorescence resonance energy transfer (FRET). We must also keep in consideration that PATJ is a large protein consisting of many PDZ binding domains, and not all of these domains have identified binding partners. Although the interaction between PALS1 and PATJ is clearly defined, we cannot rule out any influences between unknown proteins that may contribute to either the conformation or targeting of PATJ. Recently, the identification of angiomotin (AMOT) as a PATJ binding partner lends credence to the influence of Lin-7-PALS1-PATJ on trafficking. AMOT is associated with Rho-GTPase family members such as Rich1 and Cdc42 directly linking AMOT and its binding partner PATJ to the cytoskeleton (265, 293). Therefore, further biochemical studies are required to better characterize the influences of Lin-7-PALS1-PATJ as molecular scaffolds in the establishment of membrane domains.

It has become increasingly apparent that genetic control of transcription is necessary to establish and maintain epithelial polarity. We cited the use of RNA interference over the course of this work to demonstrate the affect of depletion of members of the Crumbs, Par, and Scribble protein complexes on epithelial phenotypes but we must also consider the consequences of directly inhibiting the genes from which these proteins are derived. From our results found in Chapter 3, we were able to identify a subset of genes expressed to promote the formation of tight junctions. Interestingly genes encoding conserved polarity complex proteins, only one gene, that for the protein Crb3, was specifically under transcriptional control regulating tight junction formation (Chapter 3). This data suggests that Crb3 is one of the master regulators of apico-basal

polarity. In a paper by Aigner et al., PATJ was also shown to be under transcripitional regulation by the EMT transcriptional repressor ZEB1 (4). However, Whiteman et al. demonstrated that both PATJ and PALS1 were only moderately affected by Snail-mediated transcriptional silencing (294). Given the multiple signaling pathways that feed into the EMT program, it is quite likely that individual transcription factors target only specific genes that control epithelial polarity. However, interesting questions still remain on the secondary effects of EMT mediated transcription. Since cells undergoing EMT undergo dramatic alterations in gene expression, there are presumably changes in transcription on genes not directly under the influence of EMT transcription repressors. Future work needs to be completed on the secondary affects of EMT and how these effects reinforce or work to overcome EMT phenotypes. Fortunately, advances in large-scale genomics and proteomics will allow these questions to be attacked using computational methods. The ability to data mine and investigate questions using high-throughput analysis will provide new insights to transcriptional networks and how these networks relate to changes in cellular phenotypes.

One of the major problems associated with bioinformatics based approaches to generating new data is after the data is acquired it must be validated. In the field of epithelial cell biology, validations of data previously involved using molecular biology to clone genes of interest and then insert these genes in the researcher's model of choice. Unfortunately, this method is not always practical and characterizations especially for phenotypes that aren't initially obvious. In the case of *in vitro* tissue culture modeling, genetic manipulation can be done with relative ease, however pitfalls such as clonal artifacts or cell death quite common. Additionally, it has become apparent that cells

behave differently in 2-dimesional and 3-dimensional contexts. Three-dimensional tissue culture is a technique that is growing in popularity because it takes into consideration the behavior of a cell in space (214, 245). Using space as a variable allows scientists to more sensitively monitor the relationship between generation of polarity and maintenance of apico-basal cell polarity.

In this work, we have attempted to consider the role of 3-dimensional growth when considering the role of Crb3a in epithelial cell polarity. Our studies contained here have illustrated that Crb3a is a strong inducer of polarity and that polarity is a dynamic process. Through trafficking of Crb3a, epithelial cells can form junctions, define surfaces, and importantly maintain epithelial integrity. When we consider individual epithelial cells in 3-dimensional space, as part of an entire functional epithelial sheet, we find that each cell must function as part of a whole to maintain the integrity of the epithelial sheet. Although our understanding on how Crb3a is trafficked is only beginning to become clear, we believe this work represents some of the first attempts to understand how polarity is controlled and maintain in the context of 3-dimensions. We still have limited understanding of why Crb3a is recycled only preceding apical membrane formation. Importantly, during apical lumen formation we do not understand the signals that trigger endocytosis of Crb3a into the cell, the signals that target Crb3a to the spindle pole, and the signals that insert Crb3a at the site of apical membrane. Work is currently being done in the lab to address these questions. Experiments conducted in this thesis indicate that Crb3a is a dynamic protein capable of defining the apical surface of polarized epithelial cells. Mobility assays demonstrate that apical and junctional Crb3a moves efficiently through the cell. A mobile fraction of Crb3a combined with the

bypassing of the apical recycling systems suggests the very nature of polarization is dynamic rather than static. The obvious question then becomes, what advantage does dynamic polarity give to complex organisms? Considering that the kidney is one of the major organ systems of the body responsible for filtering waste from the blood and maintaining ion balance, it can be hypothesized that the natural and constant replacement of the apical surface serves as a defense mechanism against invasion and infection. There also lies the possibility that apical shedding or exomsome secretion provides a signaling function in epithelial sheets. In the intestine for example, there are documented examples of exosomes in signaling against in host defense and growth control (171). Thus far exosome signaling has not been demonstrated in the mammalian kidney but as mentioned there does exist some precedence for the study of this phenomenon (82). We have actually tested to see if Crb3a has some signaling function in what we can only label as paracrine signaling. Since apical Crb3a has no defined function in mammalian cells (as of yet) we asked the question as to whether Crb3a in the media provides a signal to neighboring cells to facilitate any downstream signaling events. Initially, we just used media from mEGFP-Crb3a cells and placed it on wild type MDCKII cells to see if cells have the ability to uptake Crb3a from the media. These experiments were unsuccessful, however we cannot discount that there is no other signaling event taking place.

For example, in *Drosophila,* work in the last year has suggested that Crumbs is one of the upstream most components of the Warts/Hippo pathway and positively controls pathway activation by binding the FERM-binding protein Expanded (14, 77, 88, 90, 160, 233). A mammalian homologue of Expanded is yet to be identified. In the Warts/Hippo pathway, Yes-associated protein (YAP) is downstream transcription factor

and localizes to the nucleus during Warts/Hippo activation (304). However, when we overexpress Crb3a in MDCKII cells we cannot appreciably detect nuclear YAP suggesting that Crb3a overexpression may not regulate Warts/Hippo signaling in mammalian cells. It should be noted that *Drosophila* Crumbs is most similar to mammalian Crb1, and that flies do not possess a protein similar to mammalian Crb3a. This raises the interesting question of what is the evolutionary advantage of Crb3a in mammalian systems? Crb3a is obviously necessary for development of mammals so it must have a striking role in the building the complex body systems of mammals. We hope to address this issue further in the Margolis lab by building mice by both GFP-"knock-in" and conditional knockout strategies. We hope these mice will provides us insight to the role of Crb3a in the development of the kidney and other tissues as well as allow us to determine the role of Crb3a in epithelial maintenance *in vivo*.

Appendix A

FRT and FRTL5 Complete Microarray Data Sets

In Chapter 3 we presented microarray data comparing amounts of transcripts in wild type FRT cells relative to wild type FRTL5 cells. In the tables below, we have included the entire data sets for genes upregulated in both FRT cells and FRTL5 cells. Positive t-statistics indicate the gene is upregulated in FRT cells relative to FRTL5 cells and negative t-statistics indicate the gene is upregulated in FRTL5 cells relative to FRT cells.

Genes upregulated in FRT cells relative to FRTL5 cells

Symbol	Description	GenBank	t-statistic	Fold Change
Tspan8	tetraspanin 8	NM_133526	67.09	9.9
Cdh1	cadherin 1	NM_031334	62.82	8.57
Tacstd1	tumor-associated calcium signal transducer 1	BG376410	62.66	8.45
Cldn8	claudin 8	BI292090	57.71	8.64
S100a11	S100 calcium binding protein A11 (calizzarin)	BG378926	55.46	7.56
		BM387197	55.08	8.37
Ubqln2_predicted	ubiquilin 2 (predicted)	BF398140	53.22	8.58
Scd2	stearoyl-Coenzyme A desaturase 2	NM_031841	52.09	8.11
Slco4a1	solute carrier organic anion transporter family, member 4a1	AI180349	50.81	7.44
		BE108949	50.45	7.13
		AI501237	49.28	7.14
S100a6	S100 calcium binding protein A6 (calcyclin)	AF140232	49.13	8.1
		BI288769	48.49	6.65
Gpx1	glutathione peroxidase 1	S41066	48.34	7.08
S100a4	S100 calcium-binding protein A4	NM_012618	46.98	6.45
Lgals3	lectin, galactose binding, soluble 3	NM_031832	45.91	7
Manba	mannosidase, beta A, lysosomal	BM388852	45.79	6.84
Capg	capping protein (actin filament), gelsolin-like	BM384693	45.33	6.67
LOC315883	similar to phospholipid scramblase 2	AI411594	45.27	7.27
Cd74	CD74 antigen (invariant polypeptide of major histocompatibility complex, class II antigen-associated)	NM_013069	45.04	7.14
Sema4a	sema domain, immunoglobulin domain (Ig), transmembrane domain (TM) and short cytoplasmic domain, (semaphorin) 4A	AI228417	44.69	6.31
Pof1b_predicted	premature ovarian failure 1B (predicted)	BG375052	44.62	7.47
Ggh	gamma-glutamyl hydrolase	NM_012960	44.39	6.09
Tacstd2	tumor-associated calcium signal transducer 2	AA891826	43.56	6.95
RGD1308059	similar to DNA segment, Chr 4, Brigham & Womens Genetics 0951 expressed	AI408727	43.46	7.02
Fabp5	fatty acid binding protein 5, epidermal	U13253	43.45	6.94
		BG376453	42.74	7.24
RGD1308084	similar to hypothetical protein FLJ11342	BM389654	42.63	6.27
		AI599072	42.48	6.01
Gata3	GATA binding protein 3	BE118901	41.91	6.29
Cldn4	claudin 4	BE328951	41.83	7.49
Krt2-8	keratin complex 2, basic, gene 8	BF281337	41.49	6.96
Foxa1	forkhead box A1	BM383972	41.23	6.12
Nppb	natriuretic peptide precursor type B	NM_031545	41.03	5.95
LOC299339		BI278479	40.93	5.65
Atox1	ATX1 (antioxidant protein 1) homolog 1 (yeast)	NM_053359	40.64	6.08
Muc1	mucin 1, transmembrane	BI274326	40.35	6.28
Anxa8	annexin A8	BM389254	39.23	5.53
Prom1	prominin 1	NM_021751	38.98	6.04
Pof1b_predicted	premature ovarian failure 1B (predicted)	BI291859	38.94	6.12

Symbol	Description	GenBank	t-statistic	Fold Change
Cldn1	claudin 1	AI137640	38.68	5.36
Msln	mesothelin	NM_031658	38.01	6.41
Lamb3	laminin, beta 3	BE101834	37.91	6.51
Axl	AXL receptor tyrosine kinase	AI406520	37.52	6.21
Crb3	crumbs homolog 3 (Drosophila)	BI283883	37.45	5.23
Pls1_predicted	plastin 1 (I isoform) (predicted)	BM392070	37.43	5.29
		AW522833	37.42	6.53
Rab25_predicted	RAB25, member RAS oncogene family (predicted)	AA945861	37.28	5.89
Tmed6_predicted	transmembrane emp24 protein transport domain containing 6 (predicted)	BI294972	37.11	6.54
Clca6	chloride channel calcium activated 6	BI292185	37.1	5.49
LOC500040	similar to Testis derived transcript	AI177869	37.08	6.38
Myo1b	myosin Ib	NM_053986	36.93	5.68
		BF416794	36.88	6.36
Tmprss2	transmembrane protease, serine 2	AI412136	36.66	5.78
		AI600031	36.66	5.47
Igsf4a	immunoglobulin superfamily, member 4A	H31111	36.21	5.07
Fxyd2	FXYD domain-containing ion transport regulator 2	AF129400	36.01	7.02
Plk2	polo-like kinase 2 (Drosophila)	NM_031821	35.81	7.31
Mapk12	mitogen-activated protein kinase 12	NM_021746	35.7	5.78
Spint1	serine peptidase inhibitor, Kunitz type 1	BI280343	35.56	5.13
Spop	speckle-type POZ protein	BF283504	35.49	5.3
Cnksr3	Cnksr family member 3	AW253242	35.29	6.74
		AA891842	35.12	5.38
		BI274357	34.99	5.22
		BM383684	34.91	5.54
Igsf4a	immunoglobulin superfamily, member 4A	BE117767	34.88	5.83
Eva1_predicted	epithelial V-like antigen 1 (predicted)	BI282616	34.77	6.02
		BM387197	34.7	6.99
RGD1564216_predicted	similar to Myoferlin (Fer-1 like protein 3) (predicted)	AW917760	34.67	4.69
		BI274321	34.65	4.71
Htra1	HtrA serine peptidase 1	NM_031721	34.51	6.29
Itgb6	integrin, beta 6	AI070686	34.5	5.06
		BM383423	34.32	5.94
Mal	myelin and lymphocyte protein, T-cell differentiation protein	NM_012798	34.23	4.69
Tspan1	tetraspanin 1	BE349699	34.14	5.62
LOC498222	similar to specifically androgen-regulated protein	BI291703	34.07	6.32
Plat	plasminogen activator, tissue	NM_013151	33.88	4.96
		AW522835	33.87	4.56
RGD1560481_predicted	similar to hypothetical protein FLJ20171 (predicted)	BM387466	33.78	4.79
Scd2	stearoyl-Coenzyme A desaturase 2	BE107760	33.61	4.89
Gdpd3_predicted	glycerophosphodiester phosphodiesterase domain containing 3 (predicted)	BM389800	33.32	4.96
		BF389666	33.25	4.77
Hmga1	high mobility group AT-hook 1	BG378885	33.2	4.53
		BF284677	33.18	4.47
Trim35	tripartite motif protein 35	BE111791	33.13	4.56
		AI111707	33.03	4.54

Symbol	Description	GenBank	t-statistic	Fold Change
Sfn_predicted	stratifin (predicted)	BI286166	32.86	6
Slco4a1	solute carrier organic anion transporter family, member 4a1	NM_133608	32.8	4.95
		BM389293	32.8	4.48
L1cam	L1 cell adhesion molecule	NM_017345	32.57	4.42
Crim1_predicted	cysteine-rich motor neuron 1 (predicted)	BI289620	32.54	4.48
Chrna4	cholinergic receptor, nicotinic, alpha polypeptide 4	BF394332	32.47	4.54
		BI284288	32.36	4.62
		BI288775	32.23	4.62
Tmc4	transmembrane channel-like gene family 4	AI556940	32.07	4.41
Plac1	placenta-specific 1	BI293691	32.05	5.96
		AI069912	31.97	5.34
Cdh3	cadherin 3, type 1, P-cadherin (placental)	AI010270	31.91	4.68
Fcgr3	Fc receptor, IgG, low affinity III	NM_053843	31.88	4.54
B4galnt1	beta-1,4-N-acetyl-galactosaminyl transferase 1	NM_022860	31.87	4.33
		AA893164	31.85	5.26
		AI576177	31.7	5.91
Ppm1h	protein phosphatase 1H (PP2C domain containing)	AI548159	31.65	4.71
Bace2	beta-site APP-cleaving enzyme 2	BF408665	31.62	5.57
RGD1311155	similar to RIKEN cDNA 9230117N10	AI716248	31.5	7.13
Gjb5	gap junction membrane channel protein beta 5	NM_019241	31.44	4.88
Ly6a_predicted	lymphocyte antigen 6 complex, locus A (predicted)	BI291986	31.35	5.23
Hrasls3	HRAS like suppressor 3	BG378637	31.31	5.46
Vldlr	very low density lipoprotein receptor	AA849857	31.29	5.26
Mgst2_predicted	microsomal glutathione S-transferase 2 (predicted)	BI290559	31	4.29
LOC498796	hypothetical protein LOC498796	BF283267	30.69	4.16
		BE109274	30.66	4.32
Elf3	E74-like factor 3	BI279615	30.64	4.96
Hs3st1	heparan sulfate (glucosamine) 3-O-sulfotransferase 1	AF177430	30.61	5.76
		BF412036	30.56	4.58
Akap5	A kinase (PRKA) anchor protein 5	AW523875	30.48	4.44
LOC299339		AI103284	30.37	5.74
LOC304000	cell adhesion molecule JCAM	BF411017	30.3	4.5
Akr1b8	aldo-keto reductase family 1, member B8	AI233740	30.24	4.77
Anxa1	annexin A1	NM_012904	30.23	4.29
Tmem54	transmembrane protein 54	BG377582	30.18	4.1
		BI292758	30.06	4.52
Mtap_predicted	methylthioadenosine phosphorylase (predicted)	BE107396	29.95	4.36
F2r	coagulation factor II (thrombin) receptor	NM_012950	29.87	4.12
Timp1	tissue inhibitor of metalloproteinase 1	NM_053819	29.77	4.21
Lad1_predicted	ladinin (predicted)	AA799544	29.76	4.35
Cdkn2a	cyclin-dependent kinase inhibitor 2A	AF474976	29.64	4.94
Atp8b1_predicted	ATPase, Class I, type 8B, member 1 (predicted)	BM384161	29.56	4.13
RGD1311580_predicted	similar to actin filament associated protein; actin filament-associated protein, 110 kDa (predicted)	BE101285	29.48	4.39
Cldn1	claudin 1	NM_031699	29.36	4.71

Symbol	Description	GenBank	t-statistic	Fold Change
Hgfac	hepatocyte growth factor activator	BE119649	29.35	5.32
Lamc2	lamimin, gamma 2	BM385282	29.32	4.83
Vldlr	very low density lipoprotein receptor	NM_013155	29.26	6.06
Akr7a3	aldo-keto reductase family 7, member A3 (aflatoxin aldehyde reductase)	NM_013215	29.1	4.68
		BF419515	29.08	4.73
Ppp2r3a	protein phosphatase 2 (formerly 2A), regulatory subunit B", alpha	AI717707	29.07	4.03
Cldn1	claudin 1	AW917275	29.04	4.79
		BE106581	29.04	3.96
Epn3	epsin 3	BM387330	28.98	5.01
		AA997873	28.6	4.61
		BM389496	28.58	4.53
Meis1_predicted	Meis1, myeloid ecotropic viral integration site 1 homolog (mouse) (predicted)	AW532697	28.44	4.1
RGD1305347_predicted	similar to RIKEN cDNA 2610528J11 (predicted)	AA819329	28.42	5.04
		AI102833	28.41	4.45
Mawbp	MAWD binding protein	AY083160	28.36	4.03
		AW534142	28.34	4.13
Lphn2	latrophilin 2	AF081153	28.33	3.96
Elavl2	ELAV (embryonic lethal, abnormal vision, Drosophila)-like 2 (Hu antigen B)	AI145457	28.32	4.07
		AA819254	28.32	4
		BE096535	28.3	4.04
		AA800701	28.23	5.15
Cav2	caveolin 2	BE349669	28.11	4.09
RGD1561662_predicted	similar to AI661453 protein (predicted)	AI716243	28.09	4.34
		AI233227	28.07	4.14
Cxadr	coxsackie virus and adenovirus receptor	BG665433	28.07	4.1
		AI703807	28.04	4
Frk	fyn-related kinase	NM_024368	28.02	5.33
Sphk1	sphingosine kinase 1	AB049572	27.97	3.8
Dpysl3	dihydropyrimidinase-like 3	BF420803	27.94	4.21
Pkp1_predicted	plakophilin 1 (predicted)	BG371843	27.9	4.75
LOC361623		AI406517	27.9	3.8
Elavl2	ELAV (embryonic lethal, abnormal vision, Drosophila)-like 2 (Hu antigen B)	BF563441	27.8	4.07
		AI709768	27.78	5.34
Mbp	myelin basic protein	BG374506	27.78	4.16
Gstm5	glutathione S-transferase, mu 5	U86635	27.76	6.84
		AI045201	27.75	6.04
RT1-Da	RT1 class II, locus Da	Y00480	27.74	3.82
Irf6_predicted	interferon regulatory factor 6 (predicted)	BF410603	27.7	4.87
Crim1_predicted	cysteine-rich motor neuron 1 (predicted)	AI600057	27.58	4.61
Gabrp	gamma-aminobutyric acid A receptor, pi	NM_031029	27.56	5.6
		BF392317	27.53	4.06
Klf5	Kruppel-like factor 5	BM382886	27.45	3.92
Id2	inhibitor of DNA binding 2	AI008792	27.33	5.35
LOC500877	Ab1-152	AA891922	27.29	4.79
		BG377362	27.29	3.81
Cldn7	claudin 7	AJ011811	27.23	6.03
Slc22a18	solute carrier family 22 (organic cation transporter), member 18	BM391436	27.23	5.05

Symbol	Description	GenBank	t-statistic	Fold Change
Irx2	Iroquois related homeobox 2 (Drosophila)	BF563976	27.19	3.99
Abcc3	ATP-binding cassette, sub-family C (CFTR/MRP), member 3	AF072816	27.18	3.91
Cd59	CD59 antigen	NM_012925	27.12	4.81
LOC365960	similar to semaF cytoplasmic domain associated protein 2	BF285490	27.02	4.07
		AW534737	26.98	4.15
Foxq1	forkhead box Q1	NM_022858	26.89	4.51
Rrad	Ras-related associated with diabetes	NM_053338	26.83	6.22
Cav2	caveolin 2	BE349669	26.83	3.95
Tmc4	transmembrane channel-like gene family 4	AI556940	26.79	5.05
		BE111796	26.78	6.88
RT1-Bb	RT1 class II, locus Bb	BI279526	26.73	3.96
		AI178222	26.7	4.76
Nqo1	NAD(P)H dehydrogenase, quinone 1	J02679	26.7	4.73
Tpo1	developmentally regulated protein TPO1	NM_133395	26.67	5.85
RGD1308297	similar to CG10084-PA	BE117193	26.57	3.78
Bk	brain and kidney protein	U30831	26.52	4.02
Tmc4	transmembrane channel-like gene family 4	BF545988	26.46	5
Serinc2	serine incorporator 2	BF419780	26.4	6.93
		BF551377	26.32	3.65
		BI285447	26.26	4.02
RGD1309720	similar to Hypothetical protein MGC19163	BI289108	26.21	4.29
Klf4	Kruppel-like factor 4 (gut)	NM_053713	26.17	3.54
Phlda2_predicted	pleckstrin homology-like domain, family A, member 2 (predicted)	AI029402	26.1	4.73
		AW528448	26.09	3.98
		AI145306	26.08	5.17
Sh3bgrl3_predicted	SH3 domain binding glutamic acid-rich protein-like 3 (predicted)	BG666075	26.05	5.63
		BI285850	26.03	3.95
		BF558478	25.97	3.65
Fez2	fasciculation and elongation protein zeta 2 (zygin II)	AA955230	25.75	4.69
		AA998383	25.65	3.97
Id2	inhibitor of DNA binding 2	NM_013060	25.64	4.67
RGD1561394_predicted	similar to MLTK-beta (predicted)	BM390528	25.57	3.45
Ahnak	AHNAK nucleoprotein (desmoyokin)	AI407114	25.45	3.49
Klf5	Kruppel-like factor 5	NM_053394	25.34	4
Prps2	phosphoribosyl pyrophosphate synthetase 2	NM_012634	25.32	4.95
		AA800593	25.31	4.71
Aplp1	amyloid beta (A4) precursor-like protein 1	AW435479	25.29	4.19
RGD1565540_predicted	similar to ctla-2-beta protein (141 AA) (predicted)	AI230591	25.27	3.88
		BF396739	25.25	3.44
Il24	interleukin 24	NM_133311	25.18	4.43
RGD1307875_predicted	similar to FLJ23471 protein (predicted)	BG373522	25.09	4.06
		BE109381	24.93	3.68
Ndrg4	N-myc downstream regulated gene 4	BG666709	24.85	4.05
Pctk2	PCTAIRE-motif protein kinase 2	AI716206	24.81	3.37
Cln6_predicted	ceroid-lipofuscinosis, neuronal 6 (predicted)	AI105369	24.76	4.09
Ttr	transthyretin	BE098869	24.69	5.04
Lphn2	latrophilin 2	NM_134408	24.67	4.82

Symbol	Description	GenBank	t-statistic	Fold Change
		AI059853	24.64	4.62
Phyhd1	phytanoyl-CoA dioxygenase domain containing 1	BI275763	24.51	3.31
Cdx2	caudal type homeo box 2	NM_023963	24.45	3.44
Bdh1	3-hydroxybutyrate dehydrogenase, type 1	NM_053995	24.44	3.77
Mina	myc induced nuclear antigen	BI278157	24.4	3.44
Casp3	caspase 3, apoptosis related cysteine protease	U84410	24.38	3.35
Gstm1	glutathione S-transferase, mu 1	AI169331	24.33	5.15
Dpysl3	dihydropyrimidinase-like 3	BI294841	24.26	5.57
Fxyd4	FXYD domain-containing ion transport regulator 4	NM_022388	24.25	6.14
Ankrd1	ankyrin repeat domain 1 (cardiac muscle)	NM_013220	24.25	4.66
RT1-Ba	RT1 class II, locus Ba	AF307302	24.14	3.35
		BI279363	24.07	3.63
Bcor_predicted	Bcl6 interacting corepressor (predicted)	BI289386	24.06	3.5
Cst6	cystatin E/M	NM_133566	24.05	4.2
		BI291373	24.04	4.01
Lcn2	lipocalin 2	NM_130741	23.98	3.27
		BF397870	23.92	4.2
Kif16b_predicted	kinesin family member 16B (predicted)	BF420465	23.84	3.68
		BI278449	23.82	3.25
Dnajc6_predicted	DnaJ (Hsp40) homolog, subfamily C, member 6 (predicted)	AW523481	23.76	3.89
		BF560932	23.76	3.5
Cav2	caveolin 2	NM_131914	23.71	4.11
Prkcdbp	protein kinase C, delta binding protein	NM_134449	23.63	5.28
Marveld2_predicted	MARVEL (membrane-associating) domain containing 2 (predicted)	BI280967	23.56	3.38
Bspry	B-box and SPRY domain containing	AW529938	23.55	6
		AI180454	23.51	3.44
Cldn6_predicted	claudin 6 (predicted)	AI030970	23.48	3.97
Rnf39	ring finger protein 39	NM_134374	23.46	4.27
Htatip2_predicted	HIV-1 tat interactive protein 2, homolog (human) (predicted)	BG378579	23.44	3.41
Cldn3	claudin 3	NM_031700	23.4	4.01
Ces2	carboxylesterase 2 (intestine, liver)	NM_133586	23.39	4.44
Eps8l1_predicted	EPS8-like 1 (predicted)	AI715477	23.34	3.5
		BE107296	23.29	5.28
Aqp9	aquaporin 9	NM_022960	23.29	3.44
Sox4_predicted	SRY-box containing gene 4 (predicted)	AA956294	23.29	3.28
RGD1309219	similar to hypothetical protein HSPC129	BI291413	23.25	4.61
Cd79b	CD79B antigen	NM_133533	23.22	3.18
Tspan8	tetraspanin 8	AI229420	23.18	4.98
Pak1	p21 (CDKN1A)-activated kinase 1	BI281735	23.18	3.94
Casp3	caspase 3, apoptosis related cysteine protease	BM387008	23.18	3.23
LOC309169	tangerin	BI287221	23.12	3.7
		BF546029	23.12	3.2
		BM389843	23.03	3.88
Krt2-7	keratin complex 2, basic, gene 7	BI284344	22.97	6.61
Thbs1		BF558056	22.92	3.31
Cav2	caveolin 2	AI406385	22.87	3.59

Symbol	Description	GenBank	t-statistic	Fold Change
Sigirr	single immunoglobulin and toll-interleukin 1 receptor (TIR) domain	AA818702	22.86	3.33
Tnxa	tenascin XA	BM390128	22.82	3.94
Cryab	crystallin, alpha B	NM_012935	22.78	4.5
Epn3	epsin 3	BI280079	22.78	3.69
		BM388029	22.72	4.15
RGD1565016_predicted	similar to bruno-like 5, RNA binding protein (predicted)	AI012571	22.72	3.87
Ehf_predicted	ets homologous factor (predicted)	BF417773	22.71	3.71
Gm2a	GM2 ganglioside activator protein	AI717483	22.67	3.18
RGD1308084	similar to hypothetical protein FLJ11342	BE103244	22.66	4.92
RGD1304623_predicted	similar to KIAA1749 protein (predicted)	AI008974	22.65	3.51
RGD1311155	similar to RIKEN cDNA 9230117N10	BF390510	22.64	6.06
RGD1563344_predicted	similar to OTU domain containing 1 (predicted)	AI717553	22.61	3.58
Gata3	GATA binding protein 3	NM_133293	22.6	4.19
		AW433942	22.47	3.23
		BF396636	22.42	3.82
Hadhsc	L-3-hydroxyacyl-Coenzyme A dehydrogenase, short chain	AA799574	22.41	4.68
Reep6	receptor accessory protein 6	BG376982	22.35	3.75
Dtnb	dystrobrevin, beta	BE113690	22.35	3.2
		BM391896	22.32	3.24
		AI407547	22.27	3.17
Dsp	desmoplakin	AW144509	22.22	5.05
		BG378310	22.22	3.26
RGD1311316	similar to RIKEN cDNA 5730470L24	AI178732	22.11	3.07
Yc2		AA945082	22.1	4.1
		AA819868	22.08	3.41
Gjb3	gap junction membrane channel protein beta 3	NM_019240	22.02	4.07
		AI113261	22	4.79
		BM392237	21.99	3.9
Gbp2	guanylate nucleotide binding protein 2	NM_133624	21.98	3.39
Serpinb7	serine (or cysteine) proteinase inhibitor, clade B, member 7	BI292651	21.96	4.91
		AI230650	21.87	3.88
Pea15	phosphoprotein enriched in astrocytes 15	BE112895	21.8	3.53
		AI013361	21.79	4.14
Il17re	interleukin 17 receptor E	BM383766	21.78	3.18
		BI291629	21.74	3.58
Dpysl3	dihydropyrimidinase-like 3	AF389425	21.71	3.41
Cd96	CD96 antigen	BE121026	21.7	3.89
Ankrd1	ankyrin repeat domain 1 (cardiac muscle)	L81174	21.63	4.18
Acp5	acid phosphatase 5, tartrate resistant	NM_019144	21.62	3.79
Ugt1a7	UDP glycosyltransferase 1 family, polypeptide A7	AF461738	21.59	3.33
Reep6	receptor accessory protein 6	AI070350	21.49	3.88
Tm6sf1_predicted	transmembrane 6 superfamily member 1 (predicted)	BI283829	21.4	5.38
Cd9	CD9 antigen	AI227627	21.4	2.96
Csf3	colony stimulating factor 3 (granulocyte)	NM_017104	21.39	3.9
Sdc1	syndecan 1	NM_013026	21.35	5.13
Itgb4	integrin beta 4	NM_013180	21.34	3.17

Symbol	Description	GenBank	t-statistic	Fold Change
Ugt1a6	UDP glycosyltransferase 1 family, polypeptide A6	J02612	21.32	3.68
Plaur	plasminogen activator, urokinase receptor	AF007789	21.2	3.8
Myo1b	myosin Ib	AA859008	21.19	3.05
Grb2	growth factor receptor bound protein 2	BM386610	21.1	2.94
Homer2	homer homolog 2 (Drosophila)	NM_053309	21.09	3.42
LOC685067		BE108569	21.08	2.94
Lxn	latexin	NM_031655	21.04	3.09
		AI045970	20.96	3.1
Crb3	crumbs homolog 3 (Drosophila)	AI072527	20.95	3.84
		AA850472	20.95	3.09
RGD1561472_predicted	similar to mKIAA2005 protein (predicted)	BG670441	20.94	3.02
Bcl2l1	Bcl2-like 1	AF279286	20.93	3.12
LOC299339		BF389535	20.91	4.01
RGD1562428_predicted	similar to C20orf95 (predicted)	BF387347	20.88	5.45
LOC502782	similar to RIKEN cDNA 2610022G08	AW918690	20.87	2.91
Prkch	protein kinase C, eta	AA799981	20.87	2.82
Arhgap27	Rho GTPase activating protein 27	BE100015	20.83	3.47
Daf1	decay accelarating factor 1	AB032395	20.81	3.63
Elmo3	engulfment and cell motility 3, ced-12 homolog (C. elegans)	BI291645	20.79	4.66
LOC316326	similar to lung inducible neuralized-related C3HC4 RING finger protein	BF416847	20.79	3.67
Sox4_predicted	SRY-box containing gene 4 (predicted)	BI297183	20.73	3.74
Scrn1	secernin 1	BI276031	20.73	3.4
Bcat1	branched chain aminotransferase 1, cytosolic	AI102790	20.7	3.6
Ifitm1_predicted	interferon induced transmembrane protein 1 (predicted)	BG380285	20.68	3.2
Sync_predicted	syncoilin (predicted)	BF284235	20.68	2.92
Pctk2	PCTAIRE-motif protein kinase 2	BM384057	20.65	3.07
		AW536022	20.54	2.82
LOC363091	similar to hypothetical protein FLJ30973	AI103939	20.43	3.18
Sgk	serum/glucocorticoid regulated kinase	NM_019232	20.34	3.31
Sox4_predicted	SRY-box containing gene 4 (predicted)	BE115519	20.3	3.86
Hrasls5	HRAS-like suppressor family, member 5	BF409874	20.3	2.74
		BM390713	20.29	3.48
		AI178901	20.23	2.78
Clu	clusterin	AF314657	20.16	3.23
		AA892299	20.13	2.98
RGD1309676	similar to RIKEN cDNA 5730469M10	AI169367	20.11	2.94
		AA819035	20.1	3.23
RGD1561161_predicted	similar to BC067074 protein (predicted)	AI009517	20.09	3.28
RGD1562732_predicted	similar to Glutathione S-transferase, theta 3 (predicted)	BM390378	20.04	4.85
Bace2	beta-site APP-cleaving enzyme 2	BG381587	20.02	3.11
Serpinb1a	serine (or cysteine) proteinase inhibitor, clade B, member 1a	BF411331	19.99	4.9
Tpbg	trophoblast glycoprotein	NM_031807	19.97	3.21
Gsn	gelsolin	BI285576	19.94	5.98
Grb2	growth factor receptor bound protein 2	AI408674	19.94	3.59
LOC363060	similar to RIKEN cDNA 1600029D21	AI599133	19.93	2.9
LOC685652		BI282860	19.91	4.82
		BI296644	19.86	2.83

Symbol	Description	GenBank	t-statistic	Fold Change
Vat1	vesicle amine transport protein 1 homolog (T californica)	BI284849	19.85	3.14
RGD1309138_predicted	similar to hypothetical protein MGC9912 (predicted)	AW433895	19.83	3.74
Optn	optineurin	BI294994	19.83	2.92
Pak1	p21 (CDKN1A)-activated kinase 1	U23443	19.81	2.67
		AI411375	19.8	3.84
Aqp3	aquaporin 3	NM_031703	19.76	3.15
Dixdc1	DIX domain containing 1	BI296216	19.75	4.1
Dtnb	dystrobrevin, beta	BM390663	19.71	2.92
Tuft1_predicted	tuftelin 1 (predicted)	BE114778	19.66	2.88
Thnsl1	threonine synthase-like 1	BF565324	19.62	2.81
Agrn	agrin	M64780	19.6	3.05
		BI295515	19.57	2.9
		BM385296	19.55	2.77
Sh3tc1_predicted	SH3 domain and tetratricopeptide repeats 1 (predicted)	AI237897	19.54	2.74
Kat3	kynurenine aminotransferase III	BI295878	19.53	3.03
Bk	brain and kidney protein	U30831	19.52	3.35
Slc1a1	solute carrier family 1 (neuronal/epithelial high affinity glutamate transporter, system Xag), member 1	D63772	19.47	2.82
Mppe1_predicted	metallophosphoesterase 1 (predicted)	BE113263	19.38	3.23
Sdccag8	serologically defined colon cancer antigen 8	BI299261	19.28	2.66
Ccl2	chemokine (C-C motif) ligand 2	NM_031530	19.2	3.85
Sdc1	syndecan 1	BG375315	19.2	3.24
RGD1564315_predicted	similar to RIKEN cDNA 9330161F08 (predicted)	AA859508	19.13	3.96
Cpne3_predicted	copine III (predicted)	AI237636	19.07	3.3
RGD1303271	similar to chromosome 1 open reading frame 172	BM385475	18.98	2.58
		BE114751	18.95	3.1
RGD1561472_predicted	similar to mKIAA2005 protein (predicted)	AW533923	18.95	2.57
		BM388843	18.89	2.86
		AW524711	18.88	3.15
Spna1	spectrin alpha 1	AI639523	18.85	3.91
Kif12	kinesin family member 12	BI296819	18.82	2.68
		BE113381	18.79	3.65
Krt1-18	keratin complex 1, acidic, gene 18	BI286012	18.76	6.01
Bin2	bridging integrator 2	BM386830	18.74	3.05
		BF408350	18.71	2.84
		BI276505	18.71	2.64
Ocil	osteoclast inhibitory lectin	NM_130402	18.71	2.62
		AI406912	18.69	3.5
Osbpl5	oxysterol binding protein-like 5	BG372522	18.61	2.82
Cblc	Casitas B-lineage lymphoma c	BM384014	18.6	3.81
Mmp19_predicted	matrix metalloproteinase 19 (predicted)	BI294977	18.6	2.52
Zfp64	zinc finger protein 64	BI296003	18.55	3.06
Crb3	crumbs homolog 3 (Drosophila)	BF553130	18.52	3.68
		AI070306	18.5	3.06
		AA901088	18.49	2.97
Fcer2a	Fc receptor, IgE, low affinity II, alpha polypeptide	AI410068	18.43	2.69
		BI291029	18.41	3.81

Symbol	Description	GenBank	t-statistic	Fold Change
Ifit2	interferon-induced protein with tetratricopeptide repeats 2	AI009765	18.4	3.62
RGD1563437_predicted	similar to KIAA1217 (predicted)	BF291123	18.36	2.59
Kifc3	kinesin family member C3	BI295100	18.35	3.45
Serpinb7	serine (or cysteine) proteinase inhibitor, clade B, member 7	NM_130404	18.32	3.83
Bcl2l1	Bcl2-like 1	U72350	18.32	2.48
		AI236141	18.3	2.71
		BE328978	18.28	2.52
		BG378715	18.26	5.12
RGD1563506_predicted	similar to junction-mediating and regulatory protein (predicted)	AI112776	18.26	3.79
Tmprss2	transmembrane protease, serine 2	NM_130424	18.2	2.76
Rab27a	RAB27A, member RAS oncogene family	AI043615	18.2	2.53
Mfi2_predicted	antigen p97 (melanoma associated) identified by monoclonal antibodies 133.2 and 96.5 (predicted)	BF417890	18.18	4.49
Faim2	Fas apoptotic inhibitory molecule 2	AF044201	18.18	2.69
RGD1563547_predicted	RGD1563547 (predicted)	BG378463	18.16	2.93
Plcd1	phospholipase C, delta 1	NM_017035	18.16	2.69
		AI412601	18.1	2.56
RGD1309930	similar to 2810022L02Rik protein	BI275911	18.09	2.62
Pik3ap1_predicted	phosphoinositide-3-kinase adaptor protein 1 (predicted)	AW916092	18.09	2.54
Tgm1	transglutaminase 1	NM_031659	18.07	3.52
Sytl2_predicted	synaptotagmin-like 2 (predicted)	BG670294	18.07	3.08
Kcnq1	potassium voltage-gated channel, subfamily Q, member 1	NM_032073	18.07	2.79
Tmem8_predicted	transmembrane protein 8 (five membrane-spanning domains) (predicted)	AW527467	18.06	2.6
Ttll1	tubulin tyrosine ligase-like 1	AA818423	18.04	2.63
Coro2a	coronin, actin binding protein 2A	AW529016	17.99	3.61
Dock6_predicted	dedicator of cytokinesis 6 (predicted)	AI102881	17.99	2.46
		AI713223	17.97	2.47
RGD1309644_predicted	similar to Hypothetical protein KIAA0469 (predicted)	BG380058	17.96	2.56
S100a10	S100 calcium binding protein A10 (calpactin)	NM_031114	17.95	3.12
Marcks	myristoylated alanine rich protein kinase C substrate	BE111604	17.94	2.56
Vwa1	von Willebrand factor A domain containing 1	BF413643	17.92	3.2
Epb4.1l5	erythrocyte protein band 4.1-like 5	AA858925	17.9	2.63
RGD1308111_predicted	similar to zinc finger protein Cezanne; cellular zinc finger anti-NF-kappaB Cezanne (predicted)	AI716026	17.88	2.77
		BF391800	17.87	3.2
RGD1563506_predicted	similar to junction-mediating and regulatory protein (predicted)	AW532426	17.86	5.18
Kcnk6	potassium channel, subfamily K, member 6	NM_053806	17.86	3.06
RGD1307357_predicted	similar to hypothetical protein DKFZp434A1319 (predicted)	BI280278	17.86	2.44
		AI029006	17.84	2.88
Inpp1	inositol polyphosphate-1-phosphatase	BF523172	17.84	2.5
Mbnl3_predicted	muscleblind-like 3 (Drosophila) (predicted)	AI010322	17.83	3.24
Gja4	gap junction membrane channel protein alpha 4	NM_021654	17.79	3.01

Symbol	Description	GenBank	t-statistic	Fold Change
RGD1311580_predicted	similar to actin filament associated protein; actin filament-associated protein, 110 kDa (predicted)	BF409567	17.79	2.41
		BI277442	17.77	2.41
Plxnb1_predicted	plexin B1 (predicted)	BI288540	17.76	2.45
Bspry	B-box and SPRY domain containing	NM_022261	17.73	4.05
LOC501285		BF390736	17.73	2.71
Asl	argininosuccinate lyase	NM_021577	17.73	2.42
Pkp3_predicted	plakophilin 3 (predicted)	BI286045	17.71	3.94
Asb2	ankyrin repeat and SOCS box-containing protein 2	BI295982	17.69	3.18
		BE115155	17.69	3.09
		AW526790	17.67	2.51
Slc40a1	solute carrier family 39 (iron-regulated transporter), member 1	AI229664	17.67	2.42
		BM391779	17.66	3.35
		BM391096	17.66	2.44
Ifit2	interferon-induced protein with tetratricopeptide repeats 2	BE118697	17.65	4.5
		BI274487	17.63	3
Lamc2	lamimin, gamma 2	AW527269	17.61	3.64
Gas2l1_predicted	growth arrest-specific 2 like 1 (predicted)	AI172537	17.58	2.76
LOC362564		AW252401	17.51	3.33
Rassf7_predicted	Ras association (RalGDS/AF-6) domain family 7 (predicted)	BM385768	17.49	3.02
Prkch	protein kinase C, eta	NM_031085	17.47	2.43
Sec14l2	SEC14-like 2 (S. cerevisiae)	AI575603	17.44	2.42
Gstp2	glutathione S-transferase, pi 2	X02904	17.43	2.7
RGD1560915_predicted	similar to Hypothetical protein MGC30714 (predicted)	AA819250	17.42	2.66
		AI059968	17.41	3.28
Mylk_predicted	myosin, light polypeptide kinase (predicted)	AI177055	17.39	2.68
Znrf1_predicted	zinc and ring finger 1 (predicted)	BE109004	17.38	2.48
Kif16b_predicted	kinesin family member 16B (predicted)	BF397930	17.34	2.39
Inpp1	inositol polyphosphate-1-phosphatase	BI275516	17.3	2.38
Ptpn18	protein tyrosine phosphatase, non-receptor type 18	AW916153	17.29	3.39
Slc9a3r1	solute carrier family 9 (sodium/hydrogen exchanger), isoform 3 regulator 1	NM_021594	17.29	2.48
RGD1566310_predicted	similar to RIKEN cDNA 0610012C01 (predicted)	BF283013	17.26	3.08
		BM389786	17.23	2.61
Ggt1	gamma-glutamyltransferase 1	NM_053840	17.22	2.49
		BE100609	17.17	2.8
		BF283674	17.14	2.66
Nkiras2_predicted	NFKB inhibitor interacting Ras-like protein 2 (predicted)	AI406810	17.1	2.55
Cybasc3	cytochrome b, ascorbate dependent 3	AI179227	17.09	2.35
RGD1308967_predicted	similar to hypothetical protein MGC16491 (predicted)	BG372643	17.03	3.37
LOC503164	hypothetical protein LOC503164	BI289459	17.02	2.35
Marcks	myristoylated alanine rich protein kinase C substrate	M59859	16.97	2.88
Cdh23	cadherin 23 (otocadherin)	AI548870	16.96	2.57
Fut1	fucosyltransferase 1	NM_031236	16.95	2.86
		BF398618	16.89	2.28

Symbol	Description	GenBank	t-statistic	Fold Change
		BE109548	16.79	2.54
Grb7	growth factor receptor bound protein 7	NM_053403	16.77	2.78
Cdc25b	cell division cycle 25 homolog B (S. cerevisiae)	NM_133572	16.76	2.78
		BM388214	16.76	2.41
RGD1308967_predicted	similar to hypothetical protein MGC16491 (predicted)	BG373221	16.74	2.8
Inhbe	inhibin beta E	NM_031815	16.73	3.76
		BI274116	16.7	2.77
Cpeb2_predicted	cytoplasmic polyadenylation element binding protein 2 (predicted)	BG666316	16.69	2.69
		AI170382	16.65	2.7
RGD1564014_predicted	similar to ubiquitin-conjugating enzyme E2 variant 1 (predicted)	AI712728	16.64	2.72
LOC498662	similar to RIKEN cDNA 2610019F03	BI296812	16.62	2.6
Mbp	myelin basic protein	BE109730	16.6	3.31
Naprt1	nicotinate phosphoribosyltransferase domain containing 1	BF416417	16.6	2.33
RGD1304601	similar to RIKEN cDNA 5730457F11	BI274660	16.55	3.08
RGD1308297	similar to CG10084-PA	BI275975	16.54	2.34
Nudt7_predicted	nudix (nucleoside diphosphate linked moiety X)-type motif 7 (predicted)	AA944380	16.5	2.3
Mall	mal, T-cell differentiation protein-like	BM390763	16.44	2.87
Sh3gl2	SH3-domain GRB2-like 2	BM385941	16.4	2.78
Syt8	synaptotagmin 8	NM_053325	16.35	2.62
Pcbd1	pterin 4 alpha carbinolamine dehydratase/dimerization cofactor of hepatocyte nuclear factor 1 alpha (TCF1) 1	BF281220	16.35	2.48
Stx3	syntaxin 3	BI295918	16.35	2.31
Arhgap24	Rho GTPase activating protein 24	BG377201	16.34	3.72
Hspb2	heat shock 27kDa protein 2	NM_130431	16.34	2.79
RGD1565800_predicted	similar to hypothetical protein FLJ20674 (predicted)	BI292079	16.31	2.23
Sh3gl3	SH3-domain GRB2-like 3	NM_031238	16.3	3.17
Casp8	caspase 8	NM_022277	16.3	2.27
		BF398462	16.29	2.5
Padi4	peptidyl arginine deiminase, type IV	AB008803	16.29	2.35
RGD1311294_predicted	similar to Hypothetical protein C6orf60 (predicted)	BI296237	16.28	2.58
		AI764288	16.27	2.63
Mapt	microtubule-associated protein tau	BE107978	16.27	2.4
		BM392135	16.21	2.36
Cmas	cytidine monophospho-N-acetylneuraminic acid synthetase	AI172078	16.21	2.25
Stx3	syntaxin 3	NM_031124	16.2	2.25
		BE113211	16.19	2.19
Freq	frequenin homolog (Drosophila)	BE102100	16.17	5.26
St14	suppression of tumorigenicity 14 (colon carcinoma)	AB049189	16.16	2.26
RGD1560538_predicted	similar to hypothetical protein FLJ21148 (predicted)	BF417345	16.12	2.47
Sertad2	SERTA domain containing 2	BI295862	16.1	2.33
		BI277442	16.07	2.34
Cacybp	calcyclin binding protein	AW918443	16.07	2.18
Scmh1_predicted	sex comb on midleg homolog 1 (predicted)	AA924088	16.06	2.22
LOC497848		BM385981	16.05	2.35

Symbol	Description	GenBank	t-statistic	Fold Change
		AW524894	16.04	3.13
		AW433901	16.01	2.78
Ralgps2	Ral GEF with PH domain and SH3 binding motif 2	BF525299	15.93	2.47
RGD1562149_predicted	similar to mixed-lineage protein kinase 1 (predicted)	AA892737	15.93	2.4
Thbs1		AI406660	15.92	2.47
Kif3c	kinesin family member 3C	AF083330	15.89	2.53
		BM390322	15.88	2.47
		BF284519	15.87	3.87
E030032D13Rik	E030032D13Rik gene	AI136523	15.86	3.67
Prkcd	protein kinase C, delta	NM_133307	15.85	2.82
Prss22_predicted	protease, serine, 22 (predicted)	BM389391	15.84	4.27
RGD1310262_predicted	hypothetical LOC304650 (predicted)	AA891356	15.82	2.31
Timp2	tissue inhibitor of metalloproteinase 2	BF523128	15.81	2.95
		AW533071	15.79	2.47
Slc40a1	solute carrier family 39 (iron-regulated transporter), member 1	NM_133315	15.76	2.22
Evi1_predicted	ecotropic viral integration site 1 (predicted)	BI288681	15.7	2.85
		AI102173	15.68	2.89
MGC93975	similar to 2310044H10Rik protein	BI301512	15.67	2.49
Ifit3	interferon-induced protein with tetratricopeptide repeats 3	AW531805	15.65	2.26
		BE112469	15.65	2.11
Cdh23	cadherin 23 (otocadherin)	BM384374	15.64	3.29
RGD1559427_predicted	similar to BH3-only member B protein (predicted)	BF418697	15.63	2.17
Foxq1	forkhead box Q1	AI070944	15.58	5.03
Egln3	EGL nine homolog 3 (C. elegans)	NM_019371	15.58	2.29
		AI102382	15.53	3.71
		AW533313	15.51	2.82
LOC294560		BE119446	15.51	2.61
		AI102364	15.51	2.33
Dusp14_predicted	dual specificity phosphatase 14 (predicted)	AI236997	15.5	2.61
		AI677633	15.5	2.14
LOC498796	hypothetical protein LOC498796	BF549748	15.49	2.51
Gnao	guanine nucleotide binding protein, alpha o	AF413212	15.49	2.46
Adra1d	adrenergic receptor, alpha 1d	NM_024483	15.47	3.83
		BF393945	15.44	2.72
		AI408920	15.44	2.22
		BI293248	15.43	2.2
Ppap2a	phosphatidic acid phosphatase 2a	NM_022538	15.4	2.14
Pir	pirin	AI176041	15.39	3.22
Lama3	laminin, alpha 3	U61261	15.34	2.16
Frag1	FGF receptor activating protein 1	AI408972	15.32	2.48
		AA899278	15.32	2.45
Unc93b1	unc-93 homolog B1 (C. elegans)	AI234533	15.3	2.62
Jag2	jagged 2	BI274746	15.3	2.15
2-Mar	membrane-associated ring finger (C3HC4) 3	BI298096	15.28	2.14
		BE098181	15.27	2.95
Ramp2	receptor (calcitonin) activity modifying protein 2	NM_031646	15.27	2.55
		BI281808	15.24	2.09

Symbol	Description	GenBank	t-statistic	Fold Change
Irf6_predicted	interferon regulatory factor 6 (predicted)	BF557891	15.23	3.26
Il15	interleukin 15	AF015718	15.23	2.1
		AW527783	15.19	2.34
		AA997863	15.11	2.07
		AI136703	15.1	2.76
RGD1309285_predicted	similar to KIAA1636 protein (predicted)	BF522970	15.09	2.1
		AW251632	15.07	2.09
Ivns1abp_predicted	influenza virus NS1A binding protein (predicted)	AI408553	15.06	2.05
Klf5	Kruppel-like factor 5	BF561079	15.05	2.78
		AI169140	15.04	3.48
Clcf1	cardiotrophin-like cytokine factor 1	AI575844	15.04	2.28
Hnrpab	heterogeneous nuclear ribonucleoprotein A/B	NM_031330	15.04	2.13
C1galt1	core 1 UDP-galactose:N-acetylgalactosamine-alpha-R beta 1,3-galactosyltransferase	NM_022950	15.03	2.2
		AI178231	15.02	2.59
Frag1	FGF receptor activating protein 1	BG373817	15.02	2.41
LOC294560		BF563922	15	2.2
		AI229183	14.99	2.07
RGD1559427_predicted	similar to BH3-only member B protein (predicted)	BF291168	14.98	2.23
		BE116775	14.97	2.21
Vsnl1	visinin-like 1	AI227991	14.95	2.1
RGD1565561_predicted	similar to O-acyltransferase (membrane bound) domain containing 1 (predicted)	AI716936	14.94	4.11
Perp_predicted	PERP, TP53 apoptosis effector (predicted)	BI286396	14.92	2.19
		AA801395	14.91	2.74
B3galt3	UDP-Gal:betaGlcNAc beta 1,3-galactosyltransferase, polypeptide 3	AA799400	14.91	2.7
		AA817953	14.91	2.12
		AW433598	14.9	2.41
Emp1	epithelial membrane protein 1	BI275741	14.9	2.28
Atrn	attractin	AB038388	14.89	2.1
RGD1564628_predicted	similar to ubiquitin specific protease 27, X chromosome (predicted)	BE108241	14.88	2.53
Sh3yl1_predicted	Sh3 domain YSC-like 1 (predicted)	AW527403	14.87	3.1
		BI288580	14.86	2.32
Kcnk1	potassium channel, subfamily K, member 1	NM_021688	14.86	2.19
		AI177743	14.84	2.02
Marcks	myristoylated alanine rich protein kinase C substrate	M59859	14.79	2.6
		BI273710	14.75	2.05
		BF418523	14.74	2.22
		BI275934	14.72	2.59
Dennd2d_predicted	DENN/MADD domain containing 2D (predicted)	AI059486	14.72	2.11
RGD1310006	similar to RIKEN cDNA 5730421E18	AW142960	14.69	2.12
LOC685932		AI599362	14.67	3.2
Tmem5	transmembrane protein 5	BG375242	14.64	2.04
Pdgfa	platelet derived growth factor, alpha	BE100812	14.63	2
		BF396512	14.62	2.23
Mtap_predicted	methylthioadenosine phosphorylase (predicted)	BI278369	14.6	2.04

Symbol	Description	GenBank	t-statistic	Fold Change
		AI409862	14.59	3.06
Metrnl	meteorin, glial cell differentiation regulator-like	BM389126	14.59	2.37
Slc25a30	solute carrier family 25, member 30	AW530647	14.58	2.61
		AA819332	14.57	2.14
		AI230625	14.55	3
Rps6ka4_predicted	ribosomal protein S6 kinase, polypeptide 4 (predicted)	BM388595	14.54	2.2
		BF521753	14.51	2.02
Cln3	ceroid lipofuscinosis, neuronal 3, juvenile (Batten, Spielmeyer-Vogt disease)	BI285912	14.5	2.14
LOC498662	similar to RIKEN cDNA 2610019F03	AA964146	14.47	2.62
		BF394727	14.46	2.35
		BF290953	14.46	2.22
		BE121375	14.43	3.01
RGD1308432_predicted	similar to cDNA sequence BC020002 (predicted)	AA892645	14.42	2.09
Nek6	NIMA (never in mitosis gene a)-related expressed kinase 6	BF282365	14.37	3.11
Slc1a1	solute carrier family 1 (neuronal/epithelial high affinity glutamate transporter, system Xag), member 1	U39555	14.34	2.56
Arid5b_predicted	AT rich interactive domain 5B (Mrf1 like) (predicted)	AW530903	14.32	2.27
		BG667918	14.3	2.73
RGD1561596_predicted	similar to JM11 protein (predicted)	BF396751	14.3	2.02
Nfe2l3_predicted	nuclear factor, erythroid derived 2, like 3 (predicted)	BE108222	14.29	2.34
Basp1	brain abundant, membrane attached signal protein 1	BG380454	14.29	2.06
Gas2l1_predicted	growth arrest-specific 2 like 1 (predicted)	BG371690	14.26	2.24
		AI409900	14.25	2.8
		AW915533	14.25	2.29
Tpmt	thiopurine methyltransferase	NM_031329	14.24	2.22
		BF416405	14.24	2.1
		AI233825	14.22	2.27
		BI302830	14.22	2.04
Cdyl2_predicted	chromodomain protein, Y chromosome-like 2 (predicted)	AA819458	14.21	2.34
RGD1305081_predicted	similar to ionized calcium binding adapter molecule 2 (Iba2) (predicted)	BF408518	14.21	2.18
RGD1563692_predicted	similar to hypothetical protein FLJ22671 (predicted)	AI717274	14.2	2.68
Ezh1_predicted	enhancer of zeste homolog 1 (Drosophila) (predicted)	AA998678	14.2	2.25
		BI283868	14.19	2.29
S100a16_predicted	S100 calcium binding protein A16 (predicted)	AI406499	14.17	2.28
Il23a	Interleukin 23, alpha subunit p19	NM_130410	14.16	2.56
Ankrd1	ankyrin repeat domain 1 (cardiac muscle)	AW251306	14.1	3.16
Gabarapl2	GABA(A) receptor-associated protein like 2	BI303388	14.09	2
		AI179616	14.08	2.37
		AA858498	14.08	2.14
Slc9a3r1	solute carrier family 9 (sodium/hydrogen exchanger), isoform 3 regulator 1	AI577532	14.05	2.28
Basp1	brain abundant, membrane attached signal protein 1	NM_022300	14.04	2.39
RGD1308904	similar to RIKEN cDNA 5430432M24	AA901194	14.02	2.21

Symbol	Description	GenBank	t-statistic	Fold Change
Emp1	epithelial membrane protein 1	NM_012843	14.01	2.62
Fbxo2	F-box only protein 2	NM_053511	14.01	2.35
Nipsnap1	4-nitrophenylphosphatase domain and non-neuronal SNAP25-like protein homolog 1 (C. elegans)	BF554891	14.01	2.24
RGD1306284	similar to RIKEN cDNA 1110005A03	AA866227	14	2.02
		BF411062	13.97	2.42
Pea15	phosphoprotein enriched in astrocytes 15	BG662875	13.94	2.11
Vldlr	very low density lipoprotein receptor	NM_013155	13.9	3.17
Epn2	epsin 2	AW521110	13.89	2.26
Il17re	interleukin 17 receptor E	BM383766	13.84	2.63
		AW522302	13.82	2.44
Aldh3b1	aldehyde dehydrogenase 3 family, member B1	BF412690	13.8	2.5
		BF566725	13.8	2.11
		BE099804	13.79	2.27
Asahl_predicted	N-acylsphingosine amidohydrolase (acid ceramidase)-like (predicted)	AI412627	13.79	2.13
Arpc1b	actin related protein 2/3 complex, subunit 1B	NM_019289	13.72	2.17
Ua20	putative UA20 protein	AI409922	13.67	2.07
RGD1309748_predicted	similar to CG4768-PA (predicted)	BF397406	13.64	2.07
Slc5a10_predicted	solute carrier family 5 (sodium/glucose cotransporter), member 10 (predicted)	BI289660	13.63	2.14
RGD1306809_predicted	similar to hypothetical protein FLJ30596 (predicted)	BF549700	13.62	2.17
Ctsz	cathepsin Z	AA849399	13.56	2.85
Pdgfa	platelet derived growth factor, alpha	L06238	13.56	2.04
Daf1	decay accelarating factor 1	AB026903	13.55	3.09
		AI406341	13.52	3.41
Gata4	GATA binding protein 4	L22761	13.47	2.18
RGD1565927_predicted	similar to 4631422O05Rik protein (predicted)	BM389685	13.43	3.16
Crb3	crumbs homolog 3 (Drosophila)	BI283883	13.42	3.04
		BI285519	13.42	2.09
Ca3	carbonic anhydrase 3	AB030829	13.41	2.97
		BI296427	13.41	2.43
Trio	triple functional domain (PTPRF interacting)	BF554226	13.4	2.49
RGD1306658	similar to 5830411E10Rik protein	BI295501	13.4	2.03
		BE108178	13.39	2.08
Nes	nestin	NM_012987	13.37	2.5
		AT005674	13.36	2.48
Tcf2	transcription factor 2	NM_013103	13.35	3.81
		AI013328	13.34	2.22
		AW533482	13.34	2.16
		AI071024	13.33	2.44
		AA893087	13.32	2.13
		AA851361	13.32	2.12
Lypd3	Ly6/Plaur domain containing 3	NM_021759	13.31	2.17
		BF420433	13.3	2.31
Btc	betacellulin	NM_022256	13.3	2.2
Sh3glb1	SH3-domain GRB2-like B1 (endophilin)	BF283873	13.3	2.08
Mmp2	matrix metallopeptidase 2	U65656	13.26	2.96

Symbol	Description	GenBank	t-statistic	Fold Change
		AI176941	13.23	2.16
RGD1560880_predicted	similar to RIKEN cDNA 2310002J15 (predicted)	BI300388	13.23	2.13
Cugbp2	CUG triplet repeat, RNA binding protein 2	AF090695	13.19	2.02
RGD1309804	similar to hypothetical protein FLJ11218	AI044348	13.18	3.61
Ctbs	chitobiase, di-N-acetyl-	NM_031023	13.18	2.08
RGD1311307	similar to 1300014I06Rik protein	BM385779	13.16	3.76
RGD1562244_predicted	similar to SEC14 and spectrin domains 1 (predicted)	AA892491	13.15	2.15
		AI577848	13.14	2.53
		BG670559	13.04	2.24
Procr	protein C receptor, endothelial	AI137406	13	2.58
Cd96	CD96 antigen	AI764706	12.98	2.57
Slc44a4	solute carrier family 44, member 4	BI289103	12.97	3.78
		BM385170	12.96	2.02
		BI299977	12.93	2.85
		AA943752	12.92	2.11
		BM387460	12.88	2.16
RGD1308876_predicted	similar to 2610027C15Rik protein (predicted)	AI179588	12.88	2.14
		BG667935	12.85	2.37
Efha2	EF hand domain family, member A2	BF404514	12.84	2.86
Phactr1	phosphatase and actin regulator 1	AA996943	12.82	3.34
Slc25a30	solute carrier family 25, member 30	H35736	12.82	2.16
Mawbp	MAWD binding protein	AW532101	12.81	2.79
		BE111349	12.8	2.37
		AI229167	12.79	2.02
Prkar1b	protein kinase, cAMP dependent regulatory, type I, beta	BG375376	12.78	2.08
		AI454052	12.78	2.07
LOC500013		BF408536	12.77	2.06
Nipsnap1	4-nitrophenylphosphatase domain and non-neuronal SNAP25-like protein homolog 1 (C. elegans)	BI289807	12.74	2.35
Dcxr	dicarbonyl L-xylulose reductase	NM_134387	12.74	2.01
Ces1	carboxylesterase 1	AB023630	12.69	2.69
Perp_predicted	PERP, TP53 apoptosis effector (predicted)	AI598971	12.69	2.08
		AI012613	12.68	2.13
RGD1308329_predicted	similar to KIAA0869 protein (predicted)	BM390702	12.66	2.78
		AI010312	12.65	2.97
Argbp2	Arg/Abl-interacting protein ArgBP2	NM_053770	12.62	2.8
Bhlhb3	basic helix-loop-helix domain containing, class B3	NM_133303	12.53	2.12
Fcgr3	Fc receptor, IgG, low affinity III	NM_053843	12.52	2.34
Pem	placentae and embryos oncofetal gene	NM_022175	12.51	2.01
RGD1565681_predicted	similar to Prr6 protein (predicted)	AW523199	12.49	2.68
Slfn3	schlafen 3	NM_053687	12.48	5.34
		BF408801	12.46	2.96
Gcnt2	glucosaminyl (N-acetyl) transferase 2, I-branching enzyme	AI234819	12.4	2.94
RGD1311316	similar to RIKEN cDNA 5730470L24	BE102137	12.4	2.26
Krt1-19	keratin complex 1, acidic, gene 19	BI279605	12.39	2.24
Arhgap22_predicted	Rho GTPase activating protein 22 (predicted)	BM384457	12.38	2.18

Symbol	Description	GenBank	t-statistic	Fold Change
Sdpr	serum deprivation response protein	AI009714	12.37	2.49
RGD1307414_predicted	similar to RIKEN cDNA 1110067D22 (predicted)	BE095833	12.37	2.01
Ebpl_predicted	emopamil binding protein-like (predicted)	AI179635	12.23	2.65
Zfp655	zinc finger protein 655	BI292731	12.17	2.41
Cyba	cytochrome b-245, alpha polypeptide	AI232788	12.16	3.25
Slc36a4_predicted	solute carrier family 36 (proton/amino acid symporter), member 4 (predicted)	AI058947	12.14	2.59
		BF409131	12.13	2.26
RGD1562954_predicted	similar to aldo-keto reductase family 1, member C12 (predicted)	BF566188	12.12	2.71
Bik	Bcl2-interacting killer	NM_053704	12.07	3.19
		AI030349	12.02	2.23
		AI600082	11.93	2.02
RGD1560766_predicted	similar to putative protein product of HMFN2073 (predicted)	BM384831	11.89	2.4
		BF398806	11.78	2.15
		BF283210	11.77	2.45
Dap	death-associated protein	NM_022526	11.76	2.1
		AI137052	11.75	2.33
Lta	lymphotoxin A	AI113237	11.66	2.11
Slc4a11_predicted	solute carrier family 4, sodium bicarbonate transporter-like, member 11 (predicted)	BI293444	11.62	2.52
Ptprj	protein tyrosine phosphatase, receptor type, J	NM_017269	11.33	2.03
Mx1	myxovirus (influenza virus) resistance 1	X52711	11.3	3.39
LOC310013		BF409912	11.17	2.24
		BI294751	11.17	2.02
RGD1305179_predicted	similar to Nedd4 binding protein 1 (predicted)	AA965076	11.13	2.27
		BI274116	11.13	2.25
		AI715259	11.08	2
RGD1311019_predicted	similar to hypothetical protein DKFZp434H2010 (predicted)	BG372342	11.01	2.41
		BM384387	11.01	2.23
Rab27a	RAB27A, member RAS oncogene family	BM389524	10.97	2.35
		BF555947	10.86	2.66
		BF550404	10.85	2.07
Centa1	centaurin, alpha 1	U51013	10.84	2.43
		AW527651	10.84	2.17
Gmip_predicted	Gem-interacting protein (predicted)	BF544982	10.81	2.2
		AI598434	10.74	3.74
RGD1309720	similar to Hypothetical protein MGC19163	AI059270	10.74	2.25
Centa1	centaurin, alpha 1	NM_133567	10.73	2.68
Klhl2_predicted	kelch-like 2, Mayven (Drosophila) (predicted)	AI145435	10.7	2.12
Kif3c	kinesin family member 3C	NM_053486	10.68	2.26
Plekha6_predicted	pleckstrin homology domain containing, family A member 6 (predicted)	BF547014	10.63	2.12
Hbegf	heparin-binding EGF-like growth factor	NM_012945	10.59	2.8
Usp43_predicted	ubiquitin specific protease 43 (predicted)	BE120893	10.57	2.04
Mmp3	matrix metallopeptidase 3	NM_133523	10.53	2.31
Il1rn	interleukin 1 receptor antagonist	NM_022194	10.52	2.29
Npm2	nucleophosmin/nucleoplasmin 2	BE105805	10.49	2.24
Anxa1	annexin A1	AI236455	10.45	5.13

Symbol	Description	GenBank	t-statistic	Fold Change
LOC498662	similar to RIKEN cDNA 2610019F03	AA964146	10.43	2.11
Dzip1l	DAZ interacting protein 1-like	BI290883	10.43	2
		BM385061	10.41	2.38
RGD1560915_predicted	similar to Hypothetical protein MGC30714 (predicted)	AA801227	10.38	2.16
		BI296243	10.35	2.82
		BM385772	10.24	2.15
		BF419721	10.21	2.02
Trim27_predicted	tripartite motif protein 27 (predicted)	BI294862	10.15	2.22
Cpeb2_predicted	cytoplasmic polyadenylation element binding protein 2 (predicted)	AI010275	10.11	2.03
Bicc1_predicted	bicaudal C homolog 1 (Drosophila) (predicted)	BF389151	9.98	2.71
		AI408264	9.98	2.44
Lnx1_predicted	ligand of numb-protein X 1 (predicted)	BE120953	9.96	2.94
RGD1305647_predicted	similar to hypothetical protein FLJ23375 (predicted)	AI406343	9.95	2.46
RGD1563148_predicted	similar to osteoclast inhibitory lectin (predicted)	BI292042	9.92	2.11
RGD1311463	similar to RIKEN cDNA 2700007P21	AW526652	9.86	2.03
Rap2b	RAP2B, member of RAS oncogene family	BE116619	9.81	2.01
Trpv6	transient receptor potential cation channel, subfamily V, member 6	AI101583	9.66	2.27
RGD1306100_predicted	similar to RRP22 (predicted)	BF414261	9.66	2.17
Ptpn18	protein tyrosine phosphatase, non-receptor type 18	BM386565	9.64	2.03
Fgfbp1	fibroblast growth factor binding protein 1	NM_022603	9.56	2.18
Cxadr	coxsackie virus and adenovirus receptor	AI137518	9.52	2
RGD1562031_predicted	similar to GTPase activating protein testicular GAP1 (predicted)	AA818889	9.49	2.09
		BI294737	9.47	2.89
		BF399504	9.47	2.06
LOC502782	similar to RIKEN cDNA 2610022G08	AW434228	9.44	2.32
		BI286340	9.36	2.78
Ankrd1	ankyrin repeat domain 1 (cardiac muscle)	BE113012	9.34	2.92
Gna14	guanine nucleotide binding protein, alpha 14	BI289045	9.29	2.1
		AI175104	9.27	2.23
Dyrk3	dual-specificity tyrosine-(Y)-phosphorylation regulated kinase 3	BE103067	9.14	2.53
Sult2b1_predicted	sulfotransferase family, cytosolic, 2B, member 1 (predicted)	BM390571	9.03	2.09
		AI176265	9.02	2.93
Shank2	SH3/ankyrin domain gene 2	NM_133440	8.98	2.26
Dao1	D-amino acid oxidase 1	NM_053626	8.94	2.39
RGD1307749_predicted	similar to RIKEN cDNA 1600013K19 (predicted)	BG377375	8.94	2.38
Siahbp1	siah binding protein 1; FBP interacting repressor; pyrimidine tract binding splicing factor; Ro ribonucleoprotein-binding protein 1	BE100353	8.91	2.61
		AA942816	8.72	2.69
Rap2b	RAP2B, member of RAS oncogene family	NM_133410	8.55	2.27
Vgll1_predicted	vestigial like 1 homolog (Drosophila) (predicted)	BI289790	8.5	2.02
Tead2_mapped	TEA domain family member 2 (mapped)	AW142018	8.27	2.13
MGC116202		BE097451	8.17	2.3
Nrp1	neuropilin 1	AF016296	8.02	2

Symbol	Description	GenBank	t-statistic	Fold Change
Rnase4	ribonuclease, RNase A family 4	BI284831	7.98	2.06
Sla	src-like adaptor	AI500952	7.78	2.12
Grb14	growth factor receptor bound protein 14	NM_031623	7.56	2.07
		BF387305	7.52	2.05
Myo5b	myosin 5B	NM_017083	7.09	2.06
Prss35	protease, serine, 35	AA866443	7.06	3.37
Cxcl2	chemokine (C-X-C motif) ligand 2	NM_053647	7.04	4.39
Gdf15	growth differentiation factor 15	NM_019216	6.76	2.83
		AA900645	6.75	2.11
		BM389322	6.32	2.74
Cd83_predicted	CD83 antigen (predicted)	AI412355	6.08	2.5
		BI278180	6.05	2.33
Dusp5	dual specificity phosphatase 5	BE111304	5.81	3.54
Cxcl1	chemokine (C-X-C motif) ligand 1	NM_030845	5.28	2.81
Sdpr	serum deprivation response protein	AI603408	5.17	2.13
		AI008409	3.6	2.16
		AI710284	3.53	2.04

Genes upregulated in FRTL5 cells relative to FRT cells

Symbol	Description	GenBank	t-statistic	Fold Change
Sdc2	syndecan 2	AI574779	-64.02	-9.09
Ctgf	connective tissue growth factor	NM_022266	-61.13	-9
Lbp	lipopolysaccharide binding protein	BF289368	-60.48	-8.98
Tg	thyroglobulin	AF221622	-58.84	-8.88
Etnk1_predicted	ethanolamine kinase 1 (predicted)	BM391283	-55.82	-8.18
Pgcp	plasma glutamate carboxypeptidase	NM_031640	-55.67	-8.31
		AA893192	-55.42	-8.25
Sdc2	syndecan 2	AI169682	-55.08	-8.67
Mal2	mal, T-cell differentiation protein 2	AI102073	-54.38	-7.39
Rgc32	response gene to complement 32	NM_054008	-51.47	-7.25
Hhex	hematopoietically expressed homeobox	NM_024385	-50.35	-7.17
Klf2_predicted	Kruppel-like factor 2 (lung) (predicted)	BM385790	-50.21	-8.01
Gpm6a	glycoprotein m6a	BF394166	-49.68	-7
Sectm1	secreted and transmembrane 1	AI009823	-49.65	-6.91
Id4	inhibitor of DNA binding 4	BE116009	-48.74	-6.88
		BE107419	-48.07	-7.07
Cd48	CD48 antigen	X13016	-47.84	-7.2
Ctsc	cathepsin C	AW920064	-47.3	-6.76
Pros1	protein S (alpha)	U06230	-47.25	-6.67
		BF388057	-46.87	-7.09
LOC207125	unknown protein	BE118080	-46.69	-6.93
Dact2_predicted	dapper homolog 2, antagonist of beta-catenin (xenopus) (predicted)	BI288833	-46.51	-6.3
		AI112057	-46.06	-6.27
RGD1305677	similar to RIKEN cDNA 1810020E01	BE107851	-45.99	-6.21
		BG662710	-45.78	-6.37
Timp3	tissue inhibitor of metalloproteinase 3 (Sorsby fundus dystrophy, pseudoinflammatory)	AI009159	-45.67	-7.6
Tceal8	transcription elongation factor A (SII)-like 8	AI230334	-45.54	-6.3
Ndrg2	N-myc downstream regulated gene 2	NM_133583	-45.27	-7.05
Pla2g4a	phospholipase A2, group IVA (cytosolic, calcium-dependent)	NM_133551	-45.08	-7.65
Wbp5_predicted	WW domain binding protein 5 (predicted)	BG378874	-45.04	-7.5
MGC108778	similar to RIKEN cDNA 1810057C19	BM391248	-44.95	-6.22
		BF409024	-44.74	-6.51
Tg	thyroglobulin	M35965	-44.53	-7.25
		AI175045	-44.52	-7.5
Nptx1	neuronal pentraxin 1	U18772	-44.44	-6.08
Sftpc	surfactant associated protein C	AI009659	-44.42	-6.06
Sepp1	selenoprotein P, plasma, 1	AA799627	-44.42	-6.68
Tsnax	translin-associated factor X	BI283853	-43.99	-6.45
Cxcr4	chemokine (C-X-C motif) receptor 4	U54791	-43.97	-5.97
Cybrd1	cytochrome b reductase 1	AI010267	-43.53	-5.91
LOC362065	CG6210-like	BF394235	-43.15	-6.45
		AI577833	-42.95	-6.99
Slc25a4	solute carrier family 25 (mitochondrial carrier; adenine nucleotide translocator), member 4	BG666999	-42.73	-8.18
Emb	embigin	NM_053719	-42.46	-6.62

Symbol	Description	GenBank	t-statistic	Fold Change
		AI103213	-42.4	-6.44
Thrsp	thyroid hormone responsive protein	AI169092	-42.24	-7.99
Icam1	intercellular adhesion molecule 1	NM_012967	-42.2	-5.83
Timp3	tissue inhibitor of metalloproteinase 3 (Sorsby fundus dystrophy, pseudoinflammatory)	AA893169	-42.02	-9.16
Pvrl3_predicted	poliovirus receptor-related 3 (predicted)	AW525315	-41.37	-6.52
Tspyl	testis-specific protein, Y-encoded-like	BF407207	-41.32	-7.38
		BE112341	-41.21	-6.62
Cobl_predicted	cordon-bleu (predicted)	AI028942	-41.19	-5.58
		BE108374	-41.18	-5.58
Mageh1	melanoma antigen, family H, 1	H32543	-41.1	-5.79
Pgf	placental growth factor	NM_053595	-41.01	-5.88
		BI283881	-40.99	-6.15
Ania4	activity and neurotransmitter-induced early gene protein 4 (ania-4)	NM_021584	-40.74	-6.07
Cstf2t_predicted	cleavage stimulation factor, 3' pre-RNA subunit 2, tau (predicted)	AW522557	-40.71	-6.6
Fkbp9	FK506 binding protein 9	AI236786	-40.7	-5.53
		AA956784	-40.55	-5.58
		AI111767	-40.55	-6.58
RGD1560913_predicted	similar to expressed sequence AW413625 (predicted)	AA799328	-40.43	-6.86
		BI291849	-40.38	-6.33
		BG668816	-40.2	-5.66
		AA859937	-40.01	-5.45
RGD1311589_predicted	similar to RIKEN cDNA E130201N16 (predicted)	BE113624	-39.91	-6.49
Pgf	placental growth factor	BF281271	-39.89	-6.47
LOC501039		BI296353	-39.66	-6.27
		AA818380	-39.44	-5.98
Tm4sf12	transmembrane 4 superfamily member 12	AI410264	-39.44	-6.05
Napsa	napsin A aspartic peptidase	NM_031670	-39.34	-6.97
Nqo2	NAD(P)H dehydrogenase, quinone 2	AA945624	-39.32	-5.54
Timp3	tissue inhibitor of metalloproteinase 3 (Sorsby fundus dystrophy, pseudoinflammatory)	NM_012886	-39.22	-5.94
Pvrl3_predicted	poliovirus receptor-related 3 (predicted)	AI103913	-39.11	-5.41
Gpc4	glypican 4	AI071251	-39.08	-5.5
		AW142650	-39.03	-6.5
RGD1311381_predicted	similar to hypothetical protein FLJ20037 (predicted)	BI294811	-38.73	-5.26
Btg3	B-cell translocation gene 3	NM_019290	-38.72	-6.73
		BF392884	-38.62	-5.37
Tceal1	transcription elongation factor A (SII)-like 1	BF418812	-38.47	-5.26
Txnip	upregulated by 1,25-dihydroxyvitamin D-3	U30789	-38.36	-6.54
Hist1h2ai_predicted	histone 1, H2ai (predicted)	AI176481	-38.3	-5.51
Pcp4	Purkinje cell protein 4	NM_013002	-38.28	-5.9
		BG669741	-38.13	-5.72
Cybrd1	cytochrome b reductase 1	BF419070	-38.12	-5.83
Prkar2b	protein kinase, cAMP dependent regulatory, type II beta	M12492	-38.08	-6.05
Fzd1	frizzled homolog 1 (Drosophila)	AA944349	-38.06	-5.25
Slc4a5	solute carrier family 4, sodium bicarbonate cotransporter, member 5	AW529483	-37.92	-5.12
Timp3	tissue inhibitor of metalloproteinase 3 (Sorsby fundus dystrophy, pseudoinflammatory)	AI599265	-37.9	-7.03

Symbol	Description	GenBank	t-statistic	Fold Change
Spon1	spondin 1	M88469	-37.85	-5.28
Sult1d1	sulfotransferase family 1D, member 1	NM_021769	-37.58	-5.4
LOC290704		BM391364	-37.44	-5.62
Dsc2	desmocollin 2	BI279663	-37.38	-5.46
Id4	inhibitor of DNA binding 4	AI412150	-37.18	-5.07
Foxa2	forkhead box A2	NM_012743	-37.08	-5.06
		BM384088	-37.08	-5.19
Angptl4	angiopoietin-like 4	AA818262	-36.83	-5.08
Fhl1	four and a half LIM domains 1	BG673187	-36.71	-5.53
Cdkn3_predicted	cyclin-dependent kinase inhibitor 3 (predicted)	BE113362	-36.44	-5.9
MGC72567	similar to coiled-coil domain containing 8	BE107413	-36.4	-4.91
LOC499677		AA800950	-36	-4.92
Cmkor1	chemokine orphan receptor 1	NM_053352	-35.95	-6.13
Sod3	superoxide dismutase 3, extracellular	NM_012880	-35.93	-6.38
Mal2	mal, T-cell differentiation protein 2	BF555523	-35.86	-5.06
		BF396607	-35.86	-5.84
		BI286077	-35.51	-7.93
Setbp1_predicted	SET binding protein 1 (predicted)	BF396686	-35.48	-5.25
RGD1307524_predicted	similar to Friedreich ataxia region gene X123 (predicted)	AI231799	-35.35	-6.02
Crym	crystallin, mu	NM_053955	-35.34	-5.52
Ngfrap1	nerve growth factor receptor (TNFRSF16) associated protein 1	NM_053401	-35.32	-5.64
Slc5a5	solute carrier family 5 (sodium iodide symporter), member 5	NM_052983	-35.21	-6.06
Pex2	peroxin 2	AF324454	-35.19	-5.1
Egr3	early growth response 3	AA964492	-35.15	-5.2
Cxcr4	chemokine (C-X-C motif) receptor 4	AA945737	-35.04	-6
MGC114427	similar to melanoma antigen family A, 5	AI179244	-34.91	-4.94
		BM388725	-34.8	-6.58
LOC499677		BF390321	-34.65	-4.74
Tekt1	tektin 1	NM_053508	-34.63	-6.62
Adra1b	adrenergic receptor, alpha 1b	NM_016991	-34.55	-5.49
Tacc1	transforming, acidic coiled-coil containing protein 1	AI008689	-34.5	-5.89
		AI236027	-34.45	-5.23
Sdc2	syndecan 2	BG668421	-34.42	-7.74
Ass	argininosuccinate synthetase	BF283456	-34.2	-5.15
RGD1564851_predicted	similar to putative anion transporter (predicted)	AI555358	-33.93	-4.87
		BI282914	-33.75	-6.13
RGD1564105_predicted	similar to RIKEN cDNA B130052G07 (predicted)	AI409065	-33.74	-5.92
RGD1309065_predicted	similar to RIKEN cDNA 4931407K02 (predicted)	AW535172	-33.7	-4.91
Acta1	actin, alpha 1, skeletal muscle	NM_019212	-33.64	-5.39
Ddt	D-dopachrome tautomerase	NM_024131	-33.3	-5.21
MGC94782	similar to hypothetical protein MGC33926	AI010157	-33.28	-4.75
		BM386869	-33.18	-4.53
Slc25a29	solute carrier family 25 (mitochondrial carrier, palmitoylcarnitine transporter), member 29	BF555120	-33.13	-4.94
		AI231999	-33.06	-5.8
LOC681395		AW524822	-32.79	-5.02
Gpd1	glycerol-3-phosphate dehydrogenase 1 (soluble)	BI277042	-32.77	-5.69
Titf1	thyroid transcription factor 1	BF389361	-32.73	-4.91

Symbol	Description	GenBank	t-statistic	Fold Change
Tsnax	translin-associated factor X	AF262357	-32.55	-6.32
		BE109132	-32.5	-4.78
		BG380430	-32.47	-6.57
Ptges	prostaglandin E synthase	AB048730	-32.3	-5.05
		AI073219	-32.21	-4.57
RGD1309036_predicted	hypothetical LOC292874 (predicted)	AA925385	-32.01	-5.28
Rora_predicted	RAR-related orphan receptor alpha (predicted)	AI235414	-31.97	-5.87
Cxcr4	chemokine (C-X-C motif) receptor 4	AA945737	-31.95	-5.36
P2ry14	purinergic receptor P2Y, G-protein coupled, 14	U76206	-31.92	-5.93
		BE105961	-31.88	-4.65
Ctsc	cathepsin C	AI409046	-31.83	-5.71
Rhob	ras homolog gene family, member B	NM_022542	-31.8	-5.3
Tpo	thyroid peroxidase	NM_019353	-31.72	-6.83
LOC362065	CG6210-like	AI072254	-31.71	-4.69
		BM385741	-31.67	-4.51
		AI010048	-31.52	-4.69
Entpd1	ectonucleoside triphosphate diphosphohydrolase 1	AI009808	-31.48	-4.36
Ppp1r3c	protein phosphatase 1, regulatory (inhibitor) subunit 3C	BM390827	-31.27	-5.21
		BE119164	-31.24	-4.59
RGD1559803_predicted	similar to maestro (predicted)	BF283408	-31.17	-4.87
RGD1309807	similar to Fam13a1 protein	BF563961	-31.15	-4.9
		BF386199	-31.11	-4.42
		AI409042	-31.07	-4.3
Rnf125_predicted	ring finger protein 125 (predicted)	AA925710	-30.91	-5.67
		AI009713	-30.87	-4.49
Smpd3	sphingomyelin phosphodiesterase 3, neutral	NM_053605	-30.79	-5.03
RGD1563869_predicted	sim ilar to glucocorticoid induced gene 1 (predicted)	BI295240	-30.77	-5.2
Plod2	procollagen lysine, 2-oxoglutarate 5-dioxygenase 2	BI279641	-30.71	-6.02
Npepl1_predicted	aminopeptidase-like 1 (predicted)	AI411240	-30.54	-4.28
		AI406271	-30.53	-4.3
Lhx2	LIM homeobox protein 2	L06804	-30.52	-4.28
Cp	ceruloplasmin	AF202115	-30.52	-4.59
RGD1566248_predicted	similar to hypothetical protein FLJ14345 (predicted)	AI556490	-30.48	-4.37
Emp3	epithelial membrane protein 3	NM_030847	-30.38	-4.27
Hsd11b1	hydroxysteroid 11-beta dehydrogenase 1	NM_017080	-30.34	-4.43
Acy1	aminoacylase 1	AI411530	-30.33	-4.57
		BF415056	-30.32	-4.21
Enpp3	ectonucleotide pyrophosphatase/phosphodiesterase 3	NM_019370	-30.28	-4.2
		AA964074	-30.18	-4.21
Hspa4l_predicted	heat shock 70kDa protein 4-like (predicted)	BF401583	-30.16	-5.98
Edg2	endothelial differentiation, lysophosphatidic acid G-protein-coupled receptor, 2	NM_053936	-30.03	-5.13
Rasd2	RASD family, member 2	AF134409	-29.96	-4.73
Pts	6-pyruvoyl-tetrahydropterin synthase	NM_017220	-29.9	-5.2
Slc25a21	solute carrier family 25 (mitochondrial oxodicarboxylate carrier), member 21	NM_133614	-29.88	-4.25
Asph_predicted	aspartate-beta-hydroxylase (predicted)	BF561145	-29.86	-4.71
Fhl1	four and a half LIM domains 1	BI298356	-29.84	-4.33

Symbol	Description	GenBank	t-statistic	Fold Change
		AW535515	-29.8	-4.04
RGD1562987_predicted	similar to cDNA sequence BC031181 (predicted)	AI231196	-29.65	-5.7
Thrsp	thyroid hormone responsive protein	NM_012703	-29.53	-7.65
LOC499677		AI112117	-29.49	-4.36
		BE115085	-29.36	-4.75
Kcnj15	potassium inwardly-rectifying channel, subfamily J, member 15	NM_133321	-29.24	-4.11
Duox2	dual oxidase 2	NM_024141	-29.12	-4.06
		AI548028	-29.1	-4.09
		BI276341	-29.1	-4.54
		AI029492	-28.98	-5.39
RGD1311732	similar to hypothetical protein MGC15407	AI044859	-28.79	-4.94
		BM391853	-28.64	-4.8
Ctsc	cathepsin C	NM_017097	-28.62	-4.75
LOC501039		AI233213	-28.6	-6.09
Gmpr	guanosine monophosphate reductase	NM_057188	-28.57	-4.03
Cd99		AI235284	-28.49	-4.21
Nedd9	neural precursor cell expressed, developmentally down-regulated gene 9	BM392374	-28.49	-4.71
Pdpn	podoplanin	NM_019358	-28.37	-3.92
		BF565756	-28.32	-3.91
Ppp1r3c	protein phosphatase 1, regulatory (inhibitor) subunit 3C	AW530361	-28.25	-4.05
		BG380393	-28.23	-4.76
LOC361346	similar to chromosome 18 open reading frame 54	BF412754	-28.18	-5.15
Zdhhc2	zinc finger, DHHC domain containing 2	AF228917	-28.14	-4.29
Epb4.1l5	erythrocyte protein band 4.1-like 5	BE109260	-28.03	-5.19
Klhl13	kelch-like 13 (Drosophila)	AI179828	-27.85	-4.73
Dhrs3	dehydrogenase/reductase (SDR family) member 3	BI276935	-27.85	-4.86
Klf2_predicted	Kruppel-like factor 2 (lung) (predicted)	BF288243	-27.84	-6.65
Calml3	calmodulin-like 3	AI030853	-27.83	-5.29
Tfcp2l4_predicted	transcription factor CP2-like 4 (predicted)	BE109781	-27.72	-4.9
		BE111819	-27.68	-3.77
Olfml3_predicted	olfactomedin-like 3 (predicted)	BI274355	-27.64	-4.37
		BI293607	-27.58	-5.07
Ptger4	prostaglandin E receptor 4 (subtype EP4)	AI549199	-27.54	-4.03
Wnt5a	wingless-type MMTV integration site 5A	NM_022631	-27.26	-4.58
		AI411542	-27.13	-5.18
		BF549971	-26.95	-3.69
Cerk_predicted	ceramide kinase (predicted)	AW525194	-26.94	-3.7
RGD1305283_predicted	similar to RIKEN cDNA 2010110K16 (predicted)	BF403524	-26.86	-3.85
		AI408151	-26.86	-6.42
		AW524892	-26.85	-4.74
Mybph	myosin binding protein H	AI408557	-26.79	-5.13
RT1-S3	RT1 class Ib, locus S3	AJ243974	-26.69	-4.56
Gcg	glucagon	NM_012707	-26.65	-5.18
Id4	inhibitor of DNA binding 4	AW916745	-26.63	-4.56
		AI410941	-26.58	-3.69
		AI410438	-26.45	-3.66
Evl	Ena-vasodilator stimulated phosphoprotein	NM_024147	-26.44	-3.94
Thrsp	thyroid hormone responsive protein	NM_012703	-26.44	-5.56

Symbol	Description	GenBank	t-statistic	Fold Change
RGD1306981_predicted	similar to bM410K19.2.2 (novel protein similar to extra-cellular matrix proteins and chondroitin sulfate proteoglycans, variant 2) (predicted)	BM392227	-26.41	-3.62
		BG379594	-26.37	-4.47
Pip5k1a	phosphatidylinositol-4-phosphate 5-kinase, type 1 alpha	BF406008	-26.33	-6.09
Dnaja4	DnaJ (Hsp40) homolog, subfamily A, member 4	AI104324	-26.31	-3.69
Nfia	nuclear factor I/A	AB060652	-26.15	-3.54
Prdx4	peroxiredoxin 4	BI282076	-26.14	-6.29
		BI289330	-26.13	-3.99
		AI175666	-26.06	-5.18
		BI303636	-26.01	-3.94
		BM389611	-26.01	-4.02
Adora1	adenosine A1 receptor	NM_017155	-26.01	-4.31
Itpr2	inositol 1,4,5-triphosphate receptor 2	BF417289	-25.84	-4.34
Mdfic_predicted	MyoD family inhibitor domain containing (predicted)	AI411065	-25.8	-3.54
Tmem16a_predicted	transmembrane protein 16A (predicted)	BF288508	-25.64	-3.58
RT1-S3	RT1 class Ib, locus S3	AJ243973	-25.63	-4.32
Adora1	adenosine A1 receptor	M69045	-25.49	-4.48
Plekhc1	pleckstrin homology domain containing, family C (with FERM domain) member 1	BM386598	-25.44	-3.52
		AI175507	-25.4	-3.73
LOC310877	TRAF2 binding protein	BM384466	-25.37	-3.77
Kdelc2	KDEL (Lys-Asp-Glu-Leu) containing 2	BM384752	-25.25	-3.49
Osbpl1a	oxysterol binding protein-like 1A	BI289884	-25.23	-3.41
		BE111762	-25.23	-3.66
Cnn1	calponin 1	NM_031747	-25.22	-4.18
Maf	v-maf musculoaponeurotic fibrosarcoma oncogene homolog (avian)	AI180340	-25.21	-5.07
		AA818342	-25.17	-3.91
RT1-S3	RT1 class Ib, locus S3	AJ243973	-25.17	-4.17
Metrn	meteorin, glial cell differentiation regulator	BG378672	-25.11	-5.62
		BE096857	-25.09	-4.73
Cdh2	cadherin 2	NM_031333	-25.08	-3.7
		AI599873	-25.03	-4.08
Enpp5	ectonucleotide pyrophosphatase/phosphodiesterase 5	AI409048	-24.98	-3.44
		BM385726	-24.94	-3.74
Irf8	interferon regulatory factor 8	BF284262	-24.79	-3.54
LOC498425	similar to U2 small nuclear ribonucleoprotein auxiliary factor 35 kDa subunit related-protein 1 (U2(RNU2) small nuclear RNA auxillary factor 1-like 1) (SP2)	AW527413	-24.77	-3.66
Tscot_predicted	thymic stromal cotransporter (predicted)	BE108346	-24.77	-4.29
		AA925373	-24.68	-3.48
		BF389689	-24.68	-3.99
Jam3	junctional adhesion molecule 3	AA998207	-24.65	-3.38
		BG669921	-24.63	-3.5
Dmpk_predicted	dystrophia myotonica-protein kinase (predicted)	AI044427	-24.62	-4.51
RGD1564451_predicted	similar to Tribbles homolog 2 (predicted)	AI010430	-24.6	-4.32
Klf15	Kruppel-like factor 15	NM_053536	-24.59	-4.33
		BG379055	-24.58	-3.81
		BI283685	-24.57	-4.22

Symbol	Description	GenBank	t-statistic	Fold Change
		AA899900	-24.49	-3.64
		AA996921	-24.48	-3.76
LOC361346	similar to chromosome 18 open reading frame 54	AW521797	-24.47	-4.47
		BE107167	-24.46	-3.6
LOC296935		AI453854	-24.45	-4.9
		BI275030	-24.43	-3.46
Smad3	MAD homolog 3 (Drosophila)	AA997679	-24.43	-4.19
		BM385437	-24.36	-3.97
		AI578003	-24.35	-3.38
Fgfr3	fibroblast growth factor receptor 3	BF410980	-24.31	-3.87
Gfra3	glial cell line derived neurotrophic factor family receptor alpha 3	BG377887	-24.26	-3.87
Pdlim1	PDZ and LIM domain 1 (elfin)	NM_017365	-24.21	-3.95
Angptl2	angiopoietin-like 2	NM_133569	-24.17	-4.31
RGD1310681_predicted	similar to RIKEN cDNA 6720467C03 (predicted)	BE114214	-24.03	-4.86
MGC72974	Unknown (protein for MGC:72974)	BM385898	-23.98	-3.86
Kctd6_predicted	potassium channel tetramerisation domain containing 6 (predicted)	AI235964	-23.97	-3.35
Rcbtb2	regulator of chromosome condensation (RCC1) and BTB (POZ) domain containing protein 2	BE119554	-23.95	-4.09
Pmp22	peripheral myelin protein 22	AA943163	-23.93	-4.34
Azi2	5-azacytidine induced gene 2	AI177093	-23.9	-3.81
Silv_predicted	silver homolog (mouse) (predicted)	BI300443	-23.9	-3.98
Nucb2	nucleobindin 2	NM_021663	-23.88	-3.22
Pde3b	phosphodiesterase 3B	NM_017229	-23.86	-3.37
RGD1305664	similar to KIAA0672 gene product	BG380767	-23.83	-3.26
Edg2	endothelial differentiation, lysophosphatidic acid G-protein-coupled receptor, 2	AI502597	-23.77	-3.41
		BI292917	-23.73	-3.29
		BI278550	-23.73	-3.35
Slc38a1	solute carrier family 38, member 1	AF075704	-23.72	-3.25
RT1-S3	RT1 class Ib, locus S3	AF029241	-23.72	-3.45
		BF549971	-23.7	-3.43
Scarb2	scavenger receptor class B, member 2	NM_054001	-23.64	-3.28
		AI408734	-23.57	-4.62
		BI289692	-23.49	-4.02
Atf3	activating transcription factor 3	NM_012912	-23.48	-6.58
Nr4a3	nuclear receptor subfamily 4, group A, member 3	NM_031628	-23.46	-4.12
Krt10	keratin 10	BI282479	-23.41	-3.96
		AW144676	-23.36	-3.72
Sult1a1	sulfotransferase family 1A, phenol-preferring, member 1	AF394783	-23.31	-4.37
Hspb8	heat shock 22kDa protein 8	BG380282	-23.29	-3.35
		BM384930	-23.27	-4.16
		BI281630	-23.25	-3.43
		AF023090	-23.2	-3.83
Slit2	slit homolog 2 (Drosophila)	BF391439	-23.2	-5.23
Slc7a7	solute carrier family 7 (cationic amino acid transporter, y+ system), member 7	AF200684	-23.17	-3.16
		BM387112	-23.13	-4.36
		AI059603	-23.12	-4.01
RGD1561255_predicted	similar to Leucine-rich and immunoglobulin-like domains 3 (predicted)	BI300956	-23.11	-3.15
		AA956757	-23.07	-4.96

Symbol	Description	GenBank	t-statistic	Fold Change
Rrbp1_predicted	ribosome binding protein 1 homolog 180kDa (dog) (predicted)	BI282760	-23.06	-3.24
		BG371995	-23.01	-3.19
Plekhc1	pleckstrin homology domain containing, family C (with FERM domain) member 1	BE128738	-23.01	-3.47
Nr4a1	nuclear receptor subfamily 4, group A, member 1	NM_024388	-22.99	-4.29
		AI176713	-22.89	-3.19
		AA996491	-22.88	-3.08
		AI412803	-22.87	-3.22
		BF282184	-22.84	-3.17
Plekha5	pleckstrin homology domain containing, family A member 5	AI009219	-22.83	-4
		AA996760	-22.79	-3.18
Steap2_predicted	six transmembrane epithelial antigen of prostate 2 (predicted)	AA957889	-22.79	-3.56
Parp12_predicted	poly (ADP-ribose) polymerase family, member 12 (predicted)	BI285978	-22.78	-3.57
		AI578745	-22.78	-4.12
Pdzrn3_predicted	PDZ domain containing RING finger 3 (predicted)	AW532566	-22.78	-4.65
Gsta4	glutathione S-transferase, alpha 4	AI234527	-22.77	-3.91
		BI283314	-22.75	-4.41
Abca1	ATP-binding cassette, sub-family A (ABC1), member 1	AW918387	-22.73	-3.96
RGD1311732	similar to hypothetical protein MGC15407	AI547622	-22.72	-3.49
Slc14a1	solute carrier family 14 (urea transporter), member 1	BF562962	-22.7	-3.08
As3mt	arsenic (+3 oxidation state) methyltransferase	NM_080890	-22.68	-3.21
MGC94142	similar to cDNA sequence BC003324	AI408907	-22.68	-3.4
Sat2_predicted	spermidine/spermine N1-acetyl transferase 2 (predicted)	AI410221	-22.68	-4.29
Pde8a	phosphodiesterase 8A	BG377379	-22.66	-3.26
		BF398716	-22.64	-3.81
		BI274857	-22.63	-3.32
St3gal5	ST3 beta-galactoside alpha-2,3-sialyltransferase 5	NM_031337	-22.62	-3.35
St6galnac3	ST6 (alpha-N-acetyl-neuraminyl-2,3-beta-galactosyl-1,3)-N-acetylgalactosaminide alpha-2,6-sialyltransferase 3	NM_019123	-22.58	-3.95
		AI010234	-22.57	-3.22
		BF398185	-22.57	-3.24
Mcam	melanoma cell adhesion molecule	AB035507	-22.52	-3.11
Cck	cholecystokinin	NM_012829	-22.51	-3.48
Rora_predicted	RAR-related orphan receptor alpha (predicted)	BE106199	-22.4	-5.23
Glul	glutamate-ammonia ligase (glutamine synthase)	NM_017073	-22.39	-3.15
Dpp7	dipeptidylpeptidase 7	NM_031973	-22.35	-4.9
RGD1306323_predicted	similar to Protein C8orf1 (hT41) (predicted)	BM390497	-22.29	-3.02
LOC499129		BG373314	-22.28	-3.2
		AI412099	-22.28	-3.39
		AI639162	-22.25	-3.04
		AI072788	-22.21	-3.06
RGD1562587_predicted	similar to cis-Golgi matrix protein GM130 (predicted)	AA944162	-22.21	-4.22
		BE103235	-22.2	-5.05
		AA800708	-22.18	-3.51
LOC689490		AW253690	-22.17	-3.39

Symbol	Description	GenBank	t-statistic	Fold Change
Tm4sf2_mapped	transmembrane 4 superfamily member 2 (mapped)	AI234044	-22.14	-3.07
		BE116043	-22.14	-3.58
Ppic	peptidylprolyl isomerase C	BI291292	-22.12	-3.28
Igfbp5	insulin-like growth factor binding protein 5	BE104060	-22.11	-3.63
Ptges	prostaglandin E synthase	AF280967	-22.06	-2.97
Pde4d	phosphodiesterase 4D, cAMP specific	NM_017032	-22	-3.56
Crem	cAMP responsive element modulator	AW529408	-21.99	-3.42
RGD1563825_predicted	similar to ENSANGP00000020885 (predicted)	AI180253	-21.94	-3.06
RGD1562272_predicted	similar to TAF11 RNA polymerase II, TATA box binding protein (TBP)-associated factor (predicted)	BE111277	-21.92	-3.14
		AI175668	-21.92	-4.27
RGD1566282_predicted	similar to RIKEN cDNA D330045A20 (predicted)	AW142796	-21.84	-3.35
Enpp1	ectonucleotide pyrophosphatase/phosphodiesterase 1	NM_053535	-21.83	-3.34
LOC314323	transporter	AI180408	-21.77	-2.98
Id4	inhibitor of DNA binding 4	AA944139	-21.77	-3.2
Oat	ornithine aminotransferase	NM_022521	-21.73	-3.17
		AI407797	-21.67	-3.46
LOC310721	similar to 4930431B09Rik protein	BI289723	-21.66	-3.47
Map1lc3a	microtubule-associated protein 1 light chain 3 alpha	AI177372	-21.65	-3.94
		BG374285	-21.64	-3.33
Fgfr1	Fibroblast growth factor receptor 1	S54008	-21.61	-4.28
Hyal3	hyaluronoglucosaminidase 3	BF417430	-21.57	-3.21
RGD1309350_predicted	similar to transthyretin (4L369) (predicted)	BM387540	-21.52	-4.89
Gpd1	glycerol-3-phosphate dehydrogenase 1 (soluble)	NM_022215	-21.51	-3.29
Foxe1	forkhead box E1 (thyroid transcription factor 2)	Y11321	-21.51	-4.18
		AI102035	-21.51	-5.82
Ppp2r5a_predicted	protein phosphatase 2, regulatory subunit B (B56), alpha isoform (predicted)	BG673380	-21.48	-2.98
RGD1306073_predicted	similar to sallimus CG1915-PC (predicted)	BE099622	-21.38	-3.02
Tgm2	transglutaminase 2, C polypeptide	NM_019386	-21.38	-5.02
RGD1559612_predicted	similar to tigger transposable element derived 2 (predicted)	AI228340	-21.32	-2.89
Sord	sorbitol dehydrogenase	BI285149	-21.32	-3.09
Abca1	ATP-binding cassette, sub-family A (ABC1), member 1	BF284523	-21.32	-4.14
		BE108519	-21.3	-3.19
		BI294541	-21.3	-4.3
Fbxo39	F-box protein 39	AI073001	-21.11	-3.57
Pde4b	phosphodiesterase 4B, cAMP specific	AA858930	-21.06	-2.93
		BF404460	-20.97	-2.95
		AI072498	-20.94	-3.24
		AI317824	-20.94	-3.69
		AI410144	-20.93	-2.89
		BE114427	-20.79	-3.76
Spata6	spermatogenesis associated 6	NM_134392	-20.74	-3.31
Maoa	monoamine oxidase A	D00688	-20.7	-3.16
Asb9_predicted	ankyrin repeat and SOCS box-containing protein 9 (predicted)	BI288318	-20.69	-3.52
Kif7_predicted	kinesin family member 7 (predicted)	BG380625	-20.68	-3.14
Cd38	CD38 antigen	NM_013127	-20.67	-2.89

Symbol	Description	GenBank	t-statistic	Fold Change
Entpd1	ectonucleoside triphosphate diphosphohydrolase 1	NM_022587	-20.67	-2.92
RGD1564019_predicted	similar to GTPase activating RANGAP domain-like 3 (predicted)	BE098382	-20.63	-2.89
		BE116385	-20.62	-2.93
RGD1565583_predicted	similar to Protein C20orf129 homolog (predicted)	AA800742	-20.56	-2.97
Sord	sorbitol dehydrogenase	NM_017052	-20.55	-3.29
LOC499617	similar to regulatory factor X-associated protein	BG379771	-20.54	-2.99
Btbd3_predicted	BTB (POZ) domain containing 3 (predicted)	AI230481	-20.52	-3.37
RGD1561817_predicted	similar to Traf2 and NCK interacting kinase, splice variant 4 (predicted)	AW526268	-20.51	-2.79
		AW921706	-20.51	-2.8
Qki	quaking homolog, KH domain RNA binding (mouse)	BE113281	-20.47	-4.86
Plcb4	phospholipase C, beta 4	NM_024353	-20.46	-4.06
		AA858978	-20.43	-3.67
		AI235503	-20.42	-2.81
Dnajc3	DnaJ (Hsp40) homolog, subfamily C, member 3	NM_022232	-20.41	-2.87
Sema3g	sema domain, immunoglobulin domain (Ig), short basic domain, secreted, (semaphorin) 3G	BE108859	-20.37	-3.49
Notch2	notch gene homolog 2 (Drosophila)	AI011448	-20.35	-2.91
Ddr2	discoidin domain receptor family, member 2	AI575451	-20.31	-2.89
Man2a1	mannosidase 2, alpha 1	AI178793	-20.28	-2.74
		AI137898	-20.24	-3.88
Slc38a3	solute carrier family 38, member 3	AF273025	-20.19	-3.01
		AI548924	-20.17	-2.84
Uhrf1_mapped	ubiquitin-like, containing PHD and RING finger domains, 1 (mapped)	BE098732	-20.17	-2.88
Harpb64	hypertrophic agonist responsive protein B64	BG666916	-20.16	-4.88
		BM386534	-20.14	-2.72
RGD1561817_predicted	similar to Traf2 and NCK interacting kinase, splice variant 4 (predicted)	BG666454	-20.12	-2.87
Prelp	proline arginine-rich end leucine-rich repeat protein	AI011747	-20.12	-4.59
RGD1566112_predicted	similar to pleckstrin homology domain protein (5V327) (predicted)	AW521621	-20.09	-3.49
RGD1559720_predicted	RGD1559720 (predicted)	BI295767	-20.08	-3.4
Mtmr1_predicted	myotubularin related protein 1 (predicted)	AI029734	-20.06	-3.33
RGD1561985_predicted	similar to dystrobrevin alpha isoform 1 (predicted)	AI228002	-20.05	-2.72
RGD1310174_predicted	hypothetical LOC298504 (predicted)	AI178784	-20.05	-3.13
Mtac2d1	membrane targeting (tandem) C2 domain containing 1	BI302544	-20.05	-3.36
Stom	stomatin	BI295949	-20.01	-3.22
Tshr	thyroid stimulating hormone receptor	NM_012888	-20.01	-4.88
RGD1566181_predicted	similar to Deltex3 (predicted)	BI297929	-20	-3.44
Csen	calsenilin, presenilin binding protein, EF hand transcription factor	NM_032462	-19.97	-2.82
Arid5a	AT rich interactive domain 5A (Mrf1 like)	AI715395	-19.95	-2.73
		AW529927	-19.95	-3.51
		BM388957	-19.94	-3.75
		BF551311	-19.9	-2.78
Cp	ceruloplasmin	AF202115	-19.9	-2.81
Wnt4	wingless-related MMTV integration site 4	NM_053402	-19.82	-4.81
Dio1	deiodinase, iodothyronine, type I	NM_021653	-19.75	-4
Mt3	metallothionein 3	NM_053968	-19.73	-3.84

Symbol	Description	GenBank	t-statistic	Fold Change
Cachd1_predicted	cache domain containing 1 (predicted)	AI010254	-19.71	-3.64
Glul	glutamate-ammonia ligase (glutamine synthase)	BI275294	-19.7	-2.99
Mybpc2_predicted	myosin binding protein C, fast-type (predicted)	BG378588	-19.69	-3.19
Itga6	integrin, alpha 6	AI137931	-19.68	-2.67
Akap14	A kinase (PRKA) anchor protein 14	NM_021703	-19.63	-2.93
Osbpl1a	oxysterol binding protein-like 1A	AI137224	-19.63	-3.19
		AA818098	-19.62	-2.72
Moxd1	monooxygenase, DBH-like 1	AI555053	-19.55	-4.89
RGD1561749_predicted	similar to hypothetical protein MGC5528 (predicted)	AW251849	-19.54	-2.93
Sulf2	sulfatase 2	AA963797	-19.52	-4.36
		AW527767	-19.51	-3.24
Scarb1	scavenger receptor class B, member 1	AF071495	-19.5	-3.31
MGC114410	similar to Ras association (RalGDS/AF-6) domain family 6	BM383783	-19.5	-4.82
		BF283569	-19.47	-5.14
Herc3_predicted	hect domain and RLD 3 (predicted)	BI295026	-19.46	-3.48
LOC360627	similar to 65kDa FK506-binding protein	BI282959	-19.45	-3.88
LOC499417	similar to Ubiquitin-like protein SMT3A precursor (Ubiquitin-related protein SUMO-2)	BI279654	-19.41	-2.79
Maf	v-maf musculoaponeurotic fibrosarcoma oncogene homolog (avian)	AA957811	-19.39	-2.77
Klf9	Kruppel-like factor 9	BE101336	-19.38	-2.74
		BF407452	-19.36	-2.99
Abhd4_predicted	abhydrolase domain containing 4 (predicted)	AI407868	-19.35	-2.96
Hsd17b7	hydroxysteroid (17-beta) dehydrogenase 7	NM_017235	-19.35	-3.77
		AW521711	-19.34	-2.71
Tead3	TEA domain family member 3	BG372018	-19.34	-2.82
Prm2	protamine 2	NM_012873	-19.31	-3.49
Fgfr1	Fibroblast growth factor receptor 1	BI275155	-19.28	-4.1
Pdk4	pyruvate dehydrogenase kinase, isoenzyme 4	NM_053551	-19.26	-3.65
Tmepai_predicted	transmembrane, prostate androgen induced RNA (predicted)	BI274101	-19.25	-3.15
Fzd7_predicted	frizzled homolog 7 (Drosophila) (predicted)	BF411054	-19.25	-3.62
		AI235281	-19.21	-2.61
RGD1306694_predicted	similar to hypothetical protein (predicted)	BF523573	-19.21	-2.94
		BE108896	-19.19	-2.91
Clcn4-2	putative chloride channel 4-2	BG378827	-19.17	-2.67
Crem	cAMP responsive element modulator	NM_017334	-19.16	-3.53
		AI411989	-19.14	-2.73
Tcn2	transcobalamin 2	NM_022534	-19.12	-3.02
Polr3k		AI105044	-19.09	-2.89
P34	p34 protein	NM_134398	-19.08	-3.17
Cxadr	coxsackie virus and adenovirus receptor	AI412564	-19.06	-2.67
Lrp5_predicted	low density lipoprotein receptor-related protein 5 (predicted)	AW435376	-19.05	-2.7
		AI639181	-19.04	-3.2
		BI279384	-19.02	-2.71
RGD1309079	similar to Ab2-095	AI407536	-19.02	-2.75
Gpd2	glycerol-3-phosphate dehydrogenase 2, mitochondrial	U08027	-18.99	-2.63
Efemp2	EGF-containing fibulin-like extracellular matrix protein 2	BF551426	-18.99	-2.73
Grhl1_predicted	grainyhead-like 1 (Drosophila) (predicted)	BM386731	-18.94	-2.58

Symbol	Description	GenBank	t-statistic	Fold Change
		AI137509	-18.88	-2.78
		AW524563	-18.87	-2.67
Akap2	A kinase (PRKA) anchor protein 2	AI072144	-18.85	-3.04
Irak2	interleukin-1 receptor-associated kinase 2	BI274988	-18.83	-2.93
		AA892818	-18.82	-3.17
		AI317854	-18.8	-2.74
		AI548994	-18.74	-2.96
Mosc2	MOCO sulphurase C-terminal domain containing 2	NM_134410	-18.74	-3
Pak3	p21 (CDKN1A)-activated kinase 3	NM_019210	-18.74	-3.12
		BG371864	-18.69	-2.66
RGD1564596_predicted	similar to RIKEN cDNA 2010001H14 (predicted)	AI454360	-18.69	-2.99
Fads2	fatty acid desaturase 2	NM_031344	-18.67	-3.42
		AI555801	-18.63	-2.61
RGD1561724_predicted	similar to mKIAA0716 protein (predicted)	AI045668	-18.63	-3.09
Pde10a	phosphodiesterase 10A	NM_022236	-18.63	-3.29
RGD1565166_predicted	similar to MGC45438 protein (predicted)	BI274344	-18.61	-2.6
		BM389225	-18.59	-3.42
Por	P450 (cytochrome) oxidoreductase	NM_031576	-18.57	-2.58
RGD1566282_predicted	similar to RIKEN cDNA D330045A20 (predicted)	BE112948	-18.55	-2.61
		BM386808	-18.53	-2.63
Ptprg	protein tyrosine phosphatase, receptor type, G	AI556884	-18.52	-2.79
Mbip_predicted	MAP3K12 binding inhibitory protein 1 (predicted)	AI454309	-18.46	-2.51
Pde4b	phosphodiesterase 4B, cAMP specific	AF202733	-18.44	-2.66
Ptpre	protein tyrosine phosphatase, receptor type, E	D78610	-18.43	-3.36
Parvb_predicted	parvin, beta (predicted)	BI296756	-18.41	-2.8
Tst	thiosulfate sulfurtransferase	AI411117	-18.4	-2.81
Wnt5a	wingless-type MMTV integration site 5A	AI639128	-18.36	-5.11
Scarb1	scavenger receptor class B, member 1	NM_031541	-18.32	-3.38
Acp6	acid phosphatase 6, lysophosphatidic	BF555852	-18.31	-2.72
LOC652955	goliath	BM391371	-18.31	-3.73
Usp2	ubiquitin specific peptidase 2	AF106659	-18.28	-2.65
		BM384251	-18.26	-3.07
Pfkp	phosphofructokinase, platelet	BM389769	-18.23	-2.51
Efemp2	EGF-containing fibulin-like extracellular matrix protein 2	AI112299	-18.2	-2.89
RGD1561555_predicted	similar to CDNA sequence BC022692 (predicted)	BI302694	-18.18	-3.28
RGD1305797_predicted	similar to hypothetical protein FLJ33868 (predicted)	BF412784	-18.17	-2.5
Nedd9	neural precursor cell expressed, developmentally down-regulated gene 9	BF555968	-18.16	-4.09
		AA892565	-18.1	-3.89
Acp6	acid phosphatase 6, lysophosphatidic	BM386224	-18.09	-2.69
		BE097091	-18.09	-3.8
Apln	apelin, AGTRL1 ligand	AI177057	-18.08	-3
Arid5a	AT rich interactive domain 5A (Mrf1 like)	AI177813	-18.07	-2.72
		BE329352	-18.07	-3.15
Aurkb	aurora kinase B	NM_053749	-18.02	-3.35
Rasa3	RAS p21 protein activator 3	AI170661	-18.02	-3.59
		AI407050	-17.98	-3.04
Qki	quaking homolog, KH domain RNA binding (mouse)	BE102226	-17.98	-3.48

Symbol	Description	GenBank	t-statistic	Fold Change
		BI286775	-17.95	-3.62
Nol3	nucleolar protein 3 (apoptosis repressor with CARD domain)	NM_053516	-17.94	-3.5
RGD1305387	similar to RIKEN cDNA 2610207I16	BI288527	-17.93	-2.76
Abcb6	ATP-binding cassette, sub-family B (MDR/TAP), member 6	NM_080582	-17.93	-3.28
RGD1306126	similar to hypothetical protein MGC2494	BF284299	-17.91	-2.97
Hist1h2ai_predicted	histone 1, H2ai (predicted)	BE113430	-17.89	-2.78
		BE112927	-17.87	-3.76
Fzd3	frizzled homolog 3 (Drosophila)	AI029226	-17.86	-2.97
		BI282934	-17.85	-2.74
St6galnac2	ST6 (alpha-N-acetyl-neuraminyl-2,3-beta-galactosyl-1,3)-N-acetylgalactosaminide alpha-2,6-sialyltransferase 2	AA891414	-17.83	-2.71
		AI169572	-17.81	-2.4
		BE108258	-17.79	-3.06
Dnaja4	DnaJ (Hsp40) homolog, subfamily A, member 4	BM386931	-17.78	-2.43
Gprk5	G protein-coupled receptor kinase 5	NM_030829	-17.75	-2.6
		AW535897	-17.72	-2.68
Por	P450 (cytochrome) oxidoreductase	AI407454	-17.71	-2.43
		BF406329	-17.7	-2.98
		AW915423	-17.68	-2.46
Wwp1	WW domain containing E3 ubiquitin protein ligase 1	BM383223	-17.67	-2.42
Tle1_predicted	transducin-like enhancer of split 1, homolog of Drosophila E(spl) (predicted)	BG380534	-17.62	-2.52
Rgs3	regulator of G-protein signalling 3	NM_019340	-17.62	-2.57
RGD1563952_predicted	similar to Mospd2 protein (predicted)	BG667374	-17.62	-3.16
LOC499014	similar to zinc finger, DHHC domain containing 14	BI296586	-17.59	-2.53
		AI556018	-17.59	-2.73
Kif21a_predicted	kinesin family member 21A (predicted)	BE103004	-17.57	-2.73
Trp53rk_predicted	TP53 regulating kinase (predicted)	BI274525	-17.53	-2.39
Col8a1_predicted	procollagen, type VIII, alpha 1 (predicted)	BE128699	-17.52	-2.45
		AI146051	-17.47	-2.57
Zfp110	zinc finger protein 110	AI137283	-17.46	-2.41
Oprk1	opioid receptor, kappa 1	NM_017167	-17.46	-2.73
Tmem34	transmembrane protein 34	AA962979	-17.4	-2.4
		BM383081	-17.37	-2.87
		BG372099	-17.37	-3.2
Tle3	transducin-like enhancer of split 3, E(spl) homolog (Drosophila)	NM_053400	-17.36	-2.49
		AA858791	-17.36	-2.79
		BG378238	-17.35	-2.41
Boc_predicted	biregional cell adhesion molecule-related/down-regulated by oncogenes (Cdon) binding protein (predicted)	BE110539	-17.35	-2.61
Prkcz	protein kinase C, zeta	AW533298	-17.31	-2.59
		AA945751	-17.29	-4.51
Aspm_predicted	asp (abnormal spindle)-like, microcephaly associated (Drosophila) (predicted)	AW528001	-17.27	-2.82
Pde4d	phosphodiesterase 4D, cAMP specific	BF565001	-17.23	-3.18
		BF549570	-17.22	-2.97
		AI144863	-17.18	-2.35
L3mbtl3_predicted	l(3)mbt-like 3 (Drosophila) (predicted)	BI275119	-17.17	-2.7

Symbol	Description	GenBank	t-statistic	Fold Change
LOC317274	hypothetical protein LOC317274	BI288003	-17.16	-2.36
		AI410262	-17.15	-3.18
		AA819279	-17.14	-2.45
RGD1563119_predicted	similar to MADS box transcription enhancer factor 2, polypeptide C (myocyte enhancer factor 2C) (predicted)	BE104219	-17.14	-3.22
RGD1562629_predicted	similar to neurobeachin (predicted)	BM388077	-17.13	-3.47
Sesn3_predicted	sestrin 3 (predicted)	AI113325	-17.12	-2.96
RGD1305898_predicted	similar to hypothetical protein FLJ40283 (predicted)	AI555224	-17.11	-3.2
RGD1305387	similar to RIKEN cDNA 2610207I16	AA964752	-17.07	-2.41
Ghr	growth hormone receptor	AI170771	-16.98	-2.65
Ctsl	cathepsin L	AI232474	-16.97	-2.94
		AI113157	-16.95	-3.04
Enpp4_predicted	ectonucleotide pyrophosphatase/phosphodiesterase 4 (predicted)	AI170859	-16.93	-4.01
		AI043958	-16.92	-2.6
Bok	Bcl-2-related ovarian killer protein	AF051093	-16.91	-2.51
Impact		AI408713	-16.9	-3.22
		BF417576	-16.9	-5.38
Perc64	PE responsive protein c64	BI278571	-16.88	-2.53
		BF523321	-16.88	-2.64
		AI103161	-16.86	-2.28
		BI295776	-16.85	-2.31
		BF415532	-16.85	-2.97
Jundp2	Jun dimerization protein 2	BF394170	-16.83	-2.33
		AW915435	-16.83	-3.06
Pbk_predicted	PDZ binding kinase (predicted)	BG663837	-16.81	-2.64
Mic2l1	MIC2 like 1	NM_134459	-16.79	-3.74
RGD1306534_predicted	similar to P-Rex1 (predicted)	AI060225	-16.75	-2.68
Pxk	PX domain containing serine/threonine kinase	AW920759	-16.71	-2.26
MGC72974	Unknown (protein for MGC:72974)	BI275851	-16.71	-2.47
		AW529817	-16.7	-2.55
Top2a	topoisomerase (DNA) 2 alpha	BM385445	-16.67	-2.65
Cdh2	cadherin 2	AF097593	-16.67	-4.09
		BG380768	-16.64	-2.83
		BI276554	-16.6	-2.58
Ptpn22_predicted	protein tyrosine phosphatase, non-receptor type 22 (lymphoid) (predicted)	AI176755	-16.52	-2.53
		BE104039	-16.51	-2.99
Lrp4	low density lipoprotein receptor-related protein 4	AI070976	-16.5	-2.24
RGD1563224_predicted	similar to 4930438D12Rik protein (predicted)	BF284719	-16.48	-2.3
		BG379394	-16.48	-2.46
		BM383329	-16.47	-2.35
Degs1	degenerative spermatocyte homolog 1 (Drosophila)	NM_053323	-16.47	-2.51
		AW917731	-16.45	-3.43
		BE116572	-16.44	-2.38
Herpud1	homocysteine-inducible, endoplasmic reticulum stress-inducible, ubiquitin-like domain member 1	NM_053523	-16.39	-2.41
		BG376458	-16.38	-2.23
		AI406729	-16.37	-2.32
LOC497083	XK-related protein 5	AW252094	-16.37	-2.77

Symbol	Description	GenBank	t-statistic	Fold Change
Pex2	peroxin 2	BE121134	-16.34	-2.76
		AA799503	-16.33	-2.5
		BG381486	-16.31	-2.31
RGD1563950_predicted	similar to NF-kappa-B-repressing factor (Transcription factor NRF) (predicted)	BF288000	-16.29	-2.43
		BE108354	-16.29	-3.26
Dlgap1	discs, large (Drosophila) homolog-associated protein 1	NM_022946	-16.27	-3.39
		BF407449	-16.26	-3.8
Zfp354a	zinc finger protein 354A	NM_052798	-16.25	-2.73
		BF553297	-16.24	-2.41
Galnt7	UDP-N-acetyl-alpha-D-galactosamine:polypeptide N-acetylgalactosaminyltransferase 7	NM_022926	-16.2	-2.68
		BF285316	-16.2	-2.9
		BE110753	-16.19	-2.36
		BE109363	-16.18	-2.42
RGD1562933_predicted	similar to product is unknown~seizure-related gene (predicted)	BM389543	-16.15	-2.92
Ngfrap1	nerve growth factor receptor (TNFRSF16) associated protein 1	BG381021	-16.12	-2.9
RGD1564451_predicted	similar to Tribbles homolog 2 (predicted)	BE114077	-16.11	-2.32
Man2a1	mannosidase 2, alpha 1	H32368	-16.1	-2.47
Dpep1	dipeptidase 1 (renal)	L07316	-16.08	-2.6
RGD1307336	similar to hypothetical protein	AW522732	-16.08	-3.73
		BM389326	-16.06	-2.78
Impact		BG664101	-16.04	-3.5
		BG665568	-16.02	-3.58
Bai2_predicted	brain-specific angiogenesis inhibitor 2 (predicted)	AA924656	-16.01	-2.21
		AA818967	-16	-2.23
Vangl1_predicted	vang, van gogh-like 1 (Drosophila) (predicted)	AI703874	-16	-2.6
Eif2ak3	eukaryotic translation initiation factor 2 alpha kinase 3	NM_031599	-15.99	-2.37
Abhd4_predicted	abhydrolase domain containing 4 (predicted)	BM383152	-15.99	-2.61
Nmnat3	nicotinamide nucleotide adenylyltransferase 3	AA963282	-15.99	-2.67
RGD1561724_predicted	similar to mKIAA0716 protein (predicted)	AI100942	-15.95	-2.18
Cbs	cystathionine beta synthase	NM_012522	-15.93	-2.19
Impact		AA850890	-15.88	-2.72
Ppp1r1b	protein phosphatase 1, regulatory (inhibitor) subunit 1B	AA942959	-15.86	-2.73
		BI294633	-15.85	-2.23
Tcf4	transcription factor 4	BG377130	-15.8	-2.5
		BE102374	-15.8	-3.21
Elovl6	ELOVL family member 6, elongation of long chain fatty acids (yeast)	BF396857	-15.79	-2.15
Slc6a9	solute carrier family 6 (neurotransmitter transporter, glycine), member 9	M95413	-15.79	-2.52
Tparl	TPA regulated locus	AW523924	-15.75	-2.13
Sec11l3	Sec11-like 3 (S. cerevisiae)	AB022714	-15.75	-2.47
Azi2	5-azacytidine induced gene 2	AI045510	-15.73	-2.17
Sema3a	sema domain, immunoglobulin domain (Ig), short basic domain, secreted, (semaphorin) 3A	NM_017310	-15.73	-2.33
		AI412606	-15.73	-2.68
		AI704285	-15.73	-2.76
Rab38	Rab38, member of RAS oncogene family	M94043	-15.71	-2.2

Symbol	Description	GenBank	t-statistic	Fold Change
Srebf1	sterol regulatory element binding factor 1	BF398848	-15.67	-2.21
Rab27b	RAB27B, member RAS oncogene family	NM_053459	-15.64	-2.17
RGD1559673_predicted	similar to hypothetical protein PP1665 (predicted)	AA963795	-15.64	-2.27
Sc65	synaptonemal complex protein SC65	NM_021581	-15.64	-2.45
		BI294141	-15.64	-2.61
Chd7_predicted	chromodomain helicase DNA binding protein 7 (predicted)	BF523068	-15.63	-2.38
S100a1	S100 calcium binding protein A1	AI228548	-15.63	-2.8
		BE118107	-15.63	-3.98
Acot8	acyl-CoA thioesterase 8	BF282933	-15.62	-2.3
Pnldc1	poly(A)-specific ribonuclease (PARN)-like domain containing 1	AW521201	-15.61	-2.46
Mki67_predicted	antigen identified by monoclonal antibody Ki-67 (predicted)	AI714002	-15.61	-2.99
Top2a	topoisomerase (DNA) 2 alpha	BM385445	-15.61	-3.03
RGD1561019_predicted	similar to hypothetical protein (predicted)	AW530090	-15.6	-2.77
Bok	Bcl-2-related ovarian killer protein	AI227742	-15.58	-2.86
		R47022	-15.57	-2.46
		BM386212	-15.53	-2.1
		BE103021	-15.53	-2.69
		AI101660	-15.52	-2.15
		AI406363	-15.52	-2.49
		AI228600	-15.5	-2.23
RGD1307264_predicted	similar to hypothetical protein FLJ20302; similar to CG31653-PA (predicted)	BF285339	-15.47	-2.15
Agpat4	1-acylglycerol-3-phosphate O-acyltransferase 4 (lysophosphatidic acid acyltransferase, delta)	NM_133406	-15.46	-2.43
Chchd2	coiled-coil-helix-coiled-coil-helix domain containing 2	AA799736	-15.44	-2.54
Srebf1	sterol regulatory element binding factor 1	AF286470	-15.41	-2.38
Kif4	kinesin family member 4	AA859926	-15.4	-2.48
Nfia	nuclear factor I/A	D78019	-15.39	-2.15
Prc1_predicted	protein regulator of cytokinesis 1 (predicted)	BI284262	-15.38	-3.48
LOC290341		AI169116	-15.37	-2.15
RGD1564664_predicted	similar to LOC387763 protein (predicted)	AI454658	-15.37	-2.16
Rpa2	replication protein A2	BM385924	-15.36	-2.27
Slc6a9	solute carrier family 6 (neurotransmitter transporter, glycine), member 9	AW141210	-15.35	-2.53
RGD1306939	similar to mKIAA0386 protein	AI010237	-15.35	-3.6
Ctsc	cathepsin C	AA858815	-15.34	-2.58
Lgals8	lectin, galactoside-binding, soluble 8	AI411914	-15.33	-2.09
Sels	selenoprotein S	AF367467	-15.33	-2.15
Ggtl3	gamma-glutamyltransferase-like 3	NM_130423	-15.32	-2.45
		BM386385	-15.31	-2.76
		BF288135	-15.31	-2.88
		BF409676	-15.31	-2.91
Bub1b	budding uninhibited by benzimidazoles 1 homolog, beta (S. cerevisiae)	BF557145	-15.3	-3.3
		BI290860	-15.26	-2.22
		BF394102	-15.25	-2.74
Mycn_mapped	v-myc myelocytomatosis viral related oncogene, neuroblastoma derived (avian) (mapped)	BI275570	-15.24	-3.29
Lrrc8d	leucine rich repeat containing 8 family, member D	AI101427	-15.22	-2.21
Maged1	melanoma antigen, family D, 1	NM_053409	-15.2	-2.3

Symbol	Description	GenBank	t-statistic	Fold Change
Rab40b_predicted	Rab40b, member RAS oncogene family (predicted)	AA924620	-15.19	-2.19
		BI290853	-15.19	-2.61
LOC360997		BM385804	-15.17	-2.13
		BI289642	-15.14	-2.54
Rrbp1_predicted	ribosome binding protein 1 homolog 180kDa (dog) (predicted)	BI279795	-15.12	-2.18
Slc15a2	solute carrier family 15 (H+/peptide transporter), member 2	NM_031672	-15.12	-2.29
Nt5dc2	5'-nucleotidase domain containing 2	BI285551	-15.11	-2.56
Zfp347	zinc finger protein 347	AB047638	-15.1	-2.19
		AA851385	-15.1	-3.49
		BI296506	-15.07	-2.09
		BI281837	-15.07	-2.56
Abcg3	ATP-binding cassette, sub-family G (WHITE), member 3	BF282804	-15.06	-3.48
Armet_predicted	arginine-rich, mutated in early stage tumors (predicted)	AI170666	-15.02	-2.07
Pdia4	protein disulfide isomerase associated 4	NM_053849	-15.02	-2.86
		BF550315	-15.02	-3.16
Ece1	endothelin converting enzyme 1	NM_053596	-15.01	-2.13
		AW531791	-15	-2.16
		BG377427	-15	-2.76
Kifc1	kinesin family member C1	AW253880	-15	-2.8
Ucp2	uncoupling protein 2 (mitochondrial, proton carrier)	NM_019354	-14.98	-2.24
Cebpd	CCAAT/enhancer binding protein (C/EBP), delta	NM_013154	-14.98	-2.65
		BM382988	-14.92	-3.21
Map1b	microtubule-associated protein 1b	BG672052	-14.9	-2.45
LOC309891	similar to septin 10 isoform 1	AI136863	-14.88	-2.31
Bub1_predicted	budding uninhibited by benzimidazoles 1 homolog (S. cerevisiae) (predicted)	BF388785	-14.87	-2.77
		BE103930	-14.87	-3.19
Zfp629	zinc finger protein 629	BG380675	-14.86	-2.43
St6galnac1	ST6 (alpha-N-acetyl-neuraminyl-2,3-beta-galactosyl-1,3)-N-acetylgalactosaminide alpha-2,6-sialyltransferase 1	BG375792	-14.85	-3.05
Cst3	cystatin C	BG666933	-14.84	-2.05
		BF409598	-14.83	-2.23
Slc4a1	solute carrier family 4, member 1	BE113640	-14.83	-2.53
Dlg7_predicted	discs, large homolog 7 (Drosophila) (predicted)	AA874827	-14.82	-2.63
		AW533569	-14.82	-2.66
		AI412190	-14.81	-2.05
		AI601956	-14.8	-2.6
Mmp14	matrix metallopeptidase 14 (membrane-inserted)	X83537	-14.79	-2.13
RGD1307569_predicted	similar to Protein C21orf63 homolog precursor (predicted)	BF408325	-14.77	-2.34
		AW535380	-14.77	-2.4
RGD1309969	similar to RIKEN cDNA 2600010E01	AI059078	-14.77	-2.65
RGD1561413_predicted	similar to BC021442 protein (predicted)	AI137632	-14.76	-2.5
Cachd1_predicted	cache domain containing 1 (predicted)	BF567204	-14.75	-2.18
LOC294762		BE105494	-14.75	-3.15
Prickle1	prickle-like 1 (Drosophila)	AI171526	-14.74	-2.65
		BI280277	-14.73	-2.55
		BM389711	-14.67	-2.12

Symbol	Description	GenBank	t-statistic	Fold Change
Nid2	nidogen 2	BM389302	-14.65	-3.27
		AA818098	-14.61	-3.02
RGD1310360	similar to 3000004C01Rik protein	AI410054	-14.58	-2.29
Elovl2_predicted	elongation of very long chain fatty acids (FEN1/Elo2, SUR4/Elo3, yeast)-like 2 (predicted)	BG666735	-14.56	-3.26
Tmem19	transmembrane protein 19	BF289172	-14.55	-2.21
RGD1309971_predicted	similar to KIAA1126 protein (predicted)	BI296223	-14.54	-2.01
		BF542239	-14.54	-2.33
		AW251900	-14.52	-2.05
Lpin1	lipin 1	BM385286	-14.52	-2.08
		BI285321	-14.5	-2.29
Siahbp1	siah binding protein 1; FBP interacting repressor; pyrimidine tract binding splicing factor; Ro ribonucleoprotein-binding protein 1	BE113111	-14.5	-2.71
Tcfdp2_predicted	transcription factor Dp 2 (predicted)	AI177311	-14.5	-3.02
Mysm1_predicted	myb-like, SWIRM and MPN domains 1 (predicted)	BF419160	-14.49	-2.19
Ptgds2	prostaglandin D2 synthase 2	NM_031644	-14.48	-2.1
Calu	calumenin	AJ001929	-14.48	-2.18
Klf9	Kruppel-like factor 9	AI071565	-14.47	-2.1
		BG371608	-14.45	-2.08
		BF406606	-14.44	-2.11
		AW532132	-14.42	-2.64
		AI013502	-14.41	-2.29
Rasd1	RAS, dexamethasone-induced 1	AF239157	-14.39	-4.38
Hddc2_predicted	HD domain containing 2 (predicted)	BF409313	-14.35	-2.52
Ca2	carbonic anhydrase 2	NM_019291	-14.34	-3.59
Tcfcp2l2	transcription factor CP2-like 2	AI716050	-14.33	-2.21
Itpr2	inositol 1,4,5-triphosphate receptor 2	X61677	-14.29	-2.08
		AI105202	-14.27	-2.08
RGD1563246_predicted	similar to thrombospondin, type I, domain containing 2 (predicted)	BE107414	-14.26	-2.05
Tbc1d1_predicted	TBC1 domain family, member 1 (predicted)	BM383480	-14.25	-2.17
		BI278193	-14.24	-2.44
Slc6a9	solute carrier family 6 (neurotransmitter transporter, glycine), member 9	AA943735	-14.23	-2.33
		BI282008	-14.23	-2.42
		BE117009	-14.22	-2.27
		BI300566	-14.22	-2.31
Il2rb	interleukin 2 receptor, beta chain	NM_013195	-14.22	-3.79
		BI289840	-14.2	-2.52
		BI289126	-14.19	-2.14
		BE096457	-14.19	-2.77
Maf	v-maf musculoaponeurotic fibrosarcoma oncogene homolog (avian)	NM_019318	-14.16	-2.24
		AI101338	-14.16	-2.3
Itga6	integrin, alpha 6	AA955091	-14.15	-2.19
Acvr1	activin A receptor, type 1	NM_024486	-14.12	-2.18
		BI294306	-14.12	-2.23
Hspb6	heat shock protein, alpha-crystallin-related, B6	D29960	-14.1	-2.59
Smc2l1_predicted	SMC2 structural maintenance of chromosomes 2-like 1 (yeast) (predicted)	AW535052	-14.08	-2.06
		BG376748	-14.08	-2.35

Symbol	Description	GenBank	t-statistic	Fold Change
		AA963975	-14.08	-3.42
		AI407489	-14.04	-2.18
Ckap2_predicted	cytoskeleton associated protein 2 (predicted)	BI295150	-14.04	-2.38
RGD1559690_predicted	similar to hypothetical protein FLJ25416 (predicted)	BE098141	-14.03	-2.43
RGD1311381_predicted	similar to hypothetical protein FLJ20037 (predicted)	AA850950	-14.01	-2.32
Lgals3bp	lectin, galactoside-binding, soluble, 3 binding protein	AF065438	-14.01	-2.75
Slc4a4	solute carrier family 4, member 4	AF210250	-14	-2.26
		BF403558	-13.97	-2.06
		BE112536	-13.95	-2.61
Tspan5	tetraspanin 5	BG381571	-13.91	-2.01
Cd47	CD47 antigen (Rh-related antigen, integrin-associated signal transducer)	NM_019195	-13.86	-2.06
Mte1	mitochondrial acyl-CoA thioesterase 1	BF555448	-13.86	-2.14
Znf183	zinc finger protein 183 (RING finger, C3HC4 type)	AI231532	-13.86	-2.39
RGD1559992_predicted	similar to polycystic kidney disease 2 (predicted)	AA850650	-13.84	-2.06
Sept8_predicted	septin 8 (predicted)	AA943694	-13.84	-2.21
		AA850361	-13.84	-2.29
		BG372589	-13.82	-2.04
		BG379401	-13.82	-2.57
		BG381256	-13.8	-2.52
Lr8	LR8 protein	NM_134390	-13.78	-2.08
		BI295203	-13.78	-2.11
Elovl6	ELOVL family member 6, elongation of long chain fatty acids (yeast)	BE116152	-13.77	-2.7
Nab2	Ngfi-A binding protein 2	AI102530	-13.76	-2.03
Ttc23	tetratricopeptide repeat domain 23	BF284579	-13.73	-2.2
Gnpda2_predicted	glucosamine-6-phosphate deaminase 2 (predicted)	BG374650	-13.71	-2.36
		BF419415	-13.71	-2.4
		BF398091	-13.71	-2.44
Decr1	2,4-dienoyl CoA reductase 1, mitochondrial	NM_057197	-13.71	-2.8
Nusap1_predicted	nucleolar and spindle associated protein 1 (predicted)	AI711233	-13.7	-2.32
		AW525722	-13.69	-2.2
LOC306096		AI411835	-13.68	-3.47
Plunc	palate, lung, and nasal epithelium carcinoma associated	BF546645	-13.67	-2.38
Stag3	stromal antigen 3	NM_053730	-13.66	-2.95
		BF396316	-13.65	-2.23
Ube2e2	ubiquitin-conjugating enzyme E2E 2 (UBC4/5 homolog, yeast)	BM391175	-13.63	-2.01
RGD1561817_predicted	similar to Traf2 and NCK interacting kinase, splice variant 4 (predicted)	BI291396	-13.63	-2.19
Lysmd2_predicted	LysM, putative peptidoglycan-binding, domain containing 2 (predicted)	AI103948	-13.62	-2.96
Vegfc	vascular endothelial growth factor C	NM_053653	-13.62	-3.46
RGD1562686_predicted	similar to genetic suppressor element 1 (predicted)	AA963875	-13.58	-2.2
		AA964466	-13.57	-2.38
Nfasc	neurofascin	BI285436	-13.53	-2.18
Slc14a2	solute carrier family 14 (urea transporter), member 2	NM_019347	-13.53	-2.76
Sqle	squalene epoxidase	NM_017136	-13.52	-2.84

Symbol	Description	GenBank	t-statistic	Fold Change
Glul	glutamate-ammonia ligase (glutamine synthase)	BI296610	-13.51	-2.82
Ripk2	receptor (TNFRSF)-interacting serine-threonine kinase 2	BF412519	-13.49	-2.44
Foxd2_predicted	forkhead box D2 (predicted)	BI291467	-13.48	-3.57
Ccbl1	cysteine conjugate-beta lyase 1	BF400674	-13.47	-2.05
		AI454332	-13.45	-2.44
LOC305076	similar to hypothetical protein MGC29875; novel putative protein similar to YIL091C yeast hypothetical 84 kD protein from SGA1-KTR7	BI297073	-13.45	-2.53
Serpinh1	serine (or cysteine) proteinase inhibitor, clade H, member 1	BI285495	-13.39	-2.12
		BF550565	-13.37	-2.06
LOC498425	similar to U2 small nuclear ribonucleoprotein auxiliary factor 35 kDa subunit related-protein 1 (U2(RNU2) small nuclear RNA auxillary factor 1-like 1) (SP2)	BF404554	-13.35	-2.3
		AI010439	-13.35	-2.8
		AW435415	-13.33	-2.26
Abhd1	abhydrolase domain containing 1	AI105131	-13.3	-2.2
		BG378763	-13.25	-2.21
LOC302855	similar to heterogeneous nuclear ribonucleoprotein G - human	BF290678	-13.24	-3.28
Tm4sf13	transmembrane 4 superfamily member 13	AI408602	-13.21	-2.03
Trib1	tribbles homolog 1 (Drosophila)	BI290758	-13.2	-2.12
Mphosph1_predicted	M-phase phosphoprotein 1 (predicted)	BE110723	-13.2	-2.41
		AI407351	-13.16	-2.07
		BE113449	-13.15	-2.29
		AW529348	-13.15	-2.34
		AW921600	-13.09	-2.12
		AI100827	-13.09	-2.13
Fads1	fatty acid desaturase 1	NM_053445	-13.08	-2.37
Cdc20	cell division cycle 20 homolog (S. cerevisiae)	U05341	-13.08	-2.55
Stk6	serine/threonine kinase 6	AA996882	-13.07	-2.19
		AA899202	-13.04	-2
Terf1	telomeric repeat binding factor 1	AA818755	-13.03	-2.44
Cdc20	cell division cycle 20 homolog (S. cerevisiae)	U05341	-13.03	-2.61
Kif20a_predicted	kinesin family member 20A (predicted)	BE111697	-13.02	-2.8
Abhd3_predicted	abhydrolase domain containing 3 (predicted)	BG662490	-12.97	-2.28
		BE107062	-12.9	-2.44
Pltp_predicted	phospholipid transfer protein (predicted)	BI278687	-12.9	-3.23
Ppfibp2	protein tyrosine phosphatase, receptor-type, F interacting protein, binding protein 2	BE106488	-12.87	-2.28
RGD1562596_predicted	similar to mKIAA0159 protein (predicted)	AI407418	-12.86	-2.07
Sfxn1	sideroflexin 1	AA819349	-12.81	-2.26
Dnajc18	DnaJ (Hsp40) homolog, subfamily C, member 18	AI556034	-12.81	-2.63
		BE108276	-12.79	-2.57
Tm4sf1_predicted	transmembrane 4 superfamily member 1 (predicted)	AW435343	-12.78	-2.32
Asrgl1	asparaginase like 1	AF329099	-12.78	-2.78
C1s	complement component 1, s subcomponent	D88250	-12.76	-2.18
Creld2	cysteine-rich with EGF-like domains 2	BE106888	-12.76	-2.27
Ccna2	cyclin A2	AA998516	-12.76	-2.31
RGD1307736	similar to Hypothetical protein KIAA0152	AI407016	-12.71	-2.01
Dnaja4	DnaJ (Hsp40) homolog, subfamily A, member 4	BF565278	-12.69	-2.27

Symbol	Description	GenBank	t-statistic	Fold Change
Tgm2	transglutaminase 2, C polypeptide	BI275994	-12.68	-2.91
Tra1_predicted	tumor rejection antigen gp96 (predicted)	BG057543	-12.67	-2.2
		AI113308	-12.66	-2.1
		BE349670	-12.65	-2.31
Hmgcs2	3-hydroxy-3-methylglutaryl-Coenzyme A synthase 2	M33648	-12.65	-2.94
		AI145951	-12.61	-2.03
Cdca2	cell division cycle associated 2	BG381524	-12.61	-2.13
		AI170376	-12.61	-2.42
		AA894279	-12.6	-2.23
Nptxr	neuronal pentraxin receptor	BG380575	-12.6	-2.58
Ube2e2	ubiquitin-conjugating enzyme E2E 2 (UBC4/5 homolog, yeast)	AW921519	-12.58	-2.76
		BG374493	-12.57	-2.19
Aldh5a1	aldehyde dehydrogenase family 5, subfamily A1	L34821	-12.57	-2.37
Racgap1_predicted	Rac GTPase-activating protein 1 (predicted)	BF559151	-12.54	-2.09
Melk_predicted	maternal embryonic leucine zipper kinase (predicted)	BM390710	-12.54	-2.79
		BM384889	-12.53	-2.29
Rassf1	Ras association (RalGDS/AF-6) domain family 1	AI103943	-12.52	-2.24
F3	coagulation factor III	NM_013057	-12.49	-3.87
Ebf1	early B-cell factor 1	NM_053820	-12.46	-2.49
Gloxd1	glyoxalase domain containing 1	AA957707	-12.43	-2.23
Plcl3_predicted	phospholipase C-like 3 (predicted)	AI549022	-12.43	-2.98
Sah	SA rat hypertension-associated gene	BE098160	-12.41	-2.07
Spbc25	spindle pole body component 25 homolog (S. cerevisiae)	AI408269	-12.38	-2.24
Mcam	melanoma cell adhesion molecule	BI277043	-12.36	-2.52
MGC72614	Unknown (protein for MGC:72614)	AI385260	-12.35	-2.09
Ril	reversion induced LIM gene	NM_017062	-12.35	-2.5
		BE104167	-12.33	-2.08
RGD1306107_predicted	similar to chromosome 1 open reading frame 2 (predicted)	BG376030	-12.26	-2.2
Zcchc12	zinc finger, CCHC domain containing 12	AI101009	-12.26	-2.2
MGC72614	Unknown (protein for MGC:72614)	AI009530	-12.26	-2.74
Gamt	guanidinoacetate methyltransferase	NM_012793	-12.21	-2.49
		BF395101	-12.11	-2.08
		AW524864	-12.08	-2.04
Fbxo30	F-box protein 30	AI030920	-12.08	-2.17
Atad2_predicted	ATPase family, AAA domain containing 2 (predicted)	AW915567	-12.06	-2.25
Osbpl6_predicted	oxysterol binding protein-like 6 (predicted)	AA901035	-12.05	-2.36
RGD1304563_predicted	similar to RIKEN cDNA 4831426I19 (predicted)	BI301147	-12.05	-2.75
Ddt	D-dopachrome tautomerase	BE108176	-12.03	-2.09
		AA964152	-12.01	-2.25
Oprk1	opioid receptor, kappa 1	L22536	-11.99	-2.49
Ube2l6	ubiquitin-conjugating enzyme E2L 6	BI279216	-11.97	-3.01
		AA849497	-11.96	-3.03
		AI176172	-11.95	-2.51
RGD1559565_predicted	similar to EF hand domain containing 1 (predicted)	BM389214	-11.94	-2.86
		AI101499	-11.89	-2.09
Lzts1	leucine zipper, putative tumor suppressor 1	AA875041	-11.89	-2.41

Symbol	Description	GenBank	t-statistic	Fold Change
Ube2t_predicted	ubiquitin-conjugating enzyme E2T (putative) (predicted)	AW531714	-11.89	-2.51
Dhrs4	dehydrogenase/reductase (SDR family) member 4	AB062758	-11.88	-2.61
		AI579823	-11.84	-2.56
Tmod1	tropomodulin 1	NM_013044	-11.83	-2.71
Csrp1	cysteine and glycine-rich protein 1	NM_017148	-11.81	-2.02
Sc5d	sterol-C5-desaturase (fungal ERG3, delta-5-desaturase) homolog (S. cerevisae)	AB052846	-11.79	-2.15
		AI410976	-11.78	-2.17
Fgf1	fibroblast growth factor 1	BI285064	-11.77	-2.51
		BE110761	-11.75	-2.95
		BF553498	-11.73	-2.26
Hccs_predicted	holocytochrome c synthetase (predicted)	BF405032	-11.7	-2.05
		AI012120	-11.64	-2.09
Tmem23	transmembrane protein 23	AI229404	-11.63	-2.55
		BF408444	-11.6	-2.42
		BE116384	-11.57	-2.61
		AI548667	-11.55	-2.29
		AI712476	-11.54	-2.05
Nradd	neurotrophin receptor associated death domain	AI598730	-11.53	-2.07
Espl1_predicted	extra spindle poles like 1 (S. cerevisiae) (predicted)	AI385371	-11.47	-2.27
Slc25a25	solute carrier family 25 (mitochondrial carrier, phosphate carrier), member 25	AI177358	-11.46	-2.96
Depdc1b_predicted	DEP domain containing 1B (predicted)	AA899893	-11.41	-2.77
Pttg1	pituitary tumor-transforming 1	NM_022391	-11.4	-2.19
Ptprm	protein tyrosine phosphatase, receptor type, M	AI639001	-11.37	-2.21
Ccnb1	cyclin B1	L11995	-11.35	-2.39
		BM391003	-11.35	-2.44
Kif2c	kinesin family member 2C	BI274467	-11.34	-2.14
		BI299008	-11.31	-2.27
Smarcd3	SWI/SNF related, matrix associated, actin dependent regulator of chromatin, subfamily d, member 3	BG380496	-11.28	-2.07
		AI511225	-11.24	-2.05
Zfp278	zinc finger protein 278	BE112999	-11.21	-2.05
Acss1_predicted	acyl-CoA synthetase short-chain family member 1 (predicted)	AI176565	-11.2	-2.03
Tacc3	transforming, acidic coiled-coil containing protein 3	AI556917	-11.2	-2.34
		BE105762	-11.19	-2.19
		AI500762	-11.19	-2.27
Adi1	acireductone dioxygenase 1	AA997430	-11.18	-2.17
		AI072068	-11.18	-2.27
		BF562797	-11.18	-2.42
Piga_mapped	phosphatidylinositol glycan, class A (mapped)	BF409296	-11.16	-2.19
Cdc2a	cell division cycle 2 homolog A (S. pombe)	NM_019296	-11.15	-2.32
Reck_predicted	reversion-inducing-cysteine-rich protein with kazal motifs (predicted)	AW523759	-11.15	-2.7
Lass4_predicted	longevity assurance homolog 4 (S. cerevisiae) (predicted)	BE111727	-11.14	-2.27
Ccnb1	cyclin B1	X64589	-11.13	-2.21
Il6	interleukin 6	NM_012589	-11.12	-2.6
		BE120852	-11.09	-2.13
Osbpl1a	oxysterol binding protein-like 1A	AI070135	-11.08	-2.56

Symbol	Description	GenBank	t-statistic	Fold Change
Ca2	carbonic anhydrase 2	AI408948	-11.06	-2.64
Arf2	ADP-ribosylation factor 2	BE112160	-11	-2.04
Nfia	nuclear factor I/A	D78017	-10.93	-2.61
		AF151710	-10.84	-2.03
Dscr1	Down syndrome critical region homolog 1 (human)	AI170193	-10.78	-2
H2a	histone 2a	BE104595	-10.78	-2.15
Crem	cAMP responsive element modulator	BF564195	-10.77	-2.37
Cdca3	cell division cycle associated 3	BF417638	-10.71	-2.08
		AA996927	-10.67	-2.13
Ccnb2	cyclin B2	AW253821	-10.66	-2.2
Ube2c_predicted	ubiquitin-conjugating enzyme E2C (predicted)	BI296084	-10.63	-2.06
		BF397903	-10.62	-2.28
Tmod1	tropomodulin 1	AI104913	-10.62	-2.43
Tbx15_predicted	T-box 15 (predicted)	AW533075	-10.62	-2.88
		AW917486	-10.59	-2.28
MGC109491	similar to 1110007F12Rik protein	AI071166	-10.57	-2.14
RGD1562552_predicted	similar to hypothetical protein LOC340061 (predicted)	AI408343	-10.57	-2.37
Mybpc2_predicted	myosin binding protein C, fast-type (predicted)	AW533848	-10.56	-2.61
		BI303187	-10.55	-2.23
RGD1309107	similar to RIKEN cDNA 6530401L14 gene	BE109109	-10.51	-2.14
Trib1	tribbles homolog 1 (Drosophila)	BM387324	-10.44	-2.3
		AA956340	-10.43	-2.06
Etfb	electron-transfer-flavoprotein, beta polypeptide	AW252650	-10.37	-2.22
RGD1565734_predicted	similar to SNF2/RAD54 family protein (predicted)	BF397986	-10.37	-2.3
		AI232286	-10.35	-2.25
Orc1l	origin recognition complex, subunit 1-like (S.cereviaiae)	AI059490	-10.33	-2.06
Ralgps2	Ral GEF with PH domain and SH3 binding motif 2	AA926180	-10.29	-2.14
Spag5	sperm associated antigen 5	AF111111	-10.28	-2.17
Pard6g_predicted	par-6 partitioning defective 6 homolog gamma (C. elegans) (predicted)	BI295763	-10.26	-2.91
Chd1_predicted	chromodomain helicase DNA binding protein 1 (predicted)	AA875265	-10.25	-3
		BI299014	-10.18	-2.23
		BM385249	-10.18	-2.49
RGD1310784_predicted	similar to RIKEN cDNA 2810433K01 (predicted)	BE109802	-10.16	-3.04
Gas7	growth arrest specific 7	AJ131902	-10.13	-2.12
		BG378849	-10.09	-2.09
		AA818382	-10.09	-2.55
		AI234119	-10.04	-2.34
		AI599509	-10.03	-2.29
Troap_predicted	trophinin associated protein (tastin) (predicted)	BM392307	-9.96	-2.22
		BE108208	-9.93	-2.01
		BF396623	-9.91	-2
Pcbp4_predicted	poly(rC) binding protein 4 (predicted)	AW523679	-9.87	-2.05
		AI385201	-9.84	-3.07
Plk4_predicted	polo-like kinase 4 (Drosophila) (predicted)	BE109322	-9.82	-2.75
Hfe	hemochromatosis	BI299921	-9.81	-2.68
Nradd	neurotrophin receptor associated death domain	NM_139259	-9.56	-2.45
		BE102340	-9.54	-2.26

Symbol	Description	GenBank	t-statistic	Fold Change
RGD1304592_predicted	similar to KIAA0528 protein (predicted)	BF543289	-9.51	-2.2
		AI578135	-9.5	-2.07
Cdca2	cell division cycle associated 2	AW532628	-9.46	-2.19
Hey1	hairy/enhancer-of-split related with YRPW motif 1	BE107815	-9.37	-3.15
Eif2ak3	eukaryotic translation initiation factor 2 alpha kinase 3	BF398966	-9.36	-2
Stc2	stanniocalcin 2	NM_022230	-9.34	-2.03
Bmp4	bone morphogenetic protein 4	NM_012827	-9.34	-2.76
Rbbp6	retinoblastoma binding protein 6	BG373809	-9.12	-2.24
Mip1	myocardial ischemic preconditioning upregulated 1	AI548984	-9.09	-2.05
Serpina3n	serine (or cysteine) peptidase inhibitor, clade A, member 3N	NM_031531	-9.08	-2.67
Acat2	acetyl-Coenzyme A acetyltransferase 2	AI412322	-8.99	-2.04
Hmmr	hyaluronan mediated motility receptor (RHAMM)	AI171185	-8.96	-2.44
Dufd1_predicted	DUF729 domain containing 1 (predicted)	BI295614	-8.64	-2.56
Kif2c	kinesin family member 2C	NM_134472	-8.54	-2.03
E2f8	E2F transcription factor 8	AI231053	-8.54	-2.51
		AI103530	-8.5	-2.85
Cyp26b1	cytochrome P450, family 26, subfamily b, polypeptide 1	BF397093	-8.47	-2.38
Hmmr	hyaluronan mediated motility receptor (RHAMM)	AF336825	-8.37	-2.42
Zfand2a	zinc finger, AN1-type domain 2A	AI406908	-8.32	-2.39
Fshprh1	FSH primary response 1	NM_012955	-8.13	-2.35
		AI177322	-8.06	-2.97
Akap2	A kinase (PRKA) anchor protein 2	BF398063	-7.94	-2.05
		BI289438	-7.68	-2.17
RGD1305846_predicted	similar to hypothetical protein A730008H23 (predicted)	BE101323	-7.39	-2.12
LOC501039		BF399367	-7.09	-2.43
		AW522589	-6.53	-2.5
		AW434394	-6.11	-2.21
		BI298616	-6.05	-2.34
Ddit3	DNA-damage inducible transcript 3	BF403703	-5.92	-2.27
		BF408177	-5.9	-2.13
Abca1	ATP-binding cassette, sub-family A (ABC1), member 1	AI502114	-5.58	-2.47
		AI070558	-5.06	-3.42

Appendix B

Crb3a and Rab11a Dependent Apical Membrane Formation

Introduction

The deposition of transmembrane Crb3a in the apical plasma membrane requires insertion into the vesicular trafficking machinery and movement to its proper subcellular localizations. Evidence has suggested that Crb3a is responsible for the formation for a distinct apical membrane, suggesting that the trafficking of Crb3a is an early and efficient process in cell polarization. Transmembrane proteins coalesce into a post-Golgi central endosome and are segregated based on final location by Rab-family GTPases that act as sorting signals to and from each endosomal compartment (46, 99) (292). For proteins destined for the apical surface, a common apical recycling endosome (ARE) that resides just below the apical surface is the last sorting endosome before membrane insertion (9). The Rab11 family GTPAses (Rab11a, Rab11b and Rab25) are associated with the ARE (36, 81). Exocytic vesicles budded from the ARE fuse with the apical surface through Rab11-family interactions with the conserved exocyst complex and Myosin Vb based cytoskeletal association (17, 22, 145). The question still remains as to how Crb3a is trafficked to the apical surface during apical membrane establishment. We chose to

investigate Crb3a trafficking using a lumen formation model to determine how Crb3a is trafficked to the apical surface through endosomal compartments

Materials and Methods

Cell Lines and Plasmids

MDCKII cells were maintained in DMEM supplemented with 10% fetal-bovine serum and 1% penicillin-streptomycin-glutamate and appropriate selection agent where noted. PCR of Rab11a was done from a complete H.s. Rab11a EST (Invitrogen Clone ID: 5792753). H.s. Flag-Rab11a was cloned using the following PCR primers: Forward primer: TTAATT GGATCC CCACC ATG GAT TAC AAG GAC GAC GAT GAC AAG GGA GGC GGC ACC CGC GAC GAC GAG T, Reverse primer: TTTT GAATTC TTA GAT GTT CTG ACA GCA CTG CAC CTT TG. Primers were engineered to insert a BamHI restriction site followed by a Flag-epitope sequence at the 5' end and an EcoRI restriction site at the 3' end via PCR. H.s. Flag-Rab11a was cut with the appropriate restriction enzymes and ligated into pQCXIN (Clonetech) for stable transduction into GFP-Crb3a Clone 7 cells and selected using 200μg/mL Hyrgomycin (Invitrogen) and 600μg/mL G418 (Invitrogen). Flag-Rab11a S25N (dominant negative) and Flag-Rab11a Q70L (constitutively active) mutants were made via site-directed mutagenesis using Pfu Turbo (Stratagene). The following primer sequences were used for mutagenesis. S25N Forward: CCTTATTGGAGATTCTGGTGTTGGAAAGAATAATCTCCTGTCTCGATTTACTCG AAATGAG S25N Reverse: CTCATTTCGAGTAAATCGAGACAGGAGATTATTCTTTCCAACACCAGAATCTCC

AATAAGG Q70L Forward:
GCACAGATATGGGACACAGCAGGGCTAGAGCGATATCGAGCTATAACATCAGC
ATATTATCG Q70L Reverse:
CGATAATATGCTGATGTTATAGCTCGATATCGCTCTAGCCCTGCTGTGTCCCATAT
CTGTGC.

Cyst assays and statistics

MDCKII cells stably expressing plasmids of interest were dissociated using enzyme free cell dissociation buffer (Gibco Invitrogen), spun down, washed twice with PBS, and counted. Cells were then resuspended in complete growth media containing 4% Geltrex (Gibco Invitrogen) and seeded in 8-well chamber slides (Nunc), with each chamber containing a bed of 100% Geltrex. Cysts were allowed to grow in complete growth media with 4% geltrex for days indicated. Cysts were then fixed for 1 hour with 4% paraformaldhyde and permiablized with 0.1% SDS/PBS for 30 minutes followed by blocking for 1 hour in 4% goat serum/PBS (PBSG). After blocking, primary antibodies were diluted in (PBSG) and cysts were stained for 24-48 hours at 4 degrees. After three 30 minute washes with PBSG, secondary antibodies were diluted in PBSG and incubated with cysts for 24 hours. After three 30 minute washes, cysts were placed in PBS for visualization. All images were obtained using an Olympus FluoView 500 confocal laser-scanning confocal microscope at the Morphology and Image Analysis Core of the Michigan Diabetes Research and Training Center. Samples were scanned with appropriate lasers and filter sets, and images were collected at 0.5-μm intervals on an Olympus IX-71 inverted microscope using an x100 oil objective. FluoView v4.3

software was used to collect images, and subsequent preparation was performed using Adobe Creative Suite software.

For statistical analysis of Rab11a cysts, two-cell stages positive for Flag epitope staining was counted based on the criteria of possessing a single, GFP-Crb3a positive lumen that resulted in a discontinuous band of E-cadherin staining between the two cells. Statistics are a culmination of two independent experiments and *n* numbers are indicated.

Results

Dominant negative Rab11a affects initial apical membrane formation

Proteins trafficking to the apical surface can traverse a Rab11a-postive ARE en route to their final destination (36, 46). When single MDCKII cells are grown in a 3-dimensional matrix they possess Crb3a on all membrane surfaces. During mitosis and cytokinesis resulting in 2 daughter cells, a single Crb3a positive apical surface (lumen) is formed between the cells and each cell exhibits apical-basal polarity. During mitosis, monomeric eGFP-Crb3a (mEGFP-Crb3a) is endocytosed from the entire cell surface into a cytosolic vesicles and exocytosed to the cleavage furrow to establish a lumen between dividing cells (245, 246). This vesicle was revealed to be a Rab11 positive endosome (246). We generated Flag-epitope tagged versions of wild type Rab11a (Rab11a-WT); constitutively active (Q70L) Rab11a (Rab11a-CA), and dominant negative (S25N) Rab11a (Rab11a-DN) and stably expressed them in cells already stably expressing mEGFP-Crb3a (mEGFP-Crb3a/Rablla-X cells) to determine if apical surface formation is Rab11a-dependent. Single mEGFP-Crb3a/Rablla-X cells were imbedded in Geltrex and imaged after 24 hours to monitor phenotypes at the two-cell stage.

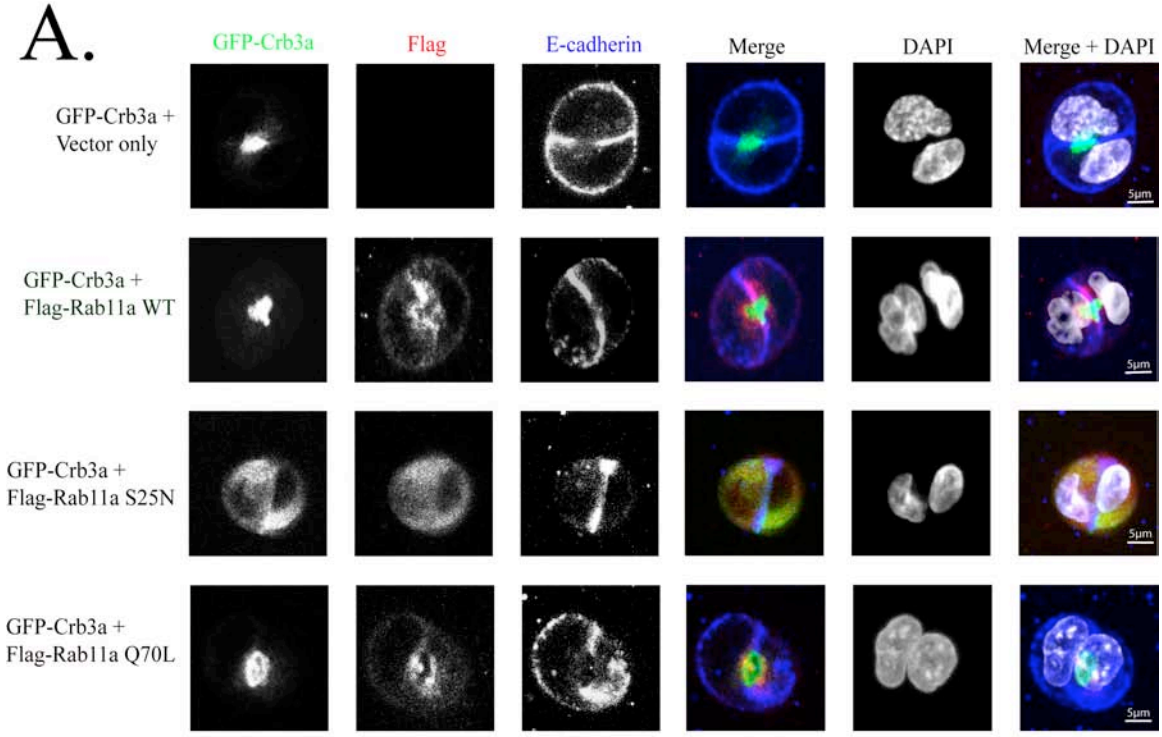
A.
GFP-Crb3a
Flag
E-cadherin
Merge
DAPI
Merge + DAPI
GFP-Crb3a + Vector only
GFP-Crb3a + Flag-Rab11a WT
GFP-Crb3a + Flag-Rab11a S25N
GFP-Crb3a + Flag-Rab11a Q70L
5μm

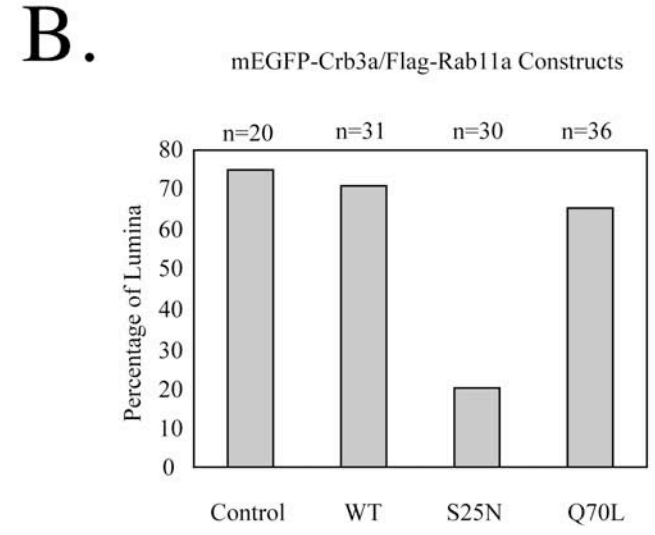
B.
mEGFP-Crb3a/Flag-Rab11a Constructs
n=20
n=31
n=30
n=36
Percentage of Lumina
80
70
60
50
40
30
20
10
0
Control
WT
S25N
Q70L

In vector only control, mEGFP-Crb3a/Rab11a-WT, and mEGFP-Crb3a/Rab11a-CA cells the majority (~70%) of two-cell stages contained a mEGFP-Crb3a positive lumen that between two cells that was also negative for E-cadherin (Figure 4-1B). In mEGFP-Crb3a/Rab11a-DN cells, mEGFP-Crb3a was able to be endocytosed from the surface at the one-cell stage, but failed to be exocytosed at the cleavage furrow at the two-cell stage thus failing to form a lumen between daughter cells in a majority (~70%) of cysts assayed. In mEGFP-Crb3a/Rab11a-DN cells, mEGFP-Crb3a accumulated sub-apically in small, dispersed puncta rather than a single, large recycling endosome.

Dominant negative Rab11a affects mature cyst formation but not polarity

At the two-cell stage in 3-dimensions, mEGFP-Crb3a/Rab11a-DN cells failed to form lumens, however we noticed that when grown in 2-dimensions (i.e. monolayers) mEGFP-Crb3a/Rab11a-DN cells appeared to form apical surfaces (data not shown). We subsequently wanted to determine if mEGFP-Crb3a/Rab11a-DN cells could form lumens at longer time points and to determine if Rab11a-DN affects polarity. To this end we grew mEGFP-Crb3a/Rab11a cells in Geltrex for 4 days to allow them to mature into full cysts with large established apical surfaces. Both mEGFP-Crb3a/Rab11a-WT and mEGFP-Crb3a/Rab11a-CA cells formed mature cysts with one solitary large lumen. The mEGFP-Crb3a/Rab11a-DN cysts however displayed multi-lumen phenotypes. The nature mEGFP-Crb3a/Rab11a-DN phenotype was such that mEGFP-Crb3a was able to form what appears to be an apical surface, but cells in general have lost the ability to coalesce apical surfaces into one solitary lumen. Rab11a has been implicated in E-cadherin

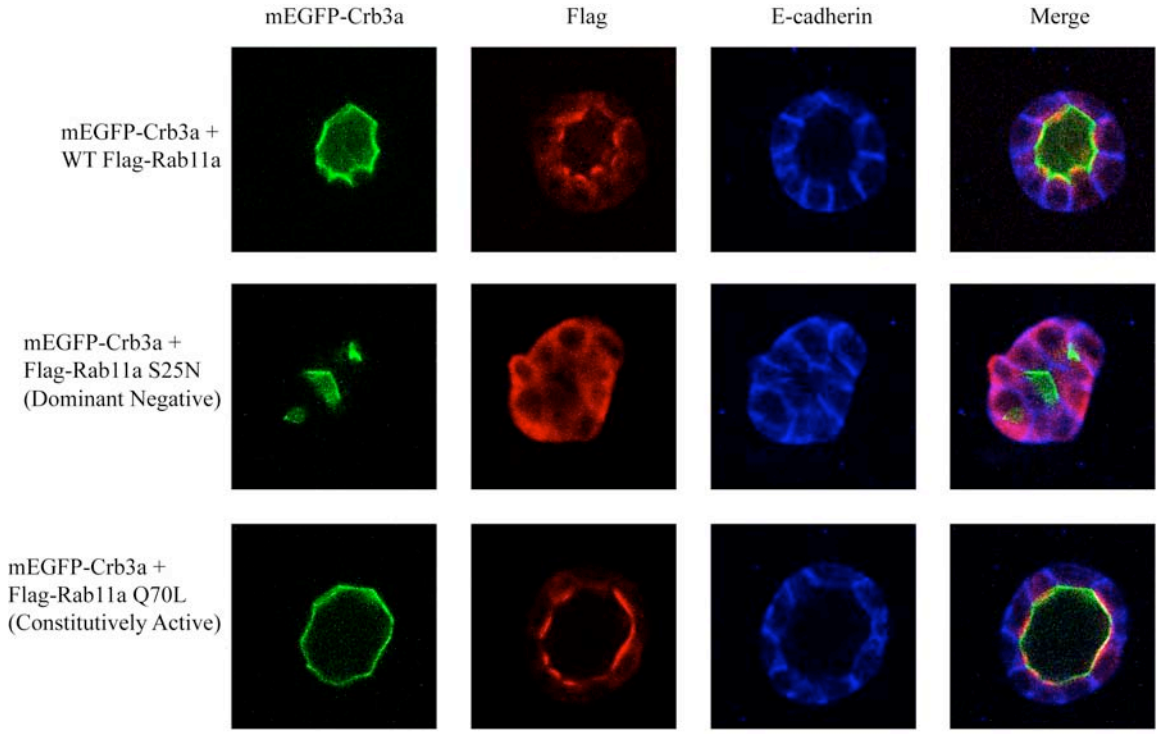
mEGFP-Crb3a
Flag
E-cadherin
Merge
mEGFP-Crb3a +
WT Flag-Rab11a
mEGFP-Crb3a +
Flag-Rab11a S25N
(Dominant Negative)
mEGFP-Crb3a +
Flag-Rab11a Q70L
(Constitutively Active)

trafficking as well, but in cyst assay E-cadherin localization remained cortical and did not appear disrupted by introduction of dominant negative Rab11a.

Discussion

Proteins trafficking to the apical membrane may traverse an apical recycling endosome (ARE) that is positive for the small GTPase Rab11a (36, 154, 250). In flies, knockout of *Rab11* leads to global trafficking defects including apical membrane defects (234). During mitosis from 1 mother cell to 2 daughter cells, wild type MDCKII cells can form a Crb3a positive apical lumen between the 2 daughter cells once mitosis is complete via coordinated endocytosis and exocytosis (246). Lumen formation models confirmed the role of Rab11a in the regulated trafficking of Crb3a during initial apical surface formation and polarization. Rab11a positive ARE have been implicated in vesicular trafficking during mitosis in multiple systems (98, 123). Rab11a is localized to the cleavage furrow of mitotic cells by interaction with Rab11-family interacting protein 3 (Rab11-FIP3) linking to cytoplasmic dynein (101-103, 295). This mechanism suggests that if Crb3a traverses Rab11-postive ARE, then functional Rab11a ARE traveling along microtubules are required for deposition of Crb3a between two daughter cells to facilitate apical lumen formation. Cells expressing mEGFP-Crb3a and dominant negative Rab11a (mEGFP-Crb3a/Rab11a-DN) did not form Crb3a positive lumina. Concurrently, during lumen formation in mEGFP-Crb3a/Rab11a-DN cells, mEGFP-Crb3 accumulated in cytosolic puncta rather than defined endosomal structures. Importantly, mEGFP-Crb3a/Rab11a-DN cells still managed to complete mitosis signifying that dominant-negative Rab11a is not affecting microtubules and the ability of cells to complete mitosis.

Although mitosis completed, we could not significantly detect Crb3a positive membranes implicating Rab11a as a regulator of apical membrane formation and specifically the exocytosis of Crb3a.

Growing mEGFP-Crb3a/Rab11a-DN cells in 3-dimesions for 4 days results in mature cysts with a multi-lumen phenotype. This phenotype is similar to those previously published, where cystic phenotypes appear to be dose-dependent on the amount of Rab11a-DN expressed (53). In confluent monolayers, mEGFP-Crb3a/Rab11a-DN cells can polarize suggesting Crb3a is sufficient to at least partially rescue trafficking defects associated with Rab11a-DN. In mEGFP-Crb3a/Rab11a-DN cysts, there also appears to be segregation of mEGFP-Crb3a onto multiple *de facto* apical surfaces yet, cells cannot establish a single lumen. Even though the cells in mEGFP-Crb3a/Rab11a-DN cysts polarized, apical surfaces established in these cysts appeared to be smaller relative to basolateral surfaces. This is consistent with data from Rab11 null *Drosophila,* where dCrumbs (the *Drosophila* homologue of Crb3a) was far more sensitive to the Rab11 knockout than other basolateral transmembrane proteins also traversing Rab-11 positive ARE (234). Importantly, even in our multi-lumen cysts we did not see colocalization of signals for Crb3a and E-cadherin. In polarized cells, a Rab11a-positive ARE is known to also contain basolateral E-cadherin in addition to apical components and Rab11a-DN caused mistargeting of E-cadherin to the apical surface (163). In our system, Crb3a was moderately overexpressed and it appears that the combination of parental wild type Rab11a and overexpressed Crb3a was enough to induce polarization. Based on previous data in MCF10A cells, we believe Crb3a provides a strong polarization cue in the establishment of tight junctions and apical membranes (69). Since Crb3a and E-cadherin

fail to overlay in mEGFP-Crb3a/Rab11a-DN cells, our observation strengthens the theory that Crb3a protein may provide a signal for segregation of apical and basolateral domains. Since Rab11a-DN expression does not confer domain mixing in the presence of Crb3a, Rab11a likely is involved in regulating spatial organization of membrane protein traffic in polarized cells and not targeting of proteins to specific domains.

Bibliography

1. **Acloque H, Adams MS, Fishwick K, Bronner-Fraser M, and Nieto MA**. Epithelial-mesenchymal transitions: the importance of changing cell state in development and disease. *J Clin Invest* 119: 1438-1449, 2009.

2. **Adachi M, Hamazaki Y, Kobayashi Y, Itoh M, Tsukita S, and Furuse M**. Similar and distinct properties of MUPP1 and Patj, two homologous PDZ domain-containing tight-junction proteins. *Mol Cell Biol* 29: 2372-2389, 2009.

3. **Adey NB, Huang L, Ormonde PA, Baumgard ML, Pero R, Byreddy DV, Tavtigian SV, and Bartel PL**. Threonine phosphorylation of the MMAC1/PTEN PDZ binding domain both inhibits and stimulates PDZ binding. *Cancer Res* 60: 35-37, 2000.

4. **Aigner K, Dampier B, Descovich L, Mikula M, Sultan A, Schreiber M, Mikulits W, Brabletz T, Strand D, Obrist P, Sommergruber W, Schweifer N, Wernitznig A, Beug H, Foisner R, and Eger A**. The transcription factor ZEB1 (deltaEF1) promotes tumour cell dedifferentiation by repressing master regulators of epithelial polarity. *Oncogene* 26: 6979-6988, 2007.

5. **Akimoto K, Mizuno K, Osada S, Hirai S, Tanuma S, Suzuki K, and Ohno S**. A new member of the third class in the protein kinase C family, PKC lambda, expressed dominantly in an undifferentiated mouse embryonal carcinoma cell line and also in many tissues and cells. *J Biol Chem* 269: 12677-12683, 1994.

6. **Alves CC, Carneiro F, Hoefler H, and Becker KF**. Role of the epithelial-mesenchymal transition regulator Slug in primary human cancers. *Front Biosci* 14: 3035-3050, 2009.

7. **Ambesi-Impiombato FS, and Coon HG**. Thyroid cells in culture. *Int Rev Cytol Suppl* 163-172, 1979.

8. **Ambesi-Impiombato FS, Parks LA, and Coon HG**. Culture of hormone-dependent functional epithelial cells from rat thyroids. *Proc Natl Acad Sci U S A* 77: 3455-3459, 1980.

9. **Apodaca G, Katz LA, and Mostov KE**. Receptor-mediated transcytosis of IgA in MDCK cells is via apical recycling endosomes. *J Cell Biol* 125: 67-86, 1994.

10. **Assemat E, Bazellieres E, Pallesi-Pocachard E, Le Bivic A, and Massey-Harroche D**. Polarity complex proteins. *Biochim Biophys Acta* 1778: 614-630, 2008.

11. **Audebert S, Navarro C, Nourry C, Chasserot-Golaz S, Lecine P, Bellaiche Y, Dupont JL, Premont RT, Sempere C, Strub JM, Van Dorsselaer A, Vitale N, and Borg JP**. Mammalian Scribble forms a tight complex with the betaPIX exchange factor. *Curr Biol* 14: 987-995, 2004.

12. **Bachmann A, Schneider M, Theilenberg E, Grawe F, and Knust E**. Drosophila Stardust is a partner of Crumbs in the control of epithelial cell polarity. *Nature* 414: 638-643, 2001.

13. **Bachmann A, Timmer M, Sierralta J, Pietrini G, Gundelfinger ED, Knust E, and Thomas U**. Cell type-specific recruitment of Drosophila Lin-7 to distinct MAGUK-based protein complexes defines novel roles for Sdt and Dlg-S97. *J Cell Sci* 117: 1899-1909, 2004.

14. **Badouel C, Gardano L, Amin N, Garg A, Rosenfeld R, Le Bihan T, and McNeill H**. The FERM-domain protein Expanded regulates Hippo pathway activity via direct interactions with the transcriptional activator Yorkie. *Dev Cell* 16: 411-420, 2009.

15. **Batlle E, Sancho E, Franci C, Dominguez D, Monfar M, Baulida J, and Garcia De Herreros A**. The transcription factor snail is a repressor of E-cadherin gene expression in epithelial tumour cells. *Nat Cell Biol* 2: 84-89, 2000.

16. **Benton R, and St Johnston D**. Drosophila PAR-1 and 14-3-3 inhibit Bazooka/PAR-3 to establish complementary cortical domains in polarized cells. *Cell* 115: 691-704, 2003.

17. **Beronja S, Laprise P, Papoulas O, Pellikka M, Sisson J, and Tepass U**. Essential function of Drosophila Sec6 in apical exocytosis of epithelial photoreceptor cells. *J Cell Biol* 169: 635-646, 2005.

18. **Bilder D**. Epithelial polarity and proliferation control: links from the Drosophila neoplastic tumor suppressors. *Genes Dev* 18: 1909-1925, 2004.

19. **Bilder D, Birnbaum D, Borg JP, Bryant P, Huigbretse J, Jansen E, Kennedy MB, Labouesse M, Legouis R, Mechler B, Perrimon N, Petit M, and Sinha P**. Collective nomenclature for LAP proteins. *Nat Cell Biol* 2: E114, 2000.

20. **Bilder D, Li M, and Perrimon N**. Cooperative regulation of cell polarity and growth by Drosophila tumor suppressors. *Science* 289: 113-116, 2000.

21. **Bilder D, and Perrimon N**. Localization of apical epithelial determinants by the basolateral PDZ protein Scribble. *Nature* 403: 676-680, 2000.

22. **Blankenship JT, Fuller MT, and Zallen JA**. The Drosophila homolog of the Exo84 exocyst subunit promotes apical epithelial identity. *J Cell Sci* 120: 3099-3110, 2007.

23. **Bohl J, Brimer N, Lyons C, and Vande Pol SB**. The stardust family protein MPP7 forms a tripartite complex with LIN7 and DLG1 that regulates the stability and localization of DLG1 to cell junctions. *J Biol Chem* 282: 9392-9400, 2007.

24. **Bolos V, Peinado H, Perez-Moreno MA, Fraga MF, Esteller M, and Cano A**. The transcription factor Slug represses E-cadherin expression and induces epithelial to mesenchymal transitions: a comparison with Snail and E47 repressors. *J Cell Sci* 116: 499-511, 2003.

25. **Borg JP, Straight SW, Kaech SM, de Taddeo-Borg M, Kroon DE, Karnak D, Turner RS, Kim SK, and Margolis B**. Identification of an evolutionarily conserved heterotrimeric protein complex involved in protein targeting. *J Biol Chem* 273: 31633-31636, 1998.

26. **Boutet A, De Frutos CA, Maxwell PH, Mayol MJ, Romero J, and Nieto MA**. Snail activation disrupts tissue homeostasis and induces fibrosis in the adult kidney. *EMBO J* 25: 5603-5613, 2006.

27. **Boutet A, Esteban MA, Maxwell PH, and Nieto MA**. Reactivation of Snail genes in renal fibrosis and carcinomas: a process of reversed embryogenesis? *Cell Cycle* 6: 638-642, 2007.

28. **Braun J, Hoang-Vu C, Dralle H, and Huttelmaier S**. Downregulation of microRNAs directs the EMT and invasive potential of anaplastic thyroid carcinomas. *Oncogene* 2010.

29. **Broniarczyk J, Olejnik-Schmidt AK, Luczak MW, Schmidt MT, Dabrowski M, Jozefiak A, Kedzia W, Kwasniewska A, and Gozdzicka-Jozefiak A**. Analysis of expression and structure of the TSG101 gene in cervical cancer cells. *Int J Mol Med* 25: 777-783, 2010.

30. **Bucci C, Wandinger-Ness A, Lutcke A, Chiariello M, Bruni CB, and Zerial M**. Rab5a is a common component of the apical and basolateral endocytic machinery in polarized epithelial cells. *Proc Natl Acad Sci U S A* 91: 5061-5065, 1994.

31. **Butz S, Okamoto M, and Sudhof TC**. A tripartite protein complex with the potential to couple synaptic vesicle exocytosis to cell adhesion in brain. *Cell* 94: 773-782, 1998.

32. **Calzada MJ, Esteban MA, Feijoo-Cuaresma M, Castellanos MC, Naranjo-Suarez S, Temes E, Mendez F, Yanez-Mo M, Ohh M, and Landazuri MO**. von Hippel-Lindau tumor suppressor protein regulates the assembly of intercellular junctions in renal cancer cells through hypoxia-inducible factor-independent mechanisms. *Cancer Res* 66: 1553-1560, 2006.

33. **Cano A, Perez-Moreno MA, Rodrigo I, Locascio A, Blanco MJ, del Barrio MG, Portillo F, and Nieto MA**. The transcription factor snail controls epithelial-mesenchymal transitions by repressing E-cadherin expression. *Nat Cell Biol* 2: 76-83, 2000.

34. **Carroll TJ, Park JS, Hayashi S, Majumdar A, and McMahon AP**. Wnt9b plays a central role in the regulation of mesenchymal to epithelial transitions underlying organogenesis of the mammalian urogenital system. *Dev Cell* 9: 283-292, 2005.

35. **Caruana G, and Bernstein A**. Craniofacial dysmorphogenesis including cleft palate in mice with an insertional mutation in the discs large gene. *Mol Cell Biol* 21: 1475-1483, 2001.

36. **Casanova JE, Wang X, Kumar R, Bhartur SG, Navarre J, Woodrum JE, Altschuler Y, Ray GS, and Goldenring JR**. Association of Rab25 and Rab11a with the apical recycling system of polarized Madin-Darby canine kidney cells. *Mol Biol Cell* 10: 47-61, 1999.

37. **Chaffer CL, Thompson EW, and Williams ED**. Mesenchymal to epithelial transition in development and disease. *Cells Tissues Organs* 185: 7-19, 2007.

38. **Chalmers AD, Pambos M, Mason J, Lang S, Wylie C, and Papalopulu N**. aPKC, Crumbs3 and Lgl2 control apicobasal polarity in early vertebrate development. *Development* 132: 977-986, 2005.

39. **Chen X, and Macara IG**. Par-3 controls tight junction assembly through the Rac exchange factor Tiam1. *Nat Cell Biol* 7: 262-269, 2005.

40. **Chen Z, Leibiger I, Katz A, and Bertorello A**. Pals-associated tight junction protein functionally links dopamine and angiotensin II to the regulation of sodium transport in renal epithelial cells. *Br J Pharmacol* 2009.

41. **Cheshire AM, Kerman BE, Zipfel WR, Spector AA, and Andrew DJ**. Kinetic and mechanical analysis of live tube morphogenesis. *Dev Dyn* 237: 2874-2888, 2008.

42. **Chudakov DM, Lukyanov S, and Lukyanov KA**. Tracking intracellular protein movements using photoswitchable fluorescent proteins PS-CFP2 and Dendra2. *Nat Protoc* 2: 2024-2032, 2007.

43. **Chudakov DM, Lukyanov S, and Lukyanov KA**. Using photoactivatable fluorescent protein Dendra2 to track protein movement. *Biotechniques* 42: 553, 555, 557 passim, 2007.

44. **Cohen AR, Woods DF, Marfatia SM, Walther Z, Chishti AH, and Anderson JM**. Human CASK/LIN-2 binds syndecan-2 and protein 4.1 and localizes to the basolateral membrane of epithelial cells. *J Cell Biol* 142: 129-138, 1998.

45. **Comer FI, and Parent CA**. Phosphoinositides specify polarity during epithelial organ development. *Cell* 128: 239-240, 2007.

46. **Cramm-Behrens CI, Dienst M, and Jacob R**. Apical cargo traverses endosomal compartments on the passage to the cell surface. *Traffic* 9: 2206-2220, 2008.

47. **Dahl U, Sjodin A, Larue L, Radice GL, Cajander S, Takeichi M, Kemler R, and Semb H**. Genetic dissection of cadherin function during nephrogenesis. *Mol Cell Biol* 22: 1474-1487, 2002.

48. **Davies BA, Lee JR, Oestreich AJ, and Katzmann DJ**. Membrane protein targeting to the MVB/lysosome. *Chem Rev* 109: 1575-1586, 2009.

49. **Delacour D, Cramm-Behrens CI, Drobecq H, Le Bivic A, Naim HY, and Jacob R**. Requirement for galectin-3 in apical protein sorting. *Curr Biol* 16: 408-414, 2006.

50. **Delacour D, Greb C, Koch A, Salomonsson E, Leffler H, Le Bivic A, and Jacob R**. Apical sorting by galectin-3-dependent glycoprotein clustering. *Traffic* 8: 379-388, 2007.

51. **Delous M, Hellman NE, Gaude HM, Silbermann F, Le Bivic A, Salomon R, Antignac C, and Saunier S**. Nephrocystin-1 and nephrocystin-4 are required for epithelial morphogenesis and associate with PALS1/PATJ and Par6. *Hum Mol Genet* 2009.

52. **den Hollander AI, ten Brink JB, de Kok YJ, van Soest S, van den Born LI, van Driel MA, van de Pol DJ, Payne AM, Bhattacharya SS, Kellner U, Hoyng CB, Westerveld A, Brunner HG, Bleeker-Wagemakers EM, Deutman AF, Heckenlively JR, Cremers FP, and Bergen AA**. Mutations in a human homologue of Drosophila crumbs cause retinitis pigmentosa (RP12). *Nat Genet* 23: 217-221, 1999.

53. **Desclozeaux M, Venturato J, Wylie FG, Kay JG, Joseph SR, Le HT, and Stow JL**. Active Rab11 and functional recycling endosome are required for E-cadherin trafficking and lumen formation during epithelial morphogenesis. *Am J Physiol Cell Physiol* 295: C545-556, 2008.

54. **Dimitratos SD, Woods DF, Stathakis DG, and Bryant PJ**. Signaling pathways are focused at specialized regions of the plasma membrane by scaffolding proteins of the MAGUK family. *Bioessays* 21: 912-921, 1999.

55. **Doerks T, Bork P, Kamberov E, Makarova O, Muecke S, and Margolis B**. L27, a novel heterodimerization domain in receptor targeting proteins Lin-2 and Lin-7. *Trends Biochem Sci* 25: 317-318, 2000.

56. **Dow LE, Brumby AM, Muratore R, Coombe ML, Sedelies KA, Trapani JA, Russell SM, Richardson HE, and Humbert PO**. hScrib is a functional homologue of the Drosophila tumour suppressor Scribble. *Oncogene* 22: 9225-9230, 2003.

57. **Dow LE, Elsum IA, King CL, Kinross KM, Richardson HE, and Humbert PO**. Loss of human Scribble cooperates with H-Ras to promote cell invasion through deregulation of MAPK signalling. *Oncogene* 27: 5988-6001, 2008.

58. **Dow LE, Kauffman JS, Caddy J, Zarbalis K, Peterson AS, Jane SM, Russell SM, and Humbert PO**. The tumour-suppressor Scribble dictates cell polarity during directed epithelial migration: regulation of Rho GTPase recruitment to the leading edge. *Oncogene* 26: 2272-2282, 2007.

59. **Dressler GR**. The cellular basis of kidney development. *Annu Rev Cell Dev Biol* 22: 509-529, 2006.

60. **Ebarasi L, He L, Hultenby K, Takemoto M, Betsholtz C, Tryggvason K, and Majumdar A**. A reverse genetic screen in the zebrafish identifies crb2b as a regulator of the glomerular filtration barrier. *Dev Biol* 2009.

61. **Ebnet K, Suzuki A, Horikoshi Y, Hirose T, Meyer Zu Brickwedde MK, Ohno S, and Vestweber D**. The cell polarity protein ASIP/PAR-3 directly associates with junctional adhesion molecule (JAM). *EMBO J* 20: 3738-3748, 2001.

62. **Etemad-Moghadam B, Guo S, and Kemphues KJ**. Asymmetrically distributed PAR-3 protein contributes to cell polarity and spindle alignment in early C. elegans embryos. *Cell* 83: 743-752, 1995.

63. **Fan S, Fogg V, Wang Q, Chen XW, Liu CJ, and Margolis B**. A novel Crumbs3 isoform regulates cell division and ciliogenesis via importin beta interactions. *J Cell Biol* 178: 387-398, 2007.

64. **Fan S, Hurd TW, Liu CJ, Straight SW, Weimbs T, Hurd EA, Domino SE, and Margolis B**. Polarity proteins control ciliogenesis via kinesin motor interactions. *Curr Biol* 14: 1451-1461, 2004.

65. **Fanning AS, and Anderson JM**. PDZ domains: fundamental building blocks in the organization of protein complexes at the plasma membrane. *J Clin Invest* 103: 767-772, 1999.

66. **Feng W, Long JF, Fan JS, Suetake T, and Zhang M**. The tetrameric L27 domain complex as an organization platform for supramolecular assemblies. *Nat Struct Mol Biol* 11: 475-480, 2004.

67. **Feng W, Wu H, Chan LN, and Zhang M**. Par-3-mediated junctional localization of the lipid phosphatase PTEN is required for cell polarity establishment. *J Biol Chem* 283: 23440-23449, 2008.

68. **Fischer E, and Pontoglio M**. Planar cell polarity and cilia. *Semin Cell Dev Biol* 20: 998-1005, 2009.

69. **Fogg VC, Liu CJ, and Margolis B**. Multiple regions of Crumbs3 are required for tight junction formation in MCF10A cells. *J Cell Sci* 118: 2859-2869, 2005.

70. **Furuse M, Hata M, Furuse K, Yoshida Y, Haratake A, Sugitani Y, Noda T, Kubo A, and Tsukita S**. Claudin-based tight junctions are crucial for the mammalian epidermal barrier: a lesson from claudin-1-deficient mice. *J Cell Biol* 156: 1099-1111, 2002.

71. **Gao L, Joberty G, and Macara IG**. Assembly of epithelial tight junctions is negatively regulated by Par6. *Curr Biol* 12: 221-225, 2002.

72. **Gao L, and Macara IG**. Isoforms of the polarity protein par6 have distinct functions. *J Biol Chem* 279: 41557-41562, 2004.

73. **Gao L, Macara IG, and Joberty G**. Multiple splice variants of Par3 and of a novel related gene, Par3L, produce proteins with different binding properties. *Gene* 294: 99-107, 2002.

74. **Garbi C, Mascia A, and Nitsch L**. Cell polarity and morphogenetic properties of Fischer rat thyroid cells (FRT) cultured in suspension or embedded in different gels. *Cell Mol Biol* 33: 293-305, 1987.

75. **Gardiol D, Kuhne C, Glaunsinger B, Lee SS, Javier R, and Banks L**. Oncogenic human papillomavirus E6 proteins target the discs large tumour suppressor for proteasome-mediated degradation. *Oncogene* 18: 5487-5496, 1999.

76. **Garrard SM, Capaldo CT, Gao L, Rosen MK, Macara IG, and Tomchick DR**. Structure of Cdc42 in a complex with the GTPase-binding domain of the cell polarity protein, Par6. *EMBO J* 22: 1125-1133, 2003.

77. **Genevet A, Polesello C, Blight K, Robertson F, Collinson LM, Pichaud F, and Tapon N**. The Hippo pathway regulates apical-domain size independently of its growth-control function. *J Cell Sci* 122: 2360-2370, 2009.

78. **Gilbert MM, Beam CK, Robinson BS, and Moberg KH**. Genetic interactions between the Drosophila tumor suppressor gene ept and the stat92E transcription factor. *PLoS One* 4: e7083, 2009.

79. **Gilbert MM, Robinson BS, and Moberg KH**. Functional interactions between the erupted/tsg101 growth suppressor gene and the DaPKC and rbf1 genes in Drosophila imaginal disc tumors. *PLoS One* 4: e7039, 2009.

80. **Goetz SC, and Anderson KV**. The primary cilium: a signalling centre during vertebrate development. *Nat Rev Genet* 11: 331-344, 2010.

81. **Goldenring JR, Shen KR, Vaughan HD, and Modlin IM**. Identification of a small GTP-binding protein, Rab25, expressed in the gastrointestinal mucosa, kidney, and lung. *J Biol Chem* 268: 18419-18422, 1993.

82. **Gonzales PA, Pisitkun T, Hoffert JD, Tchapyjnikov D, Star RA, Kleta R, Wang NS, and Knepper MA**. Large-scale proteomics and phosphoproteomics of urinary exosomes. *J Am Soc Nephrol* 20: 363-379, 2009.

83. **Gosens I, Sessa A, den Hollander AI, Letteboer SJ, Belloni V, Arends ML, Le Bivic A, Cremers FP, Broccoli V, and Roepman R**. FERM protein EPB41L5 is a novel member of the mammalian CRB-MPP5 polarity complex. *Exp Cell Res* 313: 3959-3970, 2007.

84. **Grande M, Franzen A, Karlsson JO, Ericson LE, Heldin NE, and Nilsson M**. Transforming growth factor-beta and epidermal growth factor synergistically stimulate epithelial to mesenchymal transition (EMT) through a MEK-dependent mechanism in primary cultured pig thyrocytes. *J Cell Sci* 115: 4227-4236, 2002.

85. **Gregory PA, Bracken CP, Bert AG, and Goodall GJ**. MicroRNAs as regulators of epithelial-mesenchymal transition. *Cell Cycle* 7: 3112-3118, 2008.

86. **Grifoni D, Garoia F, Bellosta P, Parisi F, De Biase D, Collina G, Strand D, Cavicchi S, and Pession A**. aPKCzeta cortical loading is associated with Lgl cytoplasmic release and tumor growth in Drosophila and human epithelia. *Oncogene* 26: 5960-5965, 2007.

87. **Grusche FA, Richardson HE, and Harvey KF**. Upstream Regulation of the Hippo Size Control Pathway. *Curr Biol* 20: R574-R582, 2010.

88. **Grzeschik NA, Parsons LM, Allott ML, Harvey KF, and Richardson HE**. Lgl, aPKC, and Crumbs regulate the Salvador/Warts/Hippo pathway through two distinct mechanisms. *Curr Biol* 20: 573-581, 2010.

89. **Hajra KM, Chen DY, and Fearon ER**. The SLUG zinc-finger protein represses E-cadherin in breast cancer. *Cancer Res* 62: 1613-1618, 2002.

90. **Hamaratoglu F, Gajewski K, Sansores-Garcia L, Morrison C, Tao C, and Halder G**. The Hippo tumor-suppressor pathway regulates apical-domain size in parallel to tissue growth. *J Cell Sci* 122: 2351-2359, 2009.

91. **Hamazaki Y, Itoh M, Sasaki H, Furuse M, and Tsukita S**. Multi-PDZ domain protein 1 (MUPP1) is concentrated at tight junctions through its possible interaction with claudin-1 and junctional adhesion molecule. *J Biol Chem* 277: 455-461, 2002.

92. **Harris KP, and Tepass U**. Cdc42 and Par proteins stabilize dynamic adherens junctions in the Drosophila neuroectoderm through regulation of apical endocytosis. *J Cell Biol* 183: 1129-1143, 2008.

93. **Harten SK, Shukla D, Barod R, Hergovich A, Balda MS, Matter K, Esteban MA, and Maxwell PH**. Regulation of renal epithelial tight junctions by the von Hippel-Lindau tumor suppressor gene involves occludin and claudin 1 and is independent of E-cadherin. *Mol Biol Cell* 20: 1089-1101, 2009.

94. **Herz HM, and Bergmann A**. Genetic analysis of ESCRT function in Drosophila: a tumour model for human Tsg101. *Biochem Soc Trans* 37: 204-207, 2009.

95. **Hildebrandt F, Attanasio M, and Otto E**. Nephronophthisis: disease mechanisms of a ciliopathy. *J Am Soc Nephrol* 20: 23-35, 2009.

96. **Hirano Y, Yoshinaga S, Ogura K, Yokochi M, Noda Y, Sumimoto H, and Inagaki F**. Solution structure of atypical protein kinase C PB1 domain and its mode of interaction with ZIP/p62 and MEK5. *J Biol Chem* 279: 31883-31890, 2004.

97. **Hirose T, Izumi Y, Nagashima Y, Tamai-Nagai Y, Kurihara H, Sakai T, Suzuki Y, Yamanaka T, Suzuki A, Mizuno K, and Ohno S**. Involvement of

ASIP/PAR-3 in the promotion of epithelial tight junction formation. *J Cell Sci* 115: 2485-2495, 2002.

98. **Hobdy-Henderson KC, Hales CM, Lapierre LA, Cheney RE, and Goldenring JR**. Dynamics of the apical plasma membrane recycling system during cell division. *Traffic* 4: 681-693, 2003.

99. **Hoekstra D, Tyteca D, and van ISC**. The subapical compartment: a traffic center in membrane polarity development. *J Cell Sci* 117: 2183-2192, 2004.

100. **Hong Y, Stronach B, Perrimon N, Jan LY, and Jan YN**. Drosophila Stardust interacts with Crumbs to control polarity of epithelia but not neuroblasts. *Nature* 414: 634-638, 2001.

101. **Horgan CP, Hanscom SR, Jolly RS, Futter CE, and McCaffrey MW**. Rab11-FIP3 binds dynein light intermediate chain 2 and its overexpression fragments the Golgi complex. *Biochem Biophys Res Commun* 394: 387-392, 2010.

102. **Horgan CP, Hanscom SR, Jolly RS, Futter CE, and McCaffrey MW**. Rab11-FIP3 links the Rab11 GTPase and cytoplasmic dynein to mediate transport to the endosomal-recycling compartment. *J Cell Sci* 123: 181-191, 2010.

103. **Horgan CP, Walsh M, Zurawski TH, and McCaffrey MW**. Rab11-FIP3 localises to a Rab11-positive pericentrosomal compartment during interphase and to the cleavage furrow during cytokinesis. *Biochem Biophys Res Commun* 319: 83-94, 2004.

104. **Horikoshi Y, Suzuki A, Yamanaka T, Sasaki K, Mizuno K, Sawada H, Yonemura S, and Ohno S**. Interaction between PAR-3 and the aPKC-PAR-6 complex is indispensable for apical domain development of epithelial cells. *J Cell Sci* 122: 1595-1606, 2009.

105. **Hoskins R, Hajnal AF, Harp SA, and Kim SK**. The C. elegans vulval induction gene lin-2 encodes a member of the MAGUK family of cell junction proteins. *Development* 122: 97-111, 1996.

106. **Hsu SC, Hazuka CD, Foletti DL, and Scheller RH**. Targeting vesicles to specific sites on the plasma membrane: the role of the sec6/8 complex. *Trends Cell Biol* 9: 150-153, 1999.

107. **Huan Y, and van Adelsberg J**. Polycystin-1, the PKD1 gene product, is in a complex containing E-cadherin and the catenins. *J Clin Invest* 104: 1459-1468, 1999.

108. **Huang L, and Muthuswamy SK**. Polarity protein alterations in carcinoma: a focus on emerging roles for polarity regulators. *Curr Opin Genet Dev* 20: 41-50, 2010.

109. **Hurd TW, Fan S, Liu CJ, Kweon HK, Hakansson K, and Margolis B**. Phosphorylation-dependent binding of 14-3-3 to the polarity protein Par3 regulates cell polarity in mammalian epithelia. *Curr Biol* 13: 2082-2090, 2003.

110. **Hurd TW, Gao L, Roh MH, Macara IG, and Margolis B**. Direct interaction of two polarity complexes implicated in epithelial tight junction assembly. *Nat Cell Biol* 5: 137-142, 2003.

111. **Iizuka-Kogo A, Ishidao T, Akiyama T, and Senda T**. Abnormal development of urogenital organs in Dlgh1-deficient mice. *Development* 134: 1799-1807, 2007.

112. **Ikeda H, and Kerppola TK**. Lysosomal localization of ubiquitinated Jun requires multiple determinants in a lysine-27-linked polyubiquitin conjugate. *Mol Biol Cell* 19: 4588-4601, 2008.

113. **Ikenouchi J, Matsuda M, Furuse M, and Tsukita S**. Regulation of tight junctions during the epithelium-mesenchyme transition: direct repression of the gene expression of claudins/occludin by Snail. *J Cell Sci* 116: 1959-1967, 2003.

114. **Irie M, Hata Y, Deguchi M, Ide N, Hirao K, Yao I, Nishioka H, and Takai Y**. Isolation and characterization of mammalian homologues of Caenorhabditis elegans lin-7: localization at cell-cell junctions. *Oncogene* 18: 2811-2817, 1999.

115. **Irizarry RA, Hobbs B, Collin F, Beazer-Barclay YD, Antonellis KJ, Scherf U, and Speed TP**. Exploration, normalization, and summaries of high density oligonucleotide array probe level data. *Biostatistics* 4: 249-264, 2003.

116. **Ishidate T, Matsumine A, Toyoshima K, and Akiyama T**. The APC-hDLG complex negatively regulates cell cycle progression from the G0/G1 to S phase. *Oncogene* 19: 365-372, 2000.

117. **Itoh M, Sasaki H, Furuse M, Ozaki H, Kita T, and Tsukita S**. Junctional adhesion molecule (JAM) binds to PAR-3: a possible mechanism for the recruitment of PAR-3 to tight junctions. *J Cell Biol* 154: 491-497, 2001.

118. **Iturrioz X, Durgan J, Calleja V, Larijani B, Okuda H, Whelan R, and Parker PJ**. The von Hippel-Lindau tumour-suppressor protein interaction with protein kinase Cdelta. *Biochem J* 397: 109-120, 2006.

119. **Ivanov AI, Young C, Den Beste K, Capaldo CT, Humbert PO, Brennwald P, Parkos CA, and Nusrat A**. Tumor suppressor scribble regulates assembly of tight junctions in the intestinal epithelium. *Am J Pathol* 176: 134-145, 2010.

120. **Izumi Y, Hirose T, Tamai Y, Hirai S, Nagashima Y, Fujimoto T, Tabuse Y, Kemphues KJ, and Ohno S**. An atypical PKC directly associates and colocalizes at the epithelial tight junction with ASIP, a mammalian homologue of Caenorhabditis elegans polarity protein PAR-3. *J Cell Biol* 143: 95-106, 1998.

121. **Jaffer ZM, and Chernoff J**. The cross-Rho'ds of cell-cell adhesion. *J Biol Chem* 279: 35123-35126, 2004.

122. **Jensen AM, and Westerfield M**. Zebrafish mosaic eyes is a novel FERM protein required for retinal lamination and retinal pigmented epithelial tight junction formation. *Curr Biol* 14: 711-717, 2004.

123. **Jing J, and Prekeris R**. Polarized endocytic transport: the roles of Rab11 and Rab11-FIPs in regulating cell polarity. *Histol Histopathol* 24: 1171-1180, 2009.

124. **Jo K, Derin R, Li M, and Bredt DS**. Characterization of MALS/Velis-1, -2, and -3: a family of mammalian LIN-7 homologs enriched at brain synapses in association with the postsynaptic density-95/NMDA receptor postsynaptic complex. *J Neurosci* 19: 4189-4199, 1999.

125. **Joberty G, Petersen C, Gao L, and Macara IG**. The cell-polarity protein Par6 links Par3 and atypical protein kinase C to Cdc42. *Nat Cell Biol* 2: 531-539, 2000.

126. **Johansson A, Driessens M, and Aspenstrom P**. The mammalian homologue of the Caenorhabditis elegans polarity protein PAR-6 is a binding partner for the Rho GTPases Cdc42 and Rac1. *J Cell Sci* 113 (Pt 18): 3267-3275, 2000.

127. **Kaech SM, Whitfield CW, and Kim SK**. The LIN-2/LIN-7/LIN-10 complex mediates basolateral membrane localization of the C. elegans EGF receptor LET-23 in vulval epithelial cells. *Cell* 94: 761-771, 1998.

128. **Kallay LM, McNickle A, Brennwald PJ, Hubbard AL, and Braiterman LT**. Scribble associates with two polarity proteins, Lgl2 and Vangl2, via distinct molecular domains. *J Cell Biochem* 99: 647-664, 2006.

129. **Kamberov E, Makarova O, Roh M, Liu A, Karnak D, Straight S, and Margolis B**. Molecular cloning and characterization of Pals, proteins associated with mLin-7. *J Biol Chem* 275: 11425-11431, 2000.

130. **Karnak D, Lee S, and Margolis B**. Identification of multiple binding partners for the amino-terminal domain of synapse-associated protein 97. *J Biol Chem* 277: 46730-46735, 2002.

131. **Karner C, Wharton KA, Jr., and Carroll TJ**. Planar cell polarity and vertebrate organogenesis. *Semin Cell Dev Biol* 17: 194-203, 2006.

132. **Karner CM, Chirumamilla R, Aoki S, Igarashi P, Wallingford JB, and Carroll TJ**. Wnt9b signaling regulates planar cell polarity and kidney tubule morphogenesis. *Nat Genet* 41: 793-799, 2009.

133. **Karp CM, Tan TT, Mathew R, Nelson D, Mukherjee C, Degenhardt K, Karantza-Wadsworth V, and White E**. Role of the polarity determinant crumbs in suppressing mammalian epithelial tumor progression. *Cancer Res* 68: 4105-4115, 2008.

134. **Katoh M**. Identification and characterization of Crumbs homolog 2 gene at human chromosome 9q33.3. *Int J Oncol* 24: 743-749, 2004.

135. **Katzmann DJ, Babst M, and Emr SD**. Ubiquitin-dependent sorting into the multivesicular body pathway requires the function of a conserved endosomal protein sorting complex, ESCRT-I. *Cell* 106: 145-155, 2001.

136. **Katzmann DJ, Odorizzi G, and Emr SD**. Receptor downregulation and multivesicular-body sorting. *Nat Rev Mol Cell Biol* 3: 893-905, 2002.

137. **Kedinger V, Alpy F, Baguet A, Polette M, Stoll I, Chenard MP, Tomasetto C, and Rio MC**. Tumor necrosis factor receptor-associated factor 4 is a dynamic tight

junction-related shuttle protein involved in epithelium homeostasis. *PLoS One* 3: e3518, 2008.

138. **Kemphues KJ, Priess JR, Morton DG, and Cheng NS**. Identification of genes required for cytoplasmic localization in early C. elegans embryos. *Cell* 52: 311-320, 1988.

139. **Kerman BE, Cheshire AM, Myat MM, and Andrew DJ**. Ribbon modulates apical membrane during tube elongation through Crumbs and Moesin. *Dev Biol* 320: 278-288, 2008.

140. **Kesarwala AH, Samrakandi MM, and Piwnica-Worms D**. Proteasome inhibition blocks ligand-induced dynamic processing and internalization of epidermal growth factor receptor via altered receptor ubiquitination and phosphorylation. *Cancer Res* 69: 976-983, 2009.

141. **Kim M, Datta A, Brakeman P, Yu W, and Mostov KE**. Polarity proteins PAR6 and aPKC regulate cell death through GSK-3beta in 3D epithelial morphogenesis. *J Cell Sci* 120: 2309-2317, 2007.

142. **Kohjima M, Noda Y, Takeya R, Saito N, Takeuchi K, and Sumimoto H**. PAR3beta, a novel homologue of the cell polarity protein PAR3, localizes to tight junctions. *Biochem Biophys Res Commun* 299: 641-646, 2002.

143. **Konig C, Yan YL, Postlethwait J, Wendler S, and Campos-Ortega JA**. A recessive mutation leading to vertebral ankylosis in zebrafish is associated with amino acid alterations in the homologue of the human membrane-associated guanylate kinase DLG3. *Mech Dev* 86: 17-28, 1999.

144. **Korinek V, Barker N, Morin PJ, van Wichen D, de Weger R, Kinzler KW, Vogelstein B, and Clevers H**. Constitutive transcriptional activation by a beta-catenin-Tcf complex in APC-/- colon carcinoma. *Science* 275: 1784-1787, 1997.

145. **Lapierre LA, Kumar R, Hales CM, Navarre J, Bhartur SG, Burnette JO, Provance DW, Jr., Mercer JA, Bahler M, and Goldenring JR**. Myosin vb is associated with plasma membrane recycling systems. *Mol Biol Cell* 12: 1843-1857, 2001.

146. **Laprise P, Beronja S, Silva-Gagliardi NF, Pellikka M, Jensen AM, McGlade CJ, and Tepass U**. The FERM protein Yurt is a negative regulatory component of the

Crumbs complex that controls epithelial polarity and apical membrane size. *Dev Cell* 11: 363-374, 2006.

147. **Laprise P, Lau KM, Harris KP, Silva-Gagliardi NF, Paul SM, Beronja S, Beitel GJ, McGlade CJ, and Tepass U**. Yurt, Coracle, Neurexin IV and the Na(+),K(+)-ATPase form a novel group of epithelial polarity proteins. *Nature* 459: 1141-1145, 2009.

148. **Laprise P, Viel A, and Rivard N**. Human homolog of disc-large is required for adherens junction assembly and differentiation of human intestinal epithelial cells. *J Biol Chem* 279: 10157-10166, 2004.

149. **Lee JM, Dedhar S, Kalluri R, and Thompson EW**. The epithelial-mesenchymal transition: new insights in signaling, development, and disease. *J Cell Biol* 172: 973-981, 2006.

150. **Lee OK, Frese KK, James JS, Chadda D, Chen ZH, Javier RT, and Cho KO**. Discs-Large and Strabismus are functionally linked to plasma membrane formation. *Nat Cell Biol* 5: 987-993, 2003.

151. **Lee S, Fan S, Makarova O, Straight S, and Margolis B**. A novel and conserved protein-protein interaction domain of mammalian Lin-2/CASK binds and recruits SAP97 to the lateral surface of epithelia. *Mol Cell Biol* 22: 1778-1791, 2002.

152. **Lemmers C, Medina E, Delgrossi MH, Michel D, Arsanto JP, and Le Bivic A**. hINADl/PATJ, a homolog of discs lost, interacts with crumbs and localizes to tight junctions in human epithelial cells. *J Biol Chem* 277: 25408-25415, 2002.

153. **Lemmers C, Michel D, Lane-Guermonprez L, Delgrossi MH, Medina E, Arsanto JP, and Le Bivic A**. CRB3 binds directly to Par6 and regulates the morphogenesis of the tight junctions in mammalian epithelial cells. *Mol Biol Cell* 15: 1324-1333, 2004.

154. **Leung SM, Ruiz WG, and Apodaca G**. Sorting of membrane and fluid at the apical pole of polarized Madin-Darby canine kidney cells. *Mol Biol Cell* 11: 2131-2150, 2000.

155. **Li L, and Cohen SN**. Tsg101: a novel tumor susceptibility gene isolated by controlled homozygous functional knockout of allelic loci in mammalian cells. *Cell* 85: 319-329, 1996.

156. **Li Y, Karnak D, Demeler B, Margolis B, and Lavie A**. Structural basis for L27 domain-mediated assembly of signaling and cell polarity complexes. *EMBO J* 23: 2723-2733, 2004.

157. **Li Z, Wang L, Hays TS, and Cai Y**. Dynein-mediated apical localization of crumbs transcripts is required for Crumbs activity in epithelial polarity. *J Cell Biol* 180: 31-38, 2008.

158. **Liew CW, Vockel M, Glassmeier G, Brandner JM, Fernandez-Ballester GJ, Schwarz JR, Schulz S, Buck F, Serrano L, Richter D, and Kreienkamp HJ**. Interaction of the human somatostatin receptor 3 with the multiple PDZ domain protein MUPP1 enables somatostatin to control permeability of epithelial tight junctions. *FEBS Lett* 583: 49-54, 2009.

159. **Lin D, Edwards AS, Fawcett JP, Mbamalu G, Scott JD, and Pawson T**. A mammalian PAR-3-PAR-6 complex implicated in Cdc42/Rac1 and aPKC signalling and cell polarity. *Nat Cell Biol* 2: 540-547, 2000.

160. **Ling C, Zheng Y, Yin F, Yu J, Huang J, Hong Y, Wu S, and Pan D**. The apical transmembrane protein Crumbs functions as a tumor suppressor that regulates Hippo signaling by binding to Expanded. *Proc Natl Acad Sci U S A* 107: 10532-10537, 2010.

161. **Lisovsky M, Dresser K, Baker S, Fisher A, Woda B, Banner B, and Lauwers GY**. Cell polarity protein Lgl2 is lost or aberrantly localized in gastric dysplasia and adenocarcinoma: an immunohistochemical study. *Mod Pathol* 22: 977-984, 2009.

162. **Liu Y**. New insights into epithelial-mesenchymal transition in kidney fibrosis. *J Am Soc Nephrol* 21: 212-222, 2010.

163. **Lock JG, and Stow JL**. Rab11 in recycling endosomes regulates the sorting and basolateral transport of E-cadherin. *Mol Biol Cell* 16: 1744-1755, 2005.

164. **Longva KE, Blystad FD, Stang E, Larsen AM, Johannessen LE, and Madshus IH**. Ubiquitination and proteasomal activity is required for transport of the EGF receptor to inner membranes of multivesicular bodies. *J Cell Biol* 156: 843-854, 2002.

165. **Lopez-Novoa JM, and Nieto MA**. Inflammation and EMT: an alliance towards organ fibrosis and cancer progression. *EMBO Mol Med* 1: 303-314, 2009.

166. **Lozano E, and Cano A**. Induction of mutual stabilization and retardation of tumor growth by coexpression of plakoglobin and E-cadherin in mouse skin spindle carcinoma cells. *Mol Carcinog* 21: 273-287, 1998.

167. **Lu H, and Bilder D**. Endocytic control of epithelial polarity and proliferation in Drosophila. *Nat Cell Biol* 7: 1232-1239, 2005.

168. **Lue RA, Marfatia SM, Branton D, and Chishti AH**. Cloning and characterization of hdlg: the human homologue of the Drosophila discs large tumor suppressor binds to protein 4.1. *Proc Natl Acad Sci U S A* 91: 9818-9822, 1994.

169. **Lynch AM, and Hardin J**. The assembly and maintenance of epithelial junctions in C. elegans. *Front Biosci* 14: 1414-1432, 2009.

170. **Makarova O, Roh MH, Liu CJ, Laurinec S, and Margolis B**. Mammalian Crumbs3 is a small transmembrane protein linked to protein associated with Lin-7 (Pals1). *Gene* 302: 21-29, 2003.

171. **Mallegol J, van Niel G, and Heyman M**. Phenotypic and functional characterization of intestinal epithelial exosomes. *Blood Cells Mol Dis* 35: 11-16, 2005.

172. **Mantovani F, and Banks L**. Regulation of the discs large tumor suppressor by a phosphorylation-dependent interaction with the beta-TrCP ubiquitin ligase receptor. *J Biol Chem* 278: 42477-42486, 2003.

173. **Mantovani F, Massimi P, and Banks L**. Proteasome-mediated regulation of the hDlg tumour suppressor protein. *J Cell Sci* 114: 4285-4292, 2001.

174. **Marshall OJ**. PerlPrimer: cross-platform, graphical primer design for standard, bisulphite and real-time PCR. *Bioinformatics* 20: 2471-2472, 2004.

175. **Martin-Belmonte F, and Mostov K**. Phosphoinositides control epithelial development. *Cell Cycle* 6: 1957-1961, 2007.

176. **Martin-Belmonte F, and Mostov K**. Regulation of cell polarity during epithelial morphogenesis. *Curr Opin Cell Biol* 20: 227-234, 2008.

177. **Martinez-Estrada OM, Culleres A, Soriano FX, Peinado H, Bolos V, Martinez FO, Reina M, Cano A, Fabre M, and Vilaro S**. The transcription factors Slug and Snail act as repressors of Claudin-1 expression in epithelial cells. *Biochem J* 394: 449-457, 2006.

178. **Marzesco AM, Janich P, Wilsch-Brauninger M, Dubreuil V, Langenfeld K, Corbeil D, and Huttner WB**. Release of extracellular membrane particles carrying the stem cell marker prominin-1 (CD133) from neural progenitors and other epithelial cells. *J Cell Sci* 118: 2849-2858, 2005.

179. **Marzesco AM, Wilsch-Brauninger M, Dubreuil V, Janich P, Langenfeld K, Thiele C, Huttner WB, and Corbeil D**. Release of extracellular membrane vesicles from microvilli of epithelial cells is enhanced by depleting membrane cholesterol. *FEBS Lett* 583: 897-902, 2009.

180. **Massari S, Perego C, Padovano V, D'Amico A, Raimondi A, Francolini M, and Pietrini G**. LIN7 mediates the recruitment of IRSp53 to tight junctions. *Traffic* 10: 246-257, 2009.

181. **Matsumine A, Ogai A, Senda T, Okumura N, Satoh K, Baeg GH, Kawahara T, Kobayashi S, Okada M, Toyoshima K, and Akiyama T**. Binding of APC to the human homolog of the Drosophila discs large tumor suppressor protein. *Science* 272: 1020-1023, 1996.

182. **McGee AW, and Bredt DS**. Identification of an intramolecular interaction between the SH3 and guanylate kinase domains of PSD-95. *J Biol Chem* 274: 17431-17436, 1999.

183. **McGee AW, Dakoji SR, Olsen O, Bredt DS, Lim WA, and Prehoda KE**. Structure of the SH3-guanylate kinase module from PSD-95 suggests a mechanism for regulated assembly of MAGUK scaffolding proteins. *Mol Cell* 8: 1291-1301, 2001.

184. **McLaughlin M, Hale R, Ellston D, Gaudet S, Lue RA, and Viel A**. The distribution and function of alternatively spliced insertions in hDlg. *J Biol Chem* 277: 6406-6412, 2002.

185. **McNeill H**. Planar cell polarity and the kidney. *J Am Soc Nephrol* 20: 2104-2111, 2009.

186. **Medina E, Lemmers C, Lane-Guermonprez L, and Le Bivic A**. Role of the Crumbs complex in the regulation of junction formation in Drosophila and mammalian epithelial cells. *Biol Cell* 94: 305-313, 2002.

187. **Metais JY, Navarro C, Santoni MJ, Audebert S, and Borg JP**. hScrib interacts with ZO-2 at the cell-cell junctions of epithelial cells. *FEBS Lett* 579: 3725-3730, 2005.

188. **Micalizzi DS, and Ford HL**. Epithelial-mesenchymal transition in development and cancer. *Future Oncol* 5: 1129-1143, 2009.

189. **Michel D, Arsanto JP, Massey-Harroche D, Beclin C, Wijnholds J, and Le Bivic A**. PATJ connects and stabilizes apical and lateral components of tight junctions in human intestinal cells. *J Cell Sci* 118: 4049-4057, 2005.

190. **Mishima A, Suzuki A, Enaka M, Hirose T, Mizuno K, Ohnishi T, Mohri H, Ishigatsubo Y, and Ohno S**. Over-expression of PAR-3 suppresses contact-mediated inhibition of cell migration in MDCK cells. *Genes Cells* 7: 581-596, 2002.

191. **Mizuno K, Suzuki A, Hirose T, Kitamura K, Kutsuzawa K, Futaki M, Amano Y, and Ohno S**. Self-association of PAR-3-mediated by the conserved N-terminal domain contributes to the development of epithelial tight junctions. *J Biol Chem* 278: 31240-31250, 2003.

192. **Moberg KH, Schelble S, Burdick SK, and Hariharan IK**. Mutations in erupted, the Drosophila ortholog of mammalian tumor susceptibility gene 101, elicit non-cell-autonomous overgrowth. *Dev Cell* 9: 699-710, 2005.

193. **Montcouquiol M, Rachel RA, Lanford PJ, Copeland NG, Jenkins NA, and Kelley MW**. Identification of Vangl2 and Scrb1 as planar polarity genes in mammals. *Nature* 423: 173-177, 2003.

194. **Montcouquiol M, Sans N, Huss D, Kach J, Dickman JD, Forge A, Rachel RA, Copeland NG, Jenkins NA, Bogani D, Murdoch J, Warchol ME, Wenthold RJ, and Kelley MW**. Asymmetric localization of Vangl2 and Fz3 indicate novel mechanisms for planar cell polarity in mammals. *J Neurosci* 26: 5265-5275, 2006.

195. **Morais-de-Sa E, Mirouse V, and St Johnston D**. aPKC phosphorylation of Bazooka defines the apical/lateral border in Drosophila epithelial cells. *Cell* 141: 509-523, 2010.

196. **Moreno-Bueno G, Cubillo E, Sarrio D, Peinado H, Rodriguez-Pinilla SM, Villa S, Bolos V, Jorda M, Fabra A, Portillo F, Palacios J, and Cano A**. Genetic profiling of epithelial cells expressing E-cadherin repressors reveals a distinct role for Snail, Slug, and E47 factors in epithelial-mesenchymal transition. *Cancer Res* 66: 9543-9556, 2006.

197. **Moreno-Bueno G, Portillo F, and Cano A**. Transcriptional regulation of cell polarity in EMT and cancer. *Oncogene* 27: 6958-6969, 2008.

198. **Morin PJ, Sparks AB, Korinek V, Barker N, Clevers H, Vogelstein B, and Kinzler KW**. Activation of beta-catenin-Tcf signaling in colon cancer by mutations in beta-catenin or APC. *Science* 275: 1787-1790, 1997.

199. **Mostov K, Su T, and ter Beest M**. Polarized epithelial membrane traffic: conservation and plasticity. *Nat Cell Biol* 5: 287-293, 2003.

200. **Musch A, Cohen D, Yeaman C, Nelson WJ, Rodriguez-Boulan E, and Brennwald PJ**. Mammalian homolog of Drosophila tumor suppressor lethal (2) giant larvae interacts with basolateral exocytic machinery in Madin-Darby canine kidney cells. *Mol Biol Cell* 13: 158-168, 2002.

201. **Nagai-Tamai Y, Mizuno K, Hirose T, Suzuki A, and Ohno S**. Regulated protein-protein interaction between aPKC and PAR-3 plays an essential role in the polarization of epithelial cells. *Genes Cells* 7: 1161-1171, 2002.

202. **Naim E, Bernstein A, Bertram JF, and Caruana G**. Mutagenesis of the epithelial polarity gene, discs large 1, perturbs nephrogenesis in the developing mouse kidney. *Kidney Int* 68: 955-965, 2005.

203. **Nakagawa S, and Huibregtse JM**. Human scribble (Vartul) is targeted for ubiquitin-mediated degradation by the high-risk papillomavirus E6 proteins and the E6AP ubiquitin-protein ligase. *Mol Cell Biol* 20: 8244-8253, 2000.

204. **Nakayama M, Goto TM, Sugimoto M, Nishimura T, Shinagawa T, Ohno S, Amano M, and Kaibuchi K**. Rho-kinase phosphorylates PAR-3 and disrupts PAR complex formation. *Dev Cell* 14: 205-215, 2008.

205. **Narayan N, Massimi P, and Banks L**. CDK phosphorylation of the discs large tumour suppressor controls its localisation and stability. *J Cell Sci* 122: 65-74, 2009.

206. **Navarro C, Nola S, Audebert S, Santoni MJ, Arsanto JP, Ginestier C, Marchetto S, Jacquemier J, Isnardon D, Le Bivic A, Birnbaum D, and Borg JP**. Junctional recruitment of mammalian Scribble relies on E-cadherin engagement. *Oncogene* 24: 4330-4339, 2005.

207. **Nieto MA**. The snail superfamily of zinc-finger transcription factors. *Nat Rev Mol Cell Biol* 3: 155-166, 2002.

208. **Nieto MA, Sargent MG, Wilkinson DG, and Cooke J**. Control of cell behavior during vertebrate development by Slug, a zinc finger gene. *Science* 264: 835-839, 1994.

209. **Nitsch L, Tramontano D, Ambesi-Impiombato FS, Quarto N, and Bonatti S**. Morphological and functional polarity of an epithelial thyroid cell line. *Eur J Cell Biol* 38: 57-66, 1985.

210. **Nix SL, Chishti AH, Anderson JM, and Walther Z**. hCASK and hDlg associate in epithelia, and their src homology 3 and guanylate kinase domains participate in both intramolecular and intermolecular interactions. *J Biol Chem* 275: 41192-41200, 2000.

211. **Noda Y, Takeya R, Ohno S, Naito S, Ito T, and Sumimoto H**. Human homologues of the Caenorhabditis elegans cell polarity protein PAR6 as an adaptor that links the small GTPases Rac and Cdc42 to atypical protein kinase C. *Genes Cells* 6: 107-119, 2001.

212. **Nola S, Sebbagh M, Marchetto S, Osmani N, Nourry C, Audebert S, Navarro C, Rachel R, Montcouquiol M, Sans N, Etienne-Manneville S, Borg JP, and Santoni MJ**. Scrib regulates PAK activity during the cell migration process. *Hum Mol Genet* 17: 3552-3565, 2008.

213. **Nolan ME, Aranda V, Lee S, Lakshmi B, Basu S, Allred DC, and Muthuswamy SK**. The polarity protein Par6 induces cell proliferation and is overexpressed in breast cancer. *Cancer Res* 68: 8201-8209, 2008.

214. **O'Brien LE, Zegers MM, and Mostov KE**. Opinion: Building epithelial architecture: insights from three-dimensional culture models. *Nat Rev Mol Cell Biol* 3: 531-537, 2002.

215. **Oh KB, Stanton MJ, West WW, Todd GL, and Wagner KU**. Tsg101 is upregulated in a subset of invasive human breast cancers and its targeted overexpression

in transgenic mice reveals weak oncogenic properties for mammary cancer initiation. *Oncogene* 26: 5950-5959, 2007.

216. **Okuda H, Saitoh K, Hirai S, Iwai K, Takaki Y, Baba M, Minato N, Ohno S, and Shuin T**. The von Hippel-Lindau tumor suppressor protein mediates ubiquitination of activated atypical protein kinase C. *J Biol Chem* 276: 43611-43617, 2001.

217. **Olsen O, Funke L, Long JF, Fukata M, Kazuta T, Trinidad JC, Moore KA, Misawa H, Welling PA, Burlingame AL, Zhang M, and Bredt DS**. Renal defects associated with improper polarization of the CRB and DLG polarity complexes in MALS-3 knockout mice. *J Cell Biol* 179: 151-164, 2007.

218. **Olsen O, Liu H, Wade JB, Merot J, and Welling PA**. Basolateral membrane expression of the Kir 2.3 channel is coordinated by PDZ interaction with Lin-7/CASK complex. *Am J Physiol Cell Physiol* 282: C183-195, 2002.

219. **Olsen O, Moore KA, Fukata M, Kazuta T, Trinidad JC, Kauer FW, Streuli M, Misawa H, Burlingame AL, Nicoll RA, and Bredt DS**. Neurotransmitter release regulated by a MALS-liprin-alpha presynaptic complex. *J Cell Biol* 170: 1127-1134, 2005.

220. **Olsen O, Wade JB, Morin N, Bredt DS, and Welling PA**. Differential localization of mammalian Lin-7 (MALS/Veli) PDZ proteins in the kidney. *Am J Physiol Renal Physiol* 288: F345-352, 2005.

221. **Ono Y, Fujii T, Ogita K, Kikkawa U, Igarashi K, and Nishizuka Y**. Protein kinase C zeta subspecies from rat brain: its structure, expression, and properties. *Proc Natl Acad Sci U S A* 86: 3099-3103, 1989.

222. **Park JS, Valerius MT, and McMahon AP**. Wnt/beta-catenin signaling regulates nephron induction during mouse kidney development. *Development* 134: 2533-2539, 2007.

223. **Patel SR, Kim D, Levitan I, and Dressler GR**. The BRCT-domain containing protein PTIP links PAX2 to a histone H3, lysine 4 methyltransferase complex. *Dev Cell* 13: 580-592, 2007.

224. **Pedersen LB, and Rosenbaum JL**. Intraflagellar transport (IFT) role in ciliary assembly, resorption and signalling. *Curr Top Dev Biol* 85: 23-61, 2008.

225. **Peinado H, Olmeda D, and Cano A**. Snail, Zeb and bHLH factors in tumour progression: an alliance against the epithelial phenotype? *Nat Rev Cancer* 7: 415-428, 2007.

226. **Penkert RR, DiVittorio HM, and Prehoda KE**. Internal recognition through PDZ domain plasticity in the Par-6-Pals1 complex. *Nat Struct Mol Biol* 11: 1122-1127, 2004.

227. **Perego C, Vanoni C, Massari S, Longhi R, and Pietrini G**. Mammalian LIN-7 PDZ proteins associate with beta-catenin at the cell-cell junctions of epithelia and neurons. *EMBO J* 19: 3978-3989, 2000.

228. **Perego C, Vanoni C, Villa A, Longhi R, Kaech SM, Frohli E, Hajnal A, Kim SK, and Pietrini G**. PDZ-mediated interactions retain the epithelial GABA transporter on the basolateral surface of polarized epithelial cells. *EMBO J* 18: 2384-2393, 1999.

229. **Petrosky KY, Ou HD, Lohr F, Dotsch V, and Lim WA**. A general model for preferential hetero-oligomerization of LIN-2/7 domains: mechanism underlying directed assembly of supramolecular signaling complexes. *J Biol Chem* 280: 38528-38536, 2005.

230. **Plant PJ, Fawcett JP, Lin DC, Holdorf AD, Binns K, Kulkarni S, and Pawson T**. A polarity complex of mPar-6 and atypical PKC binds, phosphorylates and regulates mammalian Lgl. *Nat Cell Biol* 5: 301-308, 2003.

231. **Qin Y, Capaldo C, Gumbiner BM, and Macara IG**. The mammalian Scribble polarity protein regulates epithelial cell adhesion and migration through E-cadherin. *J Cell Biol* 171: 1061-1071, 2005.

232. **Reiner A, Yekutieli D, and Benjamini Y**. Identifying differentially expressed genes using false discovery rate controlling procedures. *Bioinformatics* 19: 368-375, 2003.

233. **Robinson BS, Huang J, Hong Y, and Moberg KH**. Crumbs regulates Salvador/Warts/Hippo signaling in Drosophila via the FERM-domain protein expanded. *Curr Biol* 20: 582-590, 2010.

234. **Roeth JF, Sawyer JK, Wilner DA, and Peifer M**. Rab11 helps maintain apical crumbs and adherens junctions in the Drosophila embryonic ectoderm. *PLoS One* 4: e7634, 2009.

235. **Roh MH, Fan S, Liu CJ, and Margolis B**. The Crumbs3-Pals1 complex participates in the establishment of polarity in mammalian epithelial cells. *J Cell Sci* 116: 2895-2906, 2003.

236. **Roh MH, Liu CJ, Laurinec S, and Margolis B**. The carboxyl terminus of zona occludens-3 binds and recruits a mammalian homologue of discs lost to tight junctions. *J Biol Chem* 277: 27501-27509, 2002.

237. **Roh MH, Makarova O, Liu CJ, Shin K, Lee S, Laurinec S, Goyal M, Wiggins R, and Margolis B**. The Maguk protein, Pals1, functions as an adapter, linking mammalian homologues of Crumbs and Discs Lost. *J Cell Biol* 157: 161-172, 2002.

238. **Roh MH, and Margolis B**. Composition and function of PDZ protein complexes during cell polarization. *Am J Physiol Renal Physiol* 285: F377-387, 2003.

239. **Rohr S, Bit-Avragim N, and Abdelilah-Seyfried S**. Heart and soul/PRKCi and nagie oko/Mpp5 regulate myocardial coherence and remodeling during cardiac morphogenesis. *Development* 133: 107-115, 2006.

240. **Ruland J, Sirard C, Elia A, MacPherson D, Wakeham A, Li L, de la Pompa JL, Cohen SN, and Mak TW**. p53 accumulation, defective cell proliferation, and early embryonic lethality in mice lacking tsg101. *Proc Natl Acad Sci U S A* 98: 1859-1864, 2001.

241. **Saito RA, Watabe T, Horiguchi K, Kohyama T, Saitoh M, Nagase T, and Miyazono K**. Thyroid transcription factor-1 inhibits transforming growth factor-beta-mediated epithelial-to-mesenchymal transition in lung adenocarcinoma cells. *Cancer Res* 69: 2783-2791, 2009.

242. **Savagner P, Kusewitt DF, Carver EA, Magnino F, Choi C, Gridley T, and Hudson LG**. Developmental transcription factor slug is required for effective re-epithelialization by adult keratinocytes. *J Cell Physiol* 202: 858-866, 2005.

243. **Savagner P, Yamada KM, and Thiery JP**. The zinc-finger protein slug causes desmosome dissociation, an initial and necessary step for growth factor-induced epithelial-mesenchymal transition. *J Cell Biol* 137: 1403-1419, 1997.

244. **Schermer B, Ghenoiu C, Bartram M, Muller RU, Kotsis F, Hohne M, Kuhn W, Rapka M, Nitschke R, Zentgraf H, Fliegauf M, Omran H, Walz G, and Benzing**

T. The von Hippel-Lindau tumor suppressor protein controls ciliogenesis by orienting microtubule growth. *J Cell Biol* 175: 547-554, 2006.

245. **Schluter MA, and Margolis B**. Apical lumen formation in renal epithelia. *J Am Soc Nephrol* 20: 1444-1452, 2009.

246. **Schluter MA, Pfarr CS, Pieczynski J, Whiteman EL, Hurd TW, Fan S, Liu CJ, and Margolis B**. Trafficking of Crumbs3 during cytokinesis is crucial for lumen formation. *Mol Biol Cell* 20: 4652-4663, 2009.

247. **Schmidt-Ott KM, and Barasch J**. WNT/beta-catenin signaling in nephron progenitors and their epithelial progeny. *Kidney Int* 74: 1004-1008, 2008.

248. **Selbie LA, Schmitz-Peiffer C, Sheng Y, and Biden TJ**. Molecular cloning and characterization of PKC iota, an atypical isoform of protein kinase C derived from insulin-secreting cells. *J Biol Chem* 268: 24296-24302, 1993.

249. **Sfakianos J, Togawa A, Maday S, Hull M, Pypaert M, Cantley L, Toomre D, and Mellman I**. Par3 functions in the biogenesis of the primary cilium in polarized epithelial cells. *J Cell Biol* 179: 1133-1140, 2007.

250. **Sheff DR, Daro EA, Hull M, and Mellman I**. The receptor recycling pathway contains two distinct populations of early endosomes with different sorting functions. *J Cell Biol* 145: 123-139, 1999.

251. **Shelly M, Mosesson Y, Citri A, Lavi S, Zwang Y, Melamed-Book N, Aroeti B, and Yarden Y**. Polar expression of ErbB-2/HER2 in epithelia. Bimodal regulation by Lin-7. *Dev Cell* 5: 475-486, 2003.

252. **Shen L, Weber CR, and Turner JR**. The tight junction protein complex undergoes rapid and continuous molecular remodeling at steady state. *J Cell Biol* 181: 683-695, 2008.

253. **Shin K, Fogg VC, and Margolis B**. Tight junctions and cell polarity. *Annu Rev Cell Dev Biol* 22: 207-235, 2006.

254. **Shin K, Straight S, and Margolis B**. PATJ regulates tight junction formation and polarity in mammalian epithelial cells. *J Cell Biol* 168: 705-711, 2005.

255. **Shin K, Wang Q, and Margolis B**. PATJ regulates directional migration of mammalian epithelial cells. *EMBO Rep* 8: 158-164, 2007.

256. **Simske JS, Kaech SM, Harp SA, and Kim SK**. LET-23 receptor localization by the cell junction protein LIN-7 during C. elegans vulval induction. *Cell* 85: 195-204, 1996.

257. **Smyth GK**. Linear models and empirical bayes methods for assessing differential expression in microarray experiments. *Stat Appl Genet Mol Biol* 3: Article3, 2004.

258. **Sobrado VR, Moreno-Bueno G, Cubillo E, Holt LJ, Nieto MA, Portillo F, and Cano A**. The class I bHLH factors E2-2A and E2-2B regulate EMT. *J Cell Sci* 122: 1014-1024, 2009.

259. **Sotillos S, Diaz-Meco MT, Caminero E, Moscat J, and Campuzano S**. DaPKC-dependent phosphorylation of Crumbs is required for epithelial cell polarity in Drosophila. *J Cell Biol* 166: 549-557, 2004.

260. **Straight SW, Karnak D, Borg JP, Kamberov E, Dare H, Margolis B, and Wade JB**. mLin-7 is localized to the basolateral surface of renal epithelia via its NH(2) terminus. *Am J Physiol Renal Physiol* 278: F464-475, 2000.

261. **Straight SW, Pieczynski JN, Whiteman EL, Liu CJ, and Margolis B**. Mammalian lin-7 stabilizes polarity protein complexes. *J Biol Chem* 281: 37738-37747, 2006.

262. **Straight SW, Shin K, Fogg VC, Fan S, Liu CJ, Roh M, and Margolis B**. Loss of PALS1 expression leads to tight junction and polarity defects. *Mol Biol Cell* 15: 1981-1990, 2004.

263. **Streets AJ, Wagner BE, Harris PC, Ward CJ, and Ong AC**. Homophilic and heterophilic polycystin 1 interactions regulate E-cadherin recruitment and junction assembly in MDCK cells. *J Cell Sci* 122: 1410-1417, 2009.

264. **Stucke VM, Timmerman E, Vandekerckhove J, Gevaert K, and Hall A**. The MAGUK protein MPP7 binds to the polarity protein hDlg1 and facilitates epithelial tight junction formation. *Mol Biol Cell* 18: 1744-1755, 2007.

265. **Sugihara-Mizuno Y, Adachi M, Kobayashi Y, Hamazaki Y, Nishimura M, Imai T, Furuse M, and Tsukita S**. Molecular characterization of angiomotin/JEAP family proteins: interaction with MUPP1/Patj and their endogenous properties. *Genes Cells* 12: 473-486, 2007.

266. **Sugimoto M, Inoko A, Shiromizu T, Nakayama M, Zou P, Yonemura S, Hayashi Y, Izawa I, Sasoh M, Uji Y, Kaibuchi K, Kiyono T, and Inagaki M**. The keratin-binding protein Albatross regulates polarization of epithelial cells. *J Cell Biol* 183: 19-28, 2008.

267. **Suzuki A, Ishiyama C, Hashiba K, Shimizu M, Ebnet K, and Ohno S**. aPKC kinase activity is required for the asymmetric differentiation of the premature junctional complex during epithelial cell polarization. *J Cell Sci* 115: 3565-3573, 2002.

268. **Suzuki A, Yamanaka T, Hirose T, Manabe N, Mizuno K, Shimizu M, Akimoto K, Izumi Y, Ohnishi T, and Ohno S**. Atypical protein kinase C is involved in the evolutionarily conserved par protein complex and plays a critical role in establishing epithelia-specific junctional structures. *J Cell Biol* 152: 1183-1196, 2001.

269. **Takizawa S, Nagasaka K, Nakagawa S, Yano T, Nakagawa K, Yasugi T, Takeuchi T, Kanda T, Huibregtse JM, Akiyama T, and Taketani Y**. Human scribble, a novel tumor suppressor identified as a target of high-risk HPV E6 for ubiquitin-mediated degradation, interacts with adenomatous polyposis coli. *Genes Cells* 11: 453-464, 2006.

270. **Tan D, Li Q, Deeb G, Ramnath N, Slocum HK, Brooks J, Cheney R, Wiseman S, Anderson T, and Loewen G**. Thyroid transcription factor-1 expression prevalence and its clinical implications in non-small cell lung cancer: a high-throughput tissue microarray and immunohistochemistry study. *Hum Pathol* 34: 597-604, 2003.

271. **Tavares GA, Panepucci EH, and Brunger AT**. Structural characterization of the intramolecular interaction between the SH3 and guanylate kinase domains of PSD-95. *Mol Cell* 8: 1313-1325, 2001.

272. **Tepass U**. Crumbs, a component of the apical membrane, is required for zonula adherens formation in primary epithelia of Drosophila. *Dev Biol* 177: 217-225, 1996.

273. **Tepass U, Theres C, and Knust E**. crumbs encodes an EGF-like protein expressed on apical membranes of Drosophila epithelial cells and required for organization of epithelia. *Cell* 61: 787-799, 1990.

274. **Thiery JP**. Epithelial-mesenchymal transitions in development and pathologies. *Curr Opin Cell Biol* 15: 740-746, 2003.

275. **Thiery JP, Acloque H, Huang RY, and Nieto MA**. Epithelial-mesenchymal transitions in development and disease. *Cell* 139: 871-890, 2009.

276. **Thiery JP, and Sleeman JP**. Complex networks orchestrate epithelial-mesenchymal transitions. *Nat Rev Mol Cell Biol* 7: 131-142, 2006.

277. **Tomaic V, Gardiol D, Massimi P, Ozbun M, Myers M, and Banks L**. Human and primate tumour viruses use PDZ binding as an evolutionarily conserved mechanism of targeting cell polarity regulators. *Oncogene* 28: 1-8, 2009.

278. **Traweger A, Wiggin G, Taylor L, Tate SA, Metalnikov P, and Pawson T**. Protein phosphatase 1 regulates the phosphorylation state of the polarity scaffold Par-3. *Proc Natl Acad Sci U S A* 105: 10402-10407, 2008.

279. **Ullmer C, Schmuck K, Figge A, and Lubbert H**. Cloning and characterization of MUPP1, a novel PDZ domain protein. *FEBS Lett* 424: 63-68, 1998.

280. **Valiente M, Andres-Pons A, Gomar B, Torres J, Gil A, Tapparel C, Antonarakis SE, and Pulido R**. Binding of PTEN to specific PDZ domains contributes to PTEN protein stability and phosphorylation by microtubule-associated serine/threonine kinases. *J Biol Chem* 280: 28936-28943, 2005.

281. **van de Pavert SA, Kantardzhieva A, Malysheva A, Meuleman J, Versteeg I, Levelt C, Klooster J, Geiger S, Seeliger MW, Rashbass P, Le Bivic A, and Wijnholds J**. Crumbs homologue 1 is required for maintenance of photoreceptor cell polarization and adhesion during light exposure. *J Cell Sci* 117: 4169-4177, 2004.

282. **van Rossum AG, Aartsen WM, Meuleman J, Klooster J, Malysheva A, Versteeg I, Arsanto JP, Le Bivic A, and Wijnholds J**. Pals1/Mpp5 is required for correct localization of Crb1 at the subapical region in polarized Muller glia cells. *Hum Mol Genet* 15: 2659-2672, 2006.

283. **Vandanapu RR, Singh AK, Mikhaylova M, Reddy PP, Kreutz MR, and Sharma Y**. Structural differences between the SH3-HOOK-GuK domains of SAP90/PSD-95 and SAP97. *Protein Expr Purif* 2009.

284. **Vandenberg AL, and Sassoon DA**. Non-canonical Wnt signaling regulates cell polarity in female reproductive tract development via van gogh-like 2. *Development* 136: 1559-1570, 2009.

285. **Vasko V, Espinosa AV, Scouten W, He H, Auer H, Liyanarachchi S, Larin A, Savchenko V, Francis GL, de la Chapelle A, Saji M, and Ringel MD**. Gene expression and functional evidence of epithelial-to-mesenchymal transition in papillary thyroid carcinoma invasion. *Proc Natl Acad Sci U S A* 104: 2803-2808, 2007.

286. **Wagner KU, Krempler A, Qi Y, Park K, Henry MD, Triplett AA, Riedlinger G, Rucker IE, and Hennighausen L**. Tsg101 is essential for cell growth, proliferation, and cell survival of embryonic and adult tissues. *Mol Cell Biol* 23: 150-162, 2003.

287. **Wahab NA, and Mason RM**. A critical look at growth factors and epithelial-to-mesenchymal transition in the adult kidney. Interrelationships between growth factors that regulate EMT in the adult kidney. *Nephron Exp Nephrol* 104: e129-134, 2006.

288. **Wang Q, Chen XW, and Margolis B**. PALS1 regulates E-cadherin trafficking in mammalian epithelial cells. *Mol Biol Cell* 18: 874-885, 2007.

289. **Wang Q, Hurd TW, and Margolis B**. Tight junction protein Par6 interacts with an evolutionarily conserved region in the amino terminus of PALS1/stardust. *J Biol Chem* 279: 30715-30721, 2004.

290. **Wang Y, Du D, Fang L, Yang G, Zhang C, Zeng R, Ullrich A, Lottspeich F, and Chen Z**. Tyrosine phosphorylated Par3 regulates epithelial tight junction assembly promoted by EGFR signaling. *EMBO J* 25: 5058-5070, 2006.

291. **Wang Z, Wade P, Mandell KJ, Akyildiz A, Parkos CA, Mrsny RJ, and Nusrat A**. Raf 1 represses expression of the tight junction protein occludin via activation of the zinc-finger transcription factor slug. *Oncogene* 26: 1222-1230, 2007.

292. **Weisz OA, and Rodriguez-Boulan E**. Apical trafficking in epithelial cells: signals, clusters and motors. *J Cell Sci* 122: 4253-4266, 2009.

293. **Wells CD, Fawcett JP, Traweger A, Yamanaka Y, Goudreault M, Elder K, Kulkarni S, Gish G, Virag C, Lim C, Colwill K, Starostine A, Metalnikov P, and Pawson T**. A Rich1/Amot complex regulates the Cdc42 GTPase and apical-polarity proteins in epithelial cells. *Cell* 125: 535-548, 2006.

294. **Whiteman EL, Liu CJ, Fearon ER, and Margolis B**. The transcription factor snail represses Crumbs3 expression and disrupts apico-basal polarity complexes. *Oncogene* 27: 3875-3879, 2008.

295. **Wilson GM, Fielding AB, Simon GC, Yu X, Andrews PD, Hames RS, Frey AM, Peden AA, Gould GW, and Prekeris R**. The FIP3-Rab11 protein complex regulates recycling endosome targeting to the cleavage furrow during late cytokinesis. *Mol Biol Cell* 16: 849-860, 2005.

296. **Wodarz A, Hinz U, Engelbert M, and Knust E**. Expression of crumbs confers apical character on plasma membrane domains of ectodermal epithelia of Drosophila. *Cell* 82: 67-76, 1995.

297. **Wu H, Feng W, Chen J, Chan LN, Huang S, and Zhang M**. PDZ domains of Par-3 as potential phosphoinositide signaling integrators. *Mol Cell* 28: 886-898, 2007.

298. **Wu M, Pastor-Pareja JC, and Xu T**. Interaction between Ras(V12) and scribbled clones induces tumour growth and invasion. *Nature* 463: 545-548, 2010.

299. **Yamanaka T, Horikoshi Y, Izumi N, Suzuki A, Mizuno K, and Ohno S**. Lgl mediates apical domain disassembly by suppressing the PAR-3-aPKC-PAR-6 complex to orient apical membrane polarity. *J Cell Sci* 119: 2107-2118, 2006.

300. **Yamanaka T, Horikoshi Y, Sugiyama Y, Ishiyama C, Suzuki A, Hirose T, Iwamatsu A, Shinohara A, and Ohno S**. Mammalian Lgl forms a protein complex with PAR-6 and aPKC independently of PAR-3 to regulate epithelial cell polarity. *Curr Biol* 13: 734-743, 2003.

301. **Yamanaka T, Horikoshi Y, Suzuki A, Sugiyama Y, Kitamura K, Maniwa R, Nagai Y, Yamashita A, Hirose T, Ishikawa H, and Ohno S**. PAR-6 regulates aPKC activity in a novel way and mediates cell-cell contact-induced formation of the epithelial junctional complex. *Genes Cells* 6: 721-731, 2001.

302. **Yilmaz M, and Christofori G**. EMT, the cytoskeleton, and cancer cell invasion. *Cancer Metastasis Rev* 28: 15-33, 2009.

303. **Zavadil J, and Bottinger EP**. TGF-beta and epithelial-to-mesenchymal transitions. *Oncogene* 24: 5764-5774, 2005.

304. **Zhao B, Wei X, Li W, Udan RS, Yang Q, Kim J, Xie J, Ikenoue T, Yu J, Li L, Zheng P, Ye K, Chinnaiyan A, Halder G, Lai ZC, and Guan KL**. Inactivation of YAP oncoprotein by the Hippo pathway is involved in cell contact inhibition and tissue growth control. *Genes Dev* 21: 2747-2761, 2007.

305. **Zuo X, Guo W, and Lipschutz JH**. The exocyst protein Sec10 is necessary for primary ciliogenesis and cystogenesis in vitro. *Mol Biol Cell* 20: 2522-2529, 2009.

306. **Zurzolo C, Gentile R, Mascia A, Garbi C, Polistina C, Aloj L, Avvedimento VE, and Nitsch L**. The polarized epithelial phenotype is dominant in hybrids between polarized and unpolarized rat thyroid cell lines. *J Cell Sci* 98 (Pt 1): 65-73, 1991.